TECHNICAL REPORT

ISO/TR 12930

First edition
2014-04-01

Seismic design examples based on ISO 23469

Exemples de dimensionnement basés sur l'ISO 23469

Reference number
ISO/TR 12930:2014(E)

COPYRIGHT PROTECTED DOCUMENT

ISO copyright office
Case postale 56 • CH-1211 Geneva 20
Tel. + 41 22 749 01 11
Fax + 41 22 749 09 47
E-mail copyright@iso.org
Web www.iso.org

Published in Switzerland

Contents

Page

Foreword

ISO (the International Organization for Standardization) is a worldwide federation of national standards bodies (ISO member bodies). The work of preparing International Standards is normally carried out through ISO technical committees. Each member body interested in a subject for which a technical committee has been established has the right to be represented on that committee. International organizations, governmental and non-governmental, in liaison with ISO, also take part in the work. ISO collaborates closely with the International Electrotechnical Commission (IEC) on all matters of electrotechnical standardization.

The procedures used to develop this document and those intended for its further maintenance are described in the ISO/IEC Directives, Part 1. In particular the different approval criteria needed for the different types of ISO documents should be noted. This document was drafted in accordance with the editorial rules of the ISO/IEC Directives, Part 2. www.iso.org/directives

Attention is drawn to the possibility that some of the elements of this document may be the subject of patent rights. ISO shall not be held responsible for identifying any or all such patent rights. Details of any patent rights identified during the development of the document will be in the Introduction and/or on the ISO list of patent declarations received. www.iso.org/patents

Any trade name used in this document is information given for the convenience of users and does not constitute an endorsement.

For an explanation on the meaning of ISO specific terms and expressions related to conformity assessment, as well as information about ISO's adherence to the WTO principles in the Technical Barriers to Trade (TBT), see the following URL: Foreword - Supplementary information

The committee responsible for this document is ISO/TC 98, *Bases for design of structures*, sous-comité SC 3, *Loads, forces and other actions*.

Introduction

ISO 23469:2005 provides guidelines to be observed by experienced practicing engineers and code writers when specifying seismic actions in the design of geotechnical works. It might not be so easy for code writers and practitioners to utilize ISO 23469, because that it offers advanced philosophy and general framework of seismic design. The purpose of this Technical Report (TR) is to provide seismic design examples based on ISO 23469 for demonstrating how to utilize ISO 23469 in actual seismic designs to the code writers and the practitioners. The implementation of ISO 23469 will secure the rationality of seismic safety evaluation of the infrastructures in the world, and this TR aims at promoting the implementation.

ISO 23469 is essentially a guideline itself. Therefore, this TR should contain not explicit guidelines but design examples without using the term 'guideline'. Thus, this TR is expected to demonstrate the utilization of ISO 23469 by providing design examples with detailed explanation from the viewpoint of conformity with ISO 23469 for a kind of guidance rather than to provide the detailed recommendation of specific methodologies.

Through the development of this Technical Report, it is concluded that ISO 23469 has been and is going to be an essential and useful guideline of seismic design of geotechnical works for experienced practicing engineers and code writers.

Seismic design examples based on ISO 23469

1 Scope

This Technical Report provides seismic design examples for geotechnical works based on ISO 23469:2005 in order to demonstrate how to use this ISO standard. The design examples are intended to provide guidance to experienced practicing engineers and code writers. Geotechnical works include buried structures (e.g. buried tunnels, box culverts, pipelines, and underground storage facilities), foundations (e.g. shallow and deep foundations, and underground diaphragm walls), retaining walls (e.g. soil retaining and quay walls), pile-supported wharves and piers, earth structures (e.g. earth and rock fill dams and embankments), gravity dams, tanks, landfill and waste sites.

ISO 23469 addresses important issues for seismic actions for designing geotechnical works, including effects of site-specific response, ground displacement, soil-structure interaction and liquefaction, in a systematic manner within a consistent framework. This International Standard presents a full range of methods for the analysis of geotechnical works, ranging from simple to sophisticated, from which experienced practicing engineers can choose the most appropriate option for evaluating their performance. Therefore, this Technical Report includes well-chosen design examples that consider these important issues and covering in a balanced way the wide range of the methods of analysis and the types of model which can be used to evaluate seismic actions of geotechnical works.

2 Purpose and policy of collecting design examples

2.1 Purpose of collecting well-chosen examples

This Technical Report aims at collecting design examples that are basically conformable with ISO 23469. They are expected to be design examples dealing with important things need to be covered in ISO 23469 from the point of view of performance-based design approach. This TR should be well-balanced in included design examples;

— Focusing evaluation of reference earthquake ground motions with detailed description as a common issue.

— Having combination of simplified and detailed analyses.

— Based on simplified equivalent static analysis and detailed analysis for retaining walls, buried structures or earth structures.

— Focusing consideration of soil displacements for pile foundations and buried structures.

— Focusing evaluation of effects of liquefaction for retaining walls, earth structures, pile foundations.

— Focusing consideration of spatial variation in the ground motions for long bridges, buried structures, or dams.

— Based on site specific dynamic response by 1-D analysis.

— Based on detailed dynamic analysis by 2-D or 3-D analysis.

2.2 Concept and policy of choosing and composing

To realize the prescribed purpose of this TR, the basic concept of it is targeting to cover major distinguishing and important issues of IS23469 by all the design examples contained in this TR. Thus, the following points are another requirement for choosing and composing design examples.

— Design examples written with cares for readers in terms of conformity with requirement and recommendation in ISO 23469

— The TR should consist of several well-chosen design examples which cover the key issues of the ISO 23469 with well balance between them.

— The TR is anticipated to be well balanced among Japan, Northern America, and Europe.

— For description of manuscript, each design example is requested to

— Be cared in terms of conformity with requirement and recommendation in ISO 23469

— Have stress on methodology recommended by WG

— Be within 20 pages for a complete example and 8 pages for a sub-example basically

2.3 Development and result

After discussing the policy of collecting and choosing design examples, WG10 also had developed an expected table of contents from arguments through three Working Group meetings held in 2006 and correspondence with consideration of design practice situation in member's countries and regions. After registration of NP12825 in the end of this year, the WG10 repeatedly requested all the WG members and participants of the meetings to provide possible design examples for this Technical Report. The table of contents of the TR of design examples was almost fixed and the drafting persons for the examples were assigned in 2008 through more four WG meetings; eight examples for the first stage of specifying seismic action were expected to be prepared by three persons from Japan and one from Turkey and 28 examples for the second were hopefully to be prepared by 17 persons from Japan, three from USA, one from Greece, and one from Italy.

This NP was officially approved with the submission, in 2008, of the first Working Draft of TR12825 containing six examples, but the NWI was subsequently re-numbered as 12930 from an administrative reason. The third and final Working Draft of TR12930, which was developed through another three meetings in two years for waiting design examples to be offered from countries other than Japan was submitted to TC98/SC3 in the end of 2010 then accepted as a Draft Technical Report with a request of addition of description for a few points. The last two year period was mainly aimed at collecting examples from countries excepting Japan. Notwithstanding the total number of attendees in thirteen WG meetings is 87 and they came from Japan, USA, Greece, France, Poland, Canada, Turkey, Italy, South Africa, Germany, Morocco, Romania, and Russia (in order of total number of attendees), only prescribed persons were merely expected. Probably because that the preparing a manuscript is a tough job with few personal incentive; i.e. a completely volunteer work.

2.4 General conclusion of TR12930 obtained through its development

Eventually seven examples for the first stage and 15 examples for the second stage were successfully collected from thirteen persons consisting of eleven from Japan, one from USA, and one from Greece. The total number of the 22 well-chosen design examples can almost cover major distinguishing and important issues of IS23469 as targeting at the beginning. Through the process of preparing and editing the drafts, it was clarified that IS23469 is useful for evaluation, assessment and review in the seismic design. Furthermore, it was demonstrated that assessment for conformity with IS23469 in can be conducted in terms of provisional sentences according to Clause 3 of this TR. Thus, it is concluded that IS23469 has been and is going to be an essential and useful guideline of seismic design of geotechnical works for experienced practicing engineers and code writers.

2.5 Editors, authors and reviewers

This Technical Report has general remarks and 22 well-chosen design examples written in over 200 pages with 60 thousand words. Reviewing and editing all the manuscripts require tremendously hard works as well as the authors preparing them. Thus, the contributions of editors, authors and reviewers are shown here.

2.5.1 Editors

Prof. Shinichiro Mori, Ehime University, Japan, Convener of ISO/TC98/SC3/WG10

Prof. Kohji Ichii, Hiroshima University, Japan

The editors mainly reviewed and checked the conformity with ISO 23469 in all the manuscripts prepared by authors and added conformity codes corresponding sentences or paragraphs in their ends when necessary. The editors also revised hard-to-understand, confusing or complicated English expressions, written by some Japanese authors, by modifying the expressions and covering logical gaps.

2.5.2 Authors

Authors and Clause(s) or Subclause(s) in their charge are shown as follows:

Prof. Shinichiro Mori, Ehime University, Japan, mori@ehime-u.ac.jp

Author of Clauses 1, 2, 3, and 4, and Subclauses 5.2.2 and 5.3

Prof. Susumu Nakamura, Nihon University, Japan, s-nak@civil.ce.nihon-u.ac.jp

Author of Clause 4 and Subclauses 4.1.1, 4.2.2, and 4.3.1

Dr. Atsushi Nozu, Port and Airport Research Institute, Japan, nozu@pari.go.jp

Author of Subclauses 4.2.1 and 4.2.4

Prof. Takao Kagawa, Tottori University, Japan, kagawa@cv.tottori-u.ac.jp

Author of Subclause 4.2.3

Prof. Koji Ichii, Hiroshima University, Japan, ichiikoji@hiroshima-u.ac.jp

Author of Subclauses 5.1.1 and 5.1.5

Dr. Masaaki Yabe, Chodai Corporation, Japan, yabe-m@chodai.co.jp

Author of Subclauses 5.1.2 and 5.1.3

Dr. Shigeru Tani, National Agriculture and Food Research, Japan, stani@affrc.go.jp

Author of Subclause 5.1.4

Dr. Yoshitaka Murono, Railway Technical Research Institute, Japan, murono@rtri.or.jp

Author of Subclause 5.2.1

Prof. Kyriazis Pitilakis, Aristotle University of Thessaloniki, Greece, pitilakis@geo.civil.auth.gr

Author of Subclause 5.2.3, Member of ISO/TC98/SC3/WG10

Dr. Kiyoshi Fukutake, Shimizu Corporation, Japan, kiyoshi.fukutake@shimz.co.jp

Author of Subclauses 5.3.1, 5.3.2 and 5.3.3

Dr. Shojiro Kataoka, National Institute for Land and Infrastructure Management, Japan

kataoka-s92rc@nilim.go.jp

Author of Subclause 5.4.1

Dr. Yukio Adachi, Hanshin Expressway Company Limited, Japan

Principal author of Subclause 5.4.2

Dr. Craig A. Davis, City of Los Angeles, USA, Craig.Davis@ladwp.com

Principal author of Subclause 5.4.3, Member of ISO/TC98/SC3/WG10

Dr. Tetsuo Tobita, Kyoto University, Japan, tobita@geotech.dpri.kyoto-u.ac.jp

Author of Annex A, Member of ISO/TC98/SC3/WG10

2.5.3 Reviewers

The reviewers were basically the members of TC98/SC3/WG10 including 16 members for development of IS23469 from 12 member bodies/countries and additional 24 members from 7 member bodies/countries. They also provided great contributions throughout the development as well. The members of TC98/SC3 were also potentially to be reviewers. The mirror committee of WG10 in Japan with 34 members had been also reviewing as well as preparing the activity prior to each step in this work item.

3 Assessment for conformity with ISO 23469

Assessment of a design with regard to conformity with ISO23489 is made based on the conformity with each provisional sentence in this ISO standard.

In the main text of each sub-sub-clause for a design example, a sentence or a paragraph corresponding to a specific requirement which is provided in a sentence using “shall” in ISO 23469, shall be ended with a corresponding “code” written in parentheses for being checked in terms of conformity with provisional sentences in ISO 23469. A specific recommendation is provided in a sentence using “should” as well. Therefore, this Technical Report adopts a code description in which a code of abbreviation consists of numerals and an alphabet. In the code, consecutive numerals stand for clause, sub-clause, and sub-sub-clause, respectively in principle. An alphabet in capital letter stands for “shall” and that in lower-case letter stands for “should” in appearing order. For examples, the third sentence using “shall” in the sub-sub-clause 6.2.1 in ISO 23469 corresponds to “(621C)” and the first sentence using “should” in sub-sub-clause 8.1.4 corresponds to “(814a).” Exceptionally, zero is placed in the place for sub-clause like “(520A).”

Provisional sentences using “shall” or “should” are extracted from the main body of ISO 23469 with partial reduction if acceptable and shown in appearing order as shown in Annex A.

4 First stage of specifying seismic actions - Determination of site-specific earthquake ground motions demonstrated by design examples

For designing geotechnical works, reference earthquake motions are needed to specify as seismic actions at the first stage. In order to evaluate the reference earthquake ground motions, the motions at the firm ground are evaluated by a seismic hazard analysis based on probabilistic or deterministic approach. As the reference earthquake motions, earthquake motions at the surface of the free field or/and at a certain depth within the subsoil can be evaluated by site response analyses.

The probabilistic approach is more appropriate for the evaluation of seismic actions at scale a nation or region. In general, the probabilistic approach in some case could lead to an underestimation of local seismic action comparing with the deterministic approach.(Grooso S. and Mourgeris M. 2009a and 2009b)

Probabilistic seismic hazard analysis as probabilistic approach shall be used to determine earthquake ground motion for evaluating serviceability. The earthquake ground motion for evaluating safety shall be determined by either probabilistic or deterministic analysis is used to determine. The seismic hazard analysis should capture the characteristics of the ground motion based on the earthquake magnitude, fault type and distance with or without site parameters. More detail seismic hazard analysis should capture the near source effects and directivity effects and should be based on seismic source parameters, including the geometry of seismic faults, propagating of the fault rapture over the seismic fault, attenuation of earthquake motions from the seismic fault, and deep basin effects. The uncertainties in the model parameters of the seismic fault, attenuation relations, and deep basin effects shall be considered appropriately (621A, 621B, 621C 622a, 622b, 622c).

The seismic hazard analysis method includes empirical, semi-empirical, and theoretical method, and a combination of these methods, and shall be chosen, consistent with the degree of refinement required for analysis of the geotechnical works, based on the importance of structures, and the available information on seismic faults and deep basin structures in the vicinity of a site. Results of seismic hazard analysis, ie NEHAP in USA etc. may be available over a country or region from relevant authorities giving the representative values of earthquake ground motion for use in the subsequent analysis. (622A)

Some examples to evaluate seismic hazard analyses in term of probabilistic and deterministic approach are described in Subclause 4.2. Furthermore, some examples for site response analysis are described in Subclause 4.3.

4.1 General

4.1.1 Methodology for empirical method in deterministic approach and examples

The simplest method among empirical methods is to combine an attenuation equation of an intensity of earthquake motions at firm ground with the amplification characteristics of a site of interest. As for the indices of the intensities of the earthquake motions for design, such as maximum acceleration, maximum velocity and amplitudes of response spectra, the attenuation equations of the indices are obtained by regression analyses using earthquake motion records in terms of the magnitude of earthquakes and the hypocentral distance. Using the attenuation equations, a designer can estimate the indices of earthquake ground motions during scenario earthquakes. Recent accumulation of observed earthquake motion records led to upgraded attenuation equations that can consider the regional peculiarity or the mechanism of earthquake source. This methodology has advantages: It is easy to evaluate the characteristics of earthquake ground motion. It has been used for a long time for probabilistic hazard analysis corresponding estimated values to mean values of observed motions. (622a)

An equation developed according to a theoretical formula of earthquake ground motion is adopted as an attenuation equation. A source spectrum, S(T) consists of the terms representing both the effect of fault scale as the magnitude M and the influence of rock stiffness in the source region, where T is the object frequency.

$$S(T) = a(T)M + c(T) \tag{1}$$

The term representing the propagation of earthquake motion waves consists that of the non-elasticity attenuation and that of geometrical damping as the following equation. The hypocentral distance X represents the minimum distance from fault and the object site. Therefore, the accuracy of the focal location and area is required for more accurate estimate in focal region. (622a)

$$P(T) = -\log X - b(T)X \tag{2}$$

Adding the term associated with the relative amplification to the average ground, the final form of the attenuation equation becomes as follows.

$$\log F(T) = S(T) + P(T) + G(T) = a(T)M + c(T) - \log X - b(T)X + d(T) \quad (3)$$

For example, attenuation equations of acceleration response spectra have been developed using earthquake ground motion records of inland earthquakes observed from 1978 to 2003. Estimated acceleration response spectra as per the attenuation equations are shown in Figure 1. The equations can clearly express the difference of amplification characteristics depending on the types of ground.

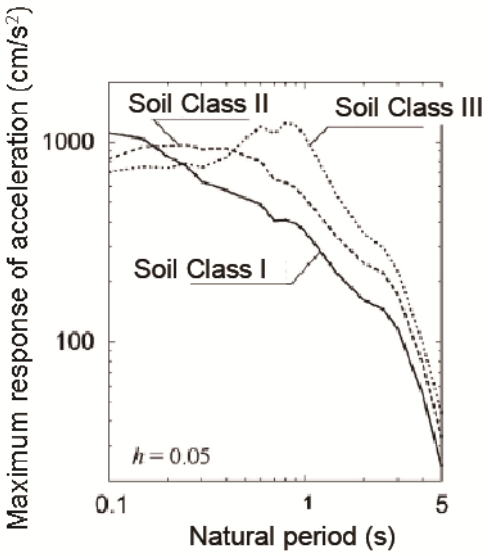

Figure 1 — Acceleration response spectrum obtained by attenuation equation

Further as variables of the fault parameters such as hypocenter depth and the earthquake type, etc. might be added to this equation. The term of the geometrical damping might be assumed 0.5logX instead of logX by considering for propagating the surface wave. The form of the attenuation equation is assumed including coefficients such as a, b, c, and d. The coefficients are evaluated by the regression analysis based on the observed seismic records. The attenuation equation has the characteristics to be applicable to evaluate the motion on the specific ground which is the same ground with that observed seismic records by used of the regression analysis. If the ground is a engineering bedrock, the characteristic value at ground surface is obtained by magnifying the amplification coefficient to the value at the engineering bedrock. (622a)

4.1.2 Examples

First of all, detail of fault plane according to fault zone between Ohoita plane and Yufuin is modeled for two planes with east part and west part based on the evaluation of the Headquarters for Earthquake Research Promotion. The fault length in east part is set to be 27 km, and the length in west part is set to be 14 km as shown in Fig.2. Moreover, this fault zone has been evaluated as the normal fault whose plane inclines the north side. The dip angle around ground surface has been known as 70 degrees based on survey. The dip angle of the fault plane was assumed to be 60 degrees considering tendency to grow the dip angle of the normal fault in the surface ground. Based on the data by the Japan Meteorological Agency, the upper and lower bound depth among fault parameters in the east part were set to 2km, 15km respectively. Those in the west part were set to 3km, 15km respectively. Therefore, the fault width in the east part and the west becomes 15km and 13km respectively. Next, fault area S required for determining the magnitude becomes 5.9×102 km2 by use of the specified fault length and width in the east and west part as the mentioned above. Based on the experimental relationship between the magnitude and the investigated fault plane in the past earthquakes, the magnitude M was set as 6.8. Minimum distance from fault plane to the design object site is set as 2km under the assumption that the value is the same with the upper bound depth of the fault plane. (622a)

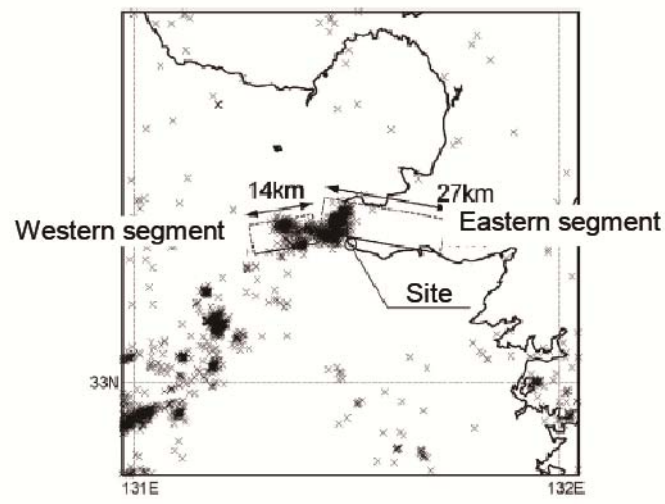

Figure 2 — Fault model at the object site

Acceleration response spectrum among the variable of earthquake ground motion is chosen to determine the seismic action on the geotechnical works. The design acceleration response spectrum at the site whose ground type is characterized as I kind is evaluated by use of the attenuation equation as mentioned above in 4.1.1. The spectrum is shown in Figure 3. As for the applicable lime of the empirical method, it has a difficulty to take into account of the investigated site-specific characteristics in terms of the fault parameters and the ground condition directly. Moreover, it can not apply to evaluate an extremely large-scale earthquake that the strong motion record has not been obtained. (623B)

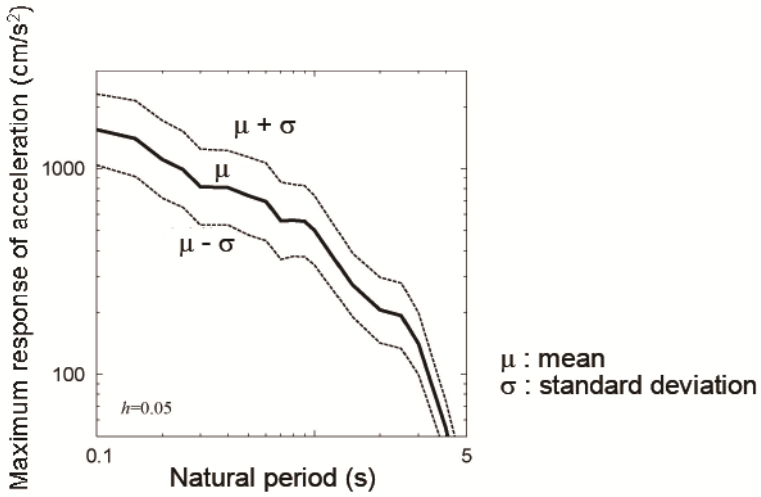

Figure 3 — Estimated acceleration response spectrum for M with 6.8, and X with 2km

4.2 Site-specific seismic hazard analysis evaluation

Site-specific seismic hazard analysis evaluation is conducted either by probabilistic approaches or deterministic ones. In general,

4.2.1 Probabilistic approach- Probabilistic seismic hazard analysis with focus on Fourier amplitude and group delay time

4.2.1.1 Outline

In general, strong ground motions are determined by three effects, namely, the source effect, the path effect and the site effect as shown in Figure 4. The source effect is defined as the effect of the rupture process of the earthquake. The path effect is defined as the effect of the materials along the propagation path from the source to the bedrock beneath the site. The site effect is defined as the effect of sediments below the site down to the bedrock. Here, the bedrock is defined as a layer with a shear wave velocity over 3000 m/s (In many cases it corresponds to fresh granite in Japan). (622a)

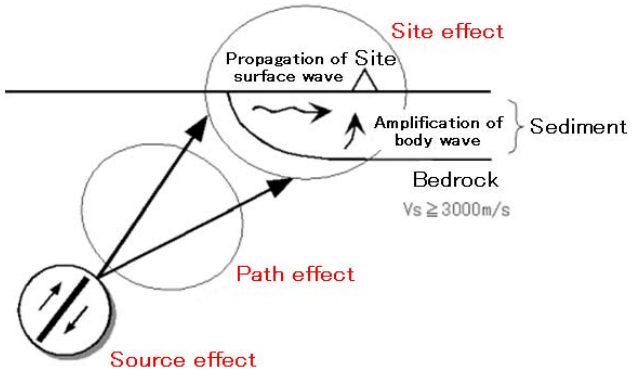

Figure 4 — Source, path and site effects

In general, the Fourier amplitude of a ground motion observed at the ground surface $O(f)$ is the product of the source effect $S(f)$, the path effect $P(f)$ and the site effect $G(f)$. (622a)

$$O(f) = S(f)P(f)G(f) \tag{4}$$

On the other hand, the group delay time of a ground motion observed at the ground surface $tgr^O(f)$ is the sum of the source effect $tgr^S(f)$, the path effect $tgr^P(f)$ and the site effect $tgr^G(f)$ (SAWADA *et al.*, 1998).

$$t_{gr}{}^{O}(f) = t_{gr}{}^{S}(f) + t_{gr}{}^{P}(f) + t_{gr}{}^{G}(f) \tag{5}$$

The group delay time is defined as the derivative of the Fourier phase with respect to angular frequency and it roughly corresponds to the arrival time of each frequency component (COHEN, 1995).

The probabilistic seismic hazard analysis (PSHA) described here (NAGAO *et al.*, 2005) is intended to deal with the source, path and site effects as strictly as possible by focusing on the Fourier amplitude and the group delay time of earthquake ground motions. The analysis uses the records of earthquake ground motions at the site of interest to account for the site effects as accurately as possible. It can generate ground motion time histories corresponding to a given annual probability of exceedance.

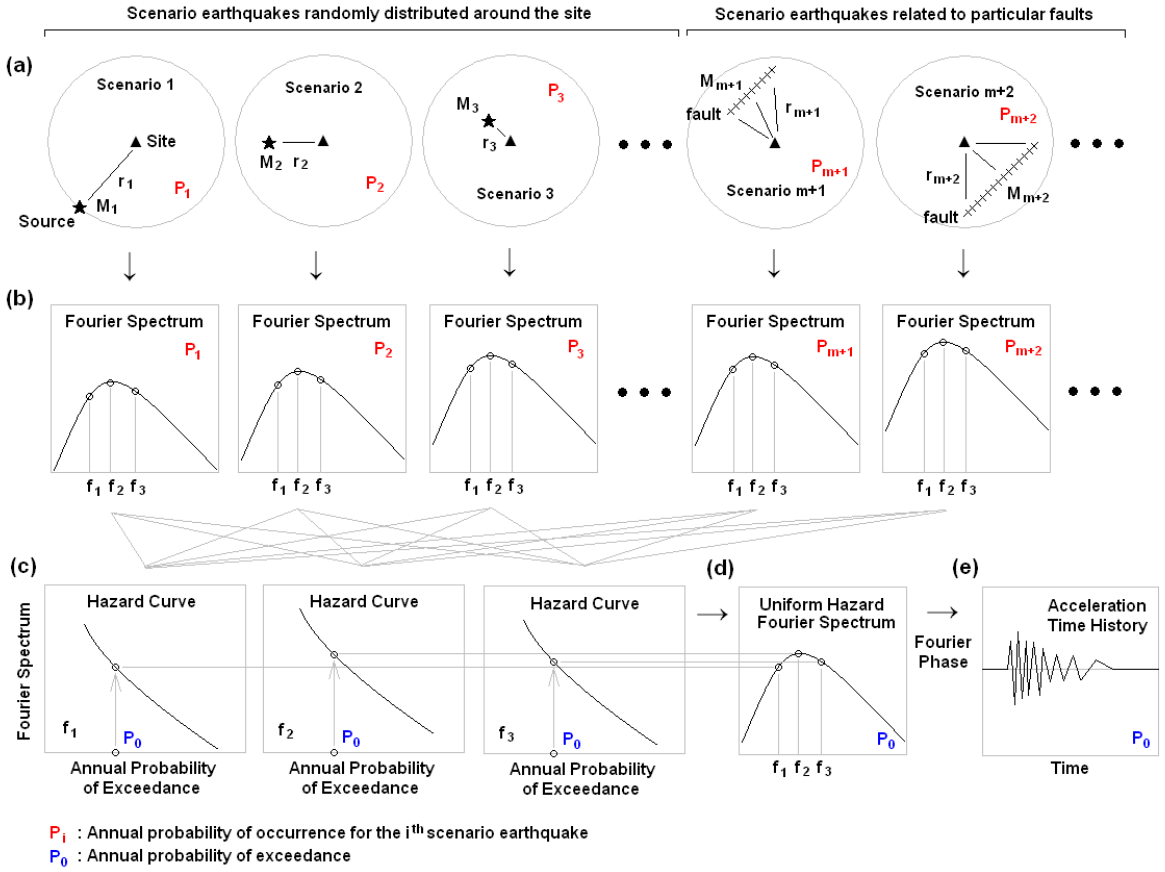

Figure 5 — Overview of the present PSHA

The overview of the present PSHA is shown in Figure 5 First, all the possible earthquake scenarios have to be considered. The scenario earthquakes fall into two categories. One is the scenario earthquakes randomly distributed around the site (background earthquakes) (Scenarios 1, 2,...*m* in Figure 5 (a)). The other is the scenario earthquakes that are related to particular faults such as active faults or plate boundaries (Scenarios *m*+1, *m*+2,...*n* in Figure 5 (a)). For each scenario, the annual probability of occurrence has to be assigned. Then, for each earthquake scenario, the Fourier amplitude spectrum at the site of interest is evaluated as shown in Figure 5 (b), taking into account the source effect, the path effect and the site effect as described later. Based on the Fourier amplitude spectra thus obtained and the relevant annual probability of occurrence, the “hazard curve” (relation between the Fourier amplitude and the annual probability of exceedance) can be obtained for each frequency (Figure 5 (c)) (the detailed procedure will be described later). If the Fourier amplitude corresponding to a given annual probability of exceedance is plotted as a function of frequency, it is called the “uniform hazard Fourier spectrum” (Figure 5 (d)). Finally, if the uniform hazard Fourier spectrum is transformed back into the time domain, it will give the ground motion time history corresponding to the annual probability of exceedance p_0 (Figure 5 (e)). For this transformation, the Fourier phase of a record at the site of interest can be used. (622c)

4.2.1.2 Evaluation of Site Amplification Factor

In this article, the amplification of Fourier amplitude spectrum caused by the sediment is called “the site amplification factor”. The evaluation of the site amplification factor is crucial in the present PSHA. It is recommended to evaluate the site amplification factor based on the seismograms obtained at the site of interest. The detailed procedure to evaluate the site amplification factor based on the seismograms is described in 4.2.2).

4.2.1.3 Earthquake scenarios and probability of occurrence

Two kinds of scenario earthquake are considered. One is the scenario earthquakes randomly distributed around the site (background earthquakes) and the other is the scenario earthquakes that are related to particular faults such as active faults or plate boundaries. For the former type of the earthquakes, a domain is assumed in which the seismicity is uniform. It is often assumed that sufficiently large earthquakes can be attributed to known faults and background earthquakes have smaller magnitudes. In the example described later, it is assumed that background earthquakes have JMA (Japan Meteorological Agency) magnitudes less than 7.

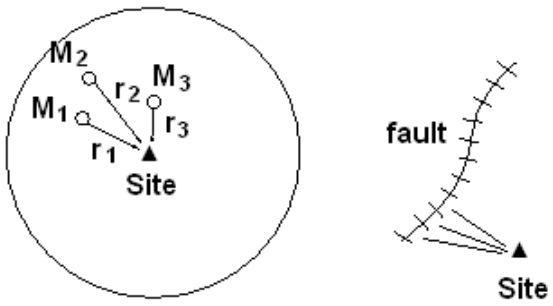

Figure 6 — Scenario earthquakes randomly distributed around the site (background earthquakes; left) and those related to particular faults (right)

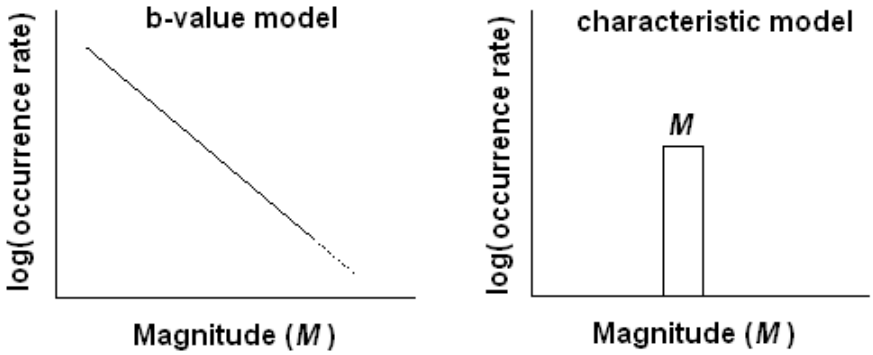

Figure 7 — Probability models for background earthquakes (left) and those for the earthquakes related to particular faults (right)

For both type of earthquakes, the annual probability of occurrence should be specified. For the background earthquakes, the earthquake catalogues are used to evaluate the annual probability of occurrence as a function of earthquake magnitude. First, the relation between the earthquake magnitude (M) and the occurrence rate of the earthquakes (N) above the magnitude is modelled as

$$\text{Log}(N) = a - bM \tag{6}$$

The model is called the “b-value model”. Taking the derivative of both sides of the equation (6), it can be shown that the logarithm of the occurrence rate of the earthquakes in the range (M, M+dM) is also linearly related to the earthquake magnitude. This relation is shown in Figure 7 (left). The parameters a and b should be determined based on the earthquake catalogue in the region. The annual probability of occurrence of the earthquakes can be determined to be consistent with the occurrence rate.

For the scenario earthquakes related to active faults, the earthquake magnitude and the annual probability of occurrence can be specified based on geological and geomorphological information. The earthquake

magnitude is typically evaluated based on the length of the fault. The annual probability of the earthquake is typically evaluated based on the length of the fault and the slip rate of the fault. For the scenario earthquake related to plate boundaries, the earthquake magnitude and the annual probability of occurrence can be evaluated based on the information on historical earthquakes.

In general, time-dependent annual probability can be incorporated in the analysis. In the example described later, time-independent annual probability is considered for simplicity, *i.e.*, the occurrence of earthquakes is assumed to be a Poisson process.

4.2.1.4 Evaluation of Fourier amplitude spectra

For each earthquake scenario, the Fourier amplitude spectrum (either at the outcrop of a firm ground or at the ground surface) at the site of interest should be evaluated, taking into account the source effect, the path effect and the site effect (Figure5(b)). (623B)

For the background earthquakes, the Fourier amplitude spectrum can be obtained as the source spectrum multiplied by the path effect and the site amplification factor. As for the site amplification factor, refer to 1)-2.

The source spectrum can be assumed to follow the ω^{-2} model (Aki, 1967). According to the ω^{-2} model, the acceleration Fourier amplitude spectrum of a seismic wave radiated from a fault (source spectrum) can be expressed as follows.

$$S(f) = C\frac{M_0}{4\pi\rho V_S^3}\frac{(2\pi f)^2}{1+(f/f_c)^2} \tag{7}$$

Where

M_0: seismic moment,

f_c: corner frequency,

ρ: density in the bedrock,

V_s: shear wave velocity in the bedrock,

C: constant.

The seismic moment is defined as follows (Aki, 1966)

$$M_0 = \mu A D_0 \tag{8}$$

Where

μ: rigidity in the bedrock,

A: area of the fault,

D_0: slip on the fault.

The constant C is the product of the radiation coefficient (in the example shown below, 0.63 is used as an averaged value), the amplification due to free surface (=2) and the coefficient representing the partition of seismic energy into two horizontal components (in the example shown below, 0.71 is used based on the assumption that the energy is equally partitioned into two horizontal components). Figure 8 shows the displacement, velocity and acceleration source spectra following the ω^{-2} model.

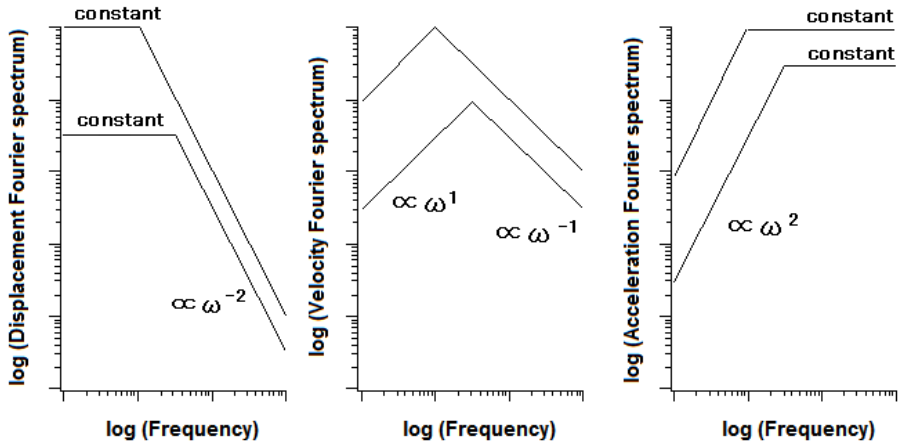

Figure 8 — Source spectra which follow the ω^{-2} model

As for the path effect, it is a common practice to take into account both the geometrical spreading and the inelastic damping as follows:

$$P(f) = \frac{1}{r}\exp(-\pi f r / Q V_S) \tag{9}$$

Where

r: hypocentral distance,

Q: Q value along the propagation path.

For the earthquakes related to particular faults, it is preferable to consider fault finiteness to estimate the Fourier amplitude spectrum at the site. This can be achieved by introducing a fault model and applying the semi empirical approach. In the semi empirical approach, a Green's function (a ground motion from a small earthquake) should be prepared, taking into account the source, path and site effects, and then superposed according to the fault model. In this process, again, the site amplification factor evaluated in 1)-2 is utilized. Details of the semi empirical approach can be found in Subclause 4.2.2). As for the Fourier phase of the Green's function, the Fourier phase of a record from a small to medium-sized earthquake at the site of interest can be used, based on the assumption that the rupture process does not have significant effects on the Fourier phase for a small to medium-sized earthquake. Although the Fourier phase of the Green's function does not have any effect on the Fourier amplitude of the calculated ground motion, it will be used to determine the Fourier phase of the calculated ground motion, which will be useful for the generation of the ground motion time history corresponding to a given annual probability of exceedance at the final step.

4.2.1.5 Evaluation of uniform hazard Fourier spectrum

Now we have evaluated the Fourier amplitude spectra for n scenario earthquakes and the relevant annual probability of occurrence. Let us consider one particular frequency for a while. Let n' (<n) denote the number of scenarios for which the Fourier spectrum at the frequency exceeds a given value x. If we sum up the annual probability of occurrence for the n' scenarios, then it will give the annual probability that the site experiences a Fourier spectrum exceeding x at the frequency. This is called the "annual probability of exceedance" and denoted here as p (x). If p (x) is plotted against x, it is called the "hazard curve" (Figure 5(c)). Then, let us find x corresponding to a given annual probability of exceedance p_0 and denote it by x_0. If we plot x_0 as a function of frequency, it is called the "uniform hazard Fourier spectrum" (Figure 5(d)). (623B)

4.2.1.6 Evaluation of ground motion time history

If the uniform hazard Fourier spectrum is transformed back into the time domain, it will give the ground motion time history corresponding to the given annual probability of exceedance p_0 (Figure 5(e)). This transformation can be achieved simply by applying an appropriate Fourier phase. To determine the Fourier phase, it is recommended to carry out the disaggregation of hazard (Bazzurro and Cornell, 1999), that is, to determine the most dominant earthquake scenario at a given level of Fourier amplitude. This process is illustrated in Figure 9 In general, the total annual probability of exceedance corresponding to a given level of Fourier amplitude is the sum of the contributions from several scenarios as shown in Figure 9 In the disaggregation, the scenario with the largest contribution is selected. The selected scenario may be dependent on the frequency. So far, it is recommended to consider the frequency range which is most important for the design of geotechnical works. For the inverse Fourier transform, the Fourier phase of the ground motion from the most dominant scenario can be used. If a scenario earthquake from a fault is most dominant, the Fourier phase of the ground motion from the fault predicted by the semi-empirical method can be used. If background earthquakes are most dominant, the Fourier phase of a record from a small to medium-sized earthquake at the site of interest can be used for the inverse Fourier transformation, based on the assumption that the rupture process does not have significant effects on the Fourier phase because of the relatively small size of the earthquake. (623B)

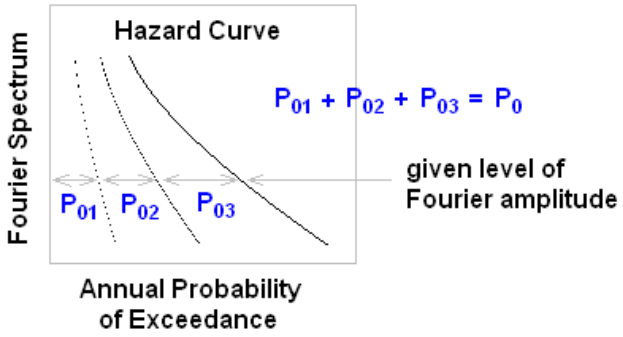

Figure 9 — Source spectra which follow the ω^{-2} model

4.2.1.7 Example of application

In this section, an example of the application of the present PSHA (NAGAO et al., 2005) is described. The analysis is applied to Kanto region, Japan. The targeted area is shown in Figure 10 Mesh A includes the Port of Tokyo. Mesh B includes Miura Peninsula. In this example, the site amplification factor for each mesh was evaluated as an average for several strong motion stations included in the mesh for demonstrating purpose. In practice, the site amplification factors should be evaluated based on the seismograms obtained at the site of interest. The evaluated site amplification factors are shown in Figure 11. These site amplification factors were evaluated at the outcrop of a firm ground. The site amplification factor for Mesh A is characterized by a relatively large amplification at lower frequencies. This is due to the thick sediments in the Kanto basin. The site amplification factor for Mesh B is relatively small for lower frequencies because Mesh B mainly covers the Miura Peninsula, which is outside the Kanto basin.

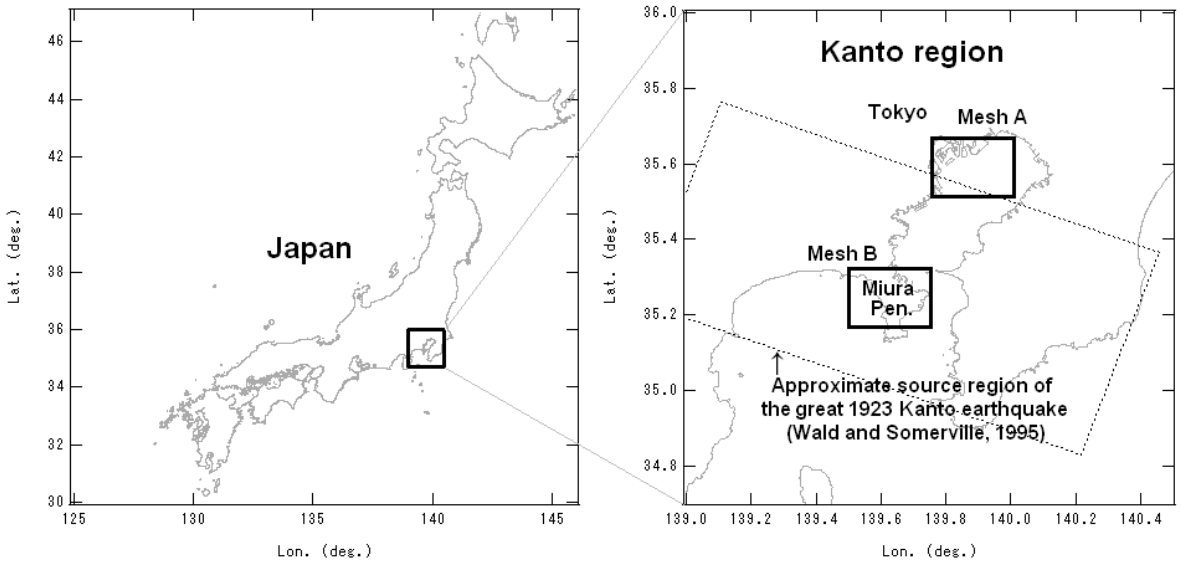

Figure 10 — Targeted area

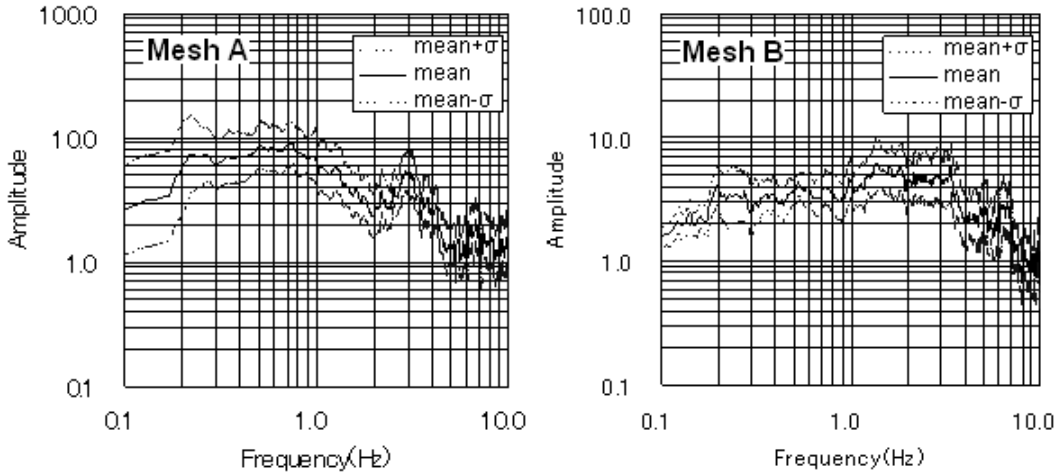

Figure 11 — Site amplification factors evaluated for Mesh A (left) and Mesh B (right)

As for the background earthquakes, two domains were considered. One domain is within 100km from the mesh (more strictly, from the center of the mesh) and 3-20 km deep. The other domain is within 100km from the mesh and 20-60 km deep. The seismicity was assumed to be uniform within the domains. The parameters for the b-value model were determined based on relevant earthquake catalogues. For these earthquakes, the seismic moments and the corner frequencies were estimated based on empirical relations (NAGAO *et al.*, 2005). The Fourier amplitude spectra at the sites for these earthquakes were calculated as a product of the source, path and site effects.

As for the earthquakes related to known faults, two kinds of earthquake were considered. One is the recurrence of the 1923 Kanto earthquake, which is a huge subduction earthquake and the other is the earthquake from active faults. For these earthquakes, fault models were introduced and the ground motions at the sites were calculated using the semi empirical method.

Approximate source region of the 1923 Kanto earthquake (Wald and Somerville, 1995) is shown in Figure 10 Source parameters shown in Table 1 (NAGAO *et al.*, 2005) were used to account for the recurrence of this earthquake. Based on the results of the waveform inversion, (Wald and Somerville, 1995), two asperities (relatively small regions on the fault where the slip and the slip velocity are especially large) were considered.

The locations of the asperities were determined based on the inversion results. The rupture starting point was randomly distributed along the bottom of the asperities.

Table 1 — Source parameters for the recurrence of the 1923 Kanto earthquake

Total area	9100km^2
Strike	290°
Dip	25°
Total moment	1.07×10^{21} Nm
Average slip	3.56m
Average stress drop	3.0MPa
Area of asperity	2002 km^2 (22%)
Average slip on asperity	7.12m
Return period	162 years
Annual probability of occurrence	6.17×10^{-3}

Figure 12 — Active faults considered for the example hazard calculation

As for the earthquakes from active faults, 21 active faults within 100 km from the site were considered as shown in Figure 12. The earthquake magnitudes were evaluated based on the length of the fault. The annual probability of each earthquake was evaluated based on the length of the fault and the slip rate of the fault. The annual probability ranged from 4.34×10^{-6} to 3.15×10^{-3}.

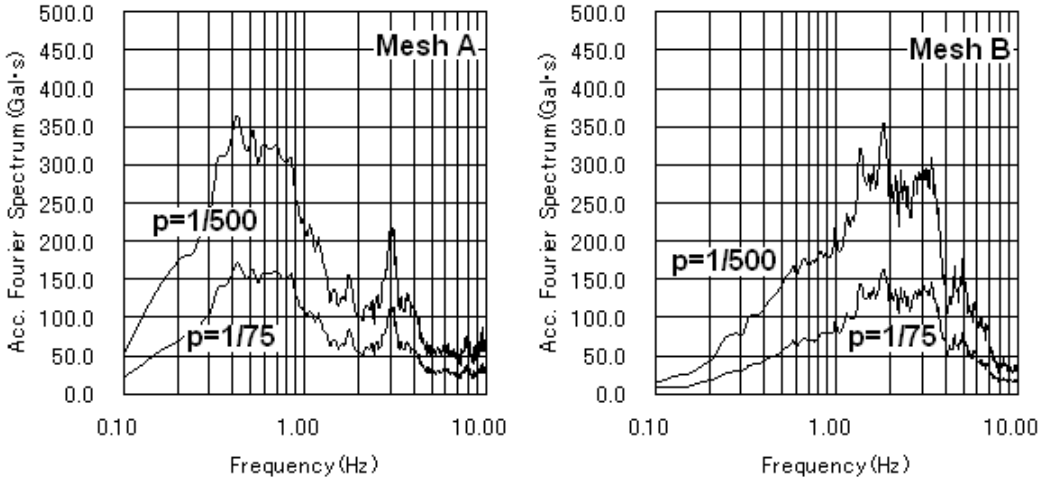

Figure 13 — Uniform hazard spectra for Mesh A (left) and Mesh B (right)

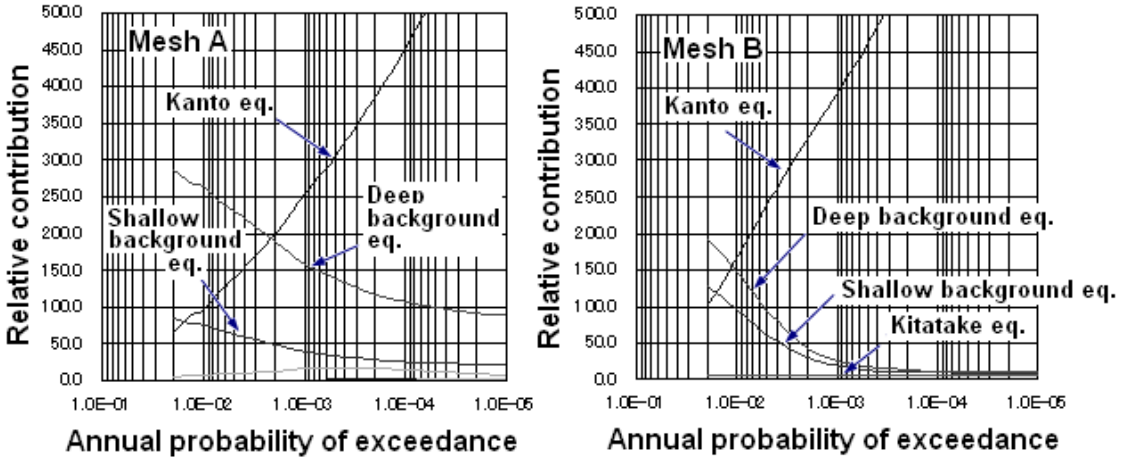

Figure 14 — Relative contributions from the scenarios for Mesh A (left) and Mesh B (right)

Uniform hazard spectra evaluated for Mesh A and Mesh B for the annual probability of exceedance of 1/75 and 1/500 are shown in Figure 13. These spectra were evaluated at the outcrop of a firm ground. For Mesh A, frequency components around 0.3-0.9 Hz are predominant. For Mesh B, frequency components around 1.0-4.0 Hz are predominant. These characteristics are consistent with the gross characteristics of the subsurface structure.

Relative contributions from the scenarios for Mesh A (left) and Mesh B (right) as functions of the annual probability of exceedance are shown in Figure 14. At the annual probability of 1/75, the contribution from the deep background earthquakes is dominant at both Mesh A and Mesh B. At the annual probability of 1/500, the contribution from the recurrence of the Kanto earthquake is dominant at both Mesh A and Mesh B. These results were used to determine the Fourier phase to obtain ground motion time histories.

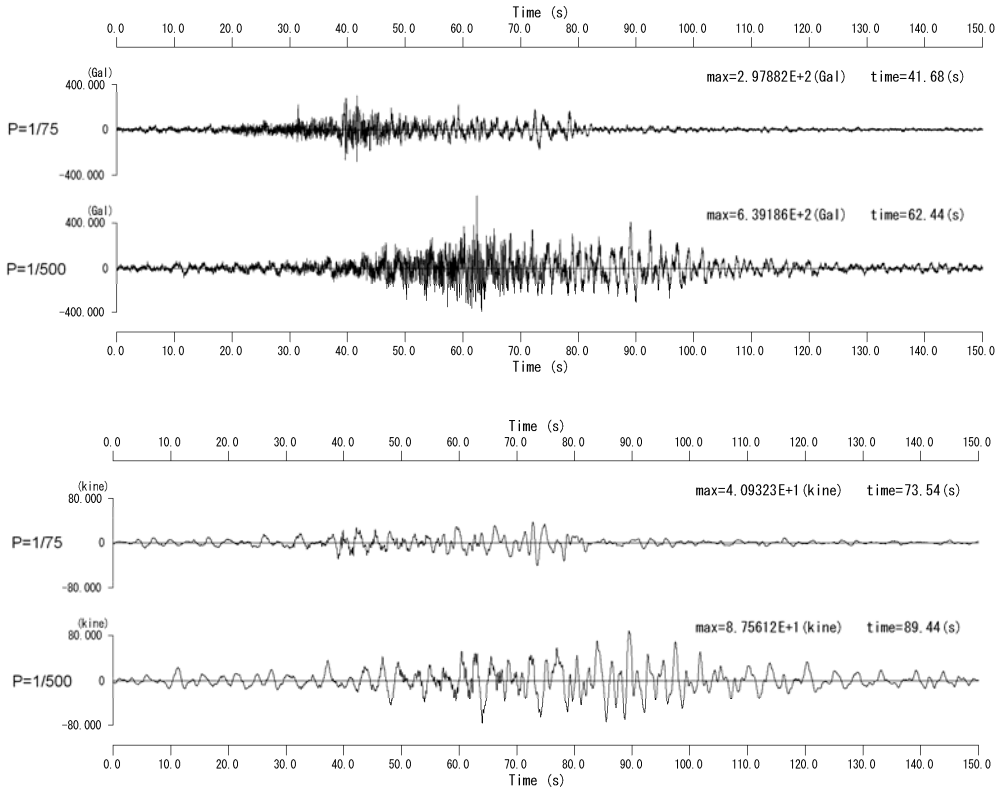

Figure 15 — Acceleration (top) and velocity (bottom) time history for Mesh A

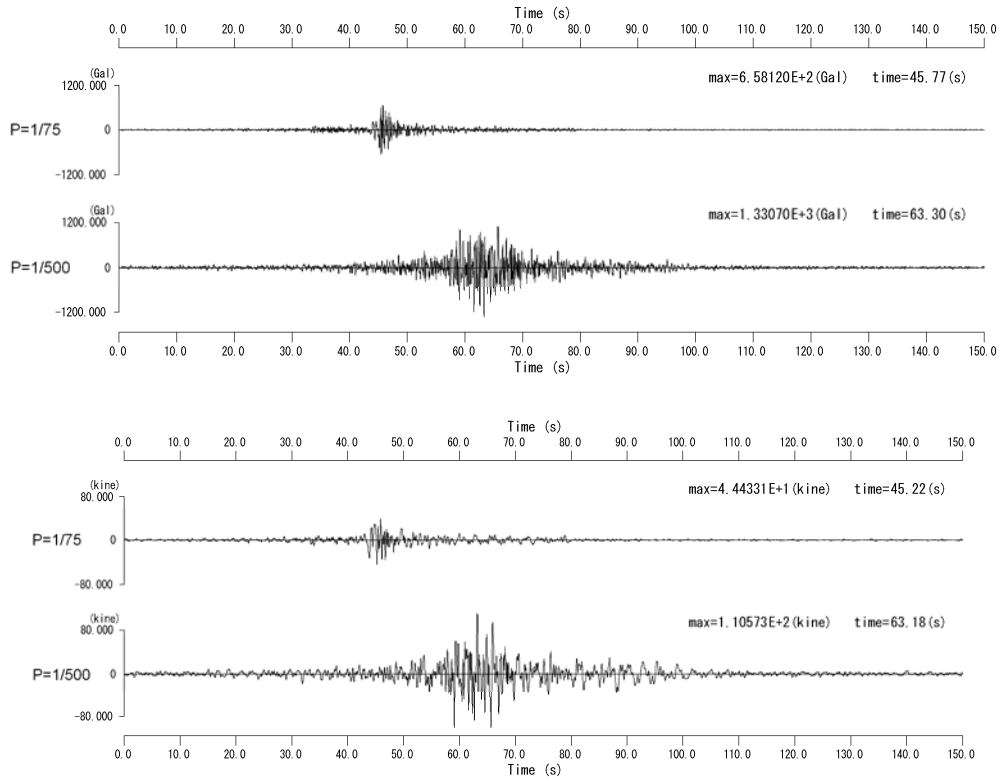

Figure 16 — Acceleration (top) and velocity (bottom) time history for Mesh B

Acceleration and velocity time histories corresponding to the annual probability of exceedance of 1/75 and 1/500 for Mesh A and Mesh B are shown in Figure 15 and Figure 16, respectively. These time histories were evaluated at the outcrop of a firm ground. The time histories for Mesh A are characterized by the predominance later phases, which can be attributed to the sediments in the Kanto basin. The ground motions for the annual probability of 1/500 have longer duration than those for the annual probability of 1/75 because, at the annual probability of 1/500, the contribution from the Kanto earthquake becomes predominant and the phase characteristics is affected by the rupture process of the Kanto earthquake. Thus, the phase characteristics of an earthquake ground motion are affected both by the source effect and the site effect. The present probabilistic seismic hazard analysis can incorporate both of these effects.

4.2.2 Site-specific approach on earthquake motions probabilistically evaluated in a LNG tank design considering a specific active fault

4.2.2.1 General procedure and design example

Guideline for Performance-Based Structural Evaluation for LNG Underground Tank was issued by Committee on Civil Engineering in Energy and Power Industries in Japan Society of Civil Engineers in 1999. The outline to evaluate the reference earthquake motion shown in the Guideline for using not only a probabilistic approach but also the combined method of the deterministic approach with probabilistic approach is described. By considering the required seismic performance for LNG underground tank, two or more levels of the earthquake ground motion are determined. First, the earthquake ground motion which occurs either once or twice during the service period is defined as Level 1 Earthquake Ground Motion. (513A)

The strongest earthquake ground motion among the realistic motion whose occurrence possibility at the object site during the service period is small is defined as Level 2 Earthquake Ground Motion. Moreover, the earthquake ground motion is specified for a few levels if necessary. As an example, the level of the motion is defined as Level 2L in case that a probability of occurrence during the service period is relatively low. The level of the motion is defined as Level 2H in case that probability of occurrence during the service period is extremely low. The design earthquake ground motion is defined at the engineering bedrock. The variable of the motion is specified as the acceleration response spectrum. The time history is evaluated by simulated earthquake motion consistent with the response spectrum. Here, Level 1 Earthquake Ground Motion is defined based on probability of occurrence in the service period. Moreover, Level 2 Earthquake Ground Motion is defined as the evaluated result at the object site to specify the scenario earthquake with the possibility generating strong earthquake ground motion by considering the occurrence probability in the service period. As the method to evaluate Level 1 and Level 2 Earthquake Ground Motions, probabilistic approach and deterministic approach are adopted.

Procedure to evaluate design earthquake ground motion described in the guideline is shown in Figure 17. In this procedure, both probabilistic approach and deterministic approach are required. Furthermore, the observed seismic record around the object site is requested to be used effectively.

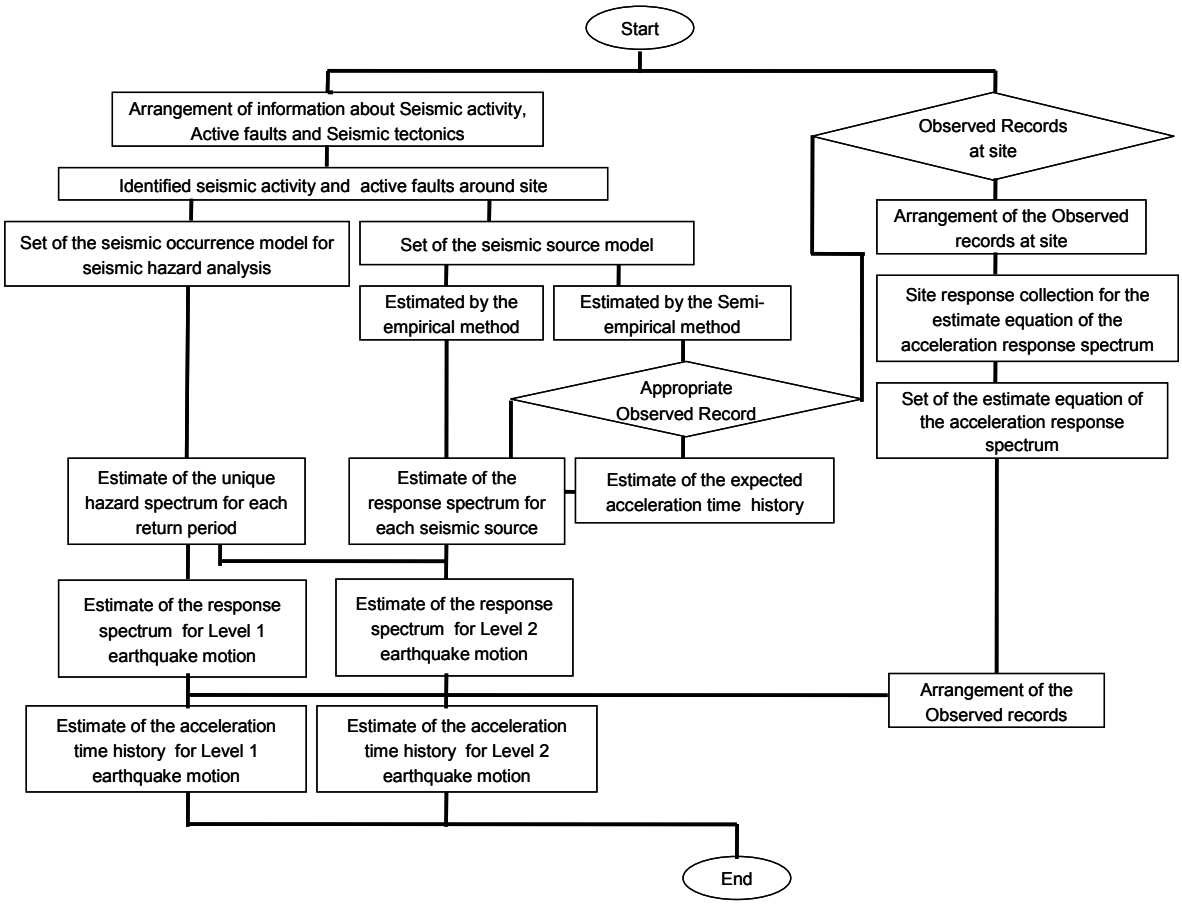

Figure 17 — Procedure of evaluating design earthquake ground motion as per LNG Design Code

In order to evaluate Level 1 earthquake motion by probabilistic approach, the occurrence probability for the service period has to be specified. As an example, 80% probability of occurrence in a 50-year period (corresponding to 31 -year return period), or 50% probability of occurrence in a 50-year period (corresponding to 71-year return period) is used. The uniform hazard spectrum of 80% probability of occurrence in a 50-year period is shown in Figure 18 as an example of Level 1 Earthquake Ground Motion (F site at Tokyo Bay). The maximal acceleration is about 150 m/s^2

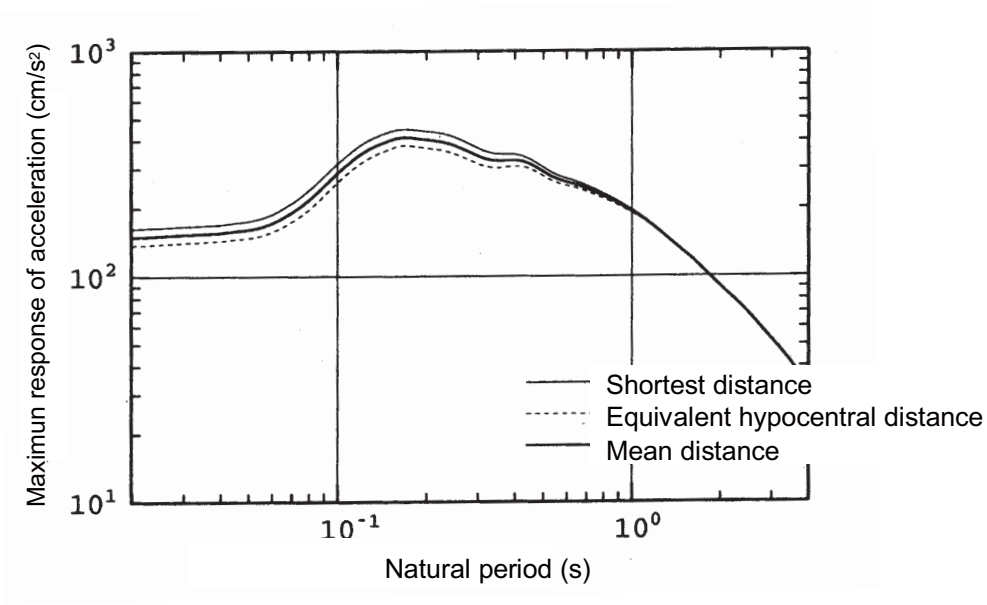

Figure 18 — Uniform hazard acceleration response spectrum for the occurrence probability 80% in 50 years

The scenario earthquake has to be modelled to evaluate Level 2 Earthquake Ground Motion as the deterministic approach. When the South Kanto Earthquake (the magnitude by Japan Meteorological Agency magnitude is 7.9) is taken into account as the scenario earthquake, the projection of the fault plane onto the ground surface is shown in Figure 19.

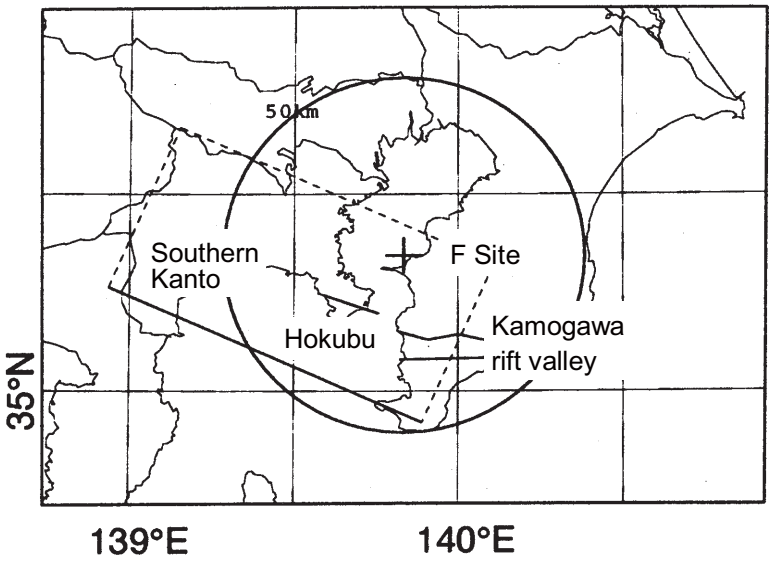

Figure 19 — Projection of the fault plane to the ground surface of the scenario earthquake

The acceleration response spectrum evaluated by not only attenuation equation method but also stochastic Green's function method are shown in Figure 20.

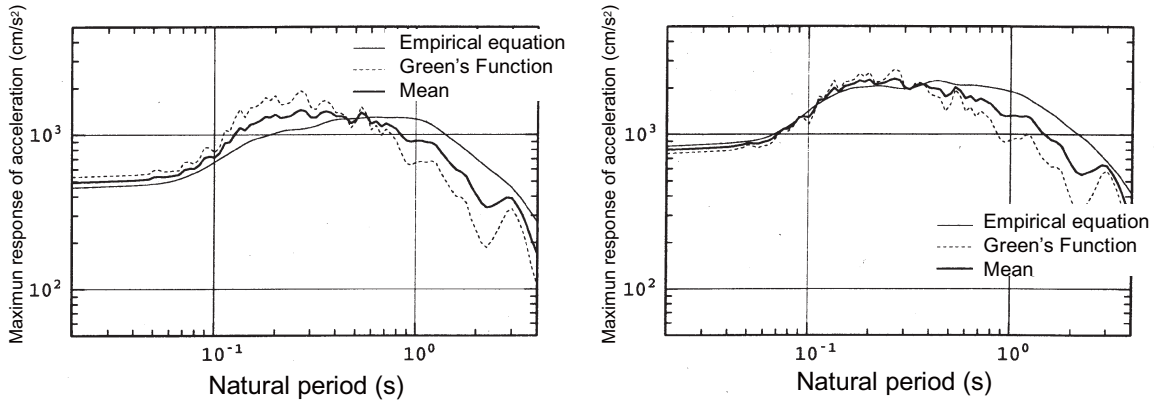

Figure 20 — Acceleration response spectrum evaluated by not only the attenuation equation but also stochastic green function method

Considering the probabilistic approach described later, the response spectrum for Level 2L, and Level 2H Earthquake Ground Motion are shown in Figure 21. Level 2L Earthquake Ground Motion is evaluated based on average Spectrum for scenario earthquake. Level 2H Earthquake Ground Motion is evaluated based on average plus standard deviation ($\mu+\sigma$) for scenario earthquake. As for the referred uniform hazard spectrum for Level 2L, and 2H Earthquake Ground Motions, probabilities of occurrence in a 50-year period are from 30% to 15% and from 15% to 5% respectively. The maximal acceleration of Level 2L Earthquake Ground Motion is evaluated as about 4.5 m/s^2 and the maximal acceleration of Level 2H Earthquake Ground Motion is evaluated as about 7.2 m/s^2.

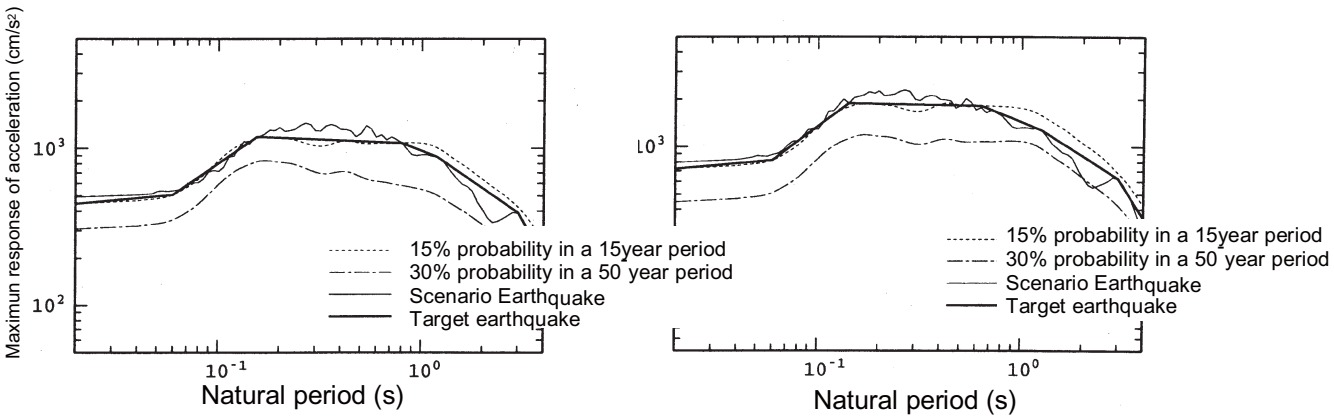

Figure 21 — Response spectrum for Level 2L, and Level 2H earthquake motion

4.2.3 Deterministic approach - Theoretical ground motion estimation based on hypothetical scenario earthquakes

4.2.3.1 Methodology for theoretical ground motion estimation

It is better to use observed ground motion information for estimating strong ground motion. However, it is rare case that we have some records with enough information at the target site. Especially for the shake map project, it is difficult to have plane information from observation records. To solve this problem, we need to assume sedimentary structure model of target area and theoretically simulate ground motions from the source fault to the target sites.

Two-stage calculation technique is popular for the theoretical simulation. First, ground motion is simulated on the engineering bedrock on which we do not need to care about non-linear site response. And next, surface ground motion is evaluated considering non-linear site response.

Evaluating ground motion at the engineering bedrock, it is ideal if we can make minute model of seismogenic zone and sedimentary structure and calculate seismic wave propagation caused by fault rupture process. However, popular methods we use for simulating wave propagation; i.e. 3-D finite difference method (GRAVES, 1996; PITARKA, 1999), require a grid model as shown in Figure 22. The methods have limitation because of finiteness of model possible and capacity of computer. At present, limitation of model is about several dozen meters. It defines limitation of shortest period to calculate around 0.5 to 2 second, depending minimum shear wave velocity of the model. Accordingly, we have to employ stochastic Green's function method introduced in section 1) for short period ground motion estimation. Stochastic Green's function methods with theoretical site response are proposed (ONISHI and HORIKE, 2000; KAGAWA, 2004) that calculate site amplification from sedimentary structure model assumed at sites. The methods are frequently used for shake map project and ground motion simulation without observed records. Main disadvantage of Stochastic Green's function method with theoretical site response is accuracy in long period range. First, the method does not treat surface wave generation and propagation because it does not consider irregular boundaries of sedimentary layers. And it does not take account of near and intermediate terms of ground motion.

To overcome the disadvantage, a hybrid method is popularly employed. The hybrid method uses a 3-D FE method for a longer period range and a stochastic Green's function method for a shorter period range. The hybrid addition is a sum of both two results weighted with the amplitude of a high-pass or a low-pass filter for each frequency. The amplitudes of the two filters are complementary for each other in order to keep the sum of the two values a unity. The filters are called 'a pair of matching filters'. It is preferable to set the central frequency of the transition zone of the matching filter, which is considered to be a boundary between deterministically and stochastically characterized ranges of frequency in terms of seismic ground motion. However, the boundary frequency is currently popular to be set approximately 1 Hz, slightly lower than the transition zone.

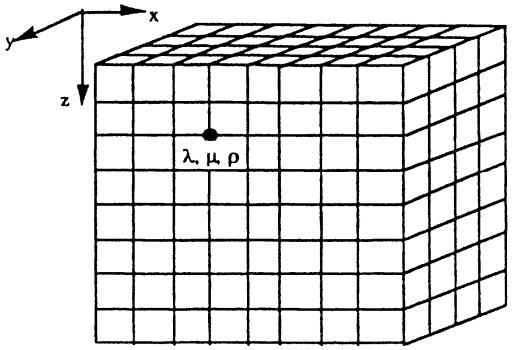

Figure 22 — Image of 3-D finite difference method

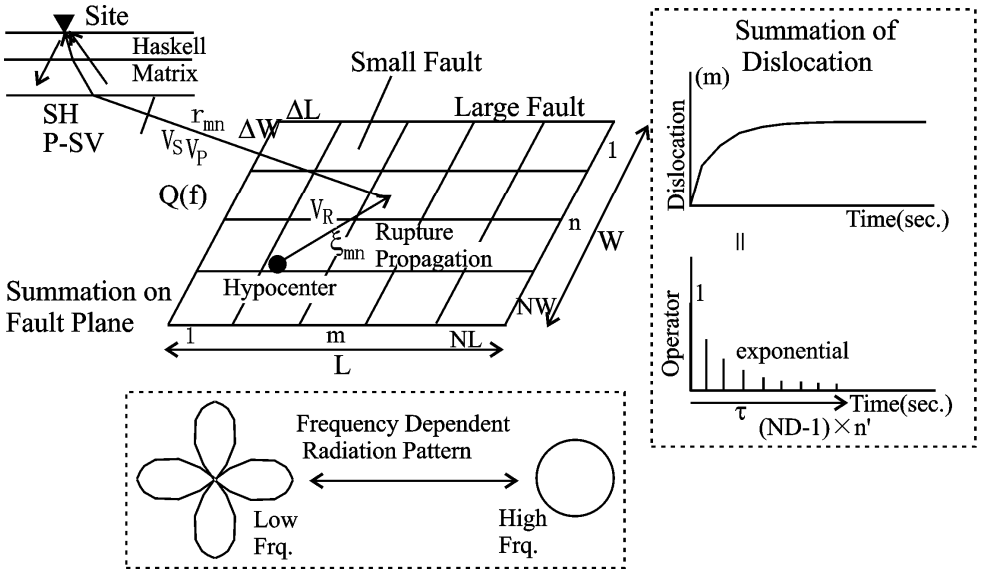

Figure 23 — Explanatory diagram of stochastic Green's function method with theoretical site response

4.2.3.2 Recipe for strong ground motion estimation

It is difficult to predict complicated fault rupture process of hypothetical earthquake. However, we are on the road to understanding the general characteristics of fault rupture process from statistical analyses of past earthquakes. Modelling asperities is a problem in progress. An asperity is the area where tectonic stresses accumulate and then they are released by strong seismic wave radiation through a fault slip dislocation in an earthquake event. It takes important role on generating strong ground motions. Using the information from the analyses, a recipe for strong ground motion estimation is proposed (IRIKURA and MIYAKE, 2001; IRIKURA et al., 2004). The recipe provides average feature of fault rupture and its parameters with their variation. Characteristic Source Model, the model of an entire fault plane and asperities in the plane as rectangular-shape areas, is employed in the recipe. On the other hand, Stochastic Source Model is popular in the world. The model has slip distributions as complicated as analysed source slip of real earthquakes. In Japan, Characteristic Source Model is popular because the model is more convenient for assuming a rupture scenario of a future earthquake than a complicated source model. Especially it works well in associating asperities with large deformation areas along the target active fault and setting worst scenario to the site considering forward directivity or focusing effect. (621C, 622a, 622b, 622A)

It is confirmed that the dominant feature of observed ground motions are simulated by Characteristic Source Model as well as the original complex slip model due to the real earthquake. The recipe for a general crustal earthquake (IRIKURA et al., 2004) is explained as follows:

Step 1: Fault Rupture Area (S = LW)

Fault length, L is assumed as the first variable of a target earthquake. Fault width, W is secondly assumed considering the maximum width defined by thickness of seismogenic zone and a dip angle. Eventually, fault rupture area, S is calculated by the production of L and W.

Step 2: Seismic Moment (M_0)

Seismic moment, M_0 is determined from fault rupture area, S using the following three-stage scaling laws.

$$S\ (km^2) = 2.23 \times 10^{-15} \times M_0^{2/3} \text{ for } M_0 < 7.5 \times 10^{25} \text{ dyne*cm: Self Similar} \quad (10)$$

$$S\ (km^2) = 4.59 \times 10^{-11} \times M_0^{1/2} \text{ for } M_0 >= 7.5 \times 10^{25} \text{ dyne*cm: Width W saturates.} \quad (11)$$

$$S\ (km^2) = 5.30 \times 10^{-25} \times M_0 \text{ for } M_0 >= 7.5 \times 10^{27} \text{ dyne*cm: Slip D Saturates.} \quad (12)$$

Step 3: Average Stress Drop ($\Delta\sigma_c$)

The value is evaluated from the crack theory (Eshelby, 1957).

$$\Delta\sigma_c = \frac{7\pi^{1.5}}{16}\frac{M_0}{S^{1.5}} \tag{13}$$

Step 4: Combined Area of Asperities (S_a)

An empirical relationship between seismic moment, M_0 and combined area of asperities, S_a (Somerville et al., 1999; IRIKURA and MIYAKE, 2001) are used. Average ratio of S_a to M_0 is approximately 0.22.

$$S_a = 0.22M_0 \tag{14}$$

Step 5: Stress Drop in Asperity ($\Delta\sigma_a$)

The value is evaluated by multiplying average stress drop, $\Delta\sigma_c$ and inverse number of area ratio derived in Step 4. The treatment is based on the asperity theory. The process introducing short-period level (Dan et al., 2001) is also used for evaluating stress drop in asperity. In the case, area ratio changes from the value 0.22 to satisfy the relationship mentioned in Step 4.

Step 6: Number of asperities (N) and their location

Number of asperities depends on the number of fault segmentation. The location of the asperities is set where accumulated surface deformation is large. The location of asperities due to late events might be an example, if the recurrence period of the target earthquake is short enough. We expect back-slip monitoring by GPS network for this purpose.

Step 7: Average Slip Ratio in Asperity (D_a)

Average slip ratio in asperity against average slip over the fault is evaluated considering the number of asperities assumed in Step 6. According to dynamic fault rupture simulations, the ratio tends to decrease with the number of asperities. Average value 2.0 is generally used. The value corresponds to the case of two asperities from statistical analysis.

Step 8: Effective Stresses in Asperity *($\Delta\sigma_a$)* and Background *($\Delta\sigma_b$)*

Effective stresses in asperity approaches to stress drop in asperity, Step 5. Effective stress in background slip is assumed about one fifth of the effective stresses in asperity from dynamic fault rupture simulations.

Step 9: Slip Velocity Function

Kostrov-type slip velocity function is generally employed. Maximum slip velocity is assumed from effective stresses. Slip duration is estimated from asperity size and rupture velocity. The results from dynamic fault rupture simulations are also used for the confirmation.

(Other Parameters) Rupture Starting Point

Rupture staring and terminating points are assumed from branching feature of target fault system (NAKATA et al., 1998).

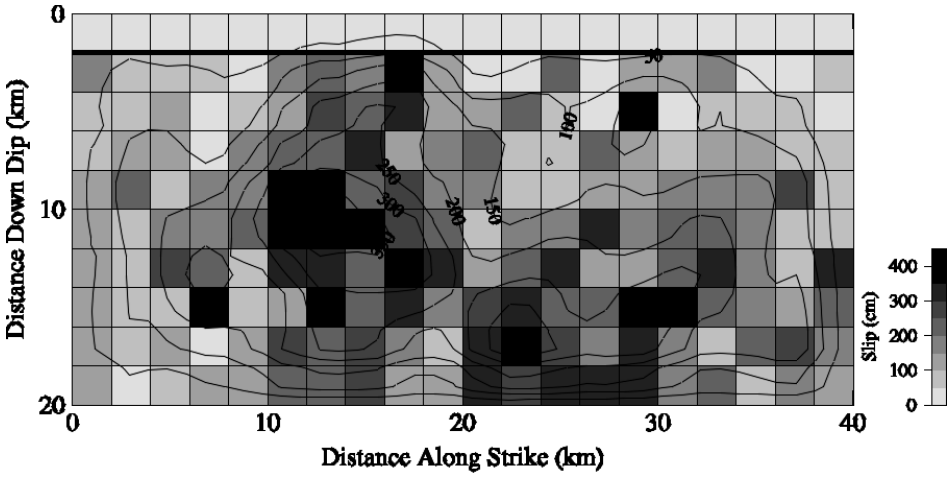

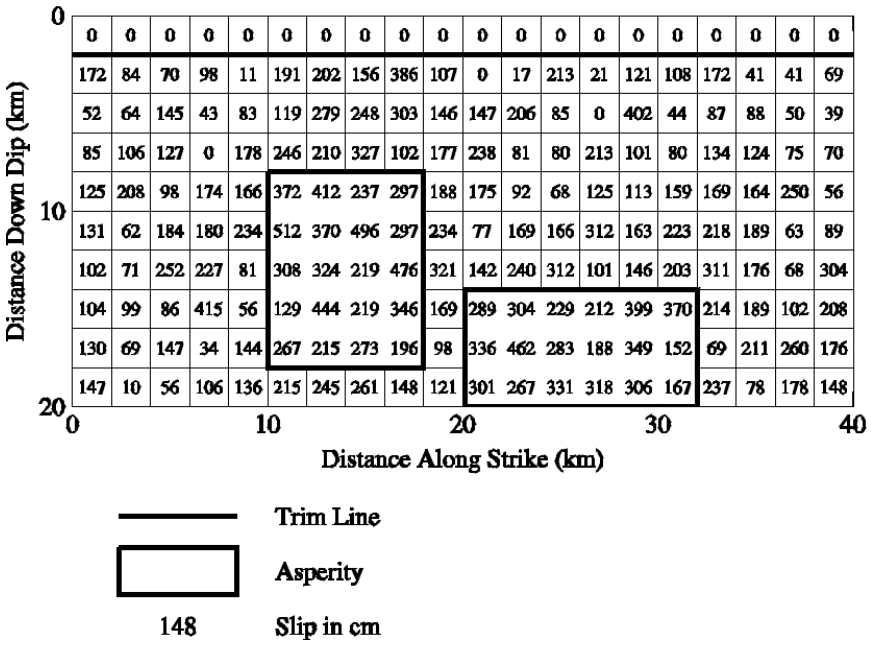

Figure 24 — Extracting a characteristic source model from a complex slip distribution derived from a source inversion analysis

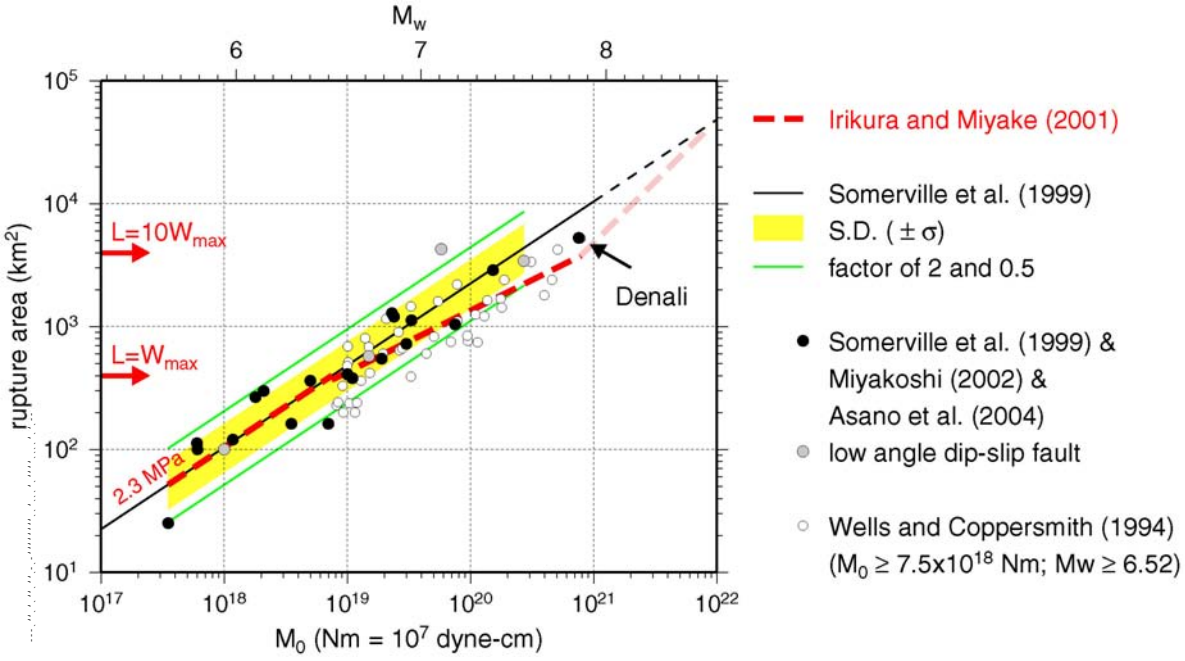

Figure 25 — Three-stage scaling models after IRIKURA et al. (2004)

4.2.3.3 Sedimentary structure model

The accuracy of sedimentary structure model affects much on the simulations of theoretical seismic wave propagation. The structure model is divided into two categories depending op the calculation methods mentioned in 2-1). One is shallow structure from surface to engineering bedrock. And the other is deep structure beneath the engineering bedrock. Physical parameters of body wave velocities, density and attenuation are required for both structure models. Parameters for non-linear site response; i.e. G-γ and h-γ properties are additionally required for shallow structure model. Irregular layered boundary model is required for calculation of 2-D or 3-D wave propagation in the deep structure. (623A, 645A, 645B)

Shallow structure models are constructed from borehole information; i.e. soil tests and logging data. It is desirable to construct a well-arranged database of borehole information gathering high quality borehole information. However, it is difficult to have homogeneous information with necessary quantity and high quality data. Interpolation from given data is generally employed to cover the wide target area supported by mesh information of soil classification and land utilization. In general borehole exploration, PS-logging of seismic waves and soil tests for non-linear site response are rarely conducted. Empirically derived relationships with standard penetration test (N-value) are employed to estimate the parameters above. It is better to use individual relationships derived from local data, however, the relationship of neighbouring area or nation wide standard relation ship is popular in practical case. (631A, 641A)

As for deep structure model, spa well drilling is the quite rare example of deep boreholes. Directly obtained information down to bedrock is lacking. Geophysical explorations are conducted to estimate deep sedimentary structure model. The most convenient technique to survey underground structure in wide area is the method using gravity anomaly, however, accuracy of data decreases in sea area. Density structure is derived from the gravity anomaly survey. Survey technique that gives highest resolution is seismic reflection survey. It uses large artificial seismic source and costs more than other survey techniques. Therefore, the area where seismic reflection surveys were conducted is limited. Another application of artificial seismic source is seismic refraction survey. It can briefly estimate sedimentary boundary structure in wide area. Using the surveys, pressure wave structure is estimated, since the artificial seismic source generally radiates. Shear waves, however, are mainly affected on strong ground motion. Shear wave structure is assumed from microtremor observation. Microtremor consists of surface waves that are sensitive for shear wave structure. (631A, 641B, 645A, 645B)

The physical explorations are not conducted to cover the target area, but the information is along a survey line or at a point. A sedimentary basin model is constructed after interpolating given data. For simulating seismic wave propagation in irregular sedimentary structure, we need model of not only sediments beneath the target site but also basin structure with surrounding mountains. The model shall be confirmed through simulations of observed small earthquake records. The records are published from some organizations at present and we can easily use them.

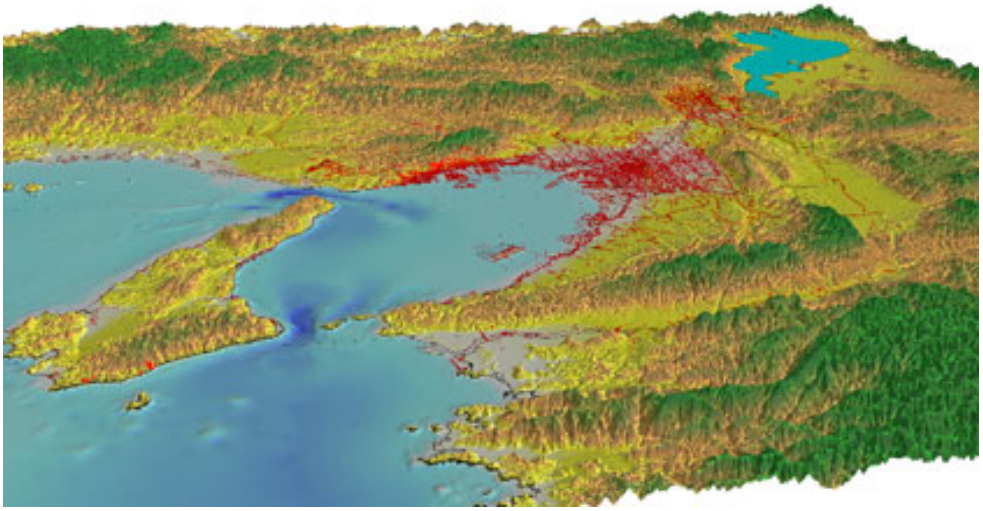

Figure 26 — Distribution of boreholes included in the database of Kansai Geo-informatics Network (2008)

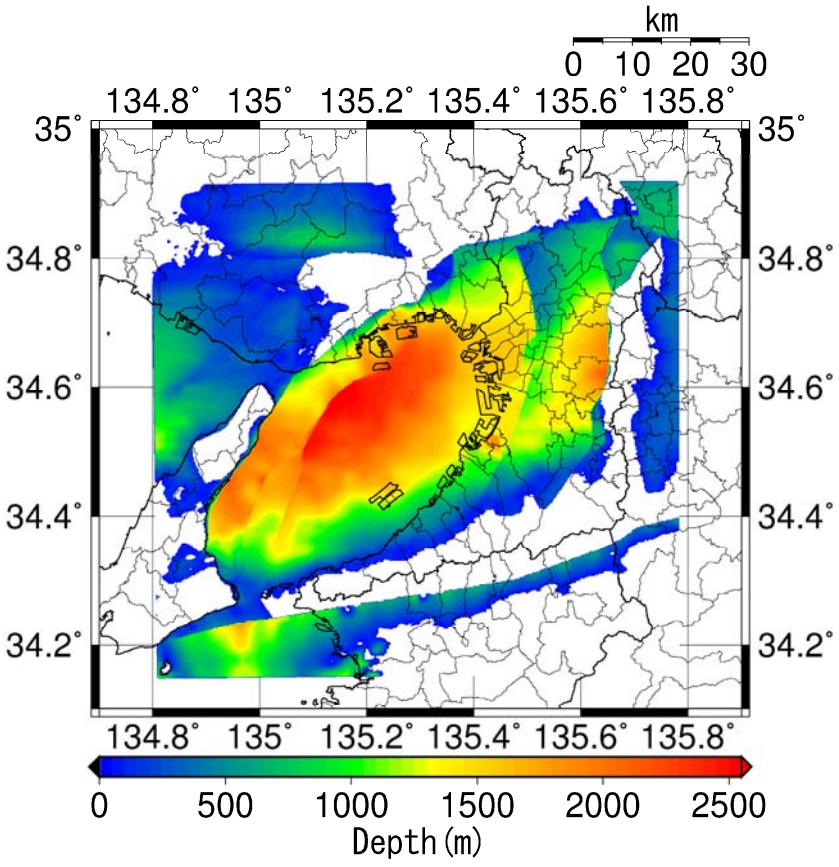

Figure 27 — Sedimentary basin model used in the project of Osaka Prefecture (2007)

4.2.3.4 Examples of strong ground motion estimation

In this section, strong ground motion estimation conducted for earthquake disaster prevention (Osaka Prefecture, 2007; Osaka City, 2007) is shown as an example.

In the Osaka sedimentary basin where Osaka Prefecture and City locate, a lot of geophysical explorations have been conducted for obtaining active fault and sedimentary structure information after the 1995 Hyogo-ken Nanbu (Kobe) earthquake. The Osaka sedimentary basin is the one of world most minutely surveyed area about deep sedimentary structure. Additionally, almost 50,000 high quality borehole data are arranged as a database (Kansai Geo-informatics Network, 2008). Using the basic information, deep and shallow sedimentary structure models are constructed. And the model was verified with ground motion records observed by high quality local network (KAGAWA et al., 2004). It is one of the most suitable areas for applying strong ground motion estimation technique. (631A)

Osaka Prefecture evaluate earthquake hazard in 3 steps (Osaka Prefecture, 2007; Osaka City, 2007). For first step, empirical method, attenuation formula and site amplification from soil classification, is applied for 12 active fault systems in and around Osaka Prefecture. Six fault systems are selected as large impact earthquake sources. Exposure population of high seismic intensity, summation of simulation meshes where JMA intensity is 6 high and larger multiplied by population in the mesh, is considered to choose the target earthquakes. As second step, 73 cases of fault rupture scenario are assumed for the six fault systems. Simulations by stochastic Green's function method are applied for the scenarios. The scenarios are set from engineering request without probability of them that there is no area where estimated ground motion is smaller enough not to consider earthquake disaster prevention. Hybrid simulation technique is applied for step 3. Long period components of five major scenarios of crustal earthquake and one subduction zone earthquake are calculated by 3-D finite difference method. Through the three-step evaluation, earthquake hazards due to the worst scenarios for Osaka Prefecture are estimated and used for disaster evaluation and following disaster mitigation plan. The ground motion waveforms are also used for presuming standard ground motion level for seismic design of public buildings.

The ground motion estimation above is a pioneering approach that provides shake maps and waveforms at where minute sedimentary structure model has been constructed, applying hybrid simulation method and recipe for strong ground motion that are considered to have the highest precision at present stage,.

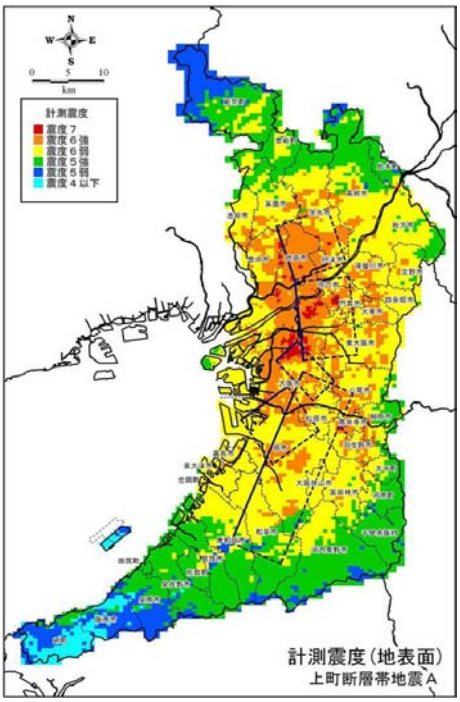

Figure 28 — Distribution of JMA seismic intensity caused by a scenario earthquake, the Uemachi fault A (Osaka Prefecture, 2007)

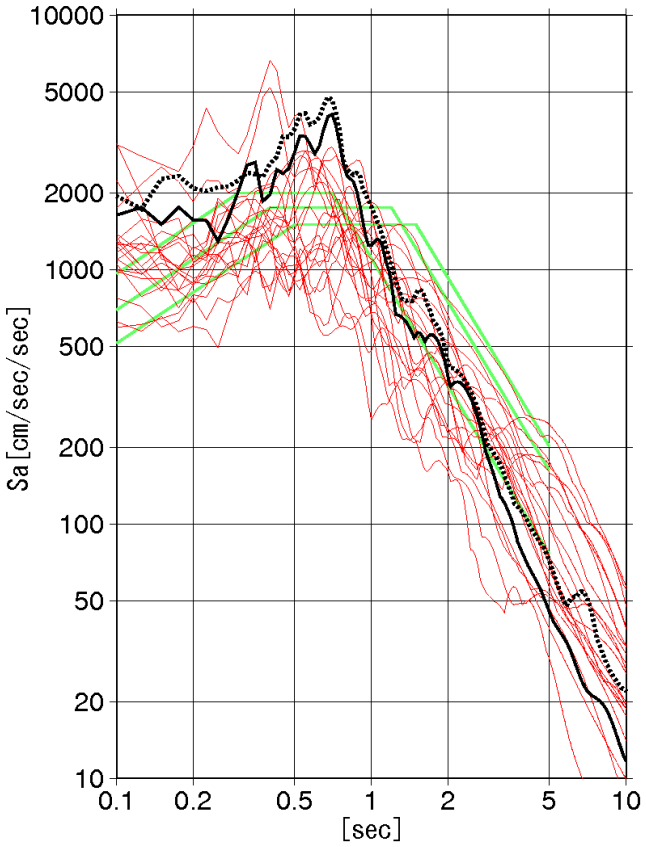

Figure 29 — Example of calculated grand motions in diluvium zones due to the scenario earthquake (Osaka Prefecture, 2007) with observed ground motion at Ojiya site due to the 2004 Chuetsu earthquake.

4.2.4 Deterministic approach - Ground motion estimation based on semi empirical approach

4.2.4.1 Outline

Generally speaking, strong ground motions are determined by three effects, namely, the source effect, the path effect and the site effect as shown in Figure 30 in Subclause 4.2.1 Among these, the site effect can be defined as the influence of sediments on strong ground motions and it includes amplification of body waves, propagation of basin-induced surface waves and so on. The existence of sediments below the site has significant effects on the amplitude, the frequency content and the duration of strong ground motions. Recent development of the nation-wide strong motion networks in Japan has greatly contributed to our understanding of the importance of the site effect. Figure 30 shows a typical example. The left panel of Figure 30 shows the topography around the Port of Sakai, western Japan. Two seismometers, namely, Sakaiminato-G (Strong Motion Earthquake Observation in Japanese Ports) and JMA (the Japan Meteorological Agency) are located in the plains of Yumigahama Peninsula. Other two seismometers, namely, SMN001 of K-NET (Kinoshita, 1998) and SMNH10 of KiK-net (Aoi *et al.*, 2000) are located in mountainous Shimane Peninsula. Observed peak ground velocities during the 2000 Tottori-ken Seibu earthquake (M_J7.3) were approximately four times larger for the plains of Yumigahama Peninsula than for mountainous Shimane Peninsula (Figure 30). Thus, evaluation of the site effect is fundamentally important to predict strong ground motions from future large earthquakes and to determine design ground motions.

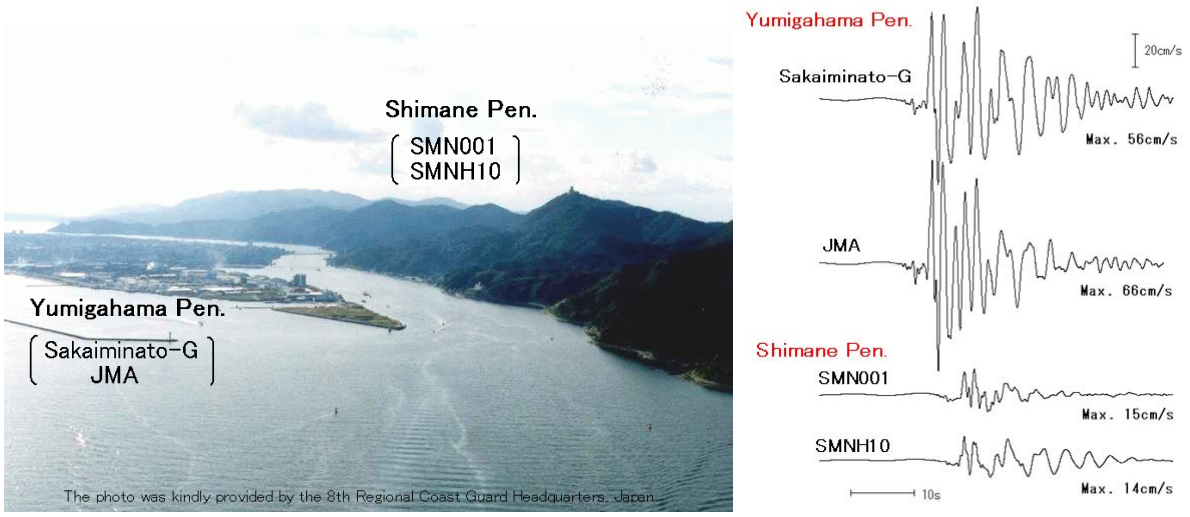

Figure 30 — The topography around the Port of Sakai, western Japan (left) and the velocity waveformsfor the fault-normal component recorded around the port during the 2000 Tottori-ken Seibu earthquake (MJ7.3). The peak ground velocities observed in the plains of Yumigahama Peninsula were approximately four times larger than those observed in mountainous Shimane Peninsula (Nozu et al., 2008).

Figure 31 shows an example of the effect of the sediments on the frequency content of strong ground motions. At Hachinohe Port, both of the Fourier spectra from the 1968 Tokachi-oki earthquake (M_J=7.9) and the 1994 Sanriku Haruka-oki earthquake (M_J=7.5) are characterized by a peak at 2.5 seconds. On the other hand, at Kansai International Airport, both of the Fourier spectra from the 1995 Hyogo-ken Nanbu earthquake (M_J=7.3) and the 2000 Tottori-ken Seibu earthquake (M_J=7.3) are characterized by a peak at 5 seconds. The difference of predominant periods can be attributed to the thickness of sediments down to the bedrock at each observation station.

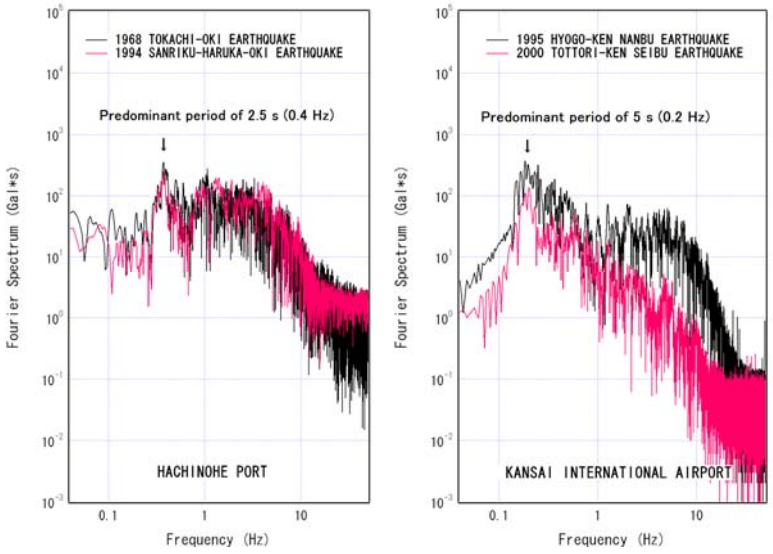

Figure 31 — Fourier spectra of past major strong motion records obtained at Hachinohe Port (NS component) and Kansai International Airport (Runway-normal component)

In principle, there are two ways to evaluate the site effect for the prediction of strong ground motions: one is the numerical evaluation based on the information on subsurface structures and the other is the empirical evaluation based on earthquake observation at the site of interest. The former type of evaluation is suitable for the areas with relatively dense information on subsurface structures, while the latter type of evaluation is

suitable for the areas with relatively high seismicity but relatively sparse information on subsurface structures. The semi-empirical approach to strong motion prediction described in this section is based on the latter type of evaluation of the site effect. Descriptions on the former type of evaluation can be found in Subclause 4.2.3.2. (622A)

The present semi empirical approach begins with the evaluation of the site amplification factors (defined here as the amplification of Fourier amplitude spectrum caused by the sediment) based on the seismograms obtained at the construction site. The approach may include temporary earthquake observations at the construction site. Because the site for the construction of important geotechnical works is often fixed years before its design procedure begins, well-organized design program will allow us to conduct temporary (typically 1-3 years in Japanese practice) observations of earthquake ground motions at the site before the design of geotechnical works. The method for the evaluation of the site amplification factors will be described in Subclause 4.2.4.2. The strong ground motions from future large earthquakes are synthesized, taking into account the rupture process of the earthquakes, together with the effect of sediments both on the Fourier amplitude and the Fourier phase of strong ground motions. The method for the synthesis will be described in Subclause 4.2.4.3. Examples of the application of the synthesis method are presented in Subclause 4.2.4.4., both for a shallow crustal earthquake and a huge subduction earthquake. (622A)

4.2.4.2 Evaluation of site amplification factor

To evaluate site amplification factors from earthquake records, an earthquake observation station sufficiently close to the construction site should be selected. In addition, it is preferable to conduct microtremor observations to make sure that the characteristics of ground motions do not differ significantly between the site of construction and the observation station. If there is no appropriate permanent earthquake observation station, it is recommended to conduct a temporary earthquake observation at the site of construction to evaluate the site amplification factor. The site amplification factor evaluated from a seismogram usually represents the amplification factor from the bedrock to the ground surface because the seismometer is located at the ground surface in many cases. The site amplification factor (from the bedrock to the outcrop of the firm ground) can be obtained by dividing the site amplification factor (from the bedrock to the ground surface) by the transfer function (from the outcrop of the firm ground to the ground surface), which is typically evaluated by the linear multiple reflection theory.

(1) Spectral inversion

The spectral inversion (Iwata and Irikura, 1986) is one of the methods to evaluate the site amplification factor at earthquake observation stations. Let us assume that the ground motions from *M* earthquakes have been observed at *N* stations. Then the Fourier spectra of the observed ground motions can be represented as the product of the source effect, the path effect and the site effect as follows.

$$O_{ij}(f) = S_i(f)P_{ij}(f)G_i(f) \tag{15}$$

Where

O_{ij}(f): Fourier spectrum of the record from the i^{th} earthquake at the j^{th} station,

S_i(f): Source effect (source spectrum) for the i^{th} earthquake,

P_{ij}(f): Path effect from the i^{th} earthquake to the j^{th} station,

G_j(f): Site effect for the j^{th} station.

The path effect can be represented as follows, taking into account the geometrical spreading and the inelastic damping.

$$P_{ij}(f) = \frac{1}{r_{ij}}\exp(-\pi f r_{ij} / QV_S) \tag{16}$$

Where

r: distance from the i^{th} earthquake to the j^{th} station,

Q: Q value along the propagation path.

By substituting the equation (2) into the equation (1) and taking the natural logarithm, one obtains

$$\log O_{ij} = -\log r_{ij} + \log S_i + \log G_j - (\log e)\pi f r_{ij} / Q V_S \quad (17)$$

In general, the numbers of the unknowns included in the equation (17) is smaller than the number of the equations, i.e., the number of the records. Thus one can solve the equation (17) by using the least square method. It should be noted, however, that the least square solutions of the equation (17) are not unique. For instance, if S_i and G_j are the least square solutions, S_i /2 and 2 G_j will also be the least square solutions. Thus, in this analysis, an additional constraint is required. One of the recommended way to give the constraint is to select a frequency-dependent reference site for which the site amplification factor is smallest among all the sites (excluding soft soil sites) and to assume that the site amplification factor is unity for this reference site (Nozu and Nagao, 2005). It is also recommended to make sure that the seismic moments estimated from the solutions of the equation (17) are in agreement with those of Centroid Moment Tensor (CMT) solutions on the average. Other recommendations on the spectral inversion can be summarized as follows.

— It is preferable to avoid records with epicentral distances larger than 150 - 200 km because the equation (16) is not applicable to long-distance records.

— It is preferable to avoid records from large earthquakes (M≥6 for example) because it is not appropriate to assume a azimuth-independent source effect S_i for large earthquakes.

— It is preferable to avoid records from small earthquakes (M<4 for example) because, for small earthquakes, the signal-to-noise ratio at low frequencies tends to be insufficient.

— It is preferable to avoid records with large amplitude to avoid the effects of soil nonlinearity.

Nozu and Nagao (2005) and Nozu *et al.* (2006) used the method to evaluate site amplification factors for strong-motion sites all over Japan including K-NET sites, KiK-net sites and sites at major ports. Medium-sized earthquakes were used, whose JMA magnitude is in the range from 4.5 to 6.0. To avoid the effects of soil nonlinearity, records with PGAs exceeding 100 cm/s^2 were excluded from the analysis. As for the path effect, geometrical spreading and nonelastic attenuation were considered. The analysis was conducted in two steps: In the first step, O_{ij} is calculated from portions of the records with duration of 40 seconds including S waves. Then, based on the equation (3), S_i is estimated. In this step, G_j is assumed to be unity for the reference site. In the second step, O_{ij} is calculated from portions of the records with duration of 160 seconds including not only S waves but also later phases. Then, based on the equation (3) and using the S_i previously determined, G_j is estimated. G_j thus estimated reflects the lengthening of ground motion duration due to local geology (e.g., Beauval *et al.*, 2003) and suitable for strong motion simulation technique described in 3). Figure 32 (left) shows the location of strong motion sites and hypocenters of the earthquakes used in the spectral inversion analysis for Kanto region. In Figure 32 (right) the seismic moments estimated from the analysis for Kanto region is compared with those of the F-net CMT solutions. F-net CMT solutions are based on very long period (0.01-0.1 Hz) surface waves. The agreement between the two seismic moments indicates that the reference site is adequately chosen and there is no serious overestimation or underestimation of the source effect. Figure 33 shows examples of site amplification factors in Kanto region. The digital data of the site amplification factors in Japan evaluated in this way are available on a CD-ROM (Nozu and Nagao, 2005).

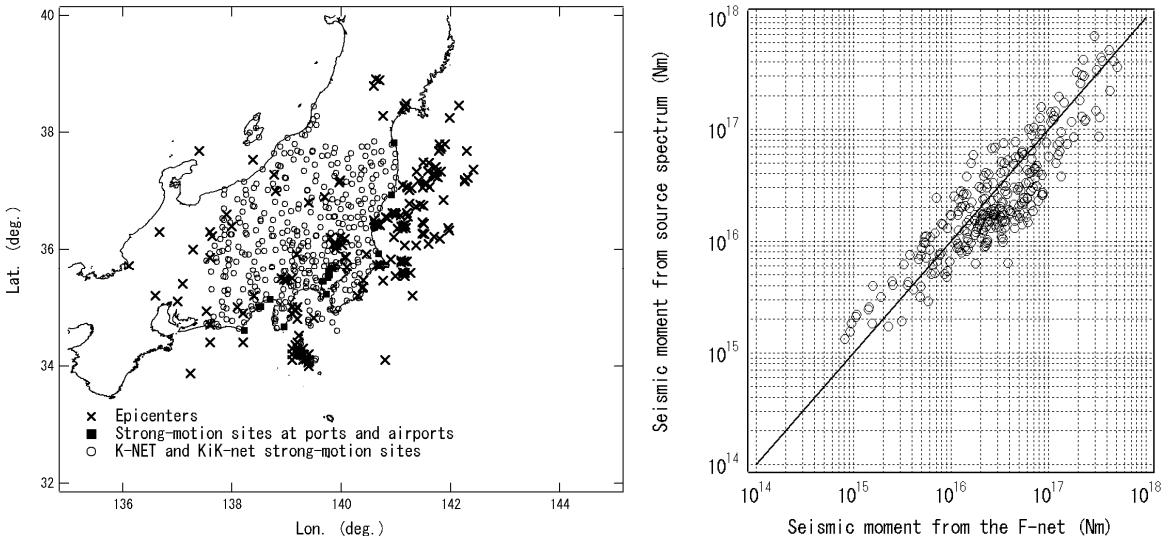

Figure 32 — (left) Location of strong motion sites and hypocenters of the earthquakes used in the spectral inversion analysis for Kanto region. (right) Comparison between the seismic moments estimated from the analysis for Kanto region and those of the F-net CMT solutions.

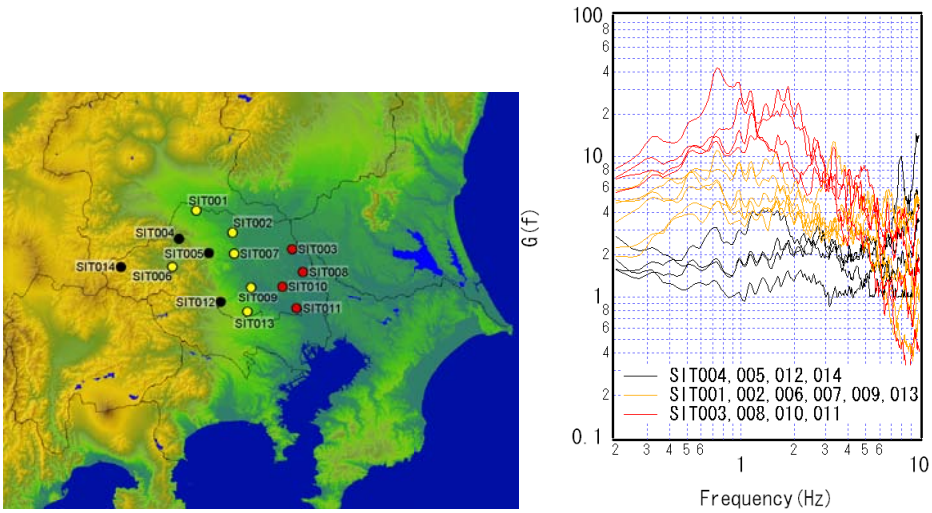

Figure 33 — Examples of site amplification factors in Kanto region. Large site amplification factors are estimated at sites located in plains (SIT003, 008, 010, 011), whereas small site amplification factors are estimated at sites located in mountains (SIT004, 005, 012, 014). Medium site amplification factor is estimated for Chichibu (SIT006), which is in a small basin surrounded by mountains (after Nozu and Nagao, 2005).

(2) Temporary earthquake observation

The term for the temporary observation should be determined taking into account the seismicity of the area. Typically, in Japan's case, a term of 1-3 years would be required. The seismometers used for the observation should cover all the frequency range for which strong ground motions should be predicted. If the predicted ground motion is intended to be used for the design of geotechnical works, the predicted ground motion should be preferable reliable down to 0.2 Hz. The trigger level should be chosen carefully. In general, a very small trigger level should be chosen to obtain as many records as possible in a limited term. It might be useful to adopt a mechanism in which the seismometer is triggered when the velocity, instead of the acceleration, exceeds certain value. The location of the observation should also be determined carefully. When it is difficult to install the seismometer just at the construction site, then microtremor observation should be conducted in and around the construction site and the seismometer should be installed within an area in which the

characteristics of microtremor can be regarded uniform. As can be seen from Figure 34 in Subclause 4.2.1, the effect of earthquake magnitude on the Fourier amplitude is especially significant for low frequencies. Fourier spectra calculated from the records of small earthquakes are often not reliable at low frequencies. To evaluate reliable site amplification factors down to low frequencies, it is important to obtain the records of relatively large (M≥4 for example) earthquakes.

(3) Evaluation of site amplification factors at a temporary station

Based on the known site amplification factors at permanent stations, the site amplification factor at a temporary station can be evaluated as follows. The first step is to find earthquakes, which are recorded both at the temporary station and the surrounding permanent stations. Then, for these earthquakes, the source spectra should be determined so that the equation (15) is satisfied for the permanent stations. It is a common practice to assume that the source spectra follow the ω^{-2} model (Aki, 1967):

$$S(f) = C\frac{M_0}{4\pi\rho V_s^3}\frac{(2\pi f)^2}{1+(f/f_c)^2} \tag{18}$$

Where

M_0: seismic moment,

f_c: corner frequency,

ñ: density in the bedrock,

V_s: shear wave velocity in the bedrock,

C: constant.

Finally, using the source spectra thus obtained and the observed spectra at the temporary station, the site amplification factor at the temporary station can be determined from the equation (15).

A simplified version of this analysis can be applied if the temporary station is very close to a permanent station for which the site amplification factor is known. In this case, these stations share the same source effect and the same path effect. Therefore, the Fourier spectral ratio of the records from the same earthquake at these stations represents the ratio of the site amplification factors. Thus, the site amplification factor for the temporary station can be easily obtained from the spectral ratios.

4.2.4.3 Evaluation of strong ground motion

To evaluate strong ground motions, the rupture process of the target earthquake should be specified. It has been revealed that the slip on the fault of a large earthquake is not uniform and there is a relatively small region called “asperities” in which the slip (and the slip velocity) is especially large. It is necessary to take into account the existence of asperities for the reliable evaluation of strong ground motions. To characterise the rupture process of a large earthquake, the “characteristic source model” is often employed. The “characteristic source models” is defined as a source model composed of rectangular asperities, within which the slip and the slip velocity is uniform. In the characteristic source model, the source parameters to be specified fall into three categories: the macroscopic parameters, the microscopic parameters and the other parameters. The macroscopic source parameters include the location of the fault, the strike of the fault, the dip of the fault, the area of the fault and the seismic moment of the fault. The microscopic parameters include the number of the asperities, the area of the asperities, the seismic moment of the asperities, the rise time of the asperities and the location of the asperities. The other parameters include the rupture starting point and the rupture velocity. The meaning of the source parameters are shown in Figure 34.

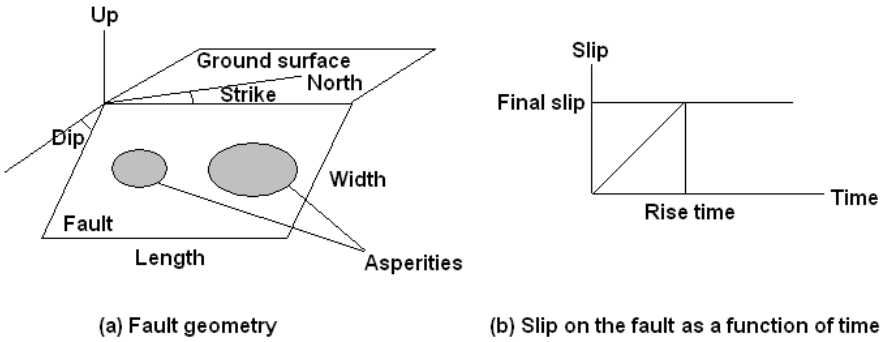

Figure 34 — Meaning of the source parameters

To calculate ground motions for a past earthquake, a source model optimized for the particular earthquake will be useful. To calculate ground motions for a future hypothetical earthquake, the source parameters should be determined based on empirical relations.). In the examples shown in Subclause 4.2.3.1.4, optimized source models for individual earthquakes are used.

There are several reliable methods for the synthesis of earthquake ground motions for a prescribed source model. In this section, the Kowada's method (Kowada, 1998; Nozu and Sugano, 2008; Nozu *et al*., 2008) is described.

First, a small earthquake should be hypothesized, whose area is equal to the area of the target asperity divided by N^2 and whose seismic moment is equal to the seismic moment of the target asperity divided by N^3. The ground motion from the small earthquake is called the "Green's function". The Fourier amplitude of the Green's function is evaluated as a product of the source effect S (f), the path effect P (f) and the site amplification factor G (f). The source effect and the path effect can be specified as follows.

$$S(f) = R_{\theta\phi} FS \cdot PRTITN \cdot \frac{M_{0e}}{4\pi\rho V_S^3} \frac{(2\pi f)^2}{1+(f/f_c)^2} \tag{19}$$

$$P(f) = \frac{1}{r}\exp(-\pi f r / Q V_S) \tag{20}$$

Where

M_{0e}: seismic moment of the small event

f_c: corner frequency of the small event

ñ: density in the bedrock

V_S: shear wave velocity in the bedrock

$R_{\theta\phi}$: radiation coefficient

FS: amplification due to free surface (=2)

$PRTITN$: coefficient representing the partition of seismic energy into two horizontal components

r: hypocentral distance for the small earthquake

Q: Q value along the propagation path.

The corner frequency of the small earthquake can be obtained from the area of the small earthquake S_e as follows (Brune, 1970; Brune, 1971).

$$f_c = 0.66 V_S \Big/ \sqrt{S_e} \tag{21}$$

As for the Fourier phase, the Fourier phase of a record at the earthquake observation station can be used. If the site amplification factor from the bedrock to the ground surface is used, the Fourier phase at the ground surface should be used. If the site amplification factor from the bedrock to the outcrop of a firm ground is used, the Fourier phase at the outcrop of the firm ground should be used. If several records are available at the site, it is recommended to choose an event, which has a similar incident angle and a similar back-azimuth with the target asperity. The Green's function in the frequency domain can be written as follows.

$$|S(f)|\ |P(f)|\ |G(f)|\ O_s(f) / |O_s(f)|_p, \tag{22}$$

Where $O_s(f)$ is the Fourier transform of a record at the site and $|O_s(f)|_p$ is its Parzen-windowed amplitude (typically the band width of 0.05 Hz is used). The time domain Green's function can be obtained as the inverse Fourier transforms of the equation (8). Finally, the time domain Green's function can be superposed as follows (e.g., Miyake *et al*., 1997).

$$U(t) = \sum_{i=1}^{N} \sum_{j=1}^{N} \left(r \big/ r_{ij} \right) f(t) * u(t - t_{ij}) \tag{23}$$

$$f(t) = \delta(t) + \left\{ 1 \big/ n' \big/ \left(1 - e^{-1} \right) \right\} \sum_{k=1}^{(N-1)n'} \left[e^{-(k-1)/(N-1)/n'} \delta\left\{ t - (k-1)\tau / (N-1) / n' \right\} \right]$$

$$t_{ij} = \left(r_{ij} - r_0 \right) \big/ V_S + \xi_{ij} / V_r$$

Where

$U(t)$: Ground motion from the asperity (designated as "large event" in Figure 35)

$u(t)$: Green's function

$f(t)$: Function to correct for the difference of slip velocity time functions for the asperity and those for the small earthquake

r: hypocentral distance for the small earthquake

r_{ij}: distance from the subfault ij to the site

ô: Rise time of the asperity

n': integer used to remove artificial periodicity

r_0 : distance from the rupture starting point to the site

î$_{ij}$: distance from the rupture starting point to the subfault ij.

V_S: shear wave velocity in the bedrock

V_r: Rupture velocity

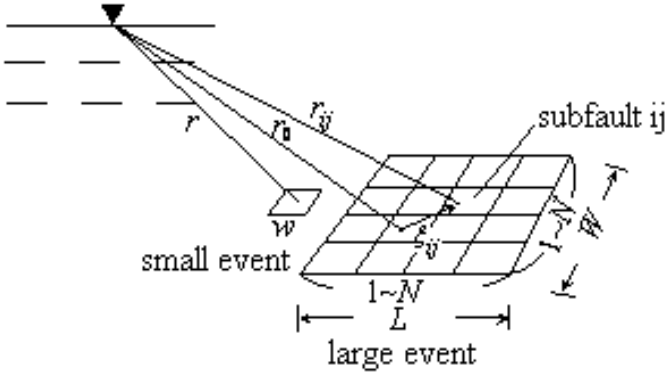

Figure 35 — Division of target fault to be superimposed by using Green's functions from divided sub-faults

The ground motion thus obtained is either at the ground surface or at the outcrop of the firm ground, depending on the site amplification factor used in the equation (8). To obtain the ground motion at the outcrop of the firm ground from the ground motion at the ground surface, the linear multiple reflection theory can be used. A computer program to synthesize strong ground motions based on the method described above is open to public from the Port and Airport Research Institute (Nozu and Sugano, 2008).

Finally, a recommended procedure to incorporate soil nonlinearity is introduced. Figure 36 shows seismic rays connecting the source and the site on a sedimentary basin. In general, the seismic rays cross the soft soil deposit somewhere in the basin before its incidence to the local soft soil deposit at the site except for the direct S wave. Therefore, when the soft soil deposit exhibit a nonlinear behaviour during a large event, the seismic waves will be affected by the soil nonlinearity more than once along the rays, except for the direct S wave. The phenomenon is referred to as the "multiple nonlinear effects" (Nozu and Morikawa, 2003; Nozu and Morikawa, 2004).

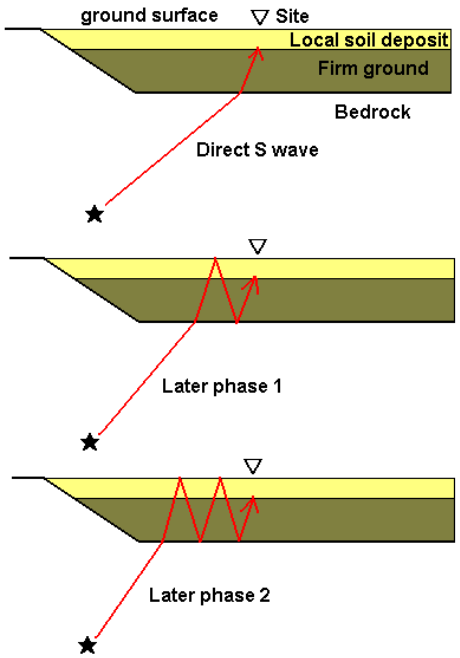

Figure 36 — Multiple nonlinear effects

In the present approach, the nonlinear effect on the seismic wave after its incidence to the local soft soil deposit is evaluated by an effective stress analysis, while the nonlinear effect on the seismic wave before its

incidence to the local soft soil deposit is evaluated by a simplified scheme using the “nonlinear parameters” (Nozu and Morikawa, 2003; Nozu and Morikawa, 2004). The latter procedure can be described as follows.

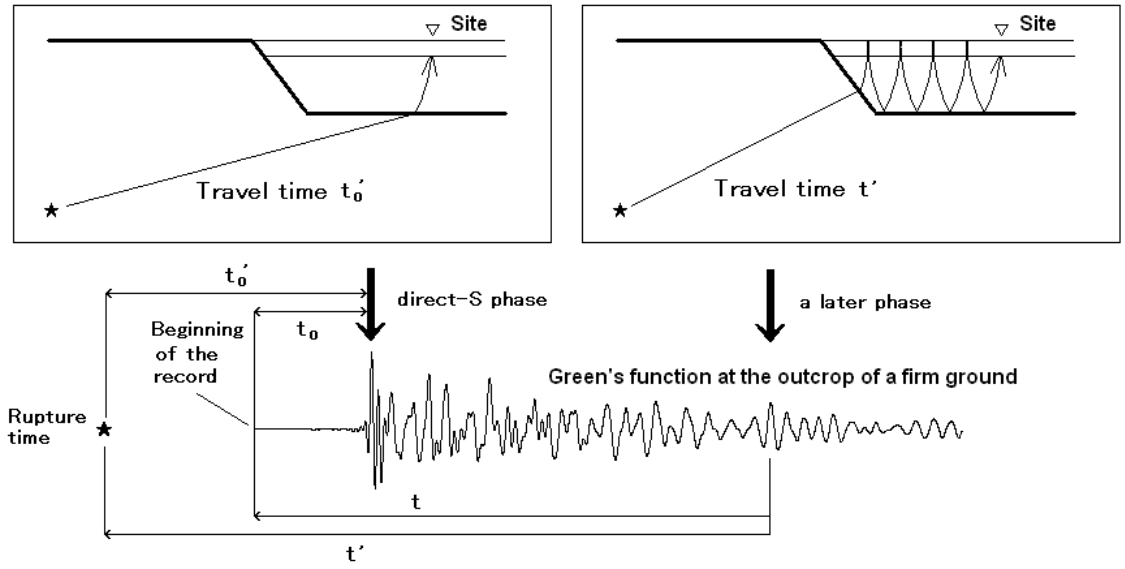

Figure 37 — Introduction of “nonlinear parameters”

A key assumption in the present method is that the delay of an arbitrary later phase found on the Green's function is caused by the trapping of the seismic ray within the sedimentary basin as schematically illustrated in Figure 37. Thus the difference of the arrival times of the direct-S phase and the later phase on the Green's function t-t_0 is approximately equal to the time for which the seismic ray corresponding to the later phase is trapped within the sedimentary basin. During a large event, the materials within the sedimentary basin can exhibit nonlinear behaviour including the reduction in shear wave velocity and the increase in damping (Beresnev and Wen, 1996). The nonlinear behavior is typically most prominent near the surface of the basin. Due to the nonlinear behaviour, the arrival time of the later phase will be delayed and its amplitude will be reduced. Two parameters, $\acute{\imath}_1$ and $\acute{\imath}_2$, are introduced to represent the deviation of the material properties of the sediments from the linear status due to the soil nonlinearity. The parameter $\acute{\imath}_1$ is defined as the averaged reduction in shear wave velocity along the ray in the sediments, that is, $\acute{\imath}_1 = V_s/V_{s0}$, where V_s is the shear wave velocity for a strong motion and V_{s0} is the shear wave velocity for a weak motion. The parameter $\acute{\imath}_2$ is defined as the averaged increase in damping factor along the ray in the sediments, that is, $\acute{\imath}_2=h-h_0$, where h is the damping factor for a strong motion and h_0 is the damping factor for a weak motion. Then, during a large event, the seismic ray corresponding to the later phase will be trapped within the sedimentary basin $1/\acute{\imath}_1$ times longer than the linear case. At the same time, the amplitude of the later phase will be reduced by a factor of $\exp[-\acute{\imath}_2 \grave{u}(t-t_0)]$, because t-t_0 is approximately equal to the time for which the seismic ray corresponding to the later phase is trapped within the sedimentary basin as discussed above. As a result, the Green's function is modified as follows:

$$g_n(t)=g(t) \qquad \text{for } t<t_0 \text{ and}$$

$$g_n(t_0+(t-t_0)/v_1)=g(t)\exp[-v_2\,\omega(t-t_0)] \quad \text{for } t>t_0, \tag{24}$$

Where g (t) is the original Green's function at the outcrop of the firm ground and $g_n(t)$ is the Green's function after modification. The parameters $\acute{\imath}_1$ and $\acute{\imath}_2$ are referred to as "the nonlinear parameters". In practice, if the Green's function is narrow-band, the corresponding angular frequency can be used in equation (10). If the Green’s function is broad-band, it is decomposed into components having different frequencies and then each component sis modified in the same manner as in the narrow-band case. Finally, the modified components are summed up.

4.2.4.4 Example of application

(1) Application to the 1995 Hyogo-ken Nanbu, Japan, earthquake (M_J7.3)

First, the method is applied to the 1995 Hyogo-ken Nanbu, Japan, earthquake, which is a shallow crustal earthquake. Using the characteristic source model by Yamada *et al.* (1999) (Figure 38), ground motions at two CEORKA (The Committee of Earthquake Observation and Research in the Kansai Area) sites in Kobe, KBU and MOT, are simulated. Site amplification factors at these sites (Nozu and Nagao, 2005) are shown in Figure 39. Based on the simulation of aftershock ground motions, the seismic moments of the asperities are re-evaluated as 3.4×10^{17} Nm, 1.3×10^{18} Nm and 2.3×10^{18} Nm for asperities 1, 2 and 4, respectively. Rise times of the asperities are 0.4s, 0.5s and 0.6s for the asperities 1, 2 and 4, respectively. The westernmost asperity was neglected in the simulation because it has little effects on the ground motions in Kobe. To determine the phase characteristics of the Green's functions, the records from an aftershock (1995/2/2 16:19) were used, whose hypocenter is shown in Figure 38. The synthetic velocity waveforms and the velocity Fourier spectra are compared with the observed ones in Figure 40 and 12, respectively. It can be clearly seen that the damaging velocity pulses generated by the asperities can be reproduced with high accuracy with the present method. The results also indicate the validity of the characteristic source model for a shallow crustal earthquake.

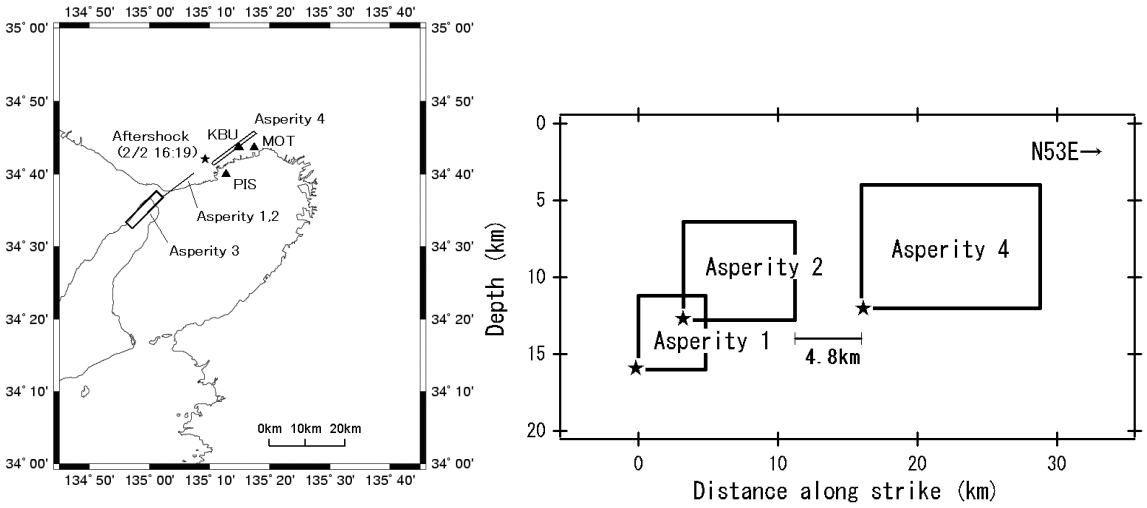

Figure 38 — Characteristic source model by Yamada et al.(1999) for the 1995 Hyogo-ken Nanbu earthquake, epicenter of the aftershock used and location of CEORKA sites KBU and MOT. Cross section shows only the Kobe side of the model.

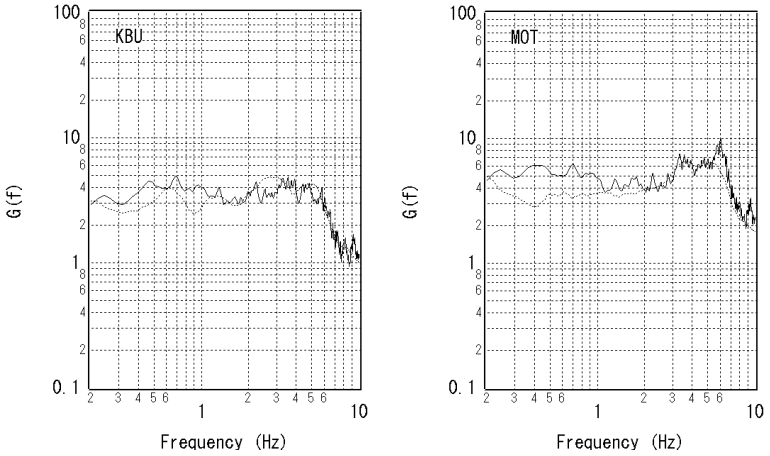

Figure 39 — Site amplification factors for CEORKA strong motions sites KBU and MOT at the ground surface estimated by Nozu and Nagao (2005) (thick lines) and those estimated by Tsurugi et al. (2002) (dotted lines).

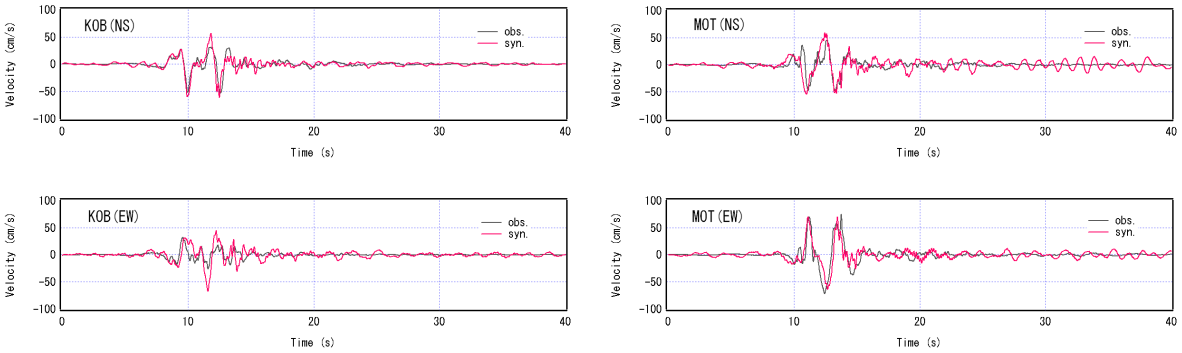

Figure 40 — Recorded (black) and simulated (red) velocity waveforms at KBU and MOT for the 1995 Hyogo-ken Nanbu earthquake.

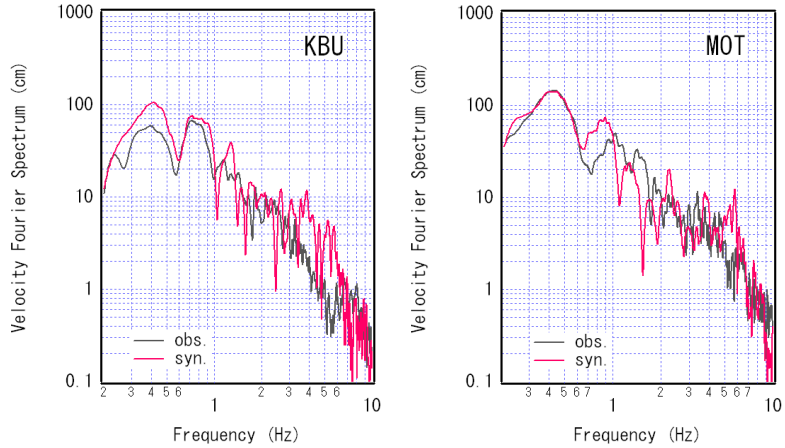

Figure 41 — Recorded (black) and simulated (red) velocity waveforms at KBU and MOT for the 1995 Hyogo-ken Nanbu earthquake.

The same source model and the same method were applied to the PIS vertical array station, where the nonlinear behaviour of the soft soil deposit was significant. Figure 42 shows the site amplification factor for PIS at the outcrop of the firm ground. To determine the phase characteristics of the Green's functions, the records from an aftershock (1995/2/18 21:37) were used. The Green's functions were modified based on the equation (10). The nonlinear parameters $\acute{\imath}_1$ = 0.91 and $\acute{\imath}_2$ = 0.06 were used. Then, the equation (9) was applied to the modified Green's functions to estimate the ground motion at the outcrop of the firm ground during the large event. Finally, an effective stress analysis (Iai *et al.*, 1992) was conducted to evaluate the nonlinear behaviour of the local soft soil layers. The parameters listed in Table 2 were used for this analysis. In this table, initial shear modulus (G_{ma}) which depends on initial mean effective stress (σ_{ma}') and internal friction angle ϕ_f' for each layer are shown as well as other parameters. Excess pore water pressure was considered for the 2nd and the 3rd layers. The synthetic velocity waveforms (0.2-2 Hz) at four depths are compared with the observed ones in Figure 43. The synthetic waveforms are consistent with the observed ones.

Table 2 — Parameters used for the effective stress analysis

Layer No.	Thickness of layer (m)	Material	Density (Mg/m^3)	initial shear modulus, G_{ma} (kPa)	initial mean effective stress, σ_{ma}' (kPa)	internal friction angle, ϕ_f'
1	3.4	Masado	1.8	79,380	63	36
2	4.6	Masado	1.8	79,380	63	36
3	1.0	Silt	1.7	74,970	143	30
4	8.0	Masado	1.8	79,380	63	36
5	13.0	Clay	1.7	74,970	143	30
6	30.0	Sand	1.8	79,380	63	36
7	23.0	Clay	1.7	74,970	143	30

Note:
1. Excess pore water pressure generation is considered for Layers 2 and 3.
   Iai's model parameters for the two layers: fp=28 deg. W1=6.0, P1=0.5, P2=0.8, C1=2.43, S1=0.005
2. Coefficient of Rayleigh damping, b=0.002
3. Masado is the Japanese name of weathered Granite soil.

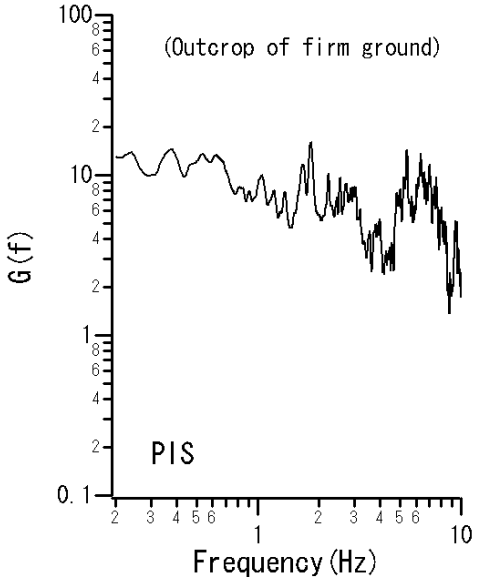

Figure 42 — Site amplification factor for PIS at the outcrop of the firm ground

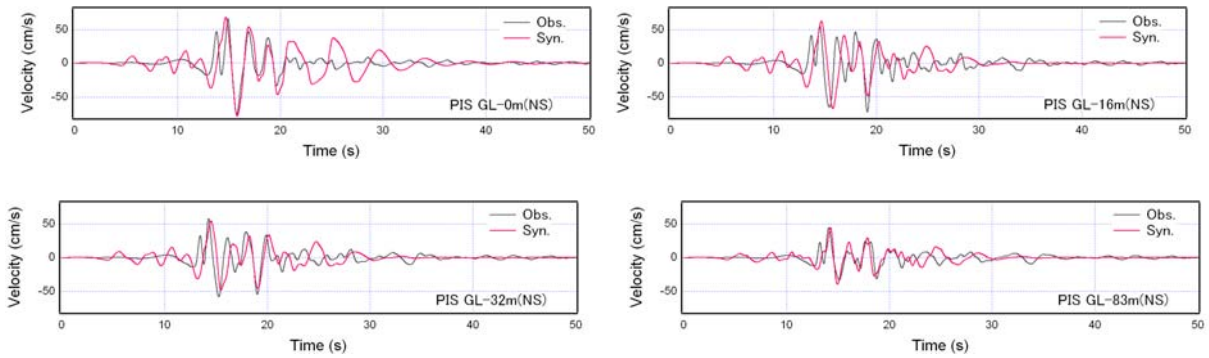

Figure 43 — Observed and synthetic velocity waveforms (0.2-2 Hz) at PIS at four depths during the 1995 Hyogo-ken Nanbu, Japan, earthquake.

(2) Application to the 2003 Tokachi-oki, Japan, earthquake (M_J8.0)

Secondly, the method is applied to the 2003 Tokachi-oki, Japan, earthquake, which is a huge subduction earthquake. Figure 44 shows the characteristic source model developed for the earthquake. The model is composed of three asperities. Ground motions at four KiK-net stations, namely, TKCH06, TKCH11, KSRH01 and TKCH02 are simulated. The site amplification factors at these sites (Nozu and Nagao, 2005) are shown in Figure 45. Although the former two stations are located close to each other, their site amplification factors are quite different. Similarly, although the latter two stations are located close to each other, their site amplification factors are quite different. The records from the aftershock 1 (2003/9/26 7:20) were in the equation (8) for the former two stations, because the effect of the asperity 1 is dominant for these stations and the aftershock 1 is close to the asperity 1. The records from the aftershock 2 (2003/9/27 17:06) were used in the equation (8) for the latter two stations, because the effect of the asperity 2 is dominant for these stations and the aftershock 2 is close to the asperity 2. The hypocenters of these aftershocks are shown in Figure 44. The synthetic velocity waveforms (0.2-1Hz) are compared with the observed ones in Figure 46. Note the significant difference of the amplitude and the duration of the observed velocity waveforms. The difference can be attributed to the site effects. The synthetic velocities are consistent with the observed ones in terms of the amplitude and duration. Thus, it is quite important to take into account the effect of sediments both on the Fourier amplitude and the Fourier phase of strong ground motions. The results also indicate the validity of the characteristic source model for a huge subduction earthquake.

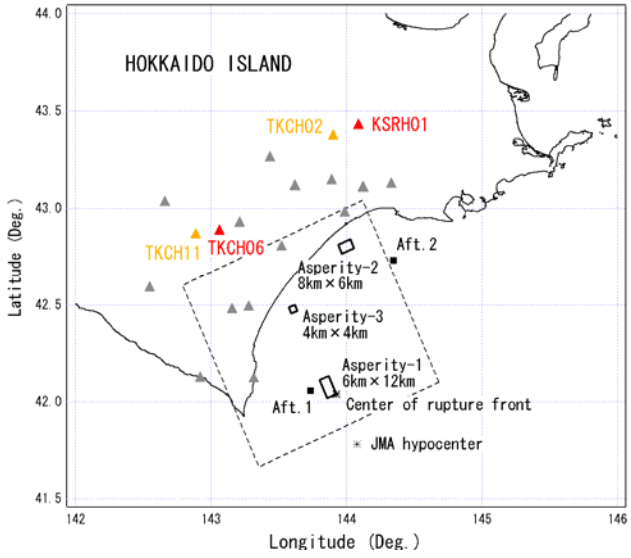

[Macroscopic parameters]Density: 3.1g/cm3, Shear wave velocity: 3.9km/s, Strike: 246, Dip: 18, Rupture starting point: (143.925E, 42.039N, d=30.1km), Rupture velocity: 2.7km/s

[Microscopic parameters]

[Asperity-1] Area: 6×12km2, Seismic moment: 4.2E+26 dyne-cm, Rise time: 0.6s, Discretization: 5×5×5

[Asperity-2] Area: 8×6km2, Seismic moment: 2.1E+26 dyne-cm, Rise time: 0.6s, Discretization: 3×3×3

Figure 44 — Characteristic source model developed for the 2003 Tokachi-oki, Japan, earthquake composed of three asperities (open rectangles). Triangles indicate strong-motion sites. Closed rectangles indicate small events whose records were used in equation (8).

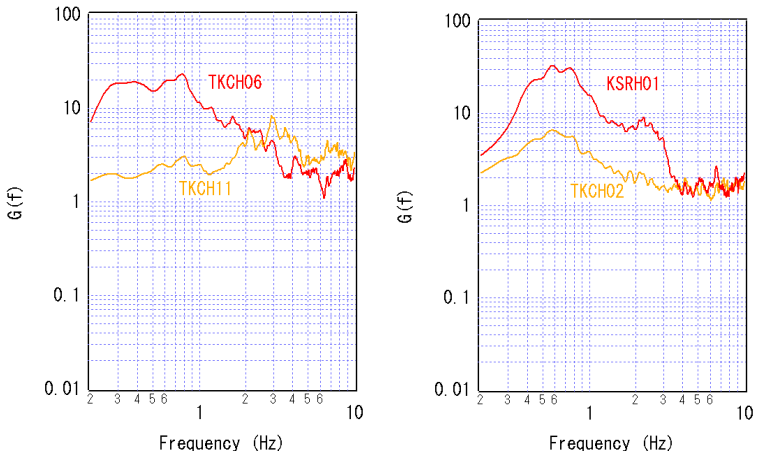

Figure 45 — Site amplification factors for TKCH06, TKCH11, KSRH01 and TKCH02 at the ground surface (Nozu and Nagao, 2005).

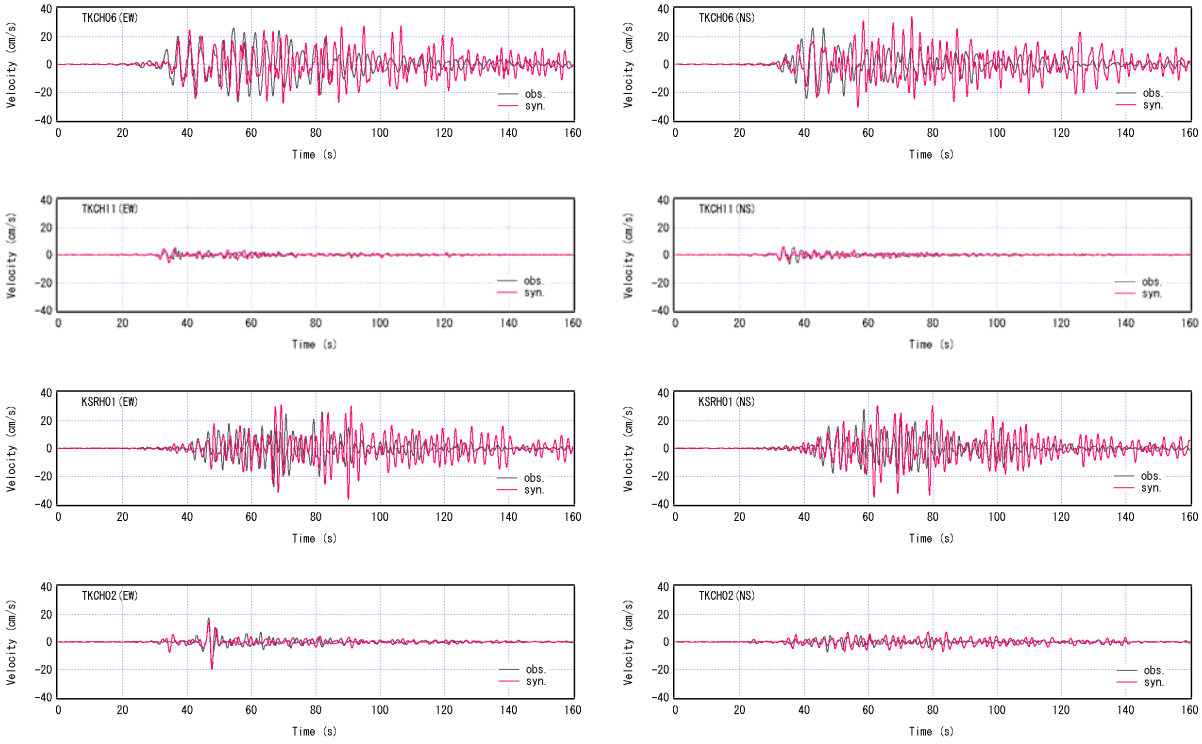

Figure 46 — Observed and synthetic velocity waveforms (0.2-1Hz) at TKCH06, TKCH11, KSRH01 and TKCH02 during the 2003 Tokachi-oki, Japan, earthquake.

4.3 Determination of earthquake ground motion to be used in site response analysis

4.3.1 Empirical and site simplified analysis approach

4.3.1.1 Simplified procedure of Seismic Deformation Method

Seismic Deformation Method, which is an equivalent static analysis method of evaluating the stress and strain in an underground structure subject to seismic soil displacement due to kinematic interaction, is commonly used for design of the underground structure. This method needs seismic soil displacements and seismic

coefficients for the masses of the structure and earth elements behind it. The seismic coefficients are determined on the basis of an empirical approach by considering the amplification in terms of the natural period of ground for design, T_G as shown in Table 3. The seismic coefficient for earth pressures acting on the buried structure is evaluated by calculating the value at the middle depth of the buried structure based on the linear interpolation technique.

As for the ground displacement, two kinds of methods to evaluate the ground displacement have been used. One is a dynamic response analysis. The other is a simplified method based on the modal analysis technique. Both methods can consider the site specific ground characteristics. Detailed explanation can be seen in Annex E of ISO 23469. In this section, the simplified method is described as follows:

Table 3 — Amplification of seismic coefficient for safety requirement for Seismic Deformation Method

Ground Type	Natural period of ground for design	Seismic coefficient at bedrock for design (limit values: lower-upper)	Seismic coefficient at ground surface (limit values: lower-upper)
Type-I	T_G<0.2	0.4 - 0.5	0.6 - 0.7
Type-II	0.2≦T_G<0.6		0.7 - 0.8
Type-III	0.6≦T_G		0.4 - 0.6

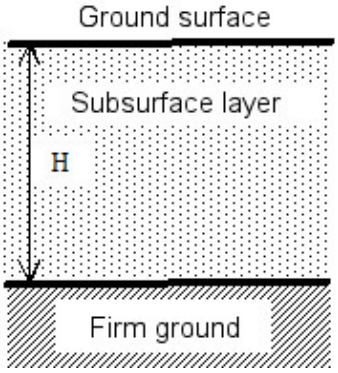

Figure 47 — Two-layer system consisting of subsurface layer on firm ground

First of all, the natural period for the 1st mode of vibration is calculated based on a two-layer system consisting of a homogeneous subsurface layer on firm ground regarded as base layer for design in terms of shear wave velocity, as shown in Figure 47. Here H denotes the thickness of the subsurface layer. Prior to the calculation, the shear wave velocity of the homogeneous subsurface layer is needed to prepare by the weighted-average of the shear wave velocities of all of the sub-layers actually composing the subsurface layer, having equivalence of the natural period for the 1st mode of vibration for the ground T_G. The displacement response spectrum $S_d(T_G, h)$ at the design bedrock is assumed to be given, where h denotes damping ratio for the system. Thus, the ground displacement distribution along the depth x in the homogeneous subsurface layer for the 1st mode of vibration $u(x)$ is induced as shown in Equation (25) on the basis of the concept of modal analysis. Converting the displacement response spectrum $S_d(T_G, h)$ to the pseudo-velocity response spectrum $S_v(T_G, h)$, one representation of the ground displacement $u(x)$ is shown in Equation (26). The other one is shown in Equation (27), which can be obtained by replacement with the product of local seismic coefficient for the ground k_h and normalized pseudo-velocity response spectrum $\overline{S}_v(T_G, h)$ in Equation (26). See E.2.2 in Annex E of ISO 23469 for reference. In reality, the displacement response spectrum is often calculated on the assumption of 20% for the damping ratio h considering the non-linerality of soil. The normalized pseudo-velocity response spectrum is calculated for acceleration time history with the maximum amplitude normalized to 1m/s^2. An example calculation is shown in the following part of this sub-sub-clause.

$$u(x) = \frac{4}{\pi} S_d(T_G, h) \cos\left(\frac{\pi x}{H}\right) \tag{25}$$

$$u(x) = \frac{2}{\pi^2} S_v(T_G, h) T_G \cos\left(\frac{\pi x}{H}\right) \tag{26}$$

$$u(x) = \frac{2}{\pi^2} k_h T_G \overline{S_v}(T_G, h) \cos\left(\frac{\pi x}{H}\right) \tag{27}$$

4.3.1.2 Natural period of an example ground

The soil profile of an example ground is shown in the left hand side of Figure 48, which provides a thickness and a shear wave velocity for each sub-layer in the subsurface layer of the example ground. The profile of shear wave velocity along the depth and the soil profile were obtained based on the results of PS logging and boring survey. The sandy gravel with a shear wave velocity of 450 m/s exists below GL -16.2 m and was regarded as bedrock for design. The subsurface layer lying above the base layer composed with sub-layers with silty or clayey soils with sand has shear wave velocity varying from 90 m/s to 270 m/s.

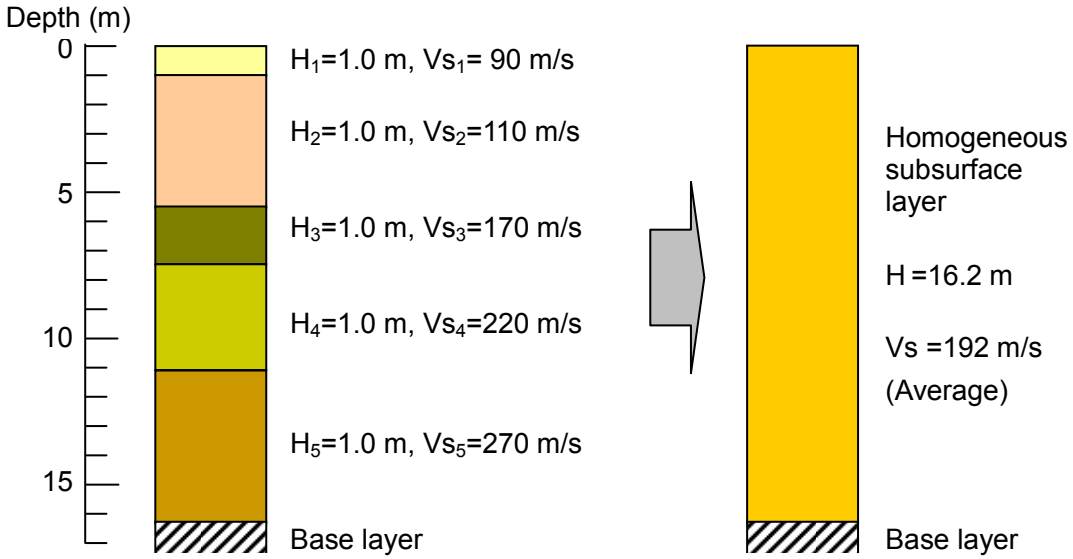

Figure 48 — Soil profile of example ground

The natural period of the ground is needed to calculate for applying to previously mentioned procedure for the calculation of ground displacement. There are two equations for the calculation of the natural period of the ground as shown in Equation 28 and Equation 29, where the thickness and the shear wave velocity of i-th sub-layer are expressed by H_i and Vs_i, respectively. Note the two equations are derived under the assumption of a rigid base.

$$T_G = 4\sum_{i=1}^{n} \frac{H_i}{Vs_i} \tag{28}$$

$$T_G = 4\frac{H}{\overline{Vs}} \tag{29}$$

,where average shear wave velocity of the subsurface layer denotes $\overline{Vs}$, which can be caluculated by

$$\bar{V}_S = \sum_{i=1}^{n} H_i Vs_i / H \tag{30}$$

The results of application of Equation 28 and Equation 29 to the example ground are shown below. Note that the two different ways for the calculation of natural period of ground differ. See an approximation for an elastic base layer shown in Equation E.8 in Annex E of ISO 23469 for reference. In this example, 0.4 second was adopted as the natural period.

$$T_G = 4 \cdot \left(\frac{1}{90} + \frac{4,4}{110} + \frac{2,0}{170} + \frac{3,6}{220} + \frac{5,2}{270} \right) = 0,4 \text{ s}$$

$$T_G = \frac{4H}{\bar{V}_S} = \frac{4 \cdot 16,2}{192} = 0,34 \text{ s}, \bar{V}_S = \frac{\left(90 \cdot 1 + 110 \cdot 4,4 + 170 \cdot 2,0 + 220 \cdot 3,6 + 270 \cdot 5,2\right)}{\left(1 + 4,4 + 2,0 + 3,6 + 5,2\right)} = 192 \text{ m/s}$$

4.3.1.3 Ground displacement

The pseudo-velocity response spectrum was given as shown in Figure 49 in this design example.

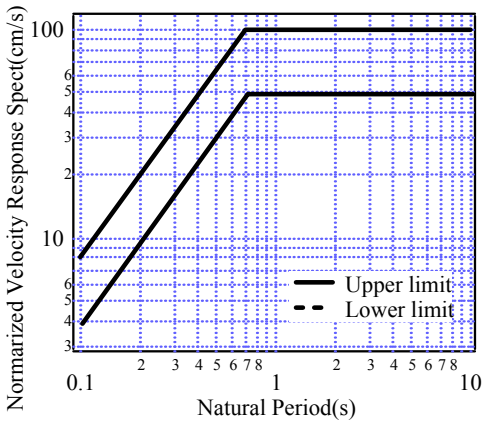

Figure 49 —pseudo-velocity spectrum for design

The value of $Sv(T_G, h)$ was determined to be 50 cm/s at T_G=0.4 s from Figure 49. The distribution of ground displacement, which is relative to the base layer, is shown in Figure 50 according to the following equation derived by substitution of relevant values into Equation 2. Maximum value of the displacement is 2.03 cm.

$$u(x) = \frac{2}{\pi^2} \cdot T_G \cdot S_v(T_G, h) \cdot \cos\left(\frac{\pi x}{2H}\right) = \frac{2}{\pi^2} \cdot 0.4 \cdot 50 \cdot \cos\left(\frac{\pi x}{2 \cdot 16.2}\right) = 2.03 \cdot \cos(0.097x)$$

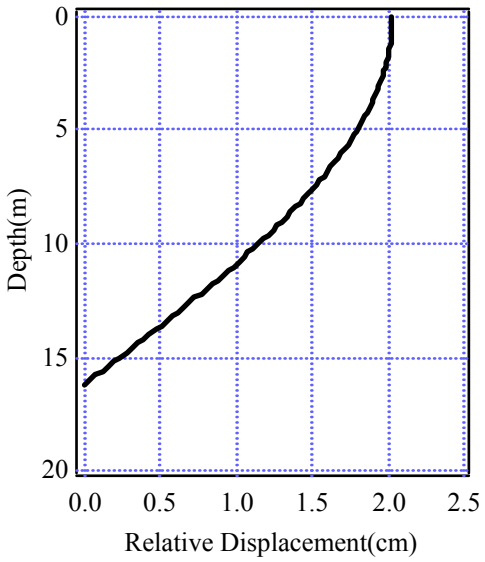

Figure 50 — Relative ground displacement distribution with depth

5 Second stage of specifying seismic actions. Seismic evaluation of geotechnical works demonstrated by design examples

5.1 Demonstrations of seismic evaluation using simplified and detailed analyses

5.1.1 Simplified static and detailed dynamic analyses in design example of gravity quay wall in port

5.1.1.1 Purpose and functions

A gravity quay wall with a water depth of 14.5m was proposed for construction. The purpose of the construction is to increase the capacity of cargo handling. Since the ship-size in commercial use is increasing in recent days, the quay wall shall be able to functional for large-scale ships. The front-water depth of the quay wall should be -14.5 m. Note this example is based on the design example shown in a seismic design guideline proposed by PIANC (2001). (511A)

5.1.1.2 Performance objectives for seismic design

Following a performance objective diagram shown in Table 4 and Table 5, which are proposed by PIANC (2001), the performance grade of this quay wall was determined to be Grade A over the life span of 50 years. The damage level classification shown in Table 4 is based on the possible consequences of failure for quay wall, considering both loss of structural stability and loss of serviceability. The concept of the grades is shown in Table 5, defined as the relationship between acceptable damage level and reference earthquake motion level. Note, the design earthquake level I (L1) is the earthquake for the reference earthquake motion for serviceability, and the design earthquake level II (L2) is the earthquake for the reference earthquake motion for safety during or after an earthquake.（512A）

The determined performance grade is based on the economic impact of the functional loss of the quay wall. Since the cargo transport by large-scale ships is an international matter, the quay wall is expected not to loss its function for the reference earthquake motion for serviceability (L1), however, limited loss of function is permissible for the severe earthquake motion (the reference earthquake motion for safety). (512a, 512b)

Table 4 Acceptable level of damage in performance-based design* (after PIANC, 2001)

Level of damage	Structural	Operational
Degree I : Serviceable	Minor or no damage	Little or no loss of serviceability
Degree II: Repairable	Controlled damage**	Short-term loss of serviceability***
Degree III: Near collapse	Extensive damage in near collapse	Long-term or complete loss of serviceability
Degree IV: Collapse****	Complete loss of structure	Complete loss of serviceability

* Considerations: Protection of human life and property, functions as an emergency base for transportation, and protection from spilling hazardous materials, if applicable, should be considered in defining the damage criteria in addition to those shown in this table.

** With limited inelastic response and/or residual deformation

*** Structure out of service for short to moderate time for repairs

**** Without significant effects on surroundings

Table 5 Performance grades S, A, B, and C (after PIANC, 2001)

Performance grade	Design earthquake	
	Level 1(L1)	Level 2(L2)
Grade S	Degree I: Serviceable	Degree I: Serviceable
Grade A	Degree I: Serviceable	Degree II: Repairable
Grade B	Degree I: Serviceable	Degree III: Near collapse
Grade C	Degree II: Repairable	Degree IV: Collapse

5.1.1.3 Reference earthquake motions

Based on seismic hazard analysis for the quay wall site, reference earthquake motions are specified as follows. The reference earthquake motions for serviceability is specified as the motions with the PGA with a probability of exceedance of 50 % during the lifespan, and the reference earthquake motions for safety is specified as the motions with the PGA with a probability of exceedance of 10 %. In this case, the former level is 0.15g and the latter level is 0.3g at the bedrock, respectively.（513A, 621A, 621B, 621C)

The details of the seismic hazard analysis are not described in the report due to the restriction of pages. Please refer to other reports to see the procedure of seismic hazard analysis. (622a, 622b, 622c, 623A)

Fault displacement is not considered in the design since no active fault was observed at the site. (611A, 650a, 650A)

5.1.1.4 Performance criteria and limit states

Performance criteria for this quay wall were determined as shown in Table 6 following PIANC(2001). These criteria were established based on the relationships between remaining function of the quay wall and damage level. Performance criteria is specified by residual displacement of the quay wall and residual tilting of the quay wall, based on the performance objective described above. Thus, the relationships between acceptable

level of damage described as engineering parameters and reference earthquake motions are summarised in Figure 51（514A,514C)

These performance criteria is not dependent on the design working life since the requested performance of the quay wall against earthquake is not dependent on the design working life in this case. However, the level or reference motion is dependent on the design working life of 50 years.（514B）

Residual displacement and residual tilting of the quay wall is somewhat difficult engineering parameters to be evaluated. However, advanced FEM analysis enables the estimation of these parameters with certain accuracy (e.g. Iai et al., 1998). The advanced FEM method shall utilized in this case since the importance of the quay wall is very high, and thus, the level of performance objective of the quay wall is also high.（514A）

Table 6 Performance criteria for a gravity quay wall (after PIANC, 2001)

Extent of damage		Degree I	Degree II	Degree III	Degree IV
Gravity wall	Normalized residual horizontal displacement (*d*/*H*)*	Less than 1.5 %	1.5～5 %	5～10 %	Larger than 10%
	Residual tilting towards the sea*	Less than 2 degrees	2～5 degrees	5～8 degrees	Larger than 8 degrees
Apron	Differential settlement between apron and non-apron areas*	Less than 0.3 m	N/A	N/A	N/A
* *d*: residual horizontal displacement; *H*: height of gravity wall					

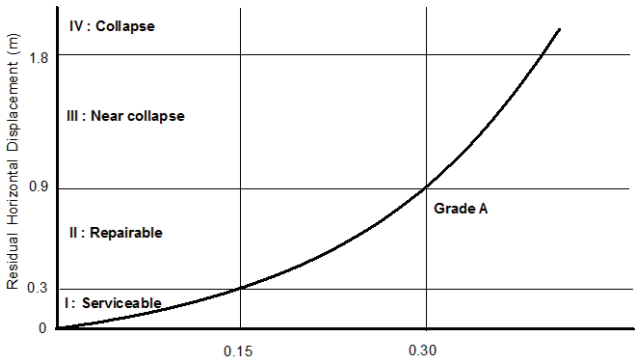

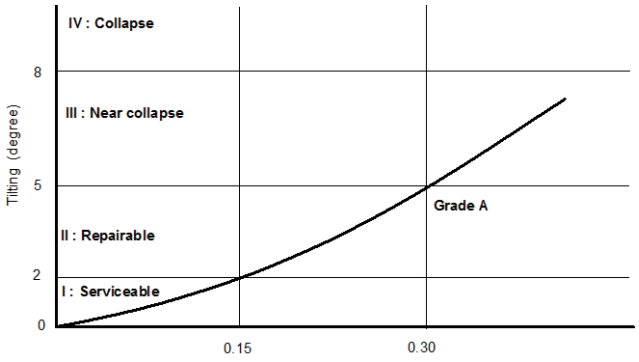

Figure 51 — Limiting curve for defining wall displacement (after PIANC, 2001)

5.1.1.5 Specific issues related to geotechnical works

Mode of failure for gravity type quay wall is very simple. Residual displacement and tilting towards sea is a major damage pattern, and other damages such as settlement of the apron are just related consequences of the seaward displacement (Inagaki, 1997). Although seismic response and soil-structure interaction affect the residual displacement and tilting significantly, these effects can be considered in advanced FEM analysis simultaneously.（515A）

5.1.1.6 Procedure for determining seismic actions

The proposed cross-section of the gravity quay wall is shown in Figure 52. It was proposed that the clay layer below the caisson wall will be removed and be replaced with sand backfill in order to attain sufficient bearing capacity. This cross section is designed empirically.

The 1st stage of determining seismic action is characterizing the firm ground motion. Figure 53 indicates the geotechnical investigation for design. The free field motion is evaluated by a one-dimensional site response analysis, and a ground surface acceleration of 0.25g was obtained. (631A, 520A, 623B)

A seismic coefficient of 0.15 for the pseudo-static analysis was determined using an empirical relation, with the parameters α = 0.6 and β= 1.0 in this case. (PIANC, 2001)

$$k_h = \alpha \times \left(a_{\max} / g\right)^{\beta} = 0.6 \times 0.25 = 0.15 \tag{31}$$

Cross-sections of the structure were proposed by the seismic coefficient. The potential for earthquake-induced phenomena (liquefaction) is investigated with sampling and laboratory test.

The 2nd stage is an advanced FEM analysis to estimate the residual displacement and residual tilting of the structure. In addition to the results of FEM analysis, a stability consideration by a pseudo-static approach is also shown in this report.（520A)

In site response analysis and FEM analysis, input earthquake motion determined with the consideration of site characteristics is necessary. In this example, a recorded motion at the site similar geotechnical condition (reclaimed land on deep alluvial clay layer) was used with modification of amplitude scales. The time history of ground motion before the modification of amplitude is shown in Figure 54. Note, this ground motion is not the original recorded motion but the corrected motion as the rock outcrop condition (2E). (623B)

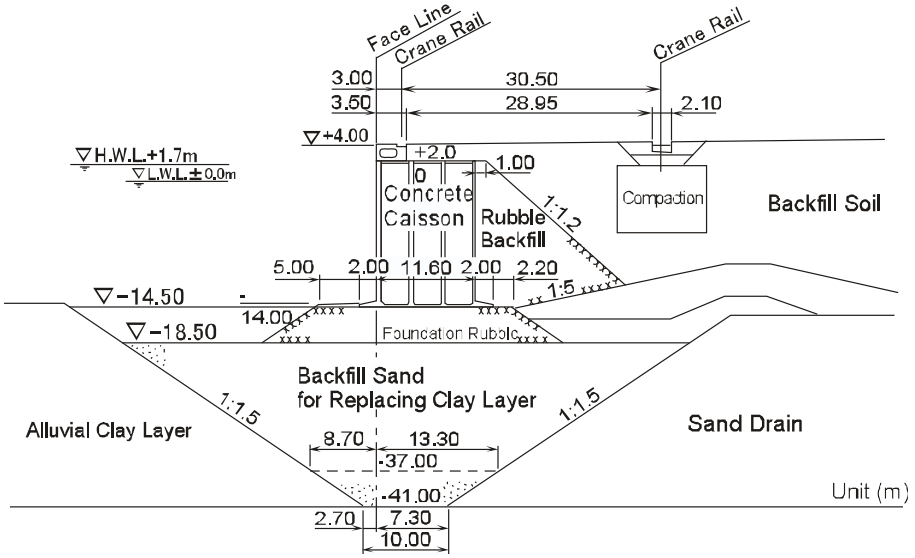

Figure 52 — Cross section of example (after PIANC, 2001)

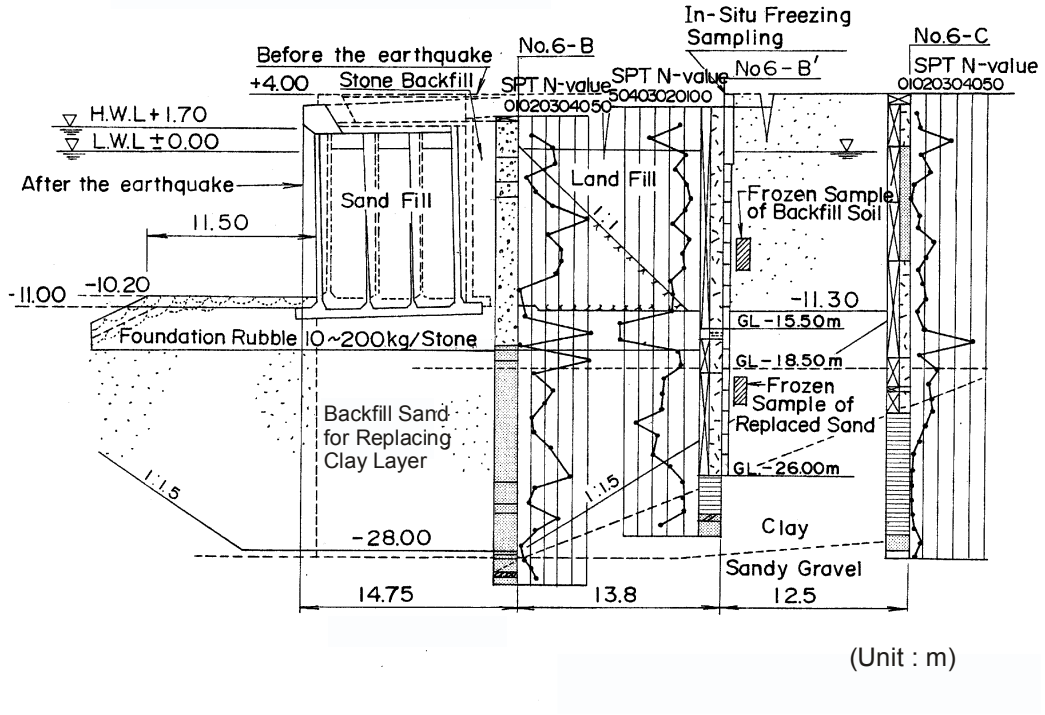

Figure 53 — Geotechnical investigations for design (after PIANC, 2001)

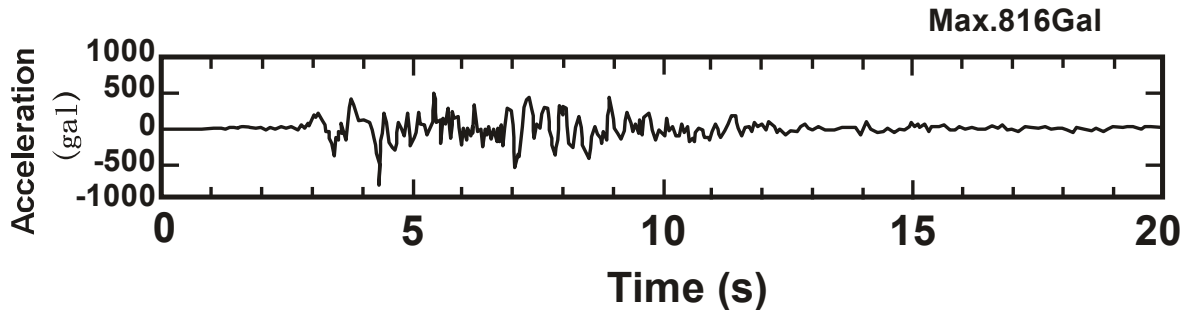

Figure 54 — Input earthquake ground motion (2E) (after PIANC, 2001)

5.1.1.7 Ground failure and other geotechnical hazards

It was proposed to remove the clay layer below the caisson wall to avoid a ground failure such as a landslide, and the area of removal were filled with sand backfill in order to attain sufficient bearing capacity. (612C)

The possibility of liquefaction is evaluated. At first, grain-size distribution is checked by the method proposed by the Ministry of Transport, Japan (PHRI, 1997; Ministry of Transport, 1999). The results shown in Figure 55 indicate the possibility of liquefaction. (612A)

Secondly, the liquefaction potential (safety factor) is assessed by in-situ blow count (N-value). Following the method proposed by the Ministry of Transport, Japan (PHRI, 1997; Ministry of Transport, 1999), equivalent N-value, N_{65}, is estimated as the index for liquefaction resistance.

$$N_{65} = \frac{N_m - 0.019(\sigma_v' - 65)}{0.0041(\sigma_v' - 65) + 1.0} \tag{32}$$

where N_m = measured SPT *N*-value of a soil layer (obtained with typical energy efficiency in Japan), σ_v' = effective overburden pressure of a soil layer (kPa). Note that the N65 should be corrected for soils with fines content, *Fc*, over 5 %. The details of the correction is not described in the report, however, following results is based on the corrected values, N_{65} = 15. Equivalent accelerations for L1 and L2 design earthquake motion levels are also estimated as the index of shear stress ratio to cause liquefaction, as follows,

$$a_{eq} = 0.7 \cdot \frac{\tau_{max}}{\sigma_v'} \cdot g \tag{33}$$

where $\tau_{\max}$ = maximum shear stress in the layer obtained from site response analysis, σ_v' = effective overburden pressure calculated. Based on the site response analysis, $a_{eq} = 175$ gal and $a_{eq} = 350$ gal were obtained for L1 and L2, respectively.

Figure 56 shows the results for the liquefaction assessment. Estimated equivalent N-value and equivalent accelerations are plotted in the figure. Zone I shows very high possibility of liquefaction, zone II shows high possibility of liquefaction, zone III shows low possibility of liquefaction, and zone IV shows very low possibility of liquefaction. Thus, the possibility of liquefaction in case of L1 level motions is low or very low; however, the possibility of liquefaction is high in case of L2 level motions. Note this liquefaction assessment should be done for all depths where in-situ blow count (N-value) were obtained, and the final conclusion of the assessment should be given from a careful consideration of the whole assessment results for all layers. The assessment results shown in Figure 56 are only an example for one layer (depth) of the site.(631B)

For an advanced FEM program, laboratory test results for samples were used to evaluate the effect of liquefaction. Parameters for soil elements in the analysis were calibrated based on the results of the geotechnical investigation; in particular, undrained cyclic properties of sand were calibrated as shown in Figure 57. (631C, 612B)

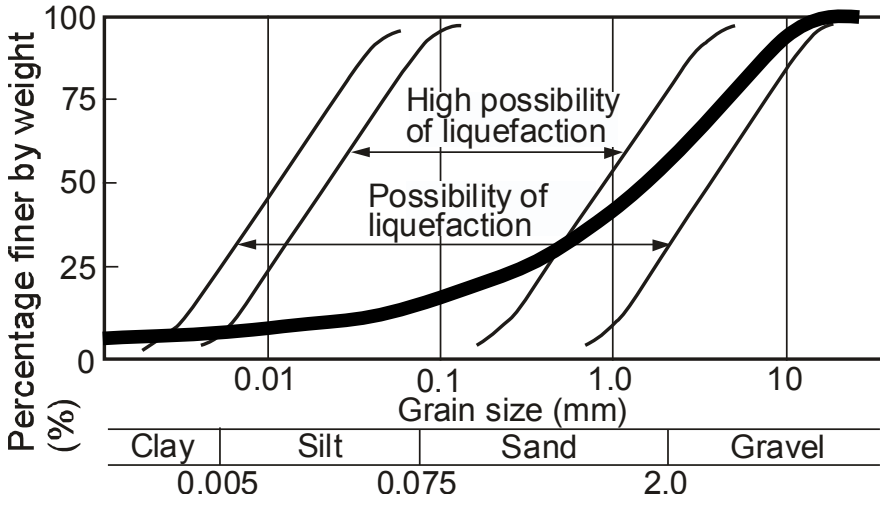

Figure 55 — Liquefaction potential assessment from grain size distribution (after Ministry of Transport, 1999)

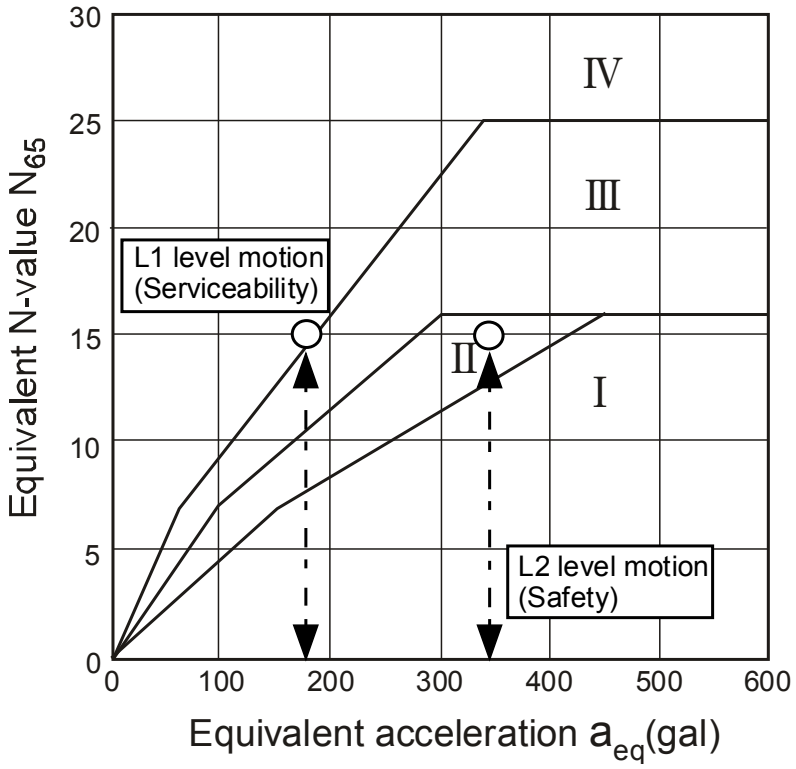

Figure 56 — Liquefaction potential assessment by in-situ blow count (after Ministry of Transport, 1999)

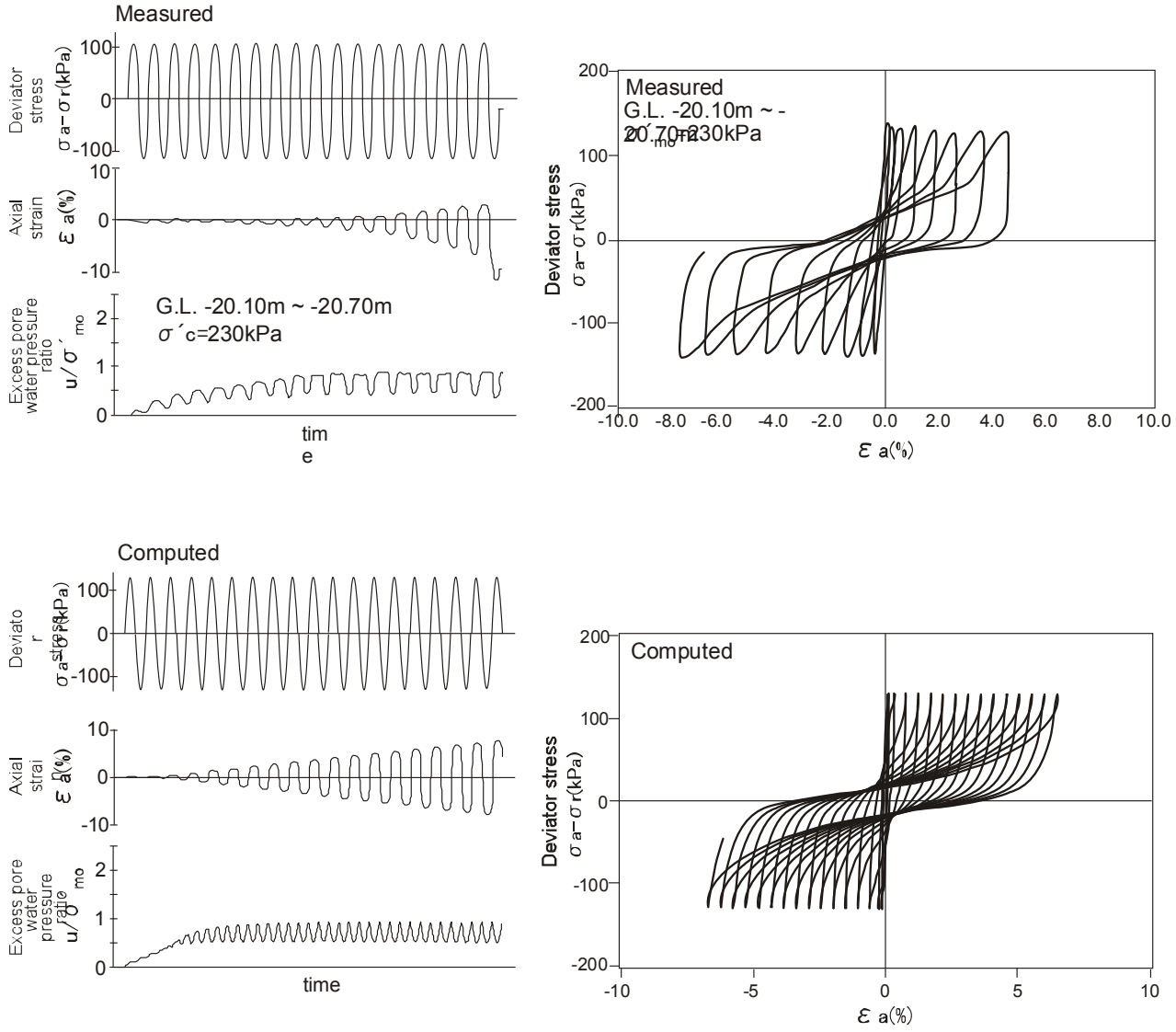

(a) Time histories

(b) Stress-strain relationships

Figure 57 — Undrained cyclic properties: laboratory test and computed results (after PIANC, 2001)

5.1.1.8 Spatial variation

Spatial variation of earthquake ground motion is not necessary to be considered since the quay walls are not firmly connected along the face line of the quay. Lateral variation of geotechnical conditions are carefully investigated by some standard penetration tests. The results of the tests indicate that geotechnical structure is quite uniform and it is no necessary to consider the effect of spatial variation of ground motions. The deep basin effects that depend on the heterogeneity below the local soil deposits was considered by utilizing an detailed technique with recorded motions at the site to synthesize the ground motion for design. (641A, 641B, 641C, 644B, 645A, 645B)

5.1.1.9 Types and models of analysis

A detailed dynamic analysis was performed. The dynamic analysis utilized the effective stress based finite element method program FLIP (Iai et al., 1992), since the applicability of the program FLIP for gravity type quay walls were confirmed many case histories including 1995 Kobe Port disaster cases. Performance criteria for design are already mentioned as shown in Table 6. Geotechnical characterization is performed by based

on geotechnical investigations. Parameters for structures and soil materials are summarized in Table 7 and Table 8, respectively. (PIANC, 2001)(711A, 711B, 712A, 713A, 715A)

Since occurrence of liquefaction is anticipated, installation of non-liquefiable material is supposed to be used in the design as geotechnical improvement. To consider the effect of improvement, four design alternatives shown in Figure 58 is considered. (715B)

Prior to a detailed dynamic analysis, a pseudo static analysis was performed for L1 earthquake motion just for a reference. Note no liquefaction occurrence is anticipated in L1 level, pseudo static approach have a certain level of applicability; however, it is not applicable to L2 level since liquefaction is anticipated in L2. (712A)

Table 7 Parameters for concrete caisson and joint elements (after PIANC, 2001)

Parameters	density (t/m^3)	Young's modulus (kPa)	shear modulus (kPa)	Poisson's ratio
Caisson	2.10	3.0×10^7	1.3×10^7	0.20
Joint elements: Friction angle δ=31 degrees (bottom of caisson); 15 degrees (behind caisson)				

Table 8 Parameters for soils and rubble (after PIANC, 2001)

Parameters	density (t/m^3)	initial shear modulus (kPa)	Poisson's ratio	internal friction angle (degrees)	phase transformation angle (degrees)
Foundation soil*	1.8	$5660\times(\sigma_{mo}')^{0.5}$	0.3	37	28
Backfill soil*	1.8	$10000\times(\sigma_{mo}')^{0.5}$	0.3	36	28
Clay	1.7	$6270\times(\sigma_{mo}')^{0.5}$	0.3	30	-
Foundation rubble and rubble backfill	2.0	$18200\times(\sigma_{mo}')^{0.5}$	0.3	40	-
* Refer to Iai et al (1992) on the parameters for dilatancy					

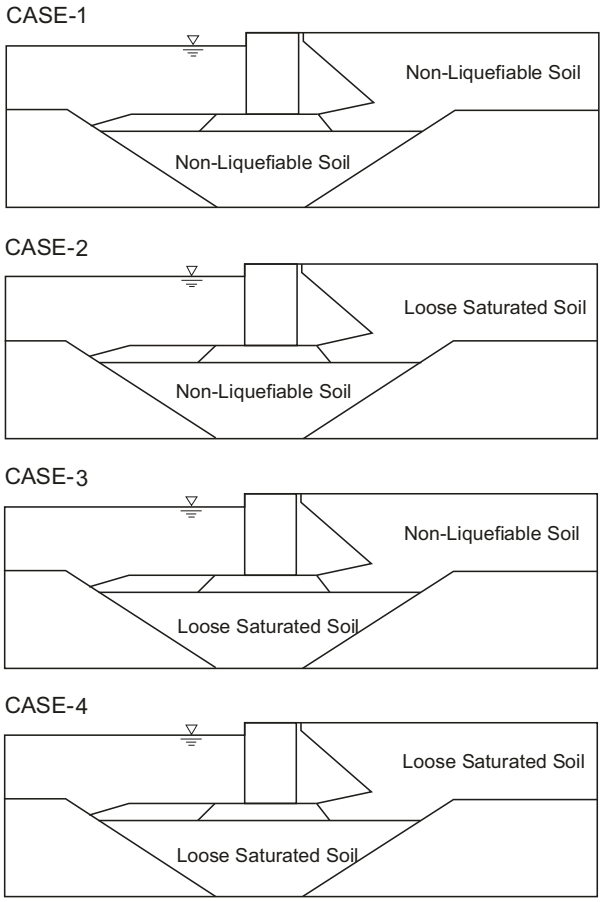

Figure 58 — Four design alternatives (after PIANC, 2001)

5.1.1.10 Simplified equivalent static analysis

The simplified cross section for pseudo static analysis is shown in Figure 59. Using the L1 acceleration of 0.35 g at bedrock, site-specific simplified dynamic analysis response was performed, and seismic coefficient of 0.15 is obtained as mentioned earlier. Note the site response analysis is conducted by a program SHAKE considering the non-liner behaviour of soils. (Schnabel et al., 1972) Therefore, seismic earth and hydro-dynamic pressure calculated by a seismic coefficient is already based on the consideration of non-liner behaviour of soils. (811B, 814a, 815a, 822A, 822B)

In this design, no seismic actions from a superstructure must be considered. Spatial variation of seismic actions is also no necessary to be considered. (811A, 811a, 811b, 812A, 812a, 813A)

(1) Active earth pressures and thrust

The active earth pressure is estimated by the active soil wedge. (Mononobe, 1924; Okabe, 1924) Since intense earthquake ground motions are not considered in this case, modification of the Mononobe-Okabe method is not utilized. The numbers with the square marks shown in Figure 60 within the soil wedge are areas in m^2 of various portions used in the analysis. Using these areas, a representative unit weight of the material above the water table, including the capping material and backfill soil, is 18 kN/m^3 (1 kN = 0.1 tf)

A representative internal friction angle for the backfill can be determined by direct averaging based on the corresponding cross-sectional areas.

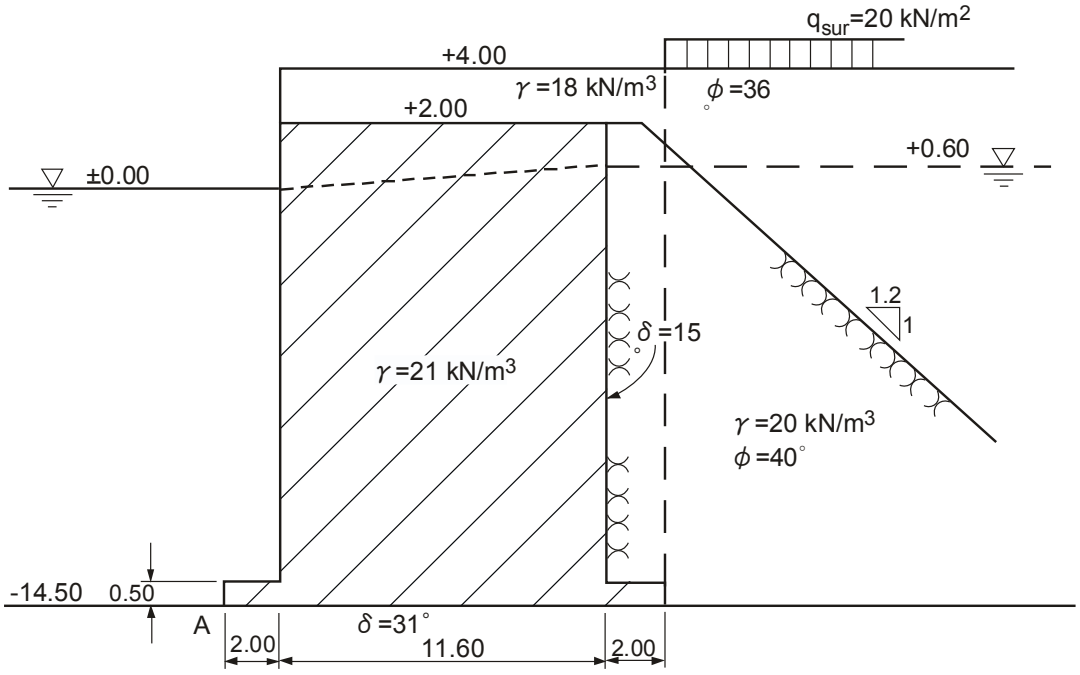

Figure 59 — Simplified cross section for pseudo-static analysis (after PIANC, 2001)

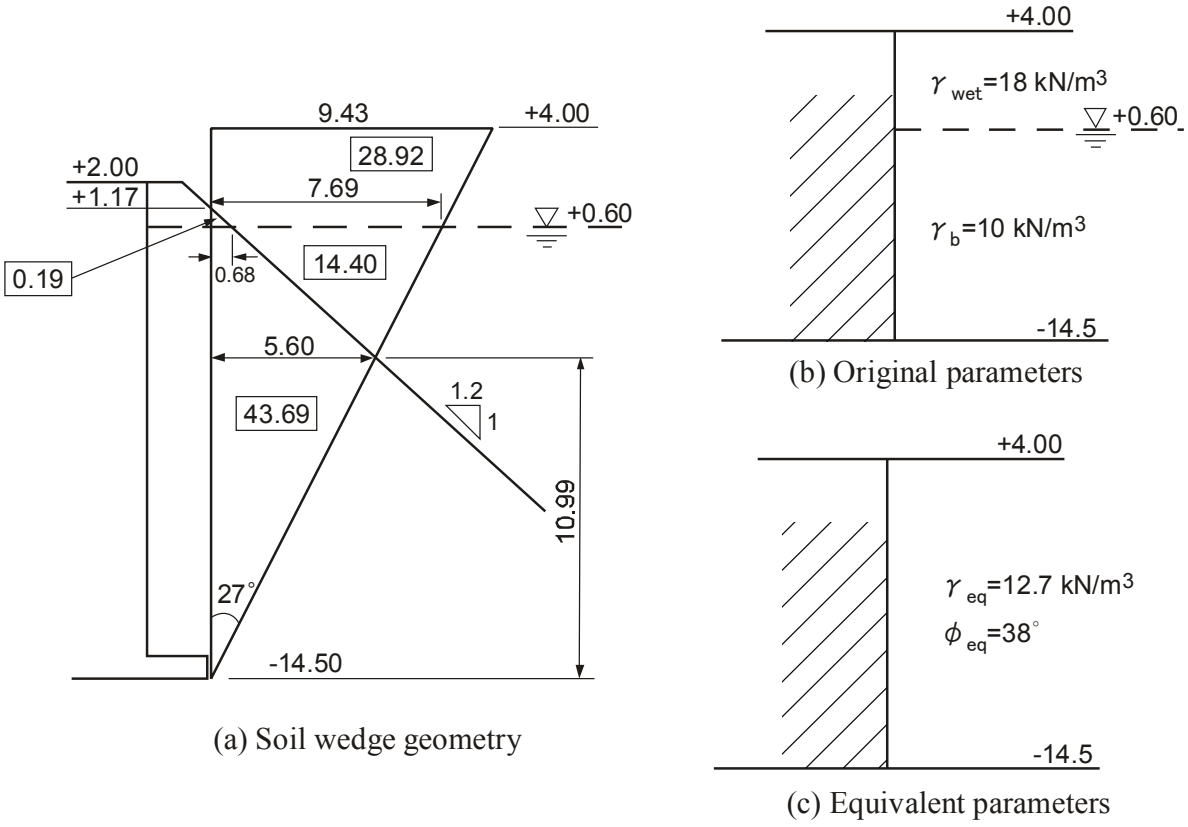

Figure 60 — Diagram for evaluating average values (after PIANC, 2001)

Assuming that half the operational surcharge is present during the earthquake, the modified seismic coefficient is derived as Kh'=0.22.

The dynamic active earth pressure coefficient of the Mononobe-Okabe method is found as:

$$K_{ae} = \frac{\cos^2(\phi - \psi)}{\cos\psi \cos(\psi + \delta)\left[1 + \sqrt{\frac{\sin(\phi + \delta)\sin(\phi - \psi)}{\cos(\delta + \psi)}}\right]^2} = 0.356$$

Note the seismic inertia angle, ψ, is defined by the following equation in the uniform field of horizontal and (downward) vertical accelerations, $k_h g$ and $k_v g$.

$$\psi = \tan^{-1}\left[\frac{k_h}{1 - k_v}\right]$$

The total earth thrust is now

$$P_{ae} = K_{ae}\frac{1}{2}\gamma_d\ (1 - k_v)H^2 = 806.6 \text{ kN/m}$$

where γ_d is the unit weight of the dry backfill.

This gives a horizontal force: $P_{ae}\cos\delta = 806.6 \times \cos 15^\circ = 779.1 \text{kN/m}$

at about 0.45×18.50=8.33m above the –14.50m elevation, and a vertical contribution

$P_{ae}\sin\delta = 806.6 \times \sin 15^\circ = 208.8 \text{kN/m}$ at the interface between structure and soil.

(2) Hydrodynamic force

The hydrodynamic force in front of the wall gives a horizontal force according to Westergaard's expression:

$$P_{dw} = \frac{7}{12}k_h \gamma_w H_w^2 = 187.6 \text{kN/m}$$

at $0.4 \times 14.5 = 5.8\text{m}$ above the -14.50m elevation.

Note where γ_w is the unit weight of seawater and H_w is the water depth, and the point of application of this force lies 0.4 H_w above mud-line. (Westergaard, 1933)

(3) Inertia and other driving forces

The wall inertia forces are estimated as follows:

cap $11.60 \times 2 \times 18 \times 0.15 = 62.6 \text{ kN/m}$ at 17.50m above bed (-14.5m)

caisson $11.60 \times 16.00 \times 21 \times 0.15 = 584.6 \text{ kN/m}$ at 8.50m above bed

footing $15.60 \times 0.5 \times 21 \times 0.15 = 24.6 \text{ kN/m}$ at 0.25m above bed

The backfill inertia force:

$2.0 \times 18.0 \times 18 \times 0.15 = 97.2 \text{ kN/m}$ at 9.50m above - 14.50m

The static bollard pull can be taken into account by reducing its value by 50%:

$50\% \times 20 = 10\,\text{kN/m}$ at 19.0m above - 14.50m

(4) Vertical forces

The resisting forces and their points of application are determined as follows (Point A is indicated in Figure 61):

cap $11.60 \times 2.0 \times 18 = 417.6\,\text{kN/m}$ at 7.8m from A

caisson $11.60 \times 1.70 \times 21 = 414.1\,\text{kN/m}$ at $\frac{11.6}{3} \times \frac{2 \times 1.40 + 2}{1.40 + 2.0} + 2 = 7.46\text{m}$ from A

$11.60 \times 14.30 \times 11 = 1824.7\,\text{kN/m}$ at 7.8m from A

footing $15.60 \times 0.50 \times 11 = 85.8\,\text{kN/m}$ at 7.8m from A

Using the backfill stone area above the water table = $\frac{1}{2} \times 0.83(1+2) + 2 \times 0.57 = 2.39\text{m}^2$, the backfill equivalent unit weight above water table is determined as

$\{20 \times 2.39 + 18 \times (2 \times 3.40 - 2.39)\} / 6.80 = 18.7\,\text{kN/m}^3$

$2.0 \times 3.40 \times 18.7 = 127.2\,\text{kN/m}$ at 14.60 m from A

$2.0 \times 13.40 \times 10 = 268\,\text{kN/m}$ at 14.60 m from A

The hydrostatic pressure due to the variation of water table gives the following forces:

$\frac{1}{2} \times 0.6^2 \times 10.2 = 1.8\,\text{kN/m}$ at $\frac{1}{3} \times 0.60 + 14.50 = 14.70\text{m}$ above -14.50m

$14.50 \times 0.60 \times 10.2 = 88.7\,\text{kN/m}$ at 7.25m above -14.50m

Uplift $\frac{1}{2} \times 0.60 \times 10.2 \times 15.60 = 47.7\,\text{kN/m}$ at $\frac{2}{3} \times 15.60 = 10.40\text{m}$ from A

It is noted that the hydrostatic pressure distribution depends on the permeability of the foundation and backfill rubble. If the latter has a much lower permeability than the former, then no uplift force is generated and the pressure diagram at the back face dies off linearly to the foundation level AB.

(5) Force and moment balance

The various forces mentioned previously act on the structure. (815a) The stabilizing moments with respect to point A are able to be calculated. The overturning moments with respect to the same point are also can be calculated. Thus, the factor of safety against overturning is

$$F_{so} = {}^{29,858.0}\!\!\diagup\!\!_{15,927.9} = 1.87$$

Depending on the definition of this factor of safety and when a non-zero angle of friction between the backfill and the wall back face is assumed, one can take the overturning moment of the earth thrust before analysing it into vertical and horizontal components.

The factor of safety against sliding is

$$F_{ss} = 3{,}298.5 \times \mu_b \diagup 1{,}836.2$$

where $\mu_b \approx \tan 31^\circ = 0.6$

Thus, $F_{ss} = 1.08$

Thus, the proposed cross section is likely to satisfy the seismic performance requirements at L1 earthquake motion. Note, in actual design, performance requirement at L2 earthquake motion should be calculated either, however, due to the fact that the effect of liquefaction is difficult to be considered in pseudo static approach, only the L1 earthquake motion cases is shown in this design example.

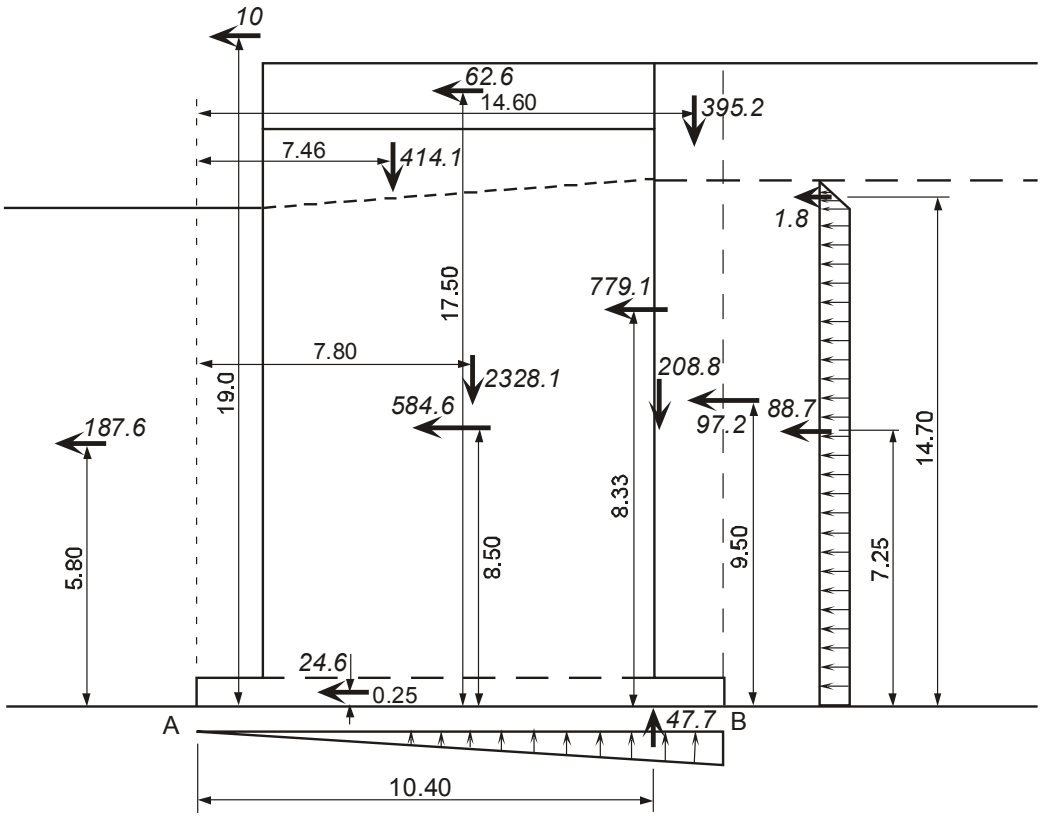

Figure 61 — Load assigning to the structure during earthquake (after PIANC, 2001)

5.1.1.11 Detailed equivalent static analysis

Detailed equivalent static analysis is not conducted in this example. (821A, 821B, 821C, 821a, 822A, 822B, 823A)

5.1.1.12 Simplified dynamic analysis

Simplified equivalent static analysis is not conducted in this example. (911A, 911B, 911C, 911a, 912A, 912B, 913A, 914a)

5.1.1.13 Detailed dynamic analysis

The cross section of the gravity quay wall was idealized into plane strain finite elements shown in Figure 62. Element size was defined small enough to allow seismic wave propagation of up to 2Hz throughout the analysis, including the liquefaction state. In order to simulate the incoming and outgoing waves through the boundaries of the analysis domain, equivalent viscous dampers were used at the boundaries. The effect of the free field motions was also taken into account by performing one dimensional response analysis at the outside fields, and assigning the free field motion through the viscous dampers. Before the earthquake response analysis, a static analysis was performed with gravity under drained conditions to simulate the stress conditions before the earthquake. The results of the static analyses were used for the initial conditions for the earthquake response analyses. (921A)

The firm ground motion is given as seismic actions for the global computational model. The ground motion is determined by a site-specific study as described in the Section 6. In this example, a recorded motion at the site similar geotechnical condition (reclaimed land on deep alluvial clay layer) was used with modification of amplitude scales. (921B, 921C)

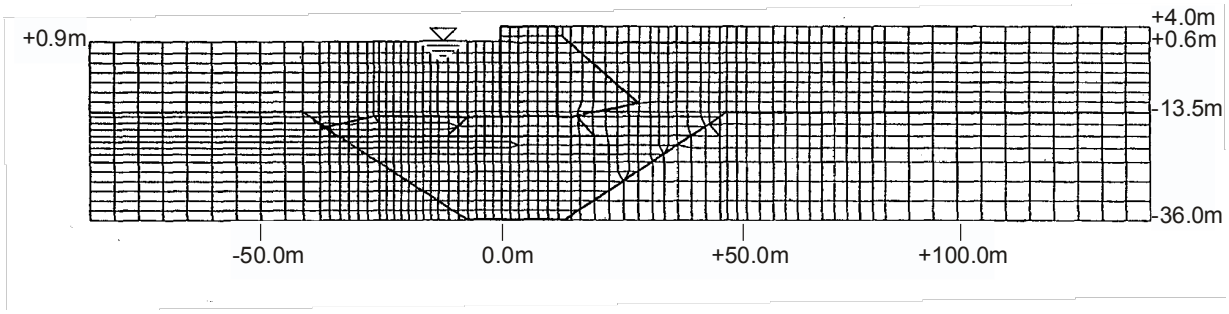

Figure 62 — Finite element mesh (after PIANC, 2001)

Concrete caisson was modelled by linear elements, with soil-structure interfaces modelled by joint elements as shown in Figure 63. The parameters are shown in Table 7. The seawater in front of the caisson was modelled as an incompressible fluid.

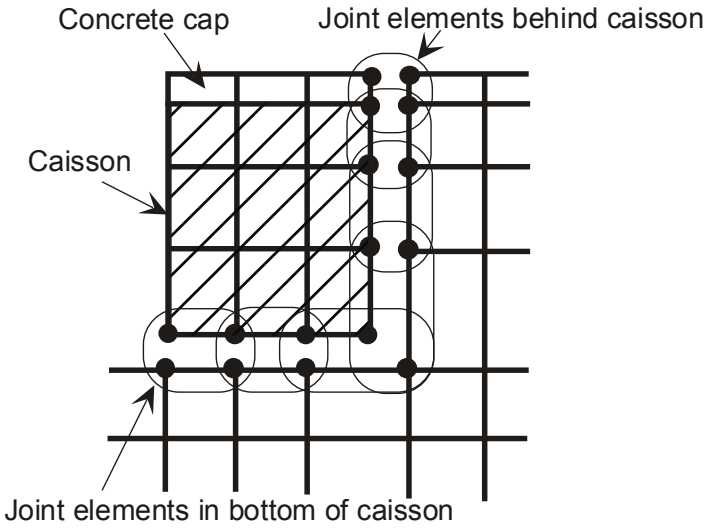

Figure 63 — Modelling of caisson structures (after PIANC, 2001)

Parameters for soil elements were calibrated based on the results of the geotechnical investigation. It should be noted that appropriate characterization of pore water pressure build-up and the increase in shear strain amplitude are important for parameter calibration, since these undrained cyclic properties significantly affect the degree of deformation of the soil-structure system. Damping characteristics of the soil profile were also carefully evaluated. The constitutive model for soil can consider the effect of liquefaction phenomena. (Iai et al., 1992)(921D, 922A)

Seismic analysis was performed for the four alternatives shown in Figure 58 over L1 and L2 earthquake motions. Computed residual deformations of the quay wall for Cases 1 and 4 for L2 earthquake motion are shown in Figure 64. The results of the analysis are summarized in Figure 65. Although all the alternatives satisfy the criteria for tilting as shown in Figure 65(b), only Case 1 satisfied the horizontal displacement criteria as shown in Figure 65(a). The remaining criteria with for differential settlement between apron and non-apron areas for L1, as shown in Table 6, are also satisfied by Case 1. Consequently, Case 1 was proposed as the recommended design.

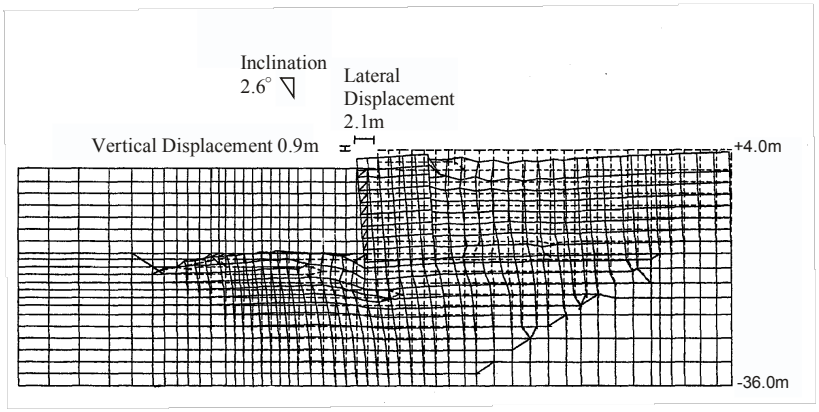

(a) Alternative case 4

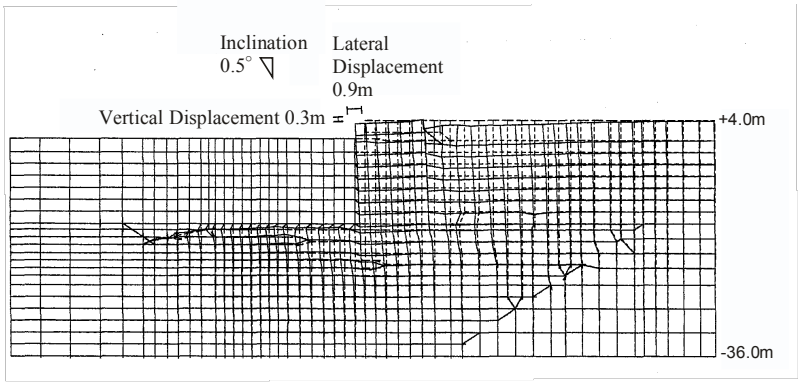

(b) Alternative case 1

Figure 64 — Computed residual deformation (after PIANC, 2001)

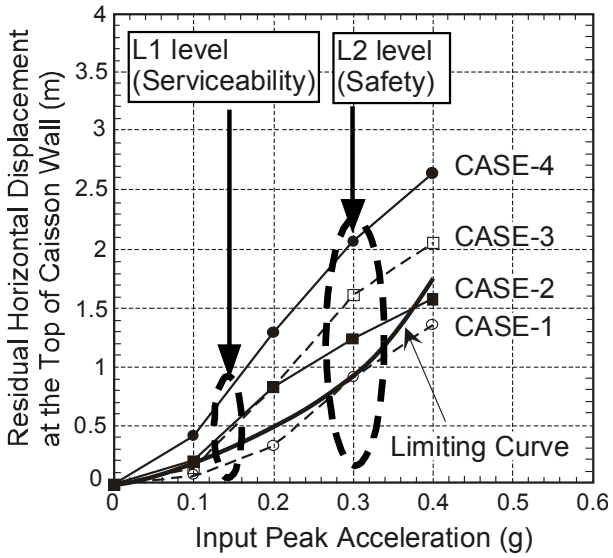

(a) Residual horizontal displacement

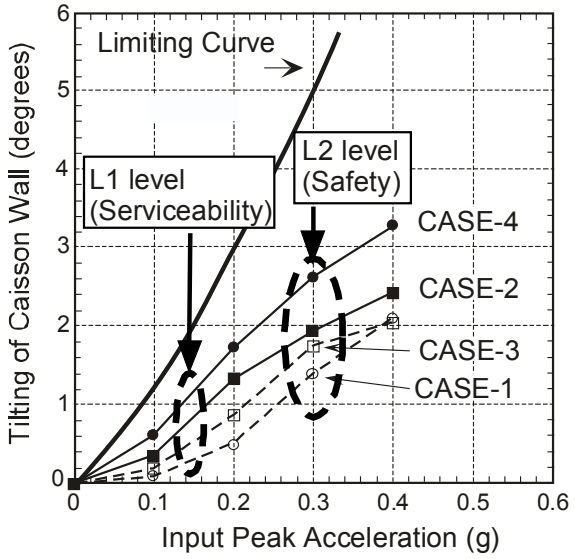

(b) Tilting

Figure 65 — Seismic response and limiting curve for acceptable damage (after PIANC, 2001)

5.1.2 Highway bridge pile foundation

5.1.2.1 Outline of the highway bridge

The highway bridge is composed of two nine-span continuous double plate girder bridges with length of 315m and 360m (Figure 66). The bridge with parallel up- and down-bound lanes is seismically isolated using seismic isolation bearings for longitudinal and transverse supports. Bridge piers are composed of an overhanging single reinforced concrete column of rectangular cross section, which is supported on a foundation of 1200-mm-diameter cast-in-place concrete piles.

Figure 67 shows the distribution of elastic S-wave velocities at the erection site obtained by elastic wave inspection, and the characteristics of dynamic deformation of soil materials constituting respective layers. (715A) There exist soft soils at the erection site. Approximately nine meters of alluvium at the surface overlies diluvium with an alternation of cohesive and sandy soil layers. Hard ground, at the engineered bedrock

surface, is found continuously at a depth of 50m or below. Approximately nine meters of alluvium are composed of approximately 5.5m of sandy soil layer, 1.0m of cohesive soil layer and 2.5m of sandy soil layer. According to the Specifications for Highway Bridges, liquefaction is likely to occur. (631B)

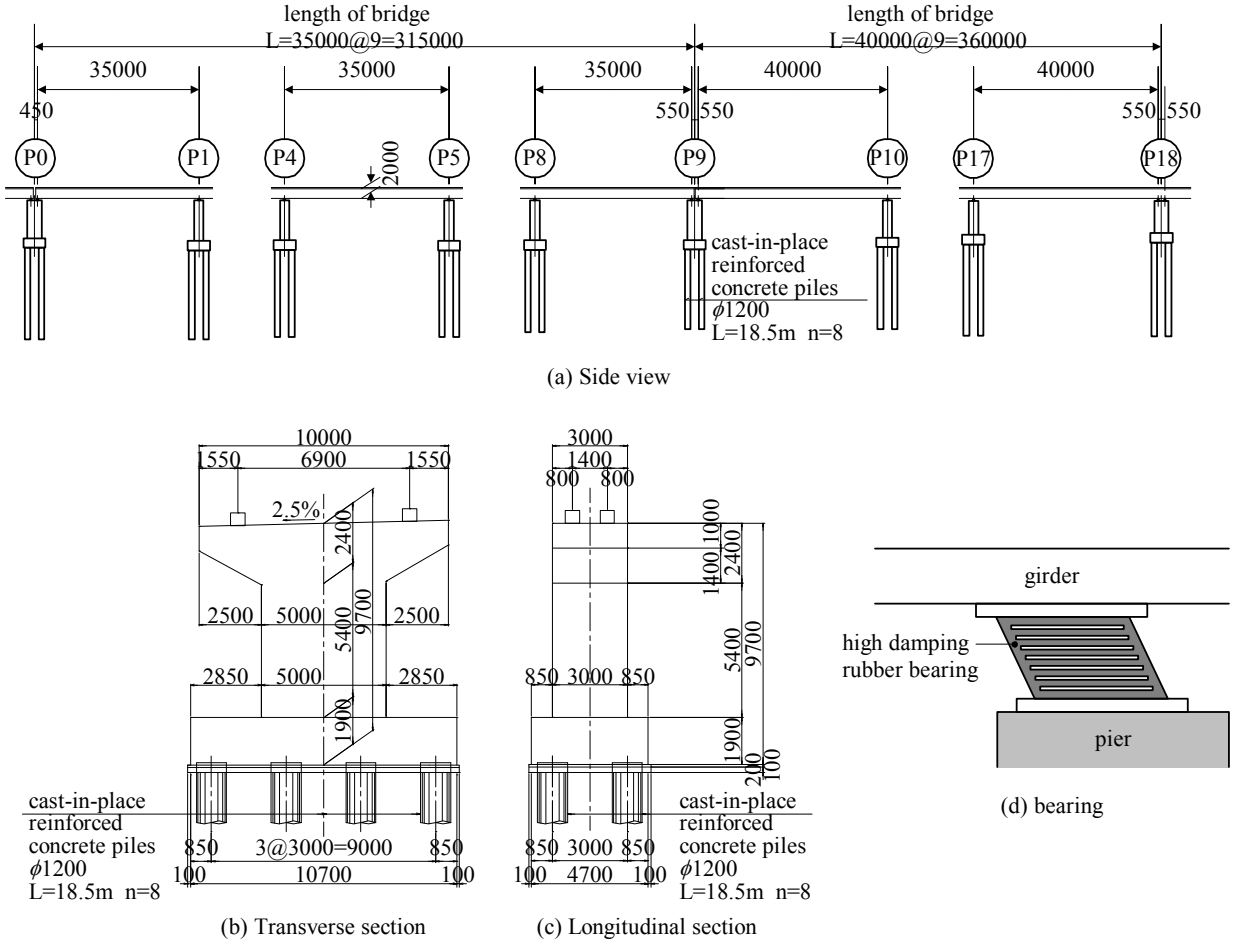

Figure 66 — Seismic isolation bridge

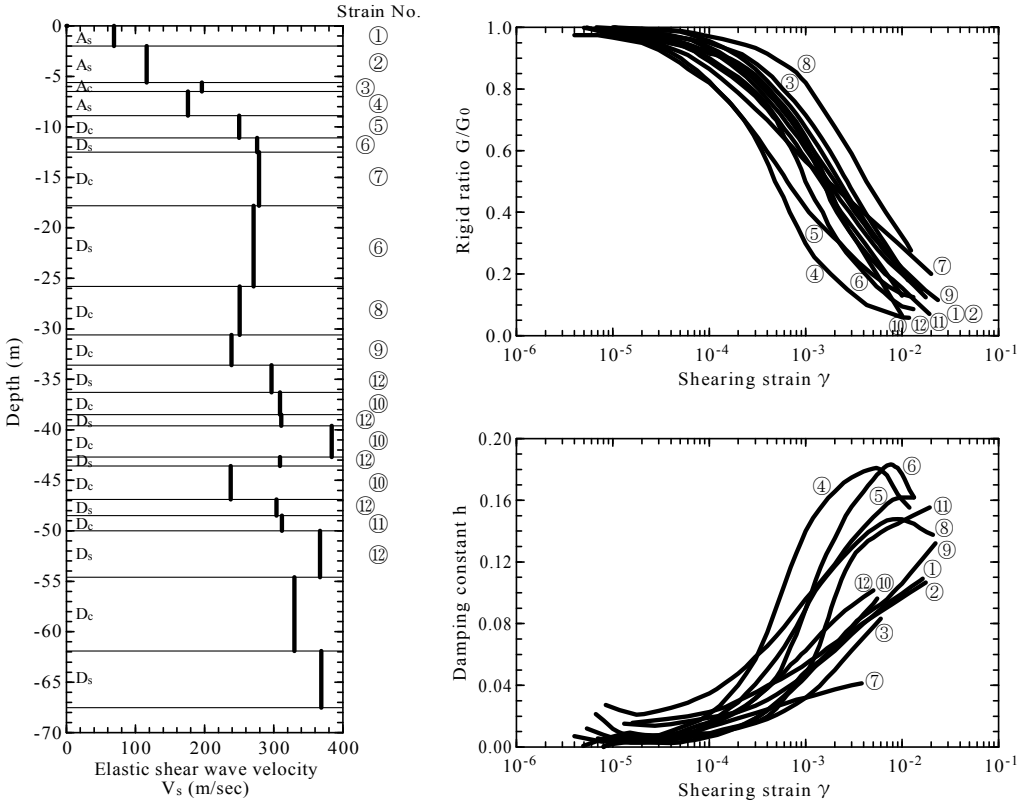

Figure 67 — Soil profile and strain-dependent characteristics

5.1.2.2 Seismic performance requirements

The bridge is designed in accordance with the Specifications for Highway Bridges (2002). The bridge is classified as Class-B in terms of importance based on the Specifications (Table 9). (511A) The seismic ground motions that should be considered in seismic design and the seismic performance requirements for Class-B bridges are listed in Table 10. Level-1 ground motion is highly likely to occur during the service life of the bridge. A ground motion of medium-size earthquake that are highly likely to occur is assumed. The probability of Level-2 ground motion occurring during the service life of the bridges is very low but the intensity of the ground motion is high. The ground motions induced by great inter-plate earthquakes with low frequency of occurrence and that caused by earthquakes in the epicentral area with an extremely low frequency such as the Hyogoken-Nambu Earthquake of January 17, 1995 were taken into consideration. (513A) Seismic performance levels 1 and 2 shown in Table 10 are defined as shown in Table 11.

Table 9 — Classification of importance of bridges[1)]

Class	Definitions
Class A bridges	Bridges other than Class B bridges
Class B bridges	Bridges of National expressways, urban expressways, designed city expressways, Honshu-Shikoku highways, and general national highways. Double-section bridges and overpasses of prefectural highways and municipal roads, and other bridges, highway viaducts, etc., especially important in view of regional disaster prevention plans, traffic strategy, etc.

Table 10 — Design Earthquake Ground Motions and Seismic Performance of Bridges[1)]

<table>
<tr><td colspan="2">Earthquake Ground Motions</td><td>Class A Bridges</td><td>Class B Bridges</td></tr>
<tr><td colspan="2">Level 1 Earthquake Ground Motion
(highly probable during the bridge service life)</td><td colspan="2">Keeping sound functions of bridges
(Seismic Performance Level 1)</td></tr>
<tr><td rowspan="2">Level 2 Earthquake Ground Motions</td><td>Type I earthquake Ground Motion (an plate boundary type earthquake with a large magnitude)</td><td rowspan="2">No critical damages
(Seismic Performance
Level 3)</td><td rowspan="2">Limited seismic damages and capable of recovering bridge functions within a short period
(Seismic Performance Level 2)</td></tr>
<tr><td>Type II earthquake Ground Motion (an Inland direct strike type earthquake like Hyogo-ken Nambu earthquake)</td></tr>
</table>

Table 11 — Seismic Performance of Bridges[1)]

<table>
<tr><td rowspan="2">Seismic Performance</td><td rowspan="2">Seismic Safety Design</td><td rowspan="2">Seismic Serviceability Design</td><td colspan="2">Seismic Repairability Design</td></tr>
<tr><td>Emergency Repairability</td><td>Permanent Repairability</td></tr>
<tr><td>Seismic Performance Level 1:
Keeping the sound functions of bridges</td><td>To ensure the safety against girder unseating</td><td>To ensure the normal functions of bridges</td><td>No repair work is needed to recover the functions</td><td>Only easy repair works are needed</td></tr>
<tr><td>Seismic Performance Level2:
Limited damages and recovery</td><td>Same as above</td><td>Capable of recovering functions within a short period after the event</td><td>Capable of recovering functions by emergency repair works</td><td>Capable of easily undertaking permanent repair works</td></tr>
<tr><td>Seismic Performance Level 3:
No critical damages</td><td>Same as above</td><td>—</td><td>—</td><td>—</td></tr>
</table>

Seismic performance levels were determined in terms of safety, serviceability and repairability from a viewpoint of seismic design. Both short- and long-term repairabilities were considered. For Class-B bridges, soundness should be maintained against level-1 ground motion, and seismic damage should be limited and the bridge should be designed to restore foundations quickly. (512a, 512b) Figure 67 shows limit states of members of seismic isolation bridge (Figure 66) that are required to achieve seismic performance Level 2 shown in Table 11. Seismic isolation bearings should be designed exclusively to behave nonlinearly. Bridge piers and foundations should be designed to have secondary plasticity. Seismic isolation bearings should be made to behave nonlinearly only to absorb the energy of bearings. Secondary plasticity of reinforced concrete bridge piers means that strain exceeding the yield strain occurs in the plastic hinge region at the base of the pier but lateral displacements at the locations of bridge piers subjected to the inertia force of superstructure are below the allowable displacements in seismic design. In the case of foundations, secondary plasticity means that no explicit point of inflection should appear in the load-displacement relationship and foundations should not yield even if a strain exceeding the yield strain occurs in the axial reinforcement in a cross section. The shear occurring in piles should be less than the shear strength of piles. The yielding of foundations is defined as one of the following states. (514A, 514B, 514C)

1) State where all piles yield

2) State where the reaction of heads of a row of piles reaches the upper limit of resistance to penetration

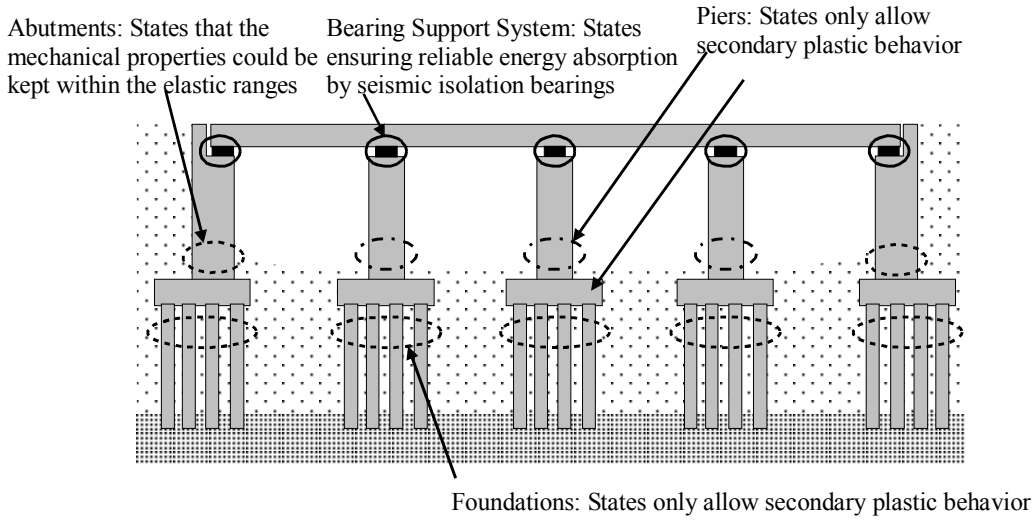

Figure 68 — Combination examples of members with consideration of plasticity or Non-linearity[1)]

5.1.2.3 Input ground motions used in seismic design and analysis model of the entire bridge

The Specifications for Highway Bridges define design ground motion as surface acceleration response spectrum with a damping factor of 5 %. For the seismic isolation bridge constructed in soft ground, the possibility of response with surface layer was pointed out. An incident wave, equivalent to Level-2 ground motion, into the engineered bedrock surface was therefore determined and used as an input ground motion to obtain surface acceleration wave considering the nonlinearity of surface ground. The surface acceleration wave was also used in seismic design of the bridge. (633A) A check was made to determine whether the bridge designed to resist design ground motion (defined at the surface level) specified in the Specifications for Highway Bridges could prove to be resistant also to the ground motion generated based on the geological conditions at the erection site and the nonlinear response of surface ground. (520A, 631A)

Figure 69 shows surface ground motions specified in the Specifications for Highway Bridges. The figure shows a ground motion induced by a great marine earthquake at the boundary between plates (Type I) and another caused by a magnitude-7-class earthquake in the epicentral area that occurs with an extremely low frequency like the 1995 Hyogoken-Nambu Earthquake (Type II). There were tree waves with the same acceleration response spectrum both for Types I and II. The average of maximum responses of three waves was used in seismic design either for Type I or II. This is because it was taken into consideration that nonlinear seismic response varied according to the phase of ground motion even where elastic acceleration response spectrum was the same. (623B)

Figure 70 shows examples of incident waves into the engineered bedrock surface (outcrop wave: 2E). For the incident wave into the engineered bedrock surface, three waves with the same elastic acceleration response spectrum were used for different ground motions. (623B)

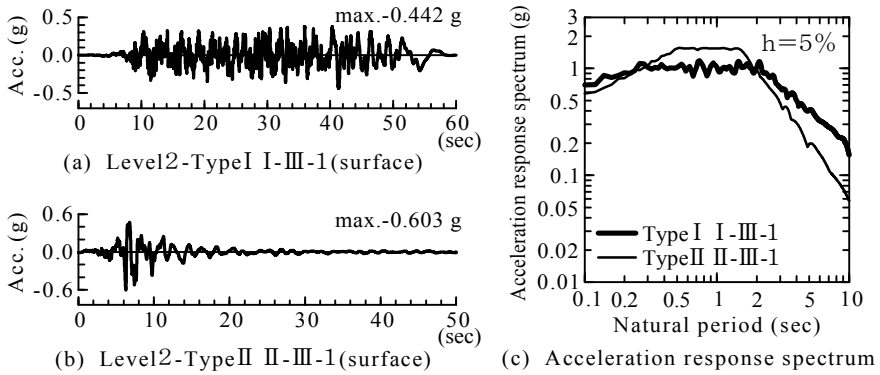

Figure 69 — Design earthquake ground motions (Time history acceleration waveform of Level2)

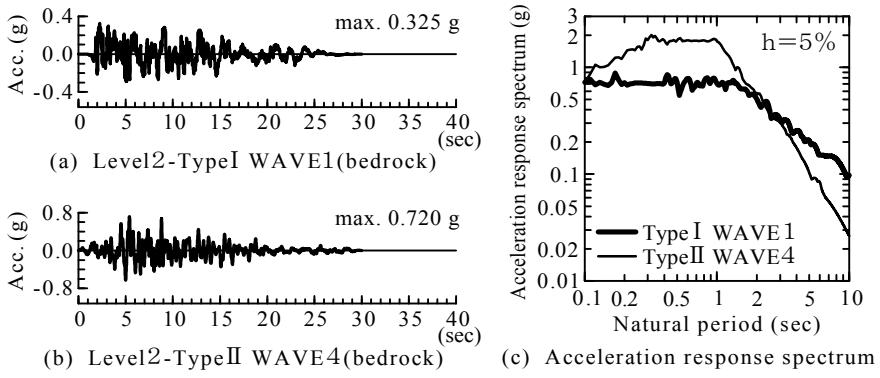

Figure 70 — Time history acceleration waveform of Level2 (Incident wave, 2E)

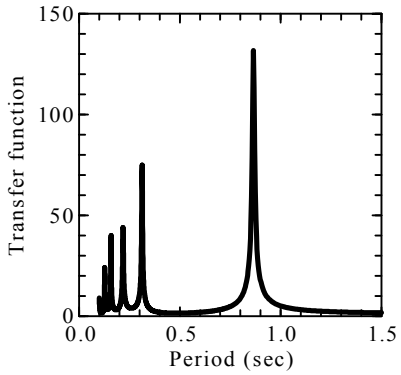

Figure 71 — Transfer function of surface layer

The acceleration waveforms shown in Figures 69 and 70 are simulated ground motions. The ground motions were obtained by selecting from recorded strong motions such ground motions as had acceleration response spectrum similar to design ground motion (acceleration response spectrum that should be achieved) and

adjusting the Fourier amplitude so that the acceleration response spectrum of the observed waveform could approximate the design ground motion while leaving the phase of observed waveform unchanged.

The incident waves shown in Figure 70 were applied to the surface layer shown in Figure 67 and a nonlinear dynamic analysis was made of the ground. The nonlinearity of the ground was represented by hyperbolic model (modified H-D model) using the dynamic deformation characteristics shown in Figure 67. Figure 71 shows frequency response function for the surface layer calculated using the initial stiffness obtained from the elastic S-wave velocities shown in Figure 67, and the damping factor at shear strain $\gamma=10^{-6}$. The predominant period was 0.87 second. It is clear that seismic response of surface layer to level-2 ground motion becomes nonlinear and the predominant period becomes longer, and there is a possibility of the ground resonating with the seismic isolation bridge. Figure 72 shows the distribution of maximum response accelerations obtained by nonlinear dynamic analysis of the ground. Figure 73 shows surface acceleration waveforms. Liquefaction was expected in the ground as described earlier, but the objective was to calculate surface acceleration waveforms. Total stress analysis was therefore made of the ground without considering the effects of liquefaction so that large response acceleration waveforms could be obtained at the surface level.

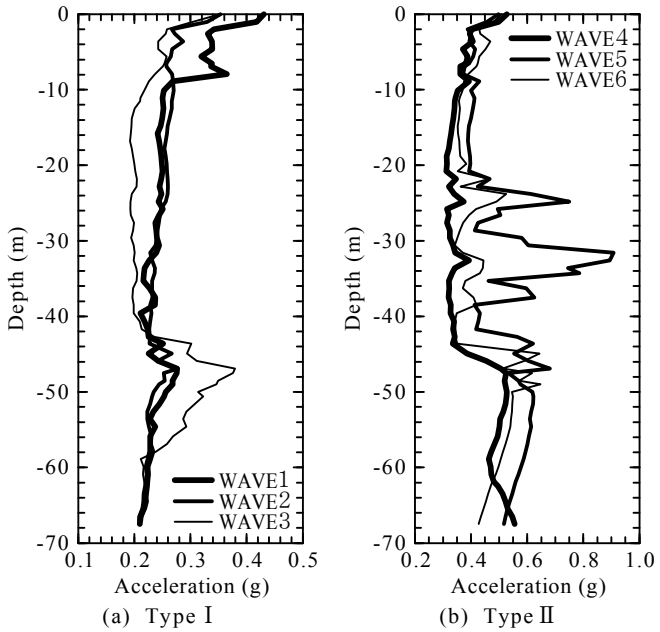

Figure 72 — Distribution of acceleration

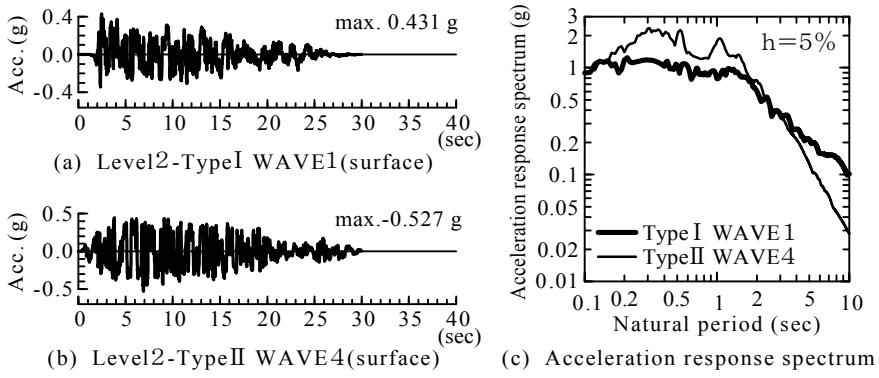

Figure 73 — Acceleration time history of ground motion at surface

The surface ground motions shown in Figures 69 and 8 were applied to the sway-rocking spring of a model of the entire bridge system (Figure 74) to make dynamic analysis. (911A, 911C) A bilinear model and a stiffness-degrading peak oriented model (Takeda model) were used to represent the seismic isolation bearings and reinforced concrete bridge piers, respectively to express their nonlinearity (Figure 75).

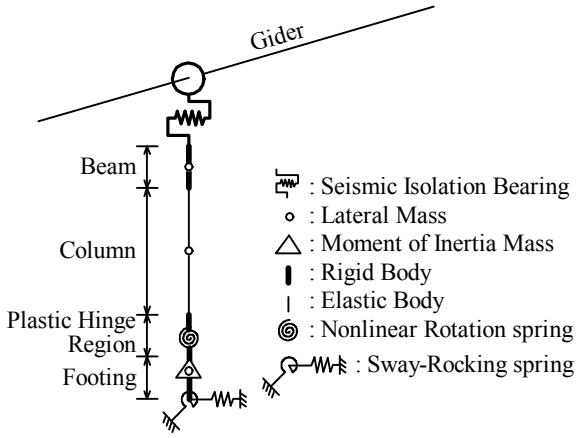

Figure 74 — Analytical model of seismic isolation bridge(Global bridge model)

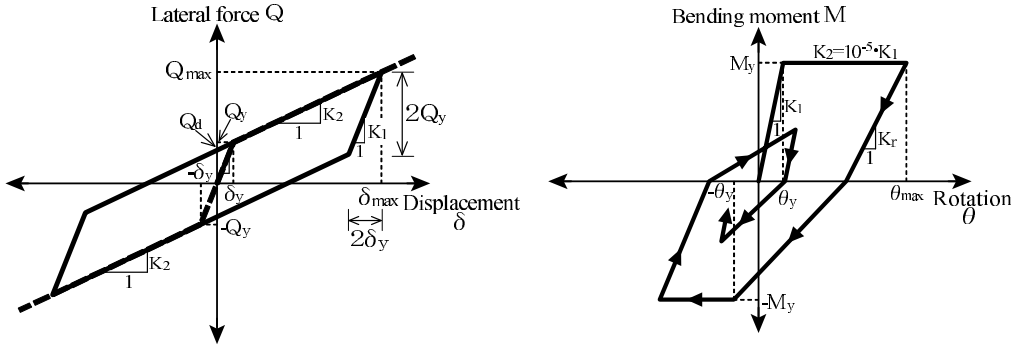

a) Seismic isolation bearing **b) RC column**

Figure 75 — Analytical model of seismic isolation bridge

5.1.2.4 Seismic design of foundations

Figure 76 shows a flow of design of pile foundations of the highway bridge. Shown here are the results for level-1 and –2 ground moti0ns. (711A, 711B, 712A)

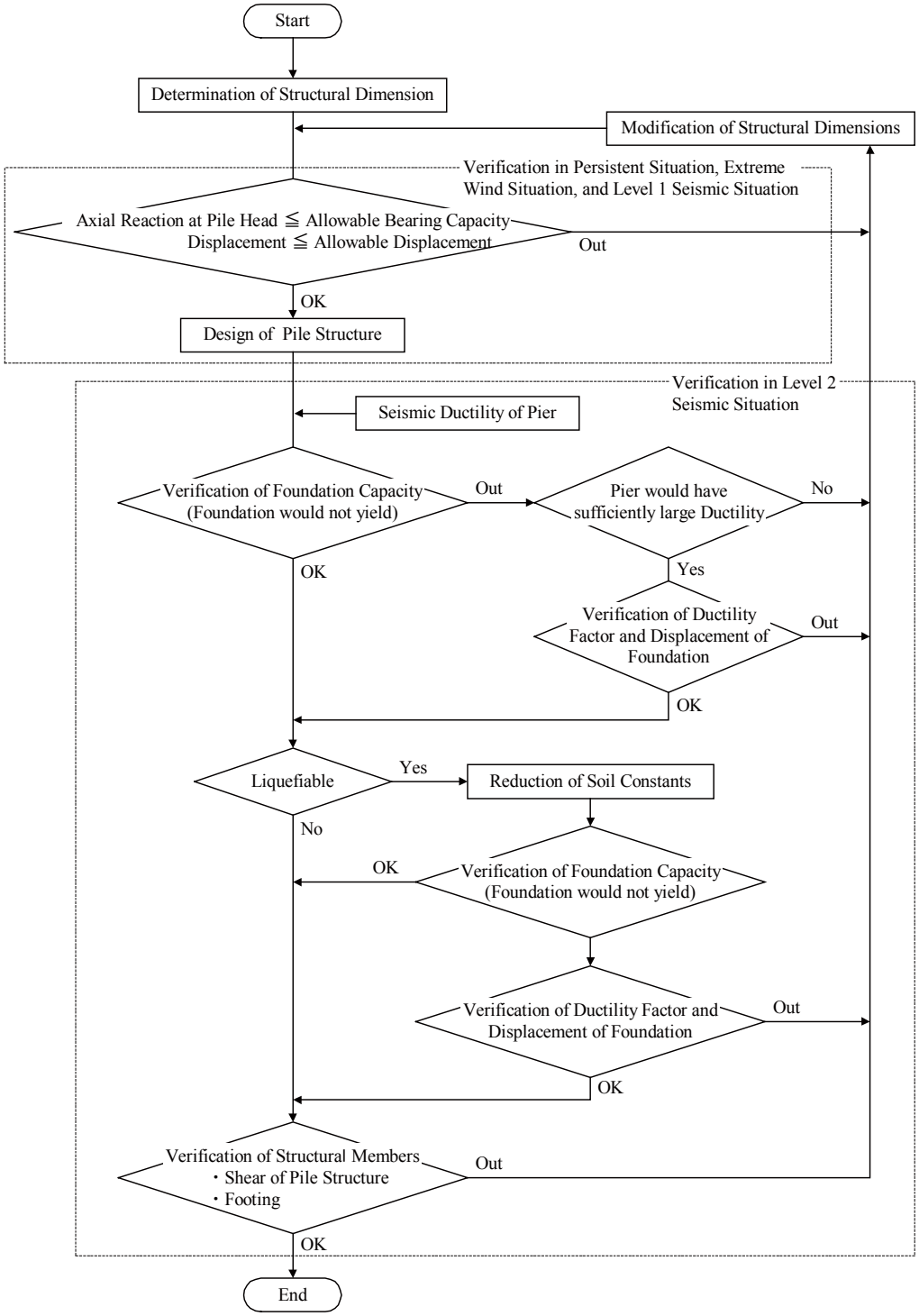

Figure 76 — Design calculation flowchart for pier pile foundations[2)]

5.1.2.4.1 Considerations of the effects of liquefaction in seismic design

Liquefaction was expected to occur during an earthquake in the alluvial sandy layer at the bridge erection site because the following three conditions were found. The factor of liquefaction (F_L) was therefore used to determine whether liquefaction would occur or not.

a) The groundwater level was within 10m below the surface ground, and the alluvial sandy layer was a saturated soil layer within 20m below the ground surface.

b) The fine particle content (FC) was 35 % or less, or the index of plasticity IP was 15 or less even where FC was higher than 35 %.

c) The mean diameter of soil particle D_{50} was 10mm or less and 10% diameter of soil particle D_{10} was 1mm or less.

Whether liquefaction would occur or not was determined by a simple method using the factor of liquefaction (F_L) expressed by

$$F_L = \frac{R}{L} = \frac{\text{dynamic shear strength ratio}}{\text{seismic shear stress ratio}} = \frac{c_W \cdot R_L}{\gamma_d \cdot k_{hg} \cdot \sigma_v / \sigma_v'} \tag{34}$$

where, c_W :correction factor based on the characteristics of ground motion, R_L :repeated triaxial strength ratio, γ_d :factor of reduction of seismic shear stress ratio in the vertical direction, k_{hg} :design lateral seismic factor of level-2 ground motion at the surface level, σ_v :total overburden pressure, and σ_v' :effective overburden pressure. Repeated triaxial strength ratio R_L varied greatly according to the characteristics of repetition of ground motions, so it was corrected using correction factor c_W according to the characteristics of Type-I or –II ground motion.

The factor of liquefaction F_L (equation 34) of fine sand deposited at a depth of 5.5m from the surface (borehole log in Figure 67) was 0.32 for Type-I ground motion or 0.35 for Type-II ground motion. Then, Liquefaction was determined to occur that could affect the bridge. The soil parameter was therefore multiplied by factor of reduction D_E for seismic design considering the effects of liquefaction. Factor of reduction D_E varied according to the factor of liquefaction, F_L. In this study, $D_E = 1/6$ for Level-2 ground motion and $D_E = 1/3$ for Level-1 ground motion.

5.1.2.4.2 Seismic design of pile foundations against level-1 ground motion

In the seismic design of pile foundations against Level-1 ground motion, the foundations were subjected to lateral force S_{FD}, bending moment M_{FD} and vertical forces W_U, W_P, W_F and W_G that were induced on the bottom surface of footing by inertia forces $k_h \cdot W_u, k_h \cdot W_p$ and $k_h \cdot W_F$, which were obtained by multiplying the weights of superstructure, bridge pier and footing to be supported by the foundations by design lateral seismic coefficient k_h which was uniformly distributed in the vertical direction (Figure 77). In seismic design against level-1 ground motion, check was made whether the axial reaction of pile at pile head was lower than the allowable resistance to penetration or allowable pullout bearing capacity of pile, whether the lateral displacement at pile head was one percent of pile diameter or less (minimum displacement should be 15 mm), and whether the compressive, tensile and shear stresses of pile did not exceed the allowable level. Figure 78 shows the distribution of bending moments in a single pile induced by Level-1 ground motion. The structural specifications for the connection between the pile and footing were determined so that the pile head could work as a rigid structure. In design, the larger of the two bending moments in the cases of rigid and hinged connection at the pile head was used for stress check.

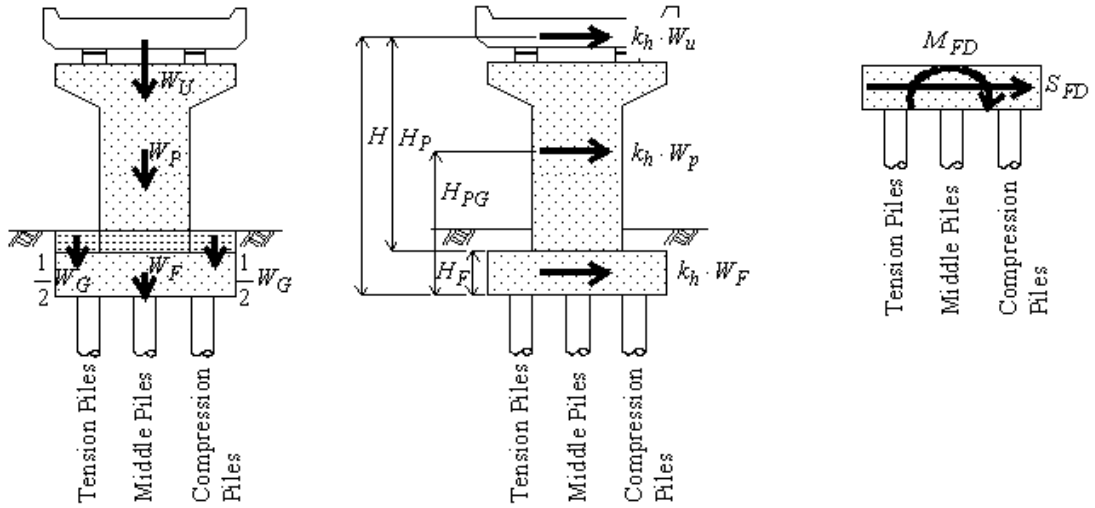

a) Dead weight **b) Inertial force** **c) Design Lateral force and moment at the bottom of a footing**

Figure 77 — Demand for a foundation

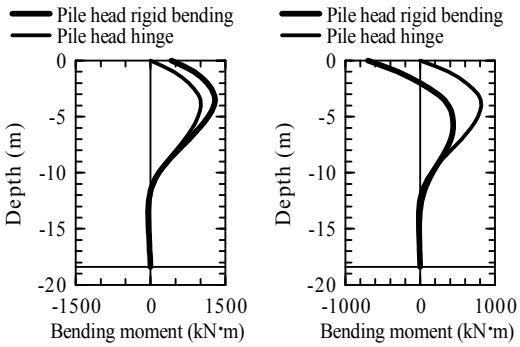

a) Longitudinal **b) Transverse**

Figure 78 — Distribution of bending moment

5.1.2.4.3 Seismic design of pile foundations against level-2 ground motion

In the seismic design of pile foundations against Level-2 ground motion, a model was used that took the nonlinearity of pile and of sway-rocking spring into consideration. One of the following two ground motions was applied to the model based on the results of nonlinear dynamic analysis of the entire bridge system shown in Figure 74 and Figure 75.

(1) Case where seismic response of reinforced concrete piers reaches the plastic area

The bridge pier and the pile foundation including the footing were considered separately (Figure 77). Lateral force and bending moment, equivalent to the ultimate lateral strength of bridge pier, were applied to the footing and underlying pile foundation under a vertical force equivalent to the self weight of the structures overlying the bottom of the footing (Figure 80). In the seismic design of pile foundation based on the ultimate lateral strength of the bridge pier, ground motion obtained by incrementing the lateral force and bending moment, equivalent to the ultimate lateral strength of bridge pier, was used. The measure was taken to control

damage to pile foundation due to strong ground motions. The Specifications for Highway Bridges adopt a factor of increment of 1.1. (811B)

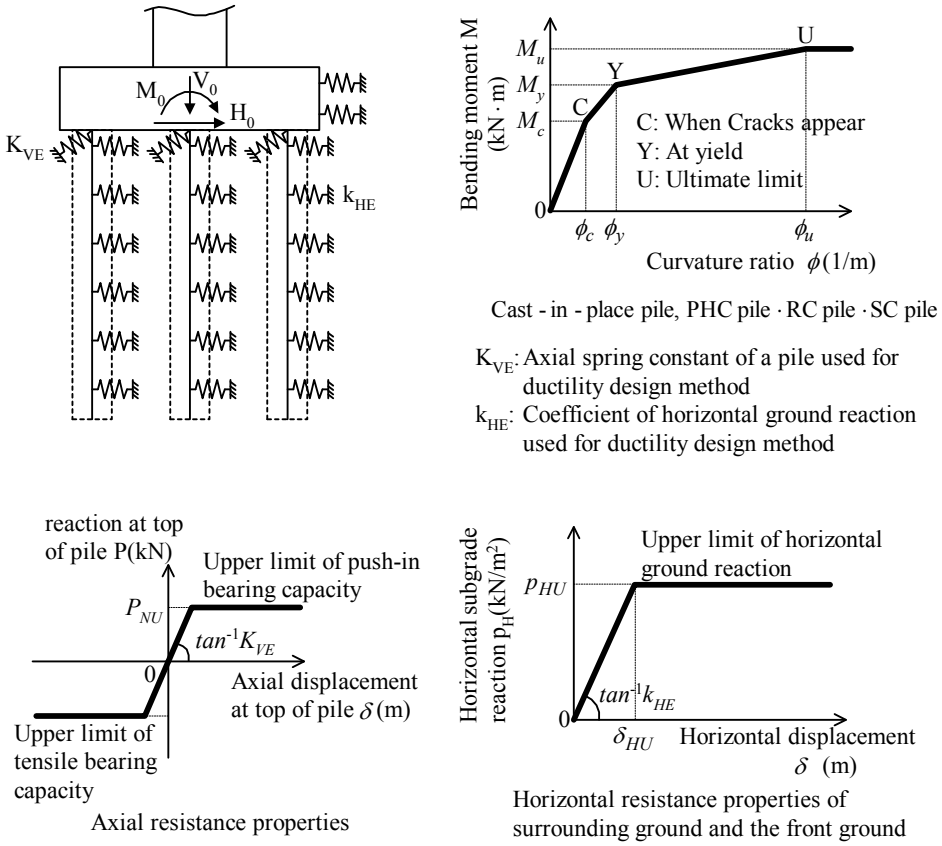

Figure 79 — Analytical model of pile foundations[2)]

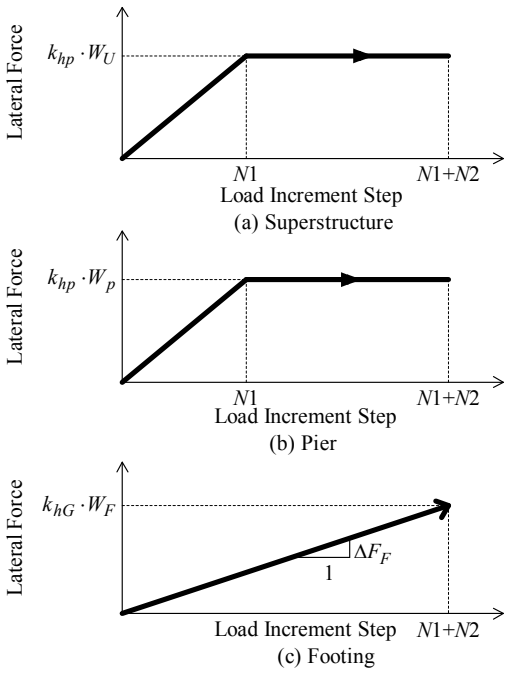

Figure 80 — Loading methods used in pushover analysis

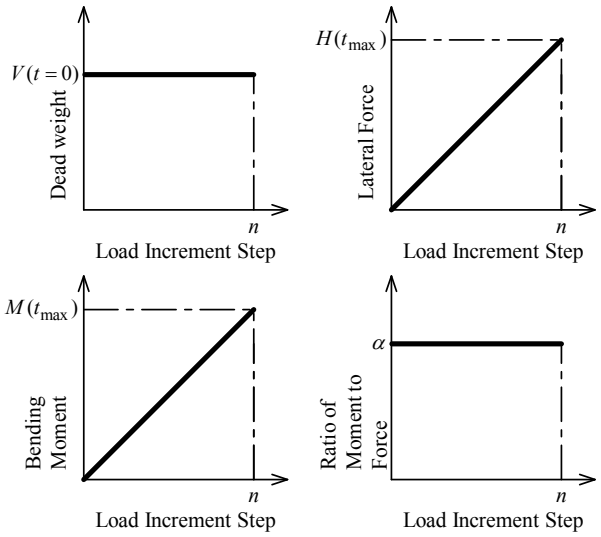

Lateral force and moment at the bottom of a footing

Figure 81 — Loading methods used in pushover analysis

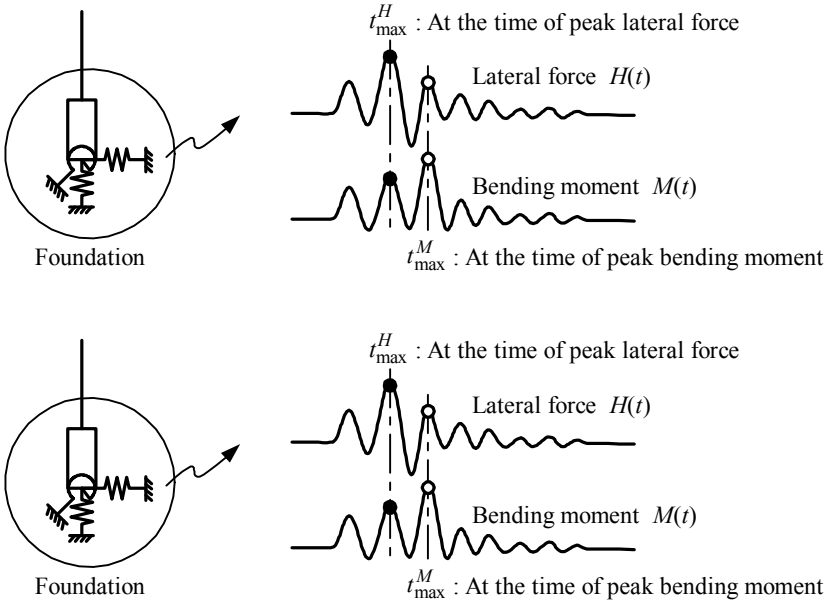

Figure 82 — Dynamic response of the analyzed seismic isolation bridge

(2) Case where the seismic response of reinforced concrete bridge pier is less than the yield response
The vertical force, lateral force and bending moment on the bottom surface of footing obtained in dynamic analysis (Figure82) were used. The vertical force, lateral force and bending moment never reached the maximum level simultaneously. The time when each of the parameters reached the maximum level was therefore considered. (911A, 911C)

a) Time when vertical force V reaches the maximum level $t^{V}_{\max} : V(t^{V}_{\max}), H(t^{V}_{\max}), M(t^{V}_{\max})$

b) Time when lateral force *H* reaches the maximum level $t^{H}_{\max} : V(t^{H}_{\max}), H(t^{H}_{\max}), M(t^{M}_{\max})$

c) Time when bending moment *M* reaches the maximum level $t^{M}_{\max} : V(t^{M}_{\max}), H(t^{M}_{\max}), M(t^{M}_{\max})$

The reinforced concrete bridge piers were positioned at the joints between girders (Figure66). As a result of dynamic analysis of the entire bridge system, it was found that no reinforced concrete bridge piers became plastic either in the longitudinal or transverse direction. The lateral force and bending moment on the bottom surface of footing obtained in dynamic analysis were gradually increased either in the longitudinal or transverse direction while maintaining their relative percentages to check the foundation (Figure81).

The Specifications for Highway Bridges stipulate that the foundations built in the ground where liquefaction is expected to occur should be checked for resistance to Level-2 ground motion in both cases where the effects of liquefaction are considered and ignored.

The results of check at the time when the most critical results were obtained in the check while the effects of liquefaction were ignored are described below. The following lateral force *H* and bending moment *M* were obtained in dynamic analysis. The vertical force *V* occurred owing to the self weight of structural elements overlying the bottom surface of footing and above.

Longitudinal direction: $V - 11{,}043kN, H = 6{,}005kN, M = 38{,}454kN \cdot m$

Transverse direction: $V = 11{,}043kN, H = 7{,}405kN, M = 52{,}924kN \cdot m$

Figure 83 shows the results of gradual increase of vertical force, lateral force and bending moment by the loading method shown in Figure81. Figure83 shows the result of checking of foundation using the lateral load-bearing capacity of foundations during an earthquake in the case where the effects of liquefaction were ignored. The vertical axis indicates the lateral force applied to the foundation, and the horizontal axis indicates the lateral displacement δ_I at the position subject to the inertia force of superstructure expressed by

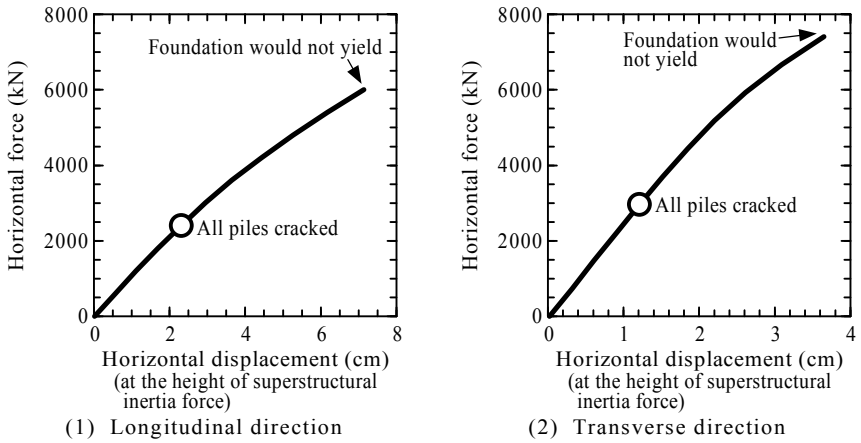

Figure 83 — Load-displacement relation obtained from pushover analysis (Disregard liquefaction)

$$\delta_I = \delta_F + \theta_F \cdot H_I \tag{35}$$

where,

δ_F : Lateral displacement of the foundation at the bottom surface of footing

θ_F : Angle of rotation of the foundation at the bottom surface of footing

H_I : Distance between the bottom surface of footing and the position subject to the inertia force of superstructure.

No explicit point of inflection appeared on the load-displacement curve of the foundation. It is therefore evident that stress did not reach the yield point in the foundation.

The reinforced concrete bridge piers under study did not become plastic in dynamic analysis. In the check of lateral load-bearing capacity of foundations during an earthquake, the vertical force, lateral force and bending moment on the bottom surface of footing obtained in dynamic analysis could be used. No effects of liquefaction were taken into consideration in dynamic analysis using the surface ground motions shown in Figures 69 and 73, and the analysis model shown in Figure 74. Practical methods available are described below.

Method 1: When liquefaction is taken into consideration, the ground motion 1.1 times the ultimate lateral strength of reinforced concrete pier equivalent to the upper limit of inertia of the structural elements overlying the footing, and the inertia of the footing are applied to check the lateral load-bearing capacity during an earthquake. This is because the analysis model shown in Figure 74 is unable to accurately trace the interaction between the seismic isolation bridge and liquefying ground and because seismic behaviour of the ground and bridge in the case of liquefaction has not been identified and the reliability of solutions obtained in analysis has yet to be known.

Method 2: Check is made using the seismic lateral load-bearing force method by applying the vertical force, lateral force and bending moment on the bottom surface of footing of an analysis model shown in Figure75 while considering no effects of liquefaction. This is because it was determined that the strength of surface acceleration wave in the case without liquefaction was higher than that in the case with liquefaction and that the forces acting on the bottom surface of footing due to the ground motion were greater than those during liquefaction.

In either case, the effects of liquefaction are taken into consideration in the lateral load-bearing model of foundation during an earthquake. In this study, the lateral load-bearing capacity during an earthquake was checked while applying ground motion 1.1 times the ultimate lateral load-bearing capacity of reinforced concrete bridge pier and the inertia of the footing shown in method 1 above.

The results of check are shown in Figure 84. It is evident that stress reached the yield point in pile foundation either in the longitudinal or in the transverse direction. In the ultimate state, the foundation of seismic isolation bridge required to achieve seismic performance 2 should have only secondary plasticity (Figure 68). Even in the case where the effects of liquefaction were taken into consideration, therefore, foundations should be designed not to yield. Then, specifications were obtained for pile cross section that could prevent foundations from becoming plastic even where liquefaction was considered. For preventing foundations shown in Figure66 from becoming plastic at the time of liquefaction, 26 D32 axial reinforcing bars (SD345) should be changed to 26 D35 bars.

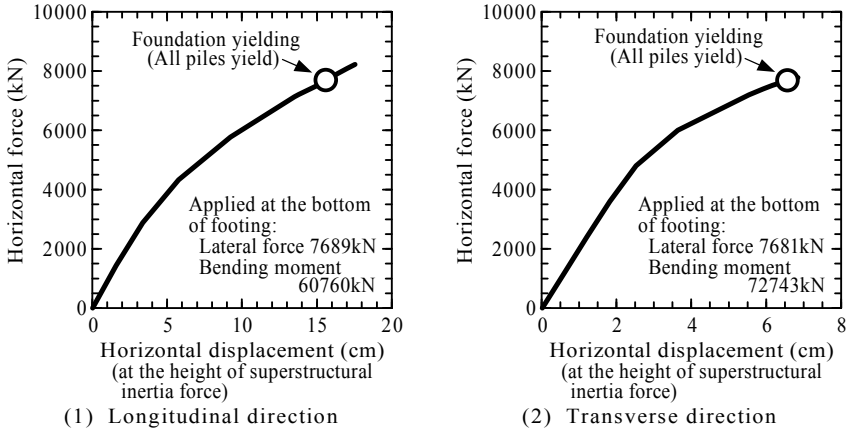

Figure 84 — Load-displacement relation obtained from pushover analysis(Liquefaction)

5.1.3 Assessment of seismic performance of the Sutong Bridge, a long cable-stayed bridge (Pile foundation)

5.1.3.1 Bridge outline

This case study focuses the assessment of seismic performance of the foundation a long cable-stayed bridge [1].

The Sutong Bridge over the Yangtze River is a cable-stayed bridge with a length of 8.2 km, the world longest cable-stayed bridges when completed. It is the main bridge in the project. The cable-stayed bridge requiring no anchorage was adopted over the Yangtze River with a width of several kilo-meters because the ground at the erection site was too soft to support the foundations of long bridges. Figure 85 provides a general view of the cable-stayed bridge. The bridge has a steel main girder and reinforced concrete pylons with a height of approximately 300 m. The multi-pile foundations are of a composite structure consisting of steel pipes and cast-in-place piles.

The natural period of the cable-stayed bridge is approximately 16 seconds in the longitudinal direction. Then, large displacement of the main girder was expected to be caused by longitudinal seismic ground motions. Reducing the displacement on the main girder was a challenge in seismic design. The reinforced concrete pylons as high as 300 m were likely to be subjected not only to their self weight but also to inertia forces caused by seismic ground motions. Ensuring that pile foundations installed to a great depth in soft ground could sufficiently resistant to earthquakes was another challenge in seismic design.

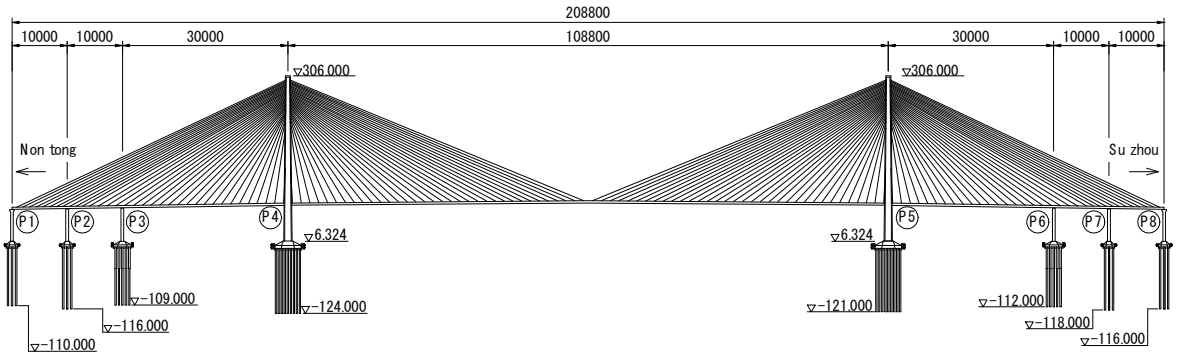

Figure 85 — General arrangement of Sutong Bridge [1]

5.1.3.2 Design seismic ground motion and seismic performance

Table12 lists the design seismic ground motions and seismic performance criteria. Seismic performance was examined to check whether the seismic performance criteria for the bridge could be met or not against seismic ground motions with return periods of 1000 and 2500 years.(512a,512b,513A) The seismic performance criteria shown in Table 12 demand that the response of major members to seismic ground motion with a return period of 1000 years should be less than allowable stress, but allow damage that causes the strain of the axial reinforcement to reach the yield strain for members that are greatly affected by seismic ground motion with a return period of 2500 years such as pylons and foundations.(514A,514B,514C,621A,621B,621C)

The design seismic ground motion acting on the cable-stayed bridge was assessed using a stochastic method.

Table 12 — Design seismic ground motion and seismic performance criteria [1]

Design seismic ground motion	Seismic performance criteria
Serviceability Limit State Ground Motions with high probability of occurrence. : Return period 1000 years.	Keeping sound functions of bridges. No repair work is needed to recover the functions.
Damage-Control Limit State Ground Motions with low probability of occurrence. : Return period 2500 years.	Limited seismic damages and capable of recovering bridge functions within a short period Capable of recovering functions by emergency repair works.

Investigations were made of the activities of earthquakes that occurred inside a radius of 300 m around the erection site and an attenuation relationship was applied.(520A,622a,622A,623A) The design seismic ground motion was defined as the acceleration response spectrum on the engineered bedrock surface (Vs ≥ 500m/sec).(715A) Figure 86 shows the distribution of elastic S-wave velocities in the ground at the position of pylon P4 of the cable-stayed bridge. A layer of soft sediment has been deposited for a depth of more than 100m above the engineered bedrock surface. Figure 87 shows amplification spectra in the ground at the positions of foundations of the cable-stayed bridge. The predominant period of the ground is 1.5 to 2.0 seconds. It is evident that long-period components are highly likely to be excited in the ground.

For the cable-stayed bridge, ten acceleration waves were generated for each return period that had acceleration response spectra equivalent to the acceleration response spectra defined on the engineered bedrock surface. The acceleration waves were generated artificially using Fourier amplitude and Fourier phase. The phase property of acceleration waves was varied by giving the phase using random numbers.(623B) Surface acceleration waves were obtained through dynamic analysis of ground motions in respective foundations using the artificially generated acceleration waves as input ground motions. The surface accelerations were made to act on a dynamic analysis model of the entire bridge. (631A)

A one-dimensional nonlinear shearing vibration system model was developed based on the dynamic properties of the ground shown in Figure 88 (631C, 715A) Surface acceleration waves were obtained through nonlinear dynamic analysis.

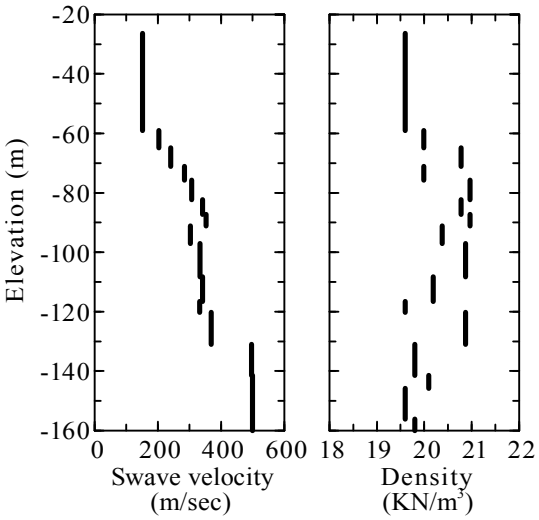

Figure 86 — Soil profile [1]

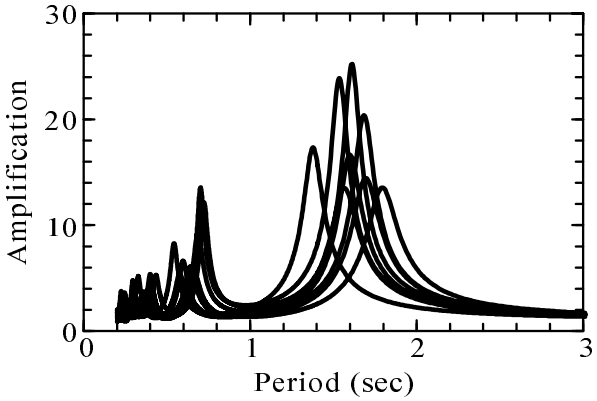

Figure 87 — Absolute amplification [1]

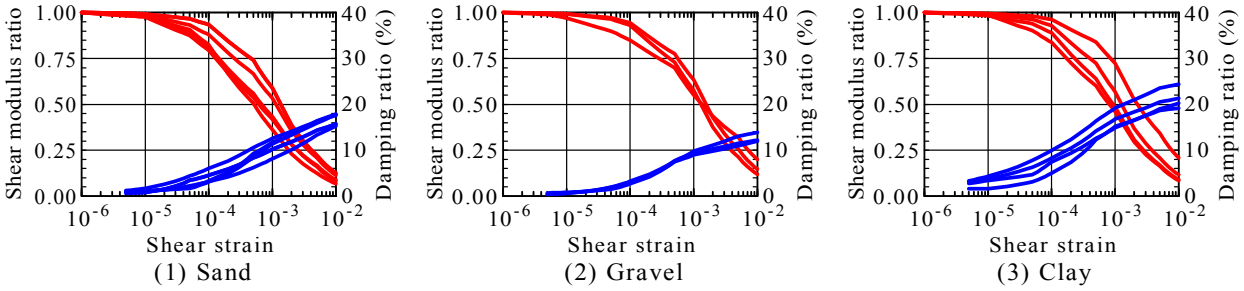

Figure 88 — Shear modulus ratios and damping ratios [1]

Figure 89 shows surface acceleration response spectra at the position of pylon P4. "Design" indicates the spectra used in seismic design of the cable-stayed bridge. "Nonlinear analysis" indicates the surface acceleration response spectra obtained by assessing the seismic performance of foundations. The cable-

stayed bridge over the Yangtze River was expected to be subject to scour during the service period. In the seismic design of the cable-stayed bridge, the effects of scour was considered in the calculation of surface acceleration waves, in the creation of a sway-rocking spring in a dynamic model, and in the seismic design of foundations. Surface acceleration waves were obtained in a case in which the effects of scour were disregarded and in other cases using models with the soils near the ground level removed according to the scour depth. (631b)

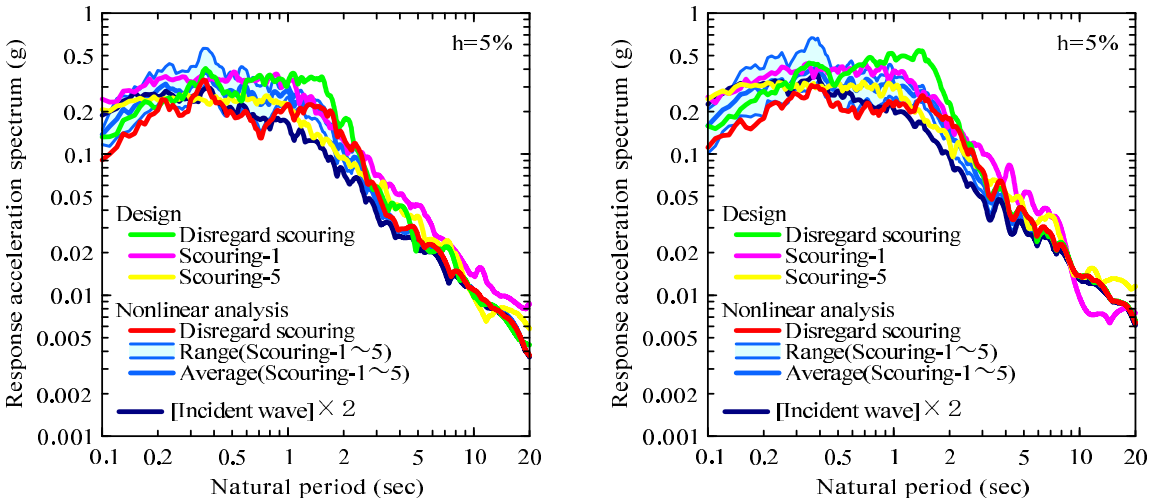

Figure 89 — Design earthquake ground motion (At the pylon P4 position)[1]

5.1.3.3 Seismic performance of foundations

Multi-pile foundations using piles with a length of approximately 120 m were adopted for the cable-stayed bridge. A 55-m section below the pile head was of a composite structure with a cast-in-place pile wrapped with a steel plate. In a 65-m section above the pile end, there was a 2500-mm-diameter cast-in-place pile. Not only a reinforced concrete pylon but also a footing between the pylon base and pile head had a heavy weighed, so 135 piles were installed at the positions of pylons.

As described earlier, the effects of scour on the cable-stayed bridge over the Yangtze River cannot be ignored. Figure 91 shows variations of outstanding pile length due to scour affecting the cable-stayed bridge. Five scour depths were assumed. When the scour depth reached level 5, the outstanding pile length was expected to be approximately 50 m. In the case where substantial scour occurred and the design seismic ground motion with a return period of 2500 years (Table12 and Figure 89) acted on the bridge, the foundations would required a size larger than currently planned unless certain degree of damage to the foundations was allowed. The probability of the seismic ground motion with a return period of 2500 years and the maximum scour expected to affect the cable-stayed bridge occurring at the same time was assumed to be extremely low. The probability of scour was considered higher than the probability of spontaneous phenomena such as earthquakes for the bridge over the Yangtze River, a large river. The effects of scour was therefore taken into consideration in the assessment of seismic performance of foundations.(515A)

The seismic loads to be used for assessing the seismic performance of foundations were determined focusing on the lateral force and bending moment acting on the lateral spring and rotational spring on the bottom surface of the footing of the sway-rocking model of the entire bridge system (Figure 92).(911A,911C) Seismic performance was assessed under two seismic loads: one composed of lateral force $H_{eq}(t^H_{\max})$, bending moment $M_{eq}(t^H_{\max})$ and vertical force $N(t^H_{\max})$ at the time when the lateral force was highest $t^H_{\max}$, and the other composed of lateral force $H_{eq}(t^M_{\max})$, bending moment $M_{eq}(t^M_{\max})$ and vertical force $N(t^M_{\max})$ at the time when the moment was highest $t^M_{\max}$.(711A,711B,712A,911A)

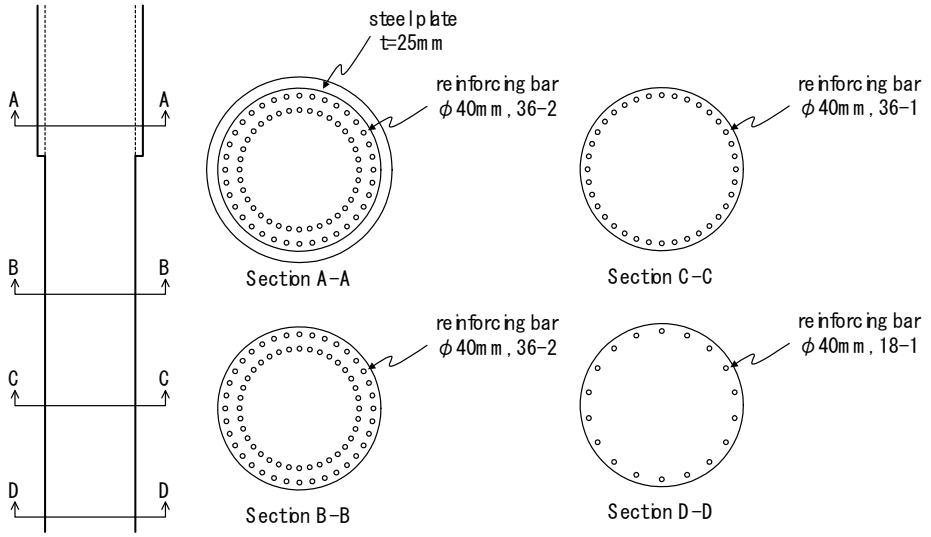

Figure 90 — Composite pile cross section [1] (not be cited: Mori)

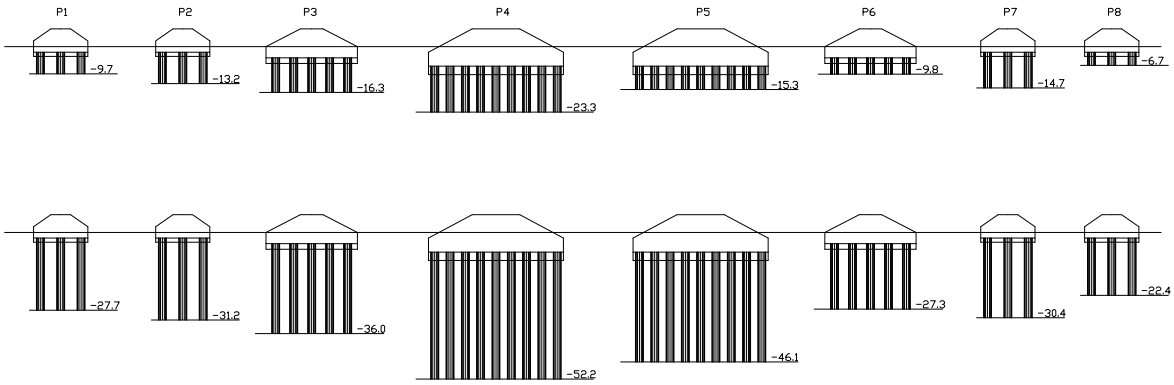

Figure 91 — Two different scouring conditions [1]

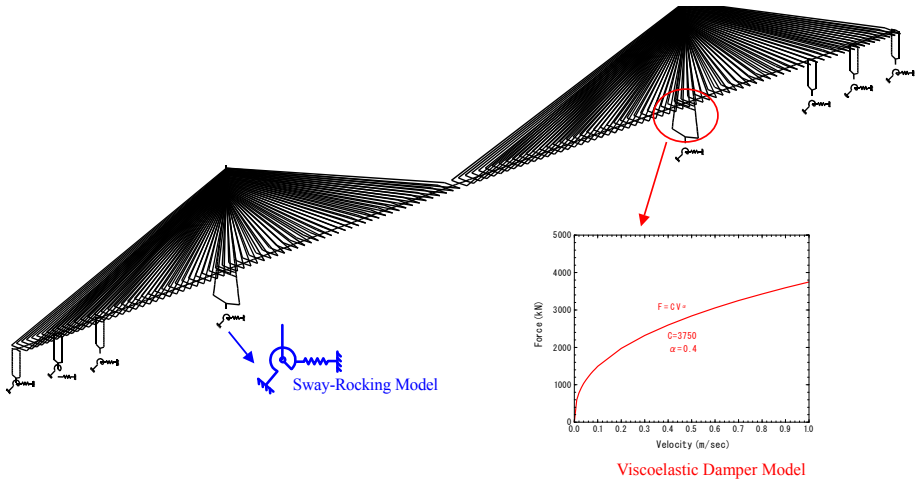

Figure 92 — Model of the entire bridge system (tentatively added by Mori)

A pushover analysis was made using an analysis model [2] that took the nonlinear properties of piles and surrounding ground into consideration (Figure 93).(713A,811B)For the nonlinear property of the composite structure to a depth of 55 m below the pile head, allowance for steel plate corrosion was considered, and flexural strength was reduced to 80% of strength at the time of complete bond between the steel plate and cast-in-place pile because the steel plate and pile were not fully bonded to each other. The method for assessing the seismic performance of foundations has been found to be able to reproduce the damage to pile foundations during the 1995 Hyogoken-Nambu Earthquake[3] and the results of tests using large foundation models under loading that caused great displacements[4), 5)].

The foundations were designed so that the damage caused by seismic ground motion with a return period of 2500 years could be held below the yield point. The point of yielding of foundations means the point when lateral displacements or angle of rotation suddenly starts increasing on the top surface of foundation (bottom surface of footing) due to plasticization of members constituting the foundation and of soil resistance. Lateral displacements or angle of rotation suddenly starts increasing on the top surface of the foundation 1) when all the axial reinforcement yield in the pile foundation or 2) when the reaction of heads of a row of piles reaches the upper limit of resistance to penetration. For the cable-stayed bridge with composite foundations with cast-in-place piles wrapped with steel plates, the yielding of the pile was defined not as the yielding of external steel plates but as the yielding of axial reinforcement in the internal cast-in-place piles.(514A,514B,514C)

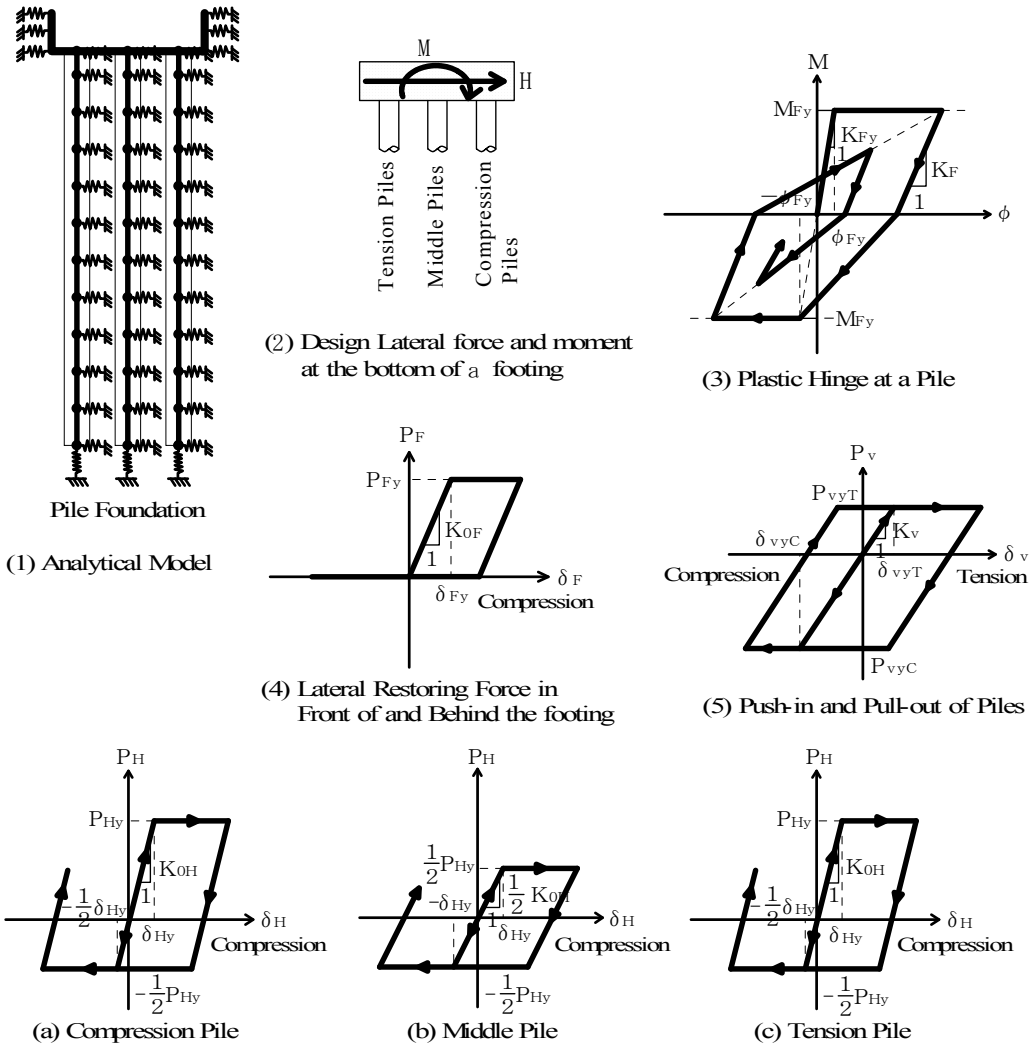

Figure 93 — Analytical model of the pile foundation system

Figure 94 shows the load-displacement relationship for foundations obtained by a pushover analysis at the position of pile P4, and the comparison between lateral force and bending moment acting on the foundation obtained by a dynamic analysis of the entire bridge. The figure shows the relationship between the lateral force and displacement at the time when the lateral force was greatest, and the relationship between bending moment and angel of rotation at the time when the bending moment was greatest. Shown are the results without scour around foundations, and at scour levels 2 and 5 when seismic ground motion with a return period of 2500 years was applied longitudinally. External steel plates and axial reinforcement in the internal cast-in-place piles yielded at scour level 2. Yielding, however, occurred not in all the piles at the position of pylon P4. Only the piles in the outermost row yielded. The pile foundation as a whole did not yield. It is clear that there remained adequate allowance for the ultimate state of piles.

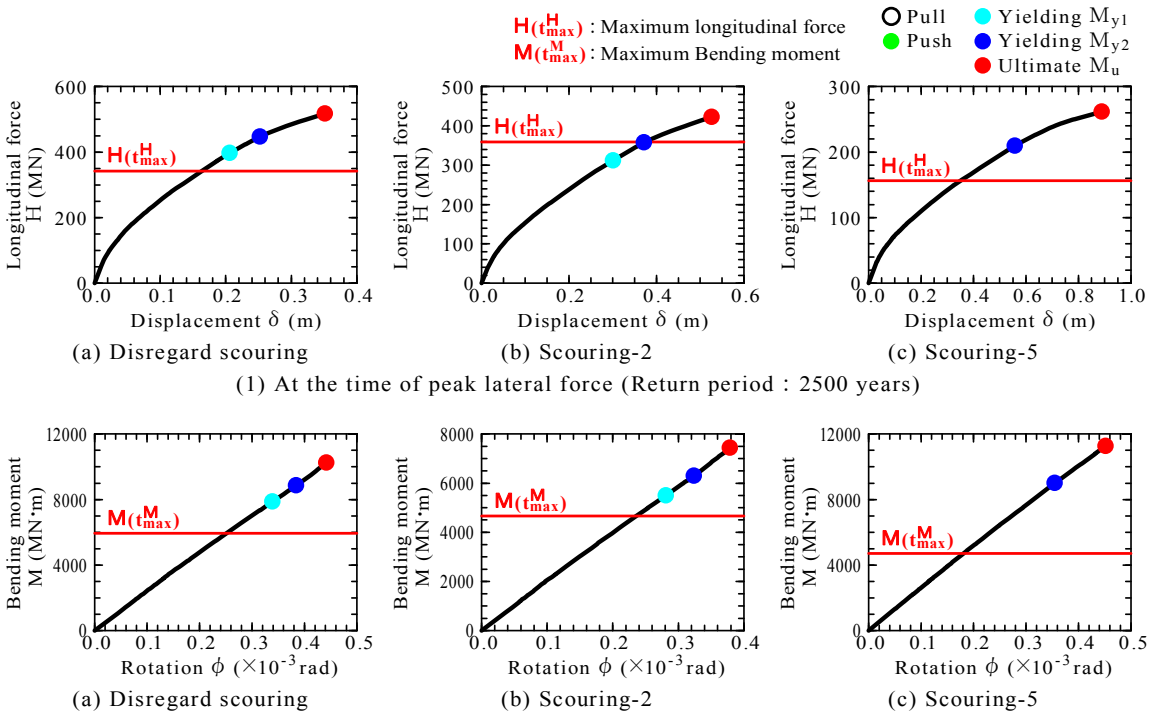

Figure 94 — Load – deformation curve for two different seismic loads [1]

A soft layer of sediment deposited above the engineered bedrock surface at the site of erection of the cable-stayed bridge. The effects of displacements of the ground during an earthquake on pile foundations could not be disregarded. In this study, attention was paid to the damage to piles subject both to the inertia forces of the structures above the bottom surface of footing and to the maximum response displacements of surrounding ground during an earthquake. (Figure 95 should be cited; added by the editor.) (811b, 812a) Figure 96 compares the bending moment distribution and flexural strength of a pile subject to the greatest damage among the pile at the position of pylon P4. The focus was on the effects of displacement of surrounding ground, so no scour was assumed. The effects of bending moment due to the inertia forces of the structures above the bottom surface of footing were predominant near the pile head. Piles yielded in some areas in the ground due to displacement. In the areas, the hardness of the ground (elastic S-wave velocity) varied and the relative displacement of ground in the upper and lower layers increased. Damage to some piles in the section below the ground level causing yielding had no effects on the seismic performance of foundations. There remained adequate allowance for the ultimate state of the pile, so such damage was allowed in seismic design.

As a result of assessment of the seismic performance of foundations, it was confirmed that the foundations at the positions of pylons could meet the seismic performance requirements against seismic ground motion with a return period of 2500 years.

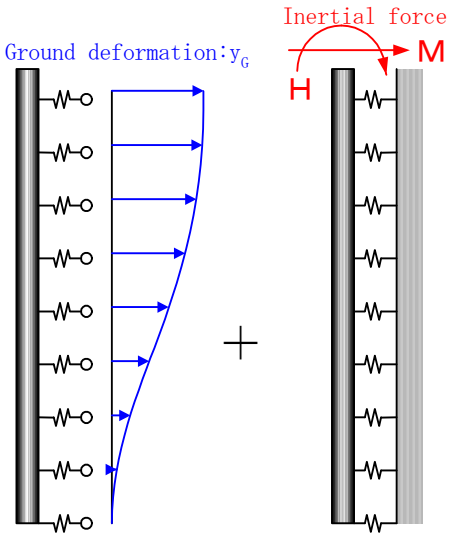

Figure 95 — Model of seismic action for pile

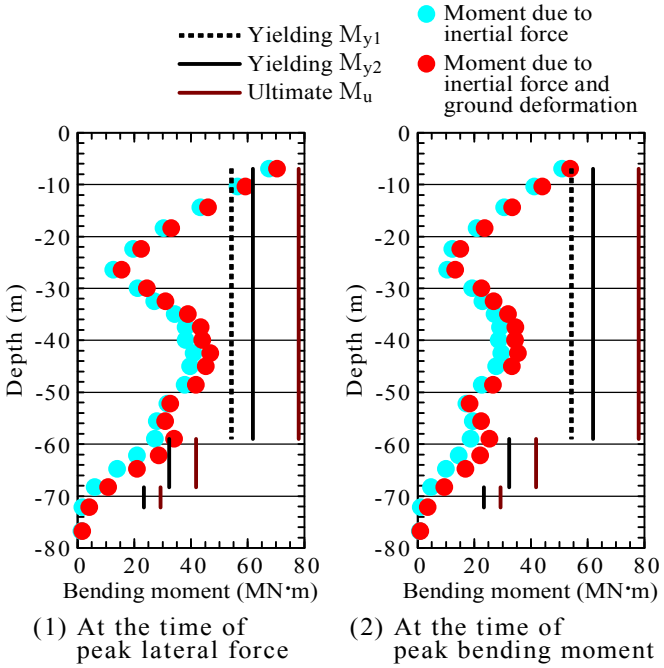

Figure 96 — Distribution of bending moments with depth [1]

5.1.4 Earth fill dam

5.1.4.1 Purpose and functions

Fill dams have been until now designed on the basis of specifications in Japan. Dam body materials, structural calculation method, and detailed construction process are specified in design standards and relevant documents. In the current design specifications, intense earthquake ground motions which rarely occur, such as those recorded during the 1995 Hyogo-ken Nanbu Earthquake, are even taken into account in dam design. Since this earthquake, the concept of performance-based design has been introduced as a kind of requirement in Japan. The shift of design philosophy from conventional specification-based design to

performance-based design for earth structures such as levee embankments, road embankments and etc. in Japan.

Because a fill dam is a water storage structure, the expected performance of the fill dam is to ensure that water stored by the dam does not flow over the dam body nor breach it during an earthquake. These overflow or breach may cause severe damage to dam's downstream area. Thus, settlement at the crest of a fill dam during an earthquake must not be exceeded a performance criterion. To ensure this required performance in design, it is essential to apply an analysis method which can accurately evaluate the possible settlement. (511A, 512a, 512b)

The following design consideration was made on the basis of the performance-based design concept, focusing on the setting process of the performance criterion index as the settlement based on the relationship of the surplus height and the settlement of a fill dam body (Tani, 2004). Public Works Research Institute (2007) announced a performance criterion incorporating a deformation verification method in which settlement is treated as an index of evaluation.

During the 2004 Niigata Chuetsu Earthquake in Japan, maximum acceleration of 558 cm/s^2 was recorded at the foundation of Kawanishi Dam. During the 2008 Iwate-Miyagi Inland Earthquake in Japan, maximum acceleration of 1,000 (cm/s^2) was recorded at the basement of the dam. It is important to verify the safety of fill dams against such intense earthquake ground motions.

5.1.4.2 Performance objectives for seismic design

The relationship between the degree of remaining functions after an earthquake and the degree of damage differs case by case depending on specifications of structures. Thus it is difficult to clarify the relationship in general. The safety of earth structures has been conventionally evaluated by an ultimate equilibrium method for the ultimate limit state. However, it is impossible to evaluate the degree of damage by a safety factor calculated by the conventional method for Level 2 Earthquake Ground Motions, which has to be considered in design.

In the conventional method, when a factor of safety is smaller than 1.0, an embankment is judged to be in a failure or a kind of instability. On the other hand, when a factor of safety is greater than 1.0, the embankment is judged to be safe. In reality, even if a factor of safety is smaller than 1.0, it would not necessarily mean an immediate failure. Therefore it is necessary to clarify that by what degree it can be judged as safe or not in terms of the quantity of anticipated displacement.

In the case of a fill dam, to keep its function as a water storage structure, the settlement related to the reservoir water level is particularly important. To estimate displacement of the dam for ensuring its safety, it is necessary to perform a detailed analysis, for example a FE analysis. If accurate residual displacements can be analyzed, the determination of a performance criterion, "to what degree of residual displacement can be allowed", is important. The performance criterion is determined in correspondence with an earthquake ground motion for design. (512A)

The settlement of crest is considered to be an index of the performance required to the water storage structure. Considering the perspective of the functions of the dam, the settlement must be kept within a range that permits the maintenance of its function for water storage against Level 2 Earthquake Ground Motions. Seismic design that stipulates performance criteria for a fill dam is started by determining the earthquake ground motion to be used for the design, and confirm that the anticipated deformation or the damage will not harm the predetermined functions. (513A)

If the function of a fill dam is to maintain stored water safely, the minimum requirements are that the elevation of the crest after an earthquake is not lower than the level of reservoir water surface. In other words, the settlement is within the allowed height of the embankment that is defined by the reservoir water level. The stored water must not overflow the crest of the dam in order to maintain the minimum required water storage function, and it may be limited to the range of the allowed height of the dam plus the height of the waves caused by the earthquake. Equations for allowed height are generally set in design standards for dam. A numerical value obtained by such an equation is the performance criteria defined as an allowable settlement, and regardless of the dam height, a minimum of 1.0 m is ensured. Note it has been reported that if large

deformation occurs (Seed, 1979), cracking, sliding, piping or other damage and alteration may occur at various locations. (514A)

According to the Technical Note by the Public Works Research Institute (2005), for the cases that slippage is not predicted on a downstream slope, there must be no possibility of piping failure. In fact, there have been almost no reports of damage to fill dams in which the settlement exceeds 0.5 m, except the cases with foundation ground liquefaction. Considering the fact, the PWRI sets the performance criterion approximately 1.0 m regardless of dam height, as a safer side judgment. Note that the criterion value was set approximately 1.0 m as the sum of 0.5 m corresponding to a confirmed value as safe settlement in actually damaged dams and 0.5 m corresponding to a considerable analysis error. (514A, 514B, 514C)

The followings are the general performance objective for a fill dam in Japan.

a) Damage shall not occur under Level 1 Earthquake Ground Motions.

b) Breaching shall not occur under Level 2 Earthquake Ground Motions.

c) Damage shall be limited to that which does not obstruct control of the stored water under Level 2 Earthquake Ground Motions (the water level can be reduced before a breach occurs).

d) It shall be possible to use the dam as before by performing only minor repair work after experience of Level 2 Earthquake Ground Motions (to maintain total reservoir functions).

The significance of the concepts, b) and c) are almost identical. Objective d) applies when the fill dam has an extremely important role in society (cases where the dam plays an extremely important role in preventing disasters downstream from its location, or where its failure to supply water for irrigation would have extremely great repercussions). In the past, this level of seismic performance was almost never demanded. (512b)

Even when the settlement is small, leaking may occur, and piping etc. causes breaching. Because it is not easily evaluated analytically, so far, a quantitative performance criterion cannot be incorporated. Thus, setting the allowable values for settlement or deformation, and the design to satisfy these values is realistic performance-based design for a fill dam. (514A)

In the case of damage to Kawanishi Dam during the Niigata Chuetsu Earthquake, the maximum acceleration of earthquake ground motion was 558 (cm/s^2) at the foot of the dam. It can be regarded as one of Level 2 Earthquake Ground Motion in contrast to earthquake ground motions recorded in the past. The displacement of the crest ranged between 20 and 40 cm. The settlement was within the allowable range, but slight surface slippage occurred on the upstream slope in the left of bank. However some work for repairing it needs suspension of irrigation water supply for one year, and thus the damage had given severe impact to the society (Tani et al., 2005). To achieve the performance objective d) “It shall be possible to use the dam as before by performing only minor repair work after Level 2 Earthquake Ground Motions in order to maintain total reservoir functions”, the required performance criteria should be quite small value of deformation based on this fact. (512b)

5.1.4.3 Procedure for determining seismic actions

As a Level 1 Earthquake Ground Motion that corresponds to the reference motion for serviceability, the lateral seismic coefficient k_h of 0.15 is used in design for a dam in a high-seismicity region. This value is generally used for the seismic design of fill dams in Japan. The slip surface analysis based on circular slip is usually conducted, and the seismic performance criterion was assumed to be a slip safety factor of 1.20 or more. (513A, 514A)

The lateral seismic coefficient $k_h = 0.35$ is used for Level 2 Earthquake Ground Motion, which corresponds to the reference motion for safety. This value is given as the seismic inertial force coefficient on ground surface, and verification of seismic performance is on the basis of the static verification method stipulated in Design Specifications for Highway Bridges (PART V Seismic Design) (JRA, 2004).

Safety against Level 2 Earthquake Ground Motions is also considered as the maximum settlement of the dam body crest is smaller than 0.5 m. This value is given considering precision of the analysis as mentioned above, and the allowable height from the full water level to the crest is 1 m in reality. (513A, 514A)

The following two kinds of motions were used as the Level 2 Earthquake Ground Motions.

1) Motions to satisfy the lower limit of acceleration response spectrum for design are shown in Figure 97 and Table 13. The acceleration time history of one of the motions was developed in compatibility with the design spectrum by using the phase characteristics of the NS component of a motion observed at Hachinohe site during the 1968 Tokachi-Oki Earthquake, and so the time history is called here as Hachinohe Wave. Moreover, another wave was prepared using the upstream-downstream component observed in ground on the left bank of Kawanishi Dam, which is a central core type fill dam with a height of 43 m in Tokamachi City, during the 2004 Niigataken Chuetsu Earthquake. So this is called here Kawanishi Wave.

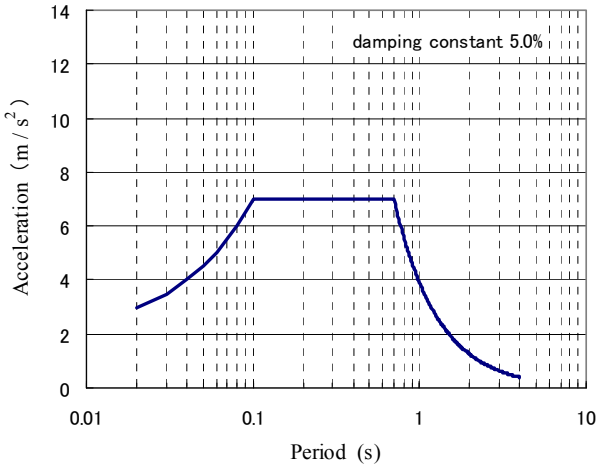

Figure 97 — Lower limit of acceleration response spectrum for serviceability limit state

Table 13 — Verification Use Lower Limit Response Spectrum (damping constant = 5%)

Range of natural period T (s)	Acceleration response S_A (gal)
0.02 <= T < 0.1	$S_A = 400 / 0.08 * (T - 0.02) + 300$
0.1 <= T <= 0.7	$S_A = 700$
0.7 < T<= 4	$S_A = 700 * (T / 0.7)^{-1.642}$

2) A motion estimated at a hypothetical site in Sendai City (North latitude 38.4013º, East longitude 141.2117º) was also taken into account for the design. This motion is developed by the statistical Green's Function Method using a fault model of the 1978 Miyagiken-Oki Earthquake shown in Figure 98, and so it is called here Miyagi Wave.

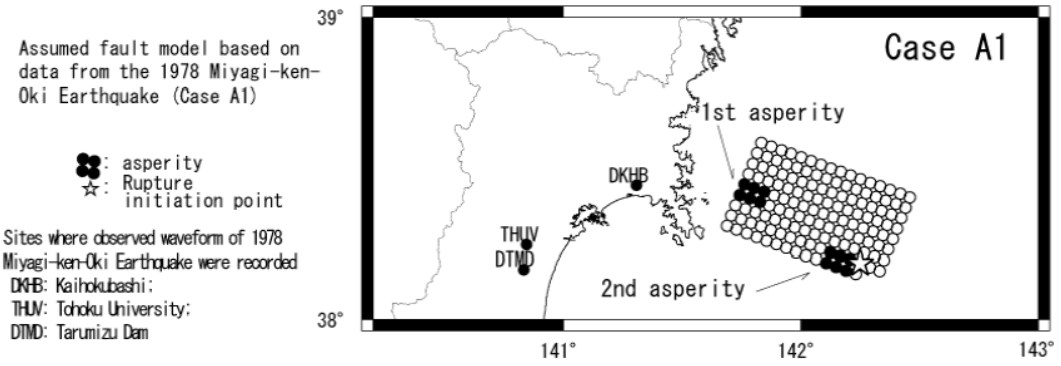

Figure 98 — Fault model for 1978 Miyagiken-Oki Earthquake

Figure 99 shows the acceleration time histories and acceleration response spectra of the three waves. The Level 2 Earthquake Ground Motion was assumed as an input motion at the bottom of the ground. (611A, 621A, 621C, 623B, 631A)

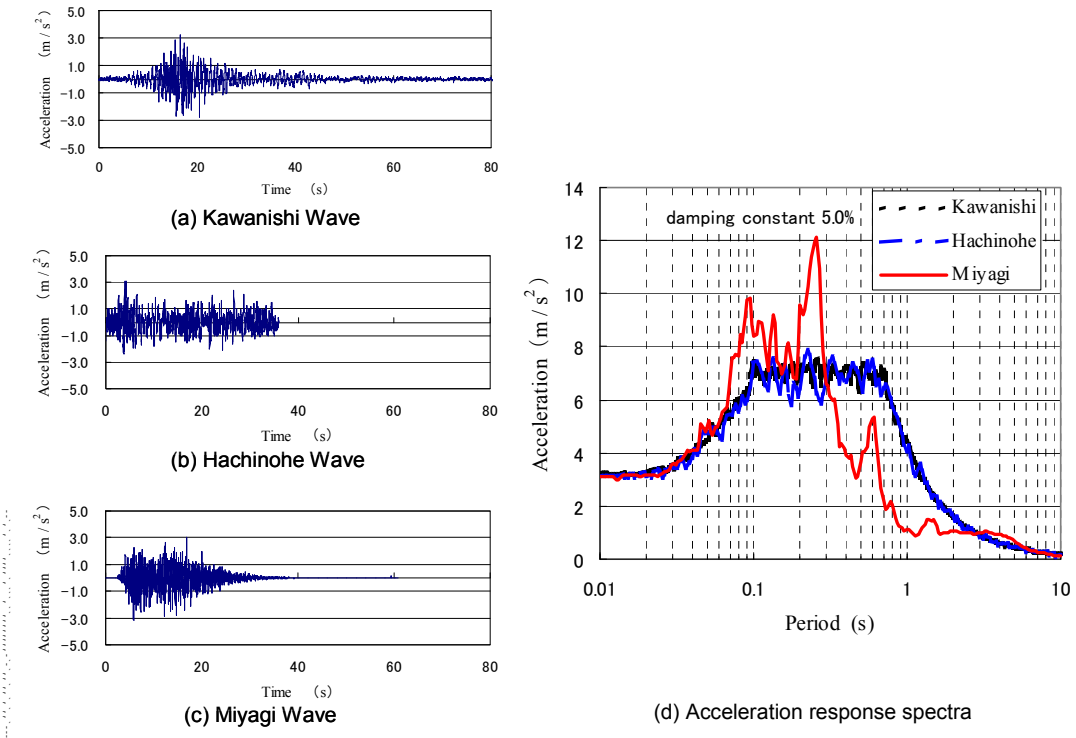

(a) Kawanishi Wave

(b) Hachinohe Wave

(c) Miyagi Wave

(d) Acceleration response spectra

Figure 99 — Acceleration time histories for design input motions and acceleration response spectra of the motions

5.1.4.4 Soil properties and models for detailed dynamic analysis

The section of a model dam is shown in Figure 100. The dam height is 36.5 m (depth from the dam body crest is 36.5 m). The crest width is 7.0 m, and gradient of the slope are 1.0:3.0 on the upstream side and 1.0:2.3 on the downstream side. The water level in design is the full reservoir level (4.0 m below the crest). Below the dam body, a foundation with N value of 20 was there with thickness of 12.0 m, while the ground below the foundation is a layer with shear wave velocity Vs = 1,500 m/s.

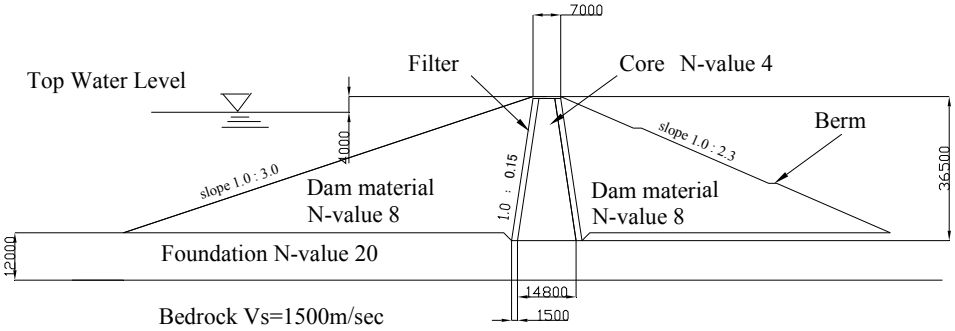

Figure 100 — Section of model dam

Figure 101 shows sections of a dam with three options of seismic reinforcement considered in the design. The details of the seismically reinforced sections are shown in Table 14: in reinforcement section (a), there is counterweight fill with crest width of 5.0 m, height of 34.5 m, upstream slope gradient of 1.0:4.0 and downstream slope gradient of 1.0:3.3, and in reinforcement section (b), there is counterweight fill with crest width of 5.0 m, height of 34.5 m, upstream and downstream slope gradients of 1.0:4.0, adding some flat area with width of 15 m in midway, and in reinforcement section (c), the top centre of the dam body was replaced with improved soil.

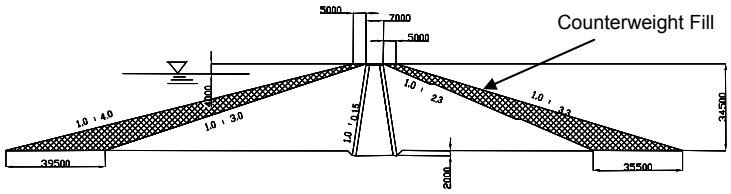

(a) Reinforcement Case a

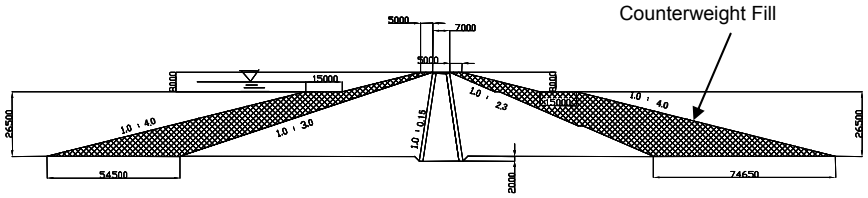

(b) Reinforcement Case b

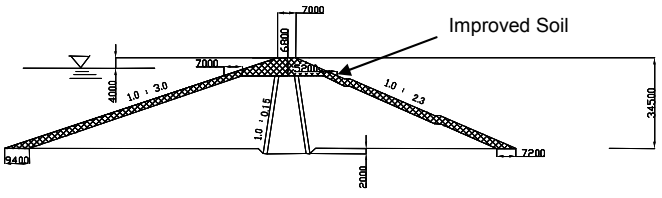

(c) Reinforcement Case c

Figure 101 —Sections of a dam with three options of seismic reinforcement

Table 14 — Specifications of reinforcement sections

	Reinforcement section a	Reinforcement section b	Reinforcement section c
Reinforcing method	Counterweight fill	Counterweight fill	Improved soil
Crest width after reinforcement	17m	17m	7m
Upstream side slope gradient	1.0 : 4.0	1.0 : 4.0	1.0 : 3.3
Downstream side slope gradient	1.0 : 3.3	1.0 : 4.0	1.0 : 2.3
Reinforced location	Outside of existing part	Outside of existing part	Inside of existing part

The materials used as the counterweight fills in reinforcement section (a) and reinforcement section (b) are the same material with that of the dam body. The improved soil in reinforcement section (c) is cohesive material with low strength.

Figure 102 shows the 2-D FE model used in the detailed dynamic analysis for design. Initial stresses, which are necessary in a nonlinear dynamic analysis, were calculated by self-weight analysis using the Mohr-Coulomb model. Boundary conditions for the self-weight analysis adopted fixed bases and vertical rollers on the both sides. During a dynamic analysis using a model shown in Figure 102, a free field was assumed for the both sides of the region, and a viscous boundary for the both sides of the region was assumed. Another viscous boundary was also set at the bottom. (921A)

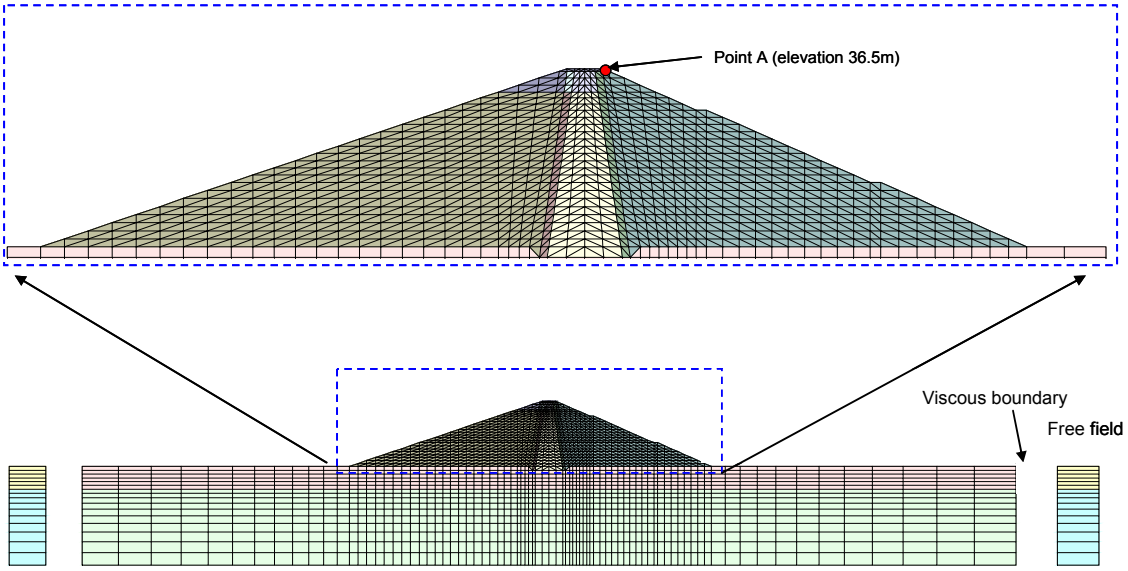

Figure 102 — 2-D FE model used in detailed dynamic analysis for design

Table 15 shows the material properties of the dam and its foundation used in the analysis. The density was set with reference to that of existing dams. A shear wave velocity was empirically evaluated on the basis of N value, and the N values of the dam body and core were set with reference to boring data from an existing dam. The internal friction angle is also set with reference to data from the existing dam. The cohesion value has a big impact on analysis results, but in this design, an empirical value was used. Rigidity was set with reference to test data in existing dams. Note the properties for dam body material, core, and filter were dependent on confining pressures, and assumed proportional to the square root of the confining pressure. The Young's modulus of the improved soil was set at 500 times the unconfined compressive strength q_u of the

improved soil. Poisson's ratio was set at 0.41 above the seepage line and at 0.49 below the seepage line, to be the static coefficient of earth pressure during self-weight analysis ranged from 0.5 to 0.33.

Table 15 — Material properties used in analysis

Material category	N value	Vs (m/s)	Saturated density (t/m^3)	Internal friction angle f (°)	Cohesion C (kN/m^2)	Rigidity (s_c=100 kN/m^2)	Young's modulus (kN/m^2)
Dam body	8	170	1.86	32	5	53 754	-
Core	4	133	1.74	28	10	30 778	-
Filter	-	-	2.17	40	0.1	203 200	-
Foundation	20	237	2.1	32.3	0.1	117 955	-
Foundation ground	-	1 500	2.2	-	-	4 950 000	-
Improved soil	-	-	1.86	10	100	-	100 000

Rayleigh damping was used in the dynamic analysis. The parameters of Rayleigh damping were set as damping of 2.5 % in the primary and secondary natural periods of the model (0.704 seconds and 0.363 seconds respectively). The constitutive equation of soil was the Mohr-Coulomb type model. In the Mohr-Coulomb type model, the non-associated flow rule which considers the plastic volume strain to be zero is used. Since the plastic volume strain is considered to be zero, volume change such as shaking down is not modelled in this analysis. And because the Mohr-Coulomb type model is a perfect plastic-elastic model, until a restoring stress reach the yield surface, it displays only elastic behaviour. After reaching the yield surface, it displays totally plastic behaviour. The non-linear numerical analysis algorithm was the initial stiffness method. Time integration was done using the Newmark-β method (γ=0.5、θ=0.25): and the analysis performed at intervals of 0.001 second. (922A)

5.1.4.5 Simplified equivalent static analysis: Slip analysis results;

Earthquake action has been evaluated both in circular slip surface analysis and 2-D FE dynamic analysis. The lateral seismic coefficient k_h = 0.15 and k_h = 0.35 were used in circular slip surface analyses for Level 1 and Level 2 Earthquake Motions respectively. The lateral seismic coefficient was considered as the uniform inertial effect to the dam body.

Table 16 is a summary of the evaluated safety factors. Figure 103 shows slip surfaces. Slip surfaces are found on the upstream side in all sections. Although the slope gradients are steeper on the downstream sides than on the upstream sides, the slip surfaces appear on the upstream sides because the shear strength on the upstream sides is lower than that of the downstream sides. This is because of the reduced effective stress as a result of the buoyancy below the water level. In the k_h = 0.15 case, the slip safety factor is greater than 1.20. In the case where k_h = 0.35, under present conditions, the safety is 0.889, and less than 1.0. Thus slippage is anticipated.

Table 16 — Slip safety factors during earthquakes

	Safety factor during earthquake (k_h=0.15)		Safety factor during earthquake (k_h=0.35)	
Reinforcing material	Dam body material	Improved soil	Dam body material	Improved soil
No countermeasure	1.357	-	0.889	-
Reinforcement section a	1.624	-	1.018	-
Reinforcement section b	1.634	-	1.018	-
Reinforcement section c	-	1.438	-	0.954

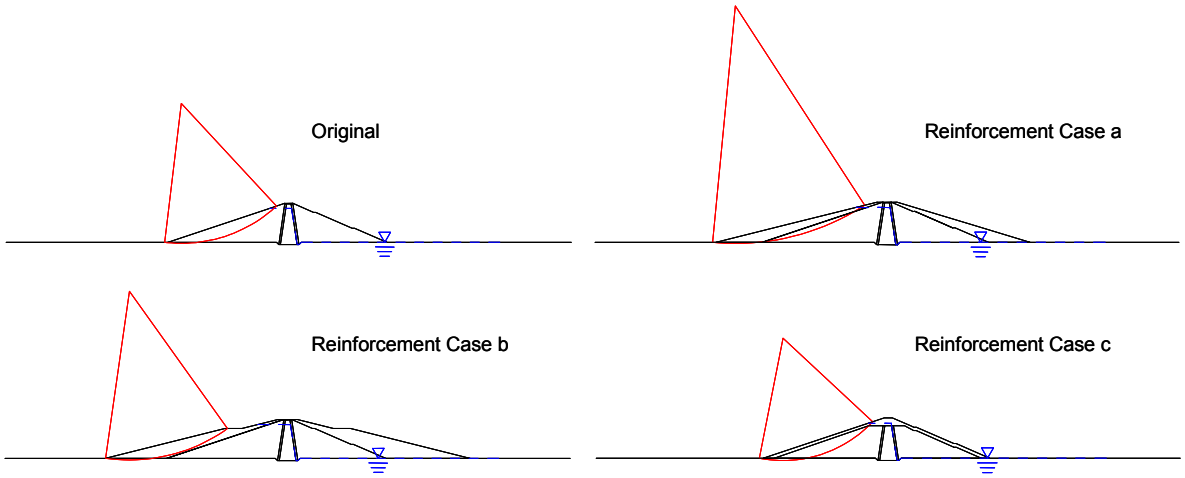

Figure 103 — Slip surface with minimum factor of safety during earthquakes

The safety factors of reinforced sections are higher than the safety factors of the section without countermeasures. Among the reinforcement sections, the safety factor of reinforcement section (c) is the lowest. The safety factors of reinforcement section (a) and reinforcement section (b) with reduced slope gradients are large. And the effect of flat area in reinforcement section (b) is clearly recognized. The slip surface forms a large arc passing through the dam body from the toe of the upstream slope to the crest of the dam. But the slip surface of reinforcement section (c) is an arc that passes through the dam body from the toe of the upstream side slope to the middle of the slope, and the arc does not pass the crest. This difference is the effect of the cohesiveness of the improved soil. The same tendency is seen in k_h = 0.35 cases.

5.1.4.1 Detailed dynamic analysis: Results of FEM dynamic analysis;

Table 17 shows the maximum settlement at the dam body obtained by FE dynamic analysis. The maximum settlement appeared near the shoulder of the downstream slope in all cases. The seismic reinforcement effects are highest in reinforcement section (c), where the inside of the existing dam body was replaced with improved soil. In this case, the maximum settlement reduced to be about 1/3 of that of the dam without countermeasures. A comparison of reinforcement section (a) and reinforcement section (b) shows that the effect of the reinforcement is higher in reinforcement section (b). The differences are the gentler slope gradient on the downstream side, existence of the flat area of 15m width, and the larger counterweight fill.

Table 17 — Maximum settlement of dam body by FE dynamic analysis

	Maximum settlement of dam body crest (m)		
Earthquake wave	Kawanishi Wave	Hachinohe Wave	Miyagi Wave
No countermeasure	0.676	0.606	0.268
Reinforcement section a	0.507	0.433	0.146
Reinforcement section b	0.384	0.326	0.073
Reinforcement section c	0.244	0.242	0.102

The settlement by the simulated Kawanishi Wave is greater than that of the simulated Hachinohe Wave although their acceleration response spectra are identical. It reveals the importance of the phase difference in the analysis results. The settlement in a case using the simulated Miyagi wave is smaller than that of other seismic waves. This is because the power near the horizontal primary natural period of 0.704 second is smaller than that of the simulated Hachinohe Wave and the simulated Kawanishi Wave.

Figure 104 and Figure 105 show deformation and the γ_{max} contour for the case with the simulated Kawanishi wave. In all cases, deformation is in severe condition on the upstream side, and the peak of γ_{max} also appears on the upstream side. The deformation might be caused by shear in deep parts of the dam body. In reinforcement section (a) and reinforcement section (b), the value of γ_{max} is high even the in the nearby of the crest. In reinforcement section (c) where the highest effects of reinforcement were found in the FEM analysis, the value of γ_{max} around the crest is small because of the effects of cohesiveness of the improved soil. Around the crest with shallow depth and low confining pressure, cohesiveness plays an important role in counting the shear strength. Consequently, it would be regarded effective to perform reinforcement with cohesive materials around the dam body crest. However, in seismic reinforcement section (c), the maximum shear strain was highest around the upstream side boundary of the improved soil and the dam body material. This is a result of the fact that the response differed around the boundary due to the differences of the stiffness of the improved soil and the dam body material. The dam design must be performed paying close attention to this point.

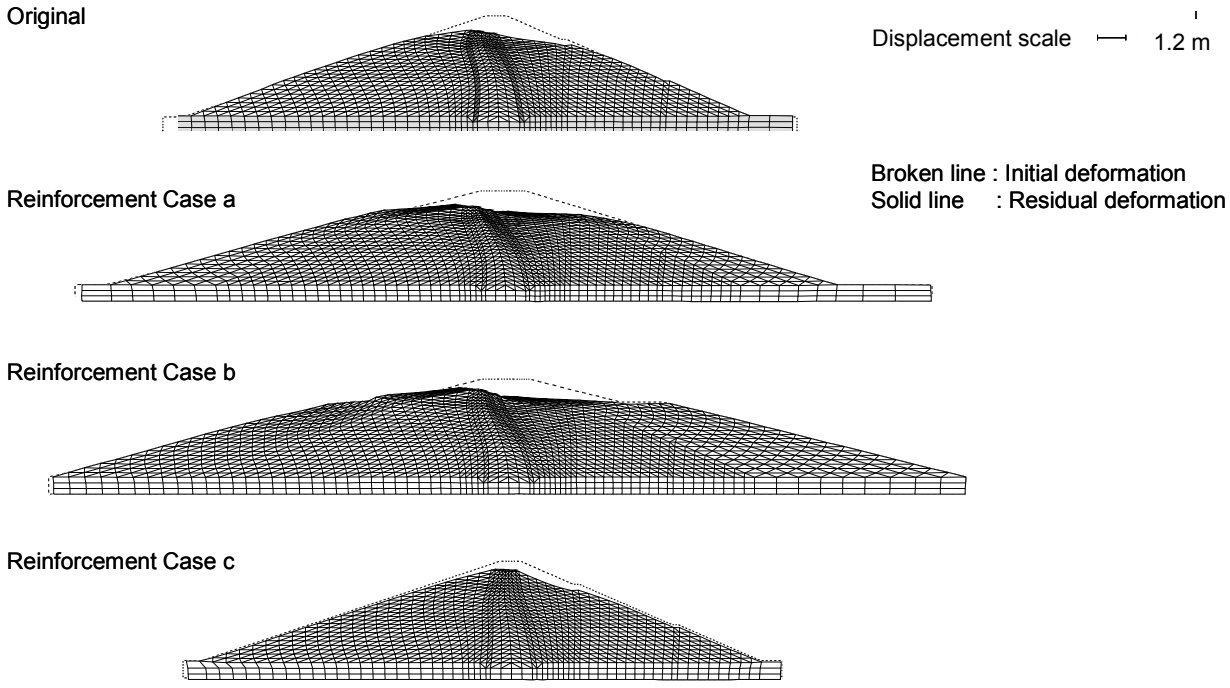

Figure 104 — Residual deformation diagram in the case of Kawanishi Wave for an input motion

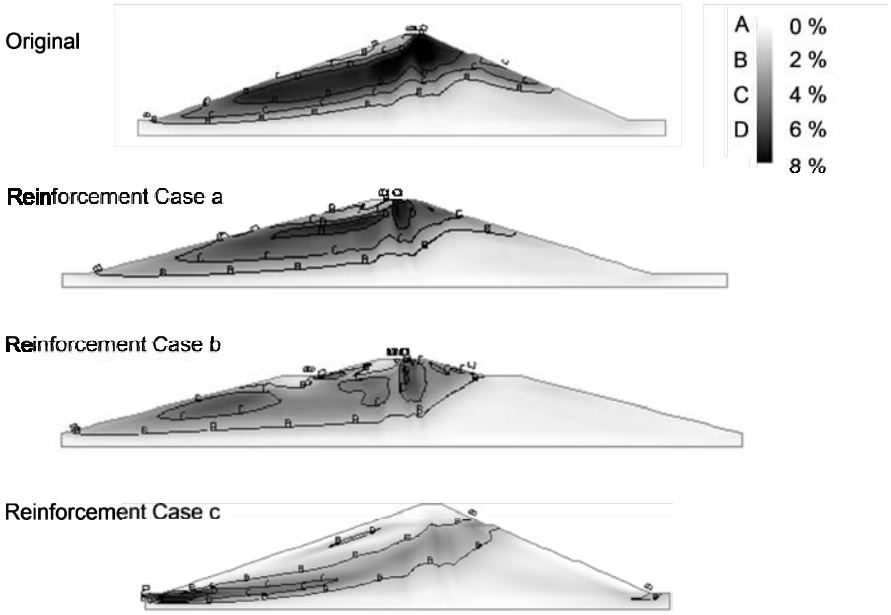

Figure 105 — Maximum shear strain (γ_{max}) diagrams in case of Kawanishi Wave for input motion

Figure 106 shows the relationship between the maximum settlement at the crest in FE analysis and the slip safety factor obtained by circular slip surface analysis. No correlation can be found. The FE analyses for reinforcement sections (a) and (b) differ despite they have roughly equal slip-safety-factors. This is because the slip surfaces with minimum safety factors in reinforcement sections (a) and (b) do not pass through the entire dam body as shown in Figure 103, shear deformation in the FE model occurs deep in the body as shown Figure 104. In other words, the slip surface analysis shows no overall shear deformation of dam body.

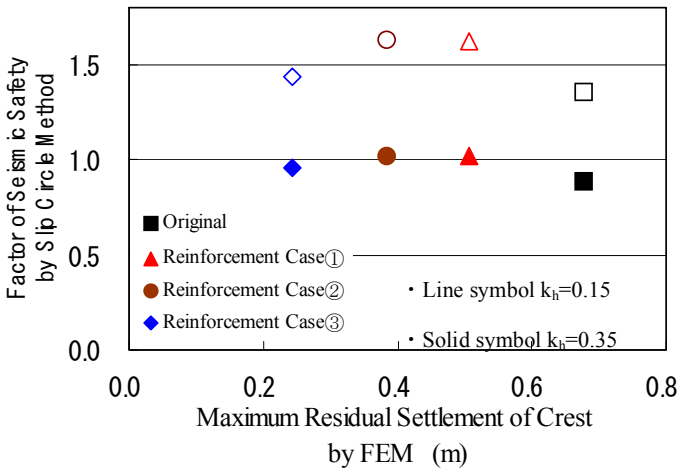

Figure 106 — Maximum shear strain (γ_{max}) diagrams in case of Kawanishi Wave for input motion

The slip safety factor of reinforcement section (c) is smallest among the reinforcement sections, but the slip surface with the minimum safety factor does not pass through the dam body crest. When the seismic performance is evaluated according to the settlement of the dam body crest, it is nonsense to consider this slip safety factor. FEM analysis considers the effects of shear deformation of the entire dam body that cannot be represented by slip surface analysis. Because the FEM analysis assumes a continuous body, it cannot clearly show the slip surface. The evaluations of seismic reinforcement effects vary depending on the failure modes which can be considered by FEM analysis. The slip surface analysis is different in this way.

Figure 107 shows the time histories of the horizontal response acceleration and the vertical displacement at the centre of the dam body crest when the simulated Kawanishi wave is used. Approximately 10 seconds later from the start, the increase of vertical displacement is observed. And it continues until approximately 45 seconds later from the start. The vertical displacement increased continuously. Figure 12 shows the distribution in depth of the maximum values of the horizontal response acceleration, maximum shear strain γ_{max}, and vertical displacement at the centre of the dam body. Near the crest, the horizontal response acceleration without countermeasures is smaller than that of the reinforcement section. This is because the acceleration cannot be transmitted easily as a consequence of strain increase and plasticization of deep parts of the dam body. Vertical displacement also observed in deep parts of the dam body on all sections. In reinforcement section (c), the quantity of vertical displacement near the crest where improved soil was used is far smaller than that of the other reinforced sections.

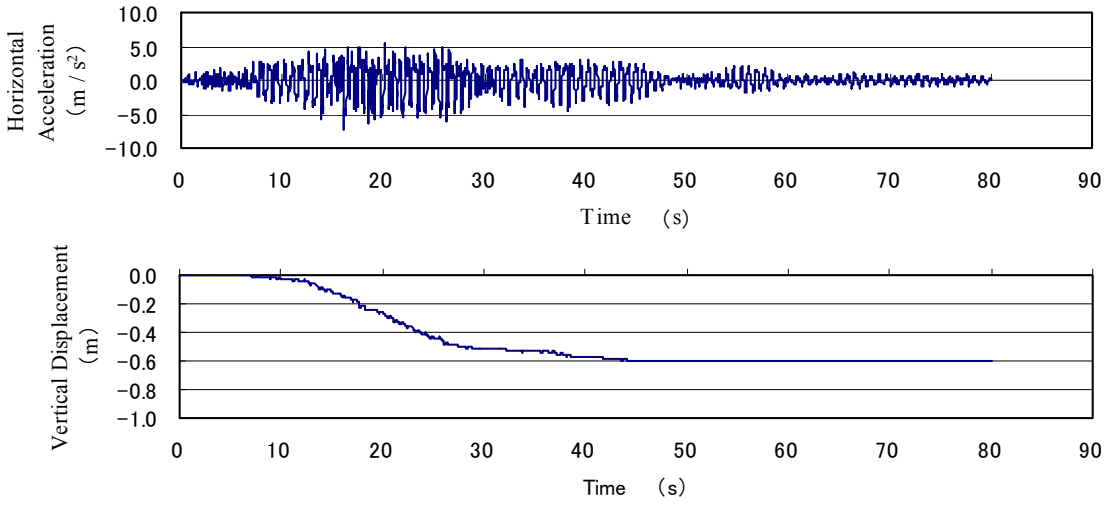

Figure 107 — Time histories of horizontal acceleration and vertical displacement at crest (Point A) of Model Dam in the case of Kawanishi Wave for an input motion

As summarized in Table 17, maximum settlement is less than 1.0 m in all case, and no countermeasure is necessary. However, this consideration indicates the reinforcement section (c) might be most effective if necessary.

5.1.5 Gravity sea wall as coastal structure

5.1.5.1 Purpose and functions

A coastal structure was proposed for construction in Hiroshima-Bay. It aims to defend the life and the property behind the coast from the coastal disaster such as storm surge, tidal waves, and tsunamis. Furthermore, considering the danger to the backyard city region, the above-mentioned functions of structure shall be maintained or recovered smoothly to prevent the secondary disaster in case of earthquake. (511A)

In this example, a typical gravity-type sea-wall is introduced.

5.1.5.2 Performance objectives for seismic design

The design working life for the structure was 50 years. The importance degree of the area is categorized as the highest class, due to the dense population and low elevation of the ground at the backyard. Since the occurrence of the tsunami is the key factor for coastal protection in earthquake, the performance objectives of the structure are defined as shown in Table 18. (512A, 512a, 512b)

Table 18 — Performance objectives

Design earthquake	Performance objectives
Level 1 (The reference earthquake motion for serviceability)	Stability of structure is secured, and the function of coastal protection is not damaged (Serviceability)
Level 2 (The reference earthquake motion for safety)	The damage is not severe, and the loss of coastal protection function can be recovered within the anticipated recovery period. (Safety)
Earthquake with Tsunami (The reference earthquake motion for safety)	The damage is limited, and the function of coastal protection is maintained. (Safety)

5.1.5.3 Reference earthquake motions

The concept for the specification of the reference earthquake motions are summarized in Table 19. The reference earthquake motion for serviceability is specified as the motion with a probability of exceedance of 50 % during the life span. Therefore, the recurrence interval of the motion is about 75 years. The reference earthquake motion for safety is specified as the motion with a maximum level of shaking intensity, possibly occur at the site in future. Note, probability of occurrence is not in consideration in specifying the reference earthquake motion for safety. The reference earthquake motion for safety considering tsunami is specified as the motion in Tonankai-Nankai earthquake, which is anticipated to occur in near future. (513A)

Table 19 — Reference earthquake motions

Reference earthquake motions	Concept
Level 1	75 years in recurrence interval
Level 2	Maximum level of the earthquake motion possibly occur at the site
Tsunami	Tonankai-Nankai earthquake

5.1.5.4 Performance criteria and limit states

The structure considered in this example is shown in Figure 108. This is a typical type of gravity-type sea wall. In case of earthquake disaster, the possible deformation is shown schematically in Figure 109. In the case history of recent earthquake disaster, the concrete retaining wall moved toward sea, and the crest of the wall settled. Considering the expected function of the structure for coastal structure, the settlement at the crest is the most important engineering parameters to be evaluated. Therefore, the performance criteria are defined by the settlement at the crest as shown in Table 20. Note, many seismic performance verification methods such as Newmark's sliding method are applicable to estimate the settlement. (514A, 514C)

The reasonable determination of allowable settlement is usually very difficult. In this case, the following equation is used.

Allowable settlement estimated by the design high tide

= | design high tide level – mean high tide level |

+ necessary height increase against the 10 year probability wave (36)

Here, the recovery of the structure assumed to be started within one month after the disaster, and the recovery might be completed one year after the disaster. In this case, the probability to encounter the high

wave beyond the 10 year probability wave height is about 10%. Thus, if the recovery can be done more quickly, the necessary height to be increased is less, and allowable settlement will be increased. Note, the design high tide level can be dependent on the design working life of the structure, and therefore, the performance criteria are also dependent on the design working life. (514B)

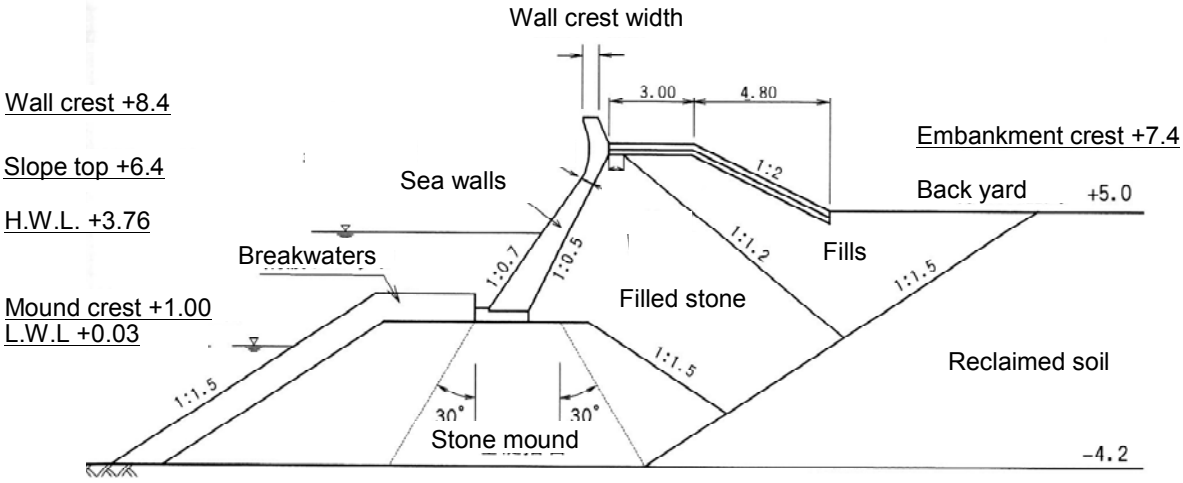

Figure 108 — Cross section of target structure

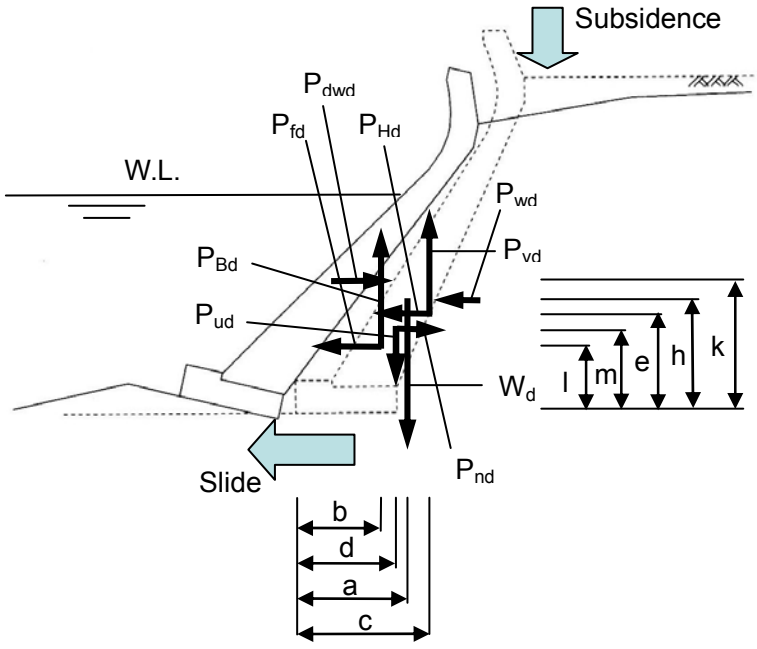

Figure 109 — Typical deformation pattern of sea wall in earthquake disaster and seismic actions

Table 20 — Performance criteria

Reference earthquake motions	Performance criteria
Level 1	Settlement at the crest is negligible.
Level 2	Settlement at the crest is less than allowable settlement estimated by the design high tide.
Tsunamis	Settlement at the crest is less than allowable settlement estimated by the tsunami height.

5.1.5.5 Specific issues related to geotechnical works

The structure is constructed on the deep soft clay layer, and the ground shaking involves the non-linear behaviour of the soft layer. The mode of failure is already shown in Figure 109, and the possibility of overtopping deformation mode is small unless the front inclination of the wall becomes steep. The proposed performance criteria already involve residual displacement. The soil-structure interaction is considered in seismic coefficient determination and the FEM analysis, both described later. (515A)

5.1.5.6 Procedure for determining seismic actions

In the design process, the firm ground motion is estimated at first. Then, the free field motion is computed. The fault displacement is no necessary to be considered at the site, since there is no active fault in the vicinity. Furthermore, the deep soft clay layers below the structure dissolve the effect of the fault movement. As the earthquake induced phenomena, the risk of ground liquefaction is evaluated. Then, the seismic action by the earthquake ground motions, and the level of ground deformation including the possibility of ground failure is evaluated. The details will be shown in the following paragraph. (520A, 650A, 650a)

5.1.5.7 Earthquake ground motions

5.1.5.7.1 Level 1 Earthquake Ground Motion

The Level 1 Earthquake Ground Motion for the site is prepared by the National Institute for Land and Infrastructure Management. This is a kind of governmental service to save the time and cost of designers. This is because the level 1 motion shall be specified by a seismic hazard analysis, and the seismic hazard analysis is a common process for various types of structures. The time history of the motion is shown in Figure 110. Note, the process to specify the Level 2 Earthquake Ground Motion is usually dependent on the type of the structure. Therefore, the specification process is not common, and so far, no general governmental service for design ground motion specification is available. (621A, 621B, 622A)

The proposed motion is based on the site amplification characteristics from earthquake base to ground surface. The site amplification characteristics is evaluated for the seismic strong motion observation point around Hiroshima port, such as Hiroshima-G (Hiroshima Port and Airport Construction Office), HRS013 (K-net Hiroshima, National Research Institute for earth science and disaster prevention) and HRH13 (Kik-net Hiroshima, National Research Institute for earth science and disaster prevention), as shown in Figure 111. Note, these motions are defined at the interface between firm ground and local soil deposit, and already reflecting the effect of the deep basin effects. And from various viewpoints such as PGA, Fourier and response spectra, it is recognized as adequate motions without any irregularities. (623A, 623B, 645B)

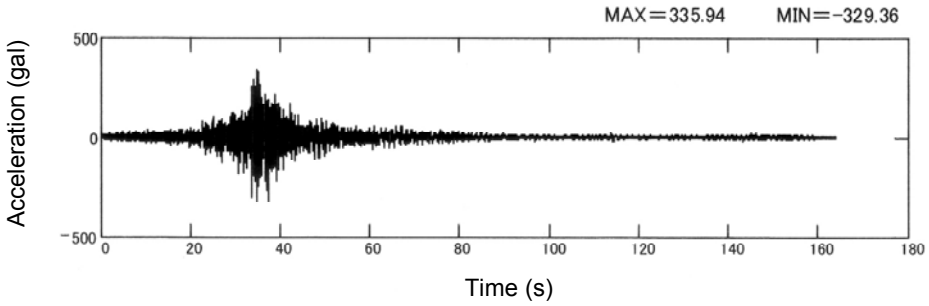

Figure 110 — Time history of Level 1 Earthquake Ground Motion

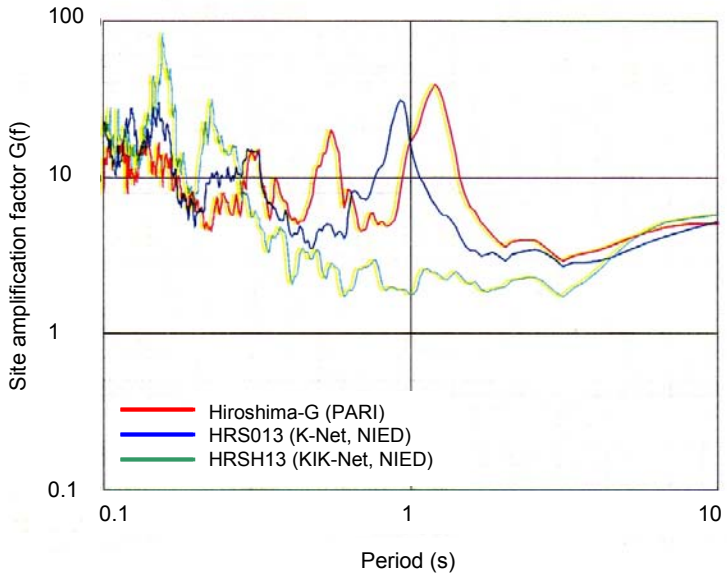

Figure 111 — Site amplification characteristics around the site

5.1.5.7.2 Level 2 Earthquake Ground Motion

The Level 2 Earthquake Ground Motion is specified by the detailed investigation of the seismic activity around the site. Here, an assumed Tonankai-Nankai earthquake and an assumed earthquake on Koi fault are specified as the earthquakes to specify the Level 2 Earthquake Ground Motions. The time histories of the motions are shown in Figure 112. (621C)

Note, these motions are also defined at the interface between firm ground and local soil deposit, and from various viewpoints such as PGA, Fourier and response spectrum, they are recognized as adequate motions without any irregularities. (623A, 623B)

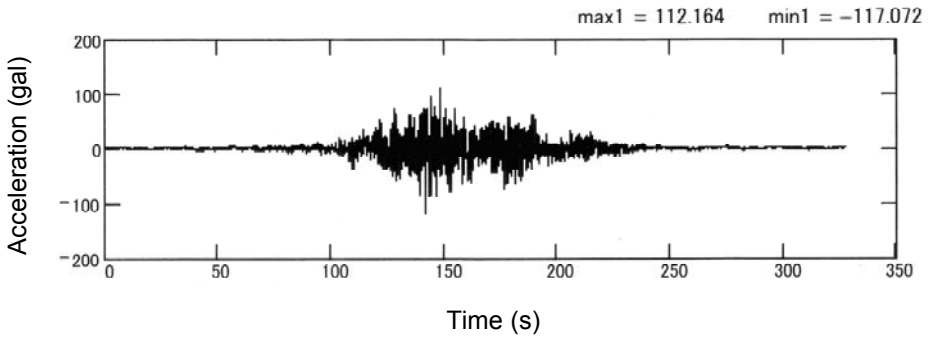

(a) Assumed Tonankai-Nankai Earthquake, PARI

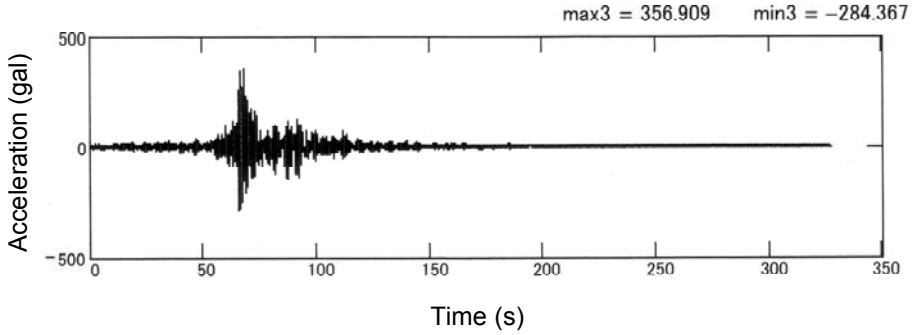

(b) Assumed Koi Fault, E22S component, by statistical Green's Function Method, PARI

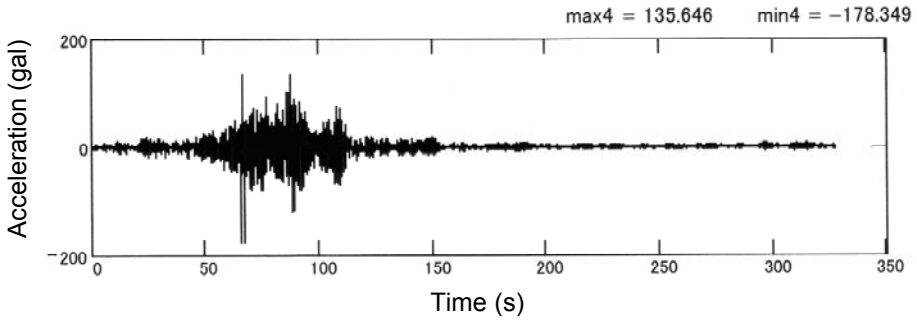

(c) Assumed Koi Fault, N22E component, by statistical Green's Function Method, PARI

Figure 112 — Level 2 Earthquake Ground Motion for checking

5.1.5.8 Seismic coefficient determinations

In the subsequent design process, seismic design coefficient is a useful variable to determine the initial cross section. The following process is used to determine the seismic coefficient. (611A)

The Fourier spectrum at ground surface obtained from one dimensional seismic response analysis is multiplied by the filter. It is to evaluate the seismic response effect of soil-structure system. The following filter is used. This one dimensional seismic response analysis is a non-linear analysis. (822A, 822B)

$$a(f)=\begin{cases} b & 0<f\le 1.0 \\ \dfrac{b}{1-\left(\dfrac{f-1.0}{1/0.34}\right)2+6.8\left(\dfrac{f-1.0}{1/0.34}\right)i} & 1.0\le f \end{cases} \tag{37}$$

a : A spectrum filter considering the frequency characteristics of the soil-structure system

f : frequency (Hz)

H : Height of quay wall (m)

H_R : Standard height of quay wall (m)

T_b : Primary natural period of behind ground (s)

T_{bR} : Standard primary natural period of behind ground (s)

T_u : Primary natural period of ground under a quay wall (s)

T_{uR} : Standard primary natural period of ground under a quay wall (s)

i : Imaginary

Figure 113 shows the filters. The filters are proposed for gravity-type quay wall and piers, but no reasonable filter is proposed for the sea walls yet. The concept of the filter is to delete the high frequency component which did not affect the deformation of the system but increase the PGA value. Figure 114 shows the Fourier spectra obtained by applying the filter. The time histories are calculated by inverse Fourier transform of these Fourier spectra.

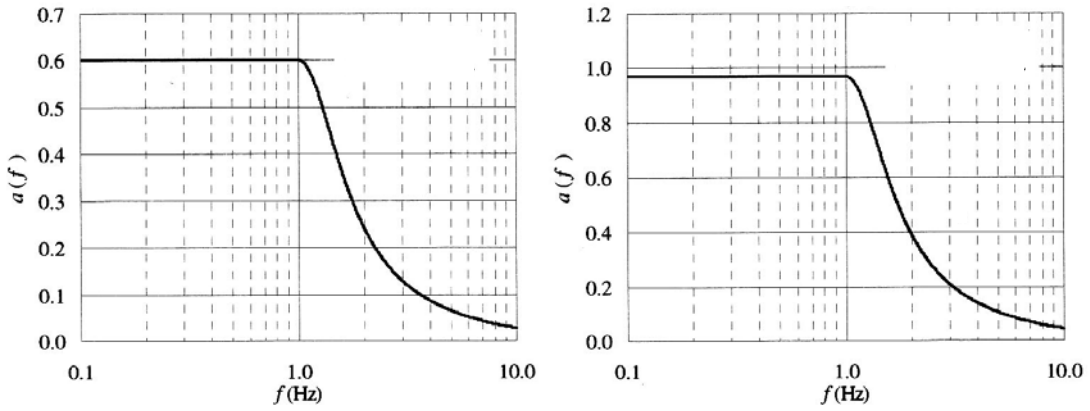

(a) Gravity-type quay walls (b) Piers

Figure 113 — Filter to consider the effect of frequency

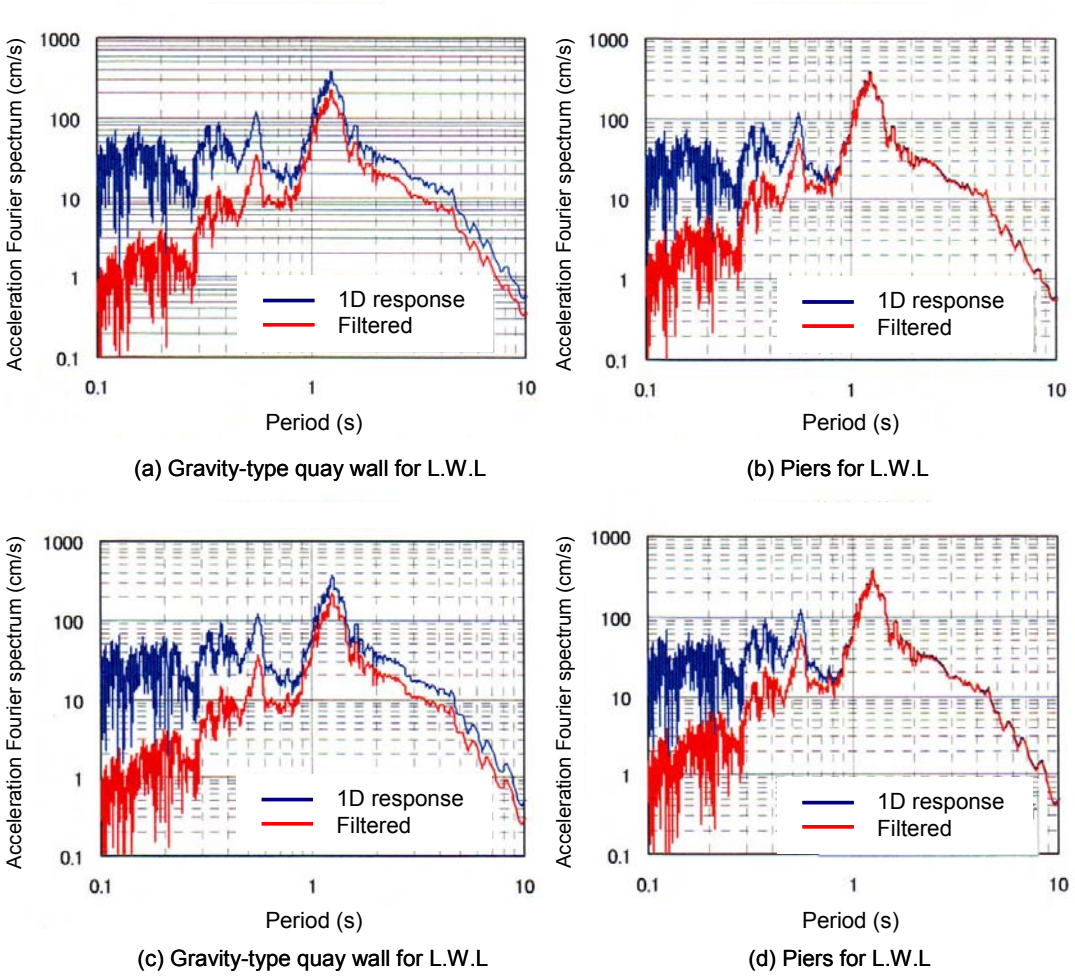

(a) Gravity-type quay wall for L.W.L

(b) Piers for L.W.L

(c) Gravity-type quay wall for L.W.L

(d) Piers for L.W.L

Figure 114 — Fourier spectra after filtering

In order to evaluate the influence of duration time of ground motion, a reduction ratio is calculated by using the time history of ground motion in Equation 3, which was derived by a regression analysis based on numerical parametric studies with nonlinear 2-D FE analyses.

$$p = 0.36 \ln\left(S / a_f\right) - 0.29 \tag{38}$$

p : Reduction ratio

S : square-root of sum of squares of ground motion after filtering (cm/s^2)

a_f : Maximum acceleration after filtering (cm/s^2)

Then, the adjusted maximum acceleration for calculation of seismic coefficient is given by the following equation using the reduction ratio.

$$a_c = p \cdot a_f \tag{39}$$

a_c : Adjusted maximum acceleration (cm/s^2)

p : Reduction ratio

a_f : Maximum acceleration after filtering (cm/s^2)

Finally, the seismic coefficient is given as follows;

$$k_{hk} = 1.78\left(\frac{D_a}{D_f}\right)^{-0.55}\frac{a_c}{g} + 0.04 \tag{40}$$

Where

k_{hk} : Characteristics value of seismic coefficient

a_c : Adjusted maximum acceleration (cm/s^2)

g : Gravity acceleration (=980cm/s^2)

D_a : Allowable horizontal displacement at the crest

D_f : Standard displacement (=10cm)

Note, this seismic coefficient is derived by the regression analysis based on numerical parametric studies, and the value is corresponding to the level of allowable displacement in horizontal. Here, the horizontal displacement of 10 cm is used as the negligible level of deformation, and based on the empirical relation; it corresponds to the 6.0 cm of deformation in vertical. The standard displacement is 10 cm, and it is used for the normalization of the equation. The determined seismic coefficients are summarized in Table 21, corresponding to the variation of tide level and type of filters.

Table 21 — Seismic coefficients for the checking

	Using the filter for Gravity-type quay wall		Using the filter for Pier-type quay wall	
Tide	L.W.L	H.W.L	L.W.L	H.W.L
a_c (cm/s2)	49.507	46.188	79.864	74.518
D_a	10.0	10.0	10.0	10.0
k_{hk}	0.13	0.12	0.19	0.18

5.1.5.9 Effects of soil liquefaction

Policies of countermeasures against soil liquefaction are summarized in Table 22.

Table 22 — Policies of countermeasure against soil liquefaction

Reference earthquake motions	Basic policy	Method for assessment of liquefaction potential
Level 1	If susceptibility of soil liquefaction is judged to be high, ground shall be treated by adequate countermeasures.	Evaluate by grain size distribution and N value. If the results are not clear, apply cyclic triaxial compression test.
Level 2 (Tsunami)	Based on the evaluated deformation in the dynamic analyses, needs of the countermeasure against the soil liquefaction shall be discussed.	Effective stress-based dynamic analysis

Evaluation of the susceptibility of liquefaction against Level 1 Earthquake Ground Motion is carried out for each layer by the method of grain size distribution and N values, as shown in Table 23. The results indicate that the susceptibility of liquefaction at the site is very low. Therefore, the risk of differential settlement is also very low. Note, in this method, the earthquake motion at the ground surface and within subsoil is adequately considered. (631A, 631B, 823A)

Table 23 — Results of evaluation of liquefaction

Soil	No	Elevation	Thickness(m)	Wet unit weight(kN/m^3)	N value	Overburden pressure (kN/m^3)	N value	Fc	N Value	Maximum shear stress (kN/m^2)	Acceleration	Evaluation of liquefaction
Backfill above the water level	1	5.00 3.00	2.00	18.0	9	18.00	12.30	14	22	1.20	45.73	IV
	2	3.00 1.27	1.73			51.57	9.79	14	18	3.40	45.23	IV
Back fill under the water level	3	1.27 -0.73	2.00	18.0	9	77.14	8.35	14	15	5.70	50.69	IV
	4	-0.73 -2.73	2.00			97.14	7.41	14	13	7.30	51.55	IV
	5	-2.73 -4.20	1.47			114.49	6.70	14	12	8.90	53.33	IV
Silt	6	-4.20 -6.50	2.30	18.0	7	133.34	4.45	25	9	11.00	56.59	III
Silty sand	7	-6.50 -8.50	2.00	18.0	5	154.84	2.41	40	5	12.80	56.71	III
Clayey silt	8	-8.50 -10.50	2.00	16.0		170.84		90		12.90	51.80	
	9	-10.50 -12.50	2.00			182.84		90		12.70	47.65	
	10	-12.50 -14.50	2.00			194.84		90		12.50	44.01	
	11	-14.50 -16.50	2.00			206.84		90		11.00	36.48	
	12	-16.50 -18.50	2.00			218.84		90		11.20	35.11	
	13	-18.50 -20.50	2.00			230.84		90		11.90	35.57	
	14	-20.50 -22.50	2.00			242.84		90		13.30	37.57	
	15	-22.50 -24.50	2.00			254.84		90		14.40	37.69	
	16	-24.50 -25.50	1.00			263.84		90		14.80	38.48	
Silty sand	17	-25.50 -27.50	2.00	20.0	9	276.84	2.66	40	5	19.40	48.07	IV
	18	-27.50 -30.00	2.50			299.34	2.32	40	5	27.70	63.48	III

I: Liquefiable
II: High probability of Liquefaction
III: Low probability of liquefaction
IV: Non-liquefaction

5.1.5.10 Spatial variation

Spatial variation along the coastal line should be considered as usual design practice. However, parts of the structures are not firmly connected along the line, and the thickness of walls will work well to prevent the inundation of waves even when a certain level of irregularity of displacement occurred. Therefore, in this case, no spatial variation in ground motion and geotechnical conditions is considered (641A, 641B, 641C, 645A)

5.1.5.11 Procedure for specifying seismic actions

In this example, the seismic performance against Level 1 Earthquake Ground Motion is conducted by the simplified equivalent static analysis, and the seismic performance against Level 2 Earthquake Ground Motion is conducted by the detailed dynamic analysis. After the selection of the type of analysis, model and the method are adequately selected, and the specification of performance criteria parameters and geotechnical characterization are follows. In this example, the type of analysis is chosen mainly by the level of complexity and non-linearity (711A, 711B, 712A)

In this example, there is no detailed equivalent static analysis and simplified dynamic analysis. (821A, 821B, 821C)

5.1.5.11.1 Simplified equivalent static analysis

Stability against sliding type deformation, over-turning, insufficient bearing capacity are examined by the seismic coefficient method. For example, the stability against the slide is checked by the following equation;

$$f_d\left(W_d + P_{vd} - P_{Bd} + P_{ud}\right) \geq \gamma_a\left(P_{Hd} + P_{wd} + P_{dwd} + P_{fd} + P_{nd}\right) \tag{41}$$

where f_d : friction factor between the basement of wall and foundation

W_d : Weight of materials that composes wall (kN/m)

P_{vd} : Sum of vertical earth pressure which acts on the wall (kN/m)

P_{Bd} : Buoyancy which acts on the wall (kN/m)

P_{ud} : Reduction of buoyancy when the tide is on the ebb (kN/m) (only during the ebb tide)

P_{Hd} : Sum of the horizontal earth pressure which acts on the wall (kN/m)

P_{wd} : Sum of the residual water pressure which acts on the wall (kN/m)

P_{dwd} : Sum of the dynamic water pressure which acts on the wall (kN/m) (only during the earthquake)

P_{fd} : Inertia force which acts on the wall (kN/m) (only during the earthquake)

P_{nd} : Sum of negative wave force which acts on the wall during the ebb (kN/m) (only during the ebb tide)

γ_a : Structural analysis factor

The followings are example calculations for the cross section shown in Figure 108.

In the Level 1 Earthquake Ground Motion at L.W.L.

$$f_d\left(W_d + P_{vd} - P_{Bd} + P_{ud}\right) = 0.600 \times \left(251.787 - 5.941 - 6.898\right) = 143.369 \quad kN/m^2$$

$$\gamma_a\left(P_{Hd} + P_{wd} + P_{dwd} + P_{fd} + P_{nd}\right) = 1.000 \times \left(61.695 + 0.376 + 0.000 + 47.840\right) = 109.911 \quad kN/m^2$$

left side / right side = 1.304 ≥ 1.0 O.K.

In the Level 1 Earthquake Ground Motion at H.W.L.

$$f_d\left(W_d + P_{vd} - P_{Bd} + P_{ud}\right) = 0.600 \times \left(251.787 - 6.077 - 54.288\right) = 114.853 \quad kN/m^2$$

$$\gamma_a\left(P_{Hd} + P_{wd} + P_{dwd} + P_{fd} + P_{nd}\right) = 1.000 \times \left(58.063 + 0.000 + 8.078 + 45.322\right) = 111.463 \quad kN/m^2$$

left side / right side = 1.030 ≥ 1.0 O.K.

The stability against the over-turning is checked by the following equation;

$$aW_d - bP_{Bd} + cP_{vd} + dP_{ud} \geq \gamma_a\left(eP_{Hd} + hP_{wd} + kP_{dwd} + lP_{fd} + mP_{nd}\right) \tag{42}$$

Where W_d: Weight of materials that composes wall (kN/m)

a Distance from the line of action of weight of wall to the toe of wall (m)

b : Distance from the line of action of buoyancy to the toe of wall (m)

c : Distance from the line of action of sum of the vertical earth pressure to the toe of wall (m)

d : Distance from the line of action of the reduce of buoyancy to the toe of wall (m)

e : Distance from the line of action of sum of the horizontal earth pressure to the bottom of wall (m)

h : Distance from the line of action of sum of the residual water pressure to the bottom of wall (m)

k : Distance from the line of action of sum of the dynamic water pressure to the bottom of wall (m)

l : Distance from the line of action of inertia forces to the bottom of wall (m)

m : Distance from the line of action of sum of negative water forces to the bottom of wall (m)

The forces and the distances dealt with in Equation 41 and Equation 42 are schematically shown in Figure 109.

The followings are example calculations for the cross section shown in Figure 108.

In the Level 1 Earthquake Ground Motion at L.W.L.

$$M_{wd} + M_{PVd} - M_{PBd} = 760.873 - 24.204 - 8.623 = 728.046 \quad kN/m \cdot m$$

$$\gamma_a\left(M_{PHd} + M_{Pwd} + M_{Pdwd} + M_{PFd}\right) = 1.100 \times \left(121.349 + 0.034 + 0.000 + 151.315\right) = 299.968 \quad kN/m \cdot m$$

left side / right side =2.427 ≥ 1.0 O.K.

In the Level 1 Earthquake Ground Motion at H.W.L.

$$M_{wd} + M_{PVd} - M_{PBd} = 760.873 - 24.296 - 106.409 = 630.168 \quad kN/m \cdot m$$

$$\gamma_a \left(M_{PHd} + M_{Pwd} + M_{Pdwd} + M_{PFd} \right) = 1.100 \times \left(117.647 + 0.000 + 8.918 + 143.351 \right) = 296.908 \quad kN/m \cdot m$$

left side / right side = 2.122 ≥ 1.0 O.K.

The bearing capacity is also checked; however, due to the limitation of pages, the detail is not described here. As a conclusion, the model design satisfies the performance criteria for reference earthquake motion for serviceability

Note, the analysis is carried out by common seismic coefficient method, and this method is regarded appropriate for the verification of serviceability. The geotechnical and material studies are carried out to determine appropriate parameters such as dynamic earth pressures. Response control and ground improvement are no necessary in this case. (713A, 715A, 715B) There is no superstructure to be considered. (811A, 811B, 811a, 811b) Non-linear behaviour of soils is considered in the estimation of seismic coefficient, and there is no large relative displacement. (812A, 813A)

5.1.5.11.2 Detailed dynamic analysis

The seismic performance against Level 2 Earthquake Ground Motion is evaluated by effective stress-based FE analysis. In this example, there is no major superstructure. Therefore, there is no major difference from a simplified dynamic analysis. (911A, 911B, 921A)

Analysis code “FLIP” (Iai et al, 19xx) is used here, considering the non-linear behaviour of soil including the effect of liquefaction. Seismic motions for an assumed Koi fault earthquake and an assumed Tonankai-Nankai earthquake are used as input motions. These motions are given as firm ground motions, by a site-specific study. (911C, 912A, 912B, 921B, 921C, 921D, 922A)

Model for numerical analysis is shown in Figure 115. Since the soil layer is uniform, no major relative displacements are expected. (913A)

Due to the restriction of pages, parameter identification for the analysis is not described here. The computed results of the dynamic analysis are summarized in Table 24 and Figure 116.

For Koi fault earthquake, the allowable settlement is as follows.

Allowable settlement

=|design high tide – mean high tide|

+ necessary height increase against the 10 years probability wave

=|C.D.L. +6.06 –C.D.L+3.76|+1.0

=3.30 m

The estimate settlement is 0.7m, and it is less than the allowable settlement.

For the Tonankai-Nankai earthquake, it is necessary that the elevation of the crest should be higher than the wave height of Tsunami. The estimated Tsunami height in this area is +0.6 m beyond the H.W.L. The height of the model wall crest is C.D.L. +8.04 m, and the H.W.L is C.D.L. +4.64 m. Thus the allowable settlement is as follows;

Allowable settlement

=8.04-4.64-0.6

=2.8 m.

The estimate settlement is 0.43 m, and it is less than the allowable settlement.

As a conclusion, the model design satisfies the performance criteria for reference earthquake motion for safety.

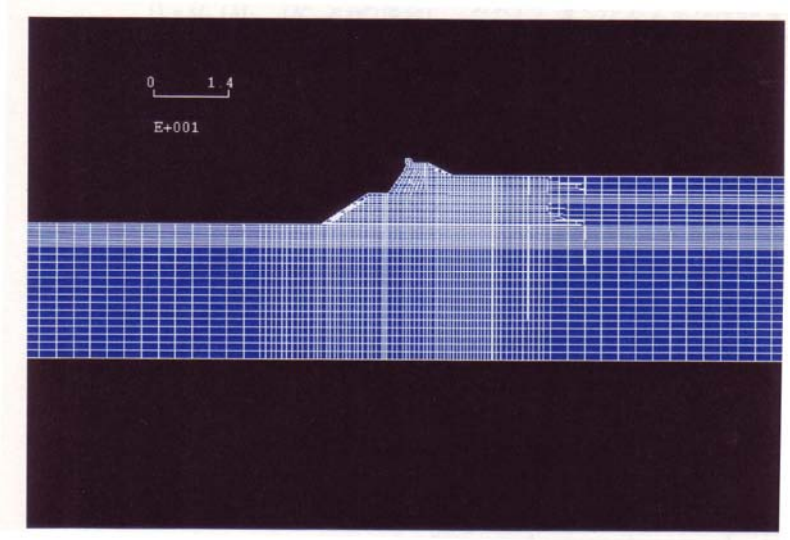

Figure 115 — FE Model for numerical analysis

Table 24 — Results of numerical analysis

Earthquake	Horizontal displacement (m)	Vertical settlement (m)
Koi fault earthquake	1.36	0.70
Tonankai-Nankai earthquake	0.53	0.43

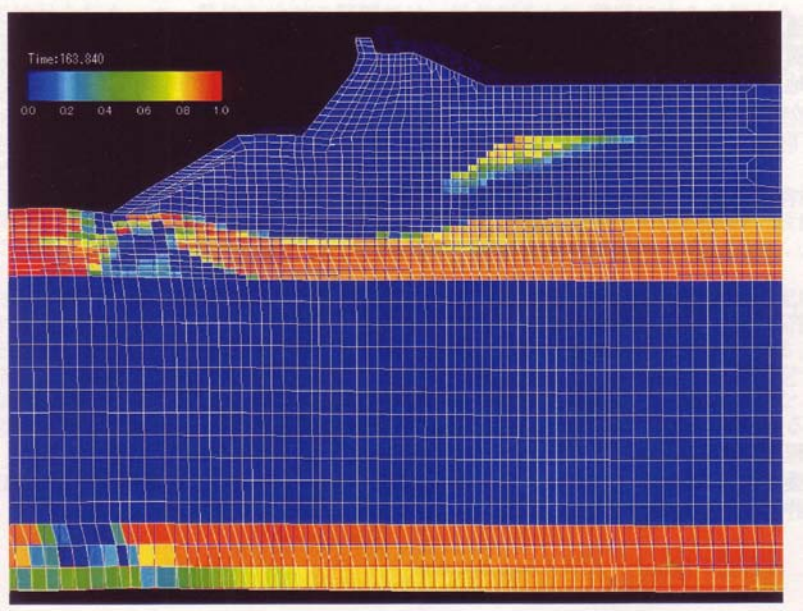

(a) Residual deformation in Koi Fault earthquake

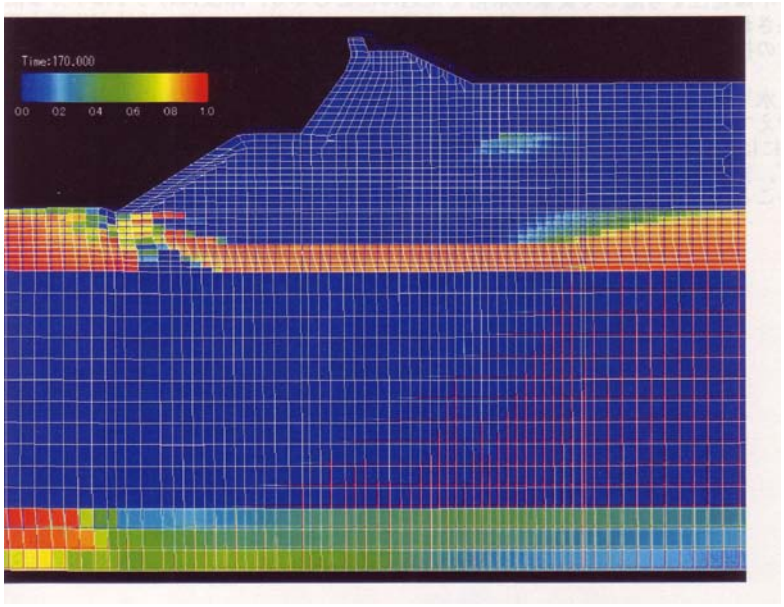

(b) Residual deformation in Tonankai-Nankai earthquake

Figure 116 — Residual deformation

5.2 Demonstrations evaluating and designing for ground displacement effects

5.2.1 Pile foundations of railway bridges

5.2.1.1 Outline of railway bridge pier

This example shows the seismic design procedure of an average railway bridge pier which was designed based on The Design Standards for Railway Structures and Commentary - Seismic Design (Railway Technical Research Institute, 1999). This design standard has been issued in December 1999 and hereafter is abbreviated as Seismic Design Standard of Railway Structure or simply Railway Standard.

The bridge pier is composed of an overhanging reinforced concrete column of rectangular cross section, which is supported by a foundation of nine 1200-mm-diameter cast-in-place concrete piles (Figure 117). The bridge is designed and constructed for the Japanese high-speed bullet train which is called “Shinkansen”. (511A)

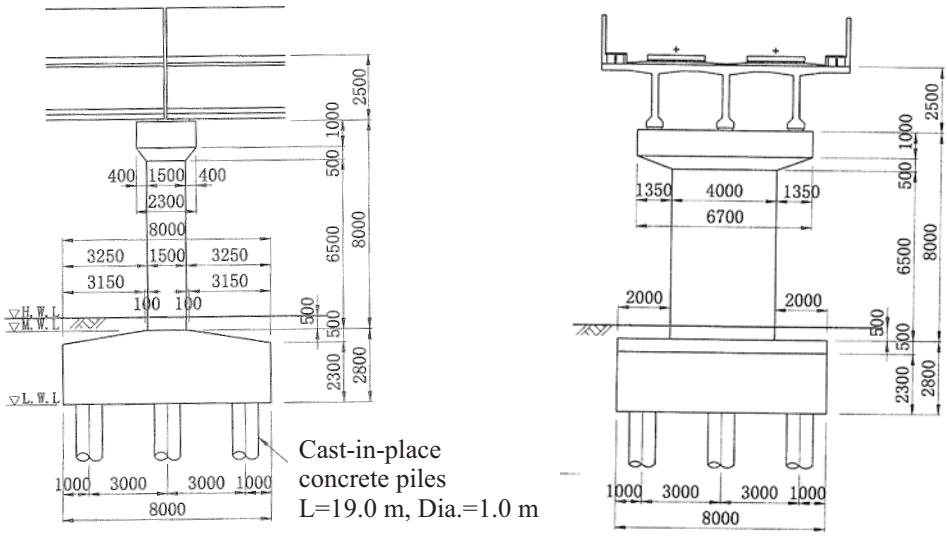

(a) Longitudinal direction **(b) Transverse direction**

Figure 117 — Reinforced concrete bridge pier (Unit: mm when no unit shown)

The soil profiles and properties of soil layers are summarized in Table 25. The N-value (N_{50}) and the shear velocity Vs have been given on the basis of the results obtained by in-situ tests. The dynamic properties, such as strain-dependencies of shear modulus and hysteretic damping, have been defined by cyclic loading tri-axial tests. (641C)

Table 25 — Soil properties

Depth (m)	Soil	Vs (m/s)	ρ (t/m^3)	N_{50}
-2.6	Sand	146	1.8	10
-7.6	Sand	167	1.8	15
-13.6	Clay	135	1.5	4
-18.0	Clay	183	1.6	10
-19.0	Sand	251	2.0	50

5.2.1.2 Seismic performance requirements

5.2.1.2.1 Importance of structure

The importance of a structure is defined with regard to the operating speed and number of trains and the difficulty of recovery in an event damaging to the structure. According to Railway Standard, structures are classified to be the important structures as follows: a) structures for the “Shinkansen” railway network and metropolitan passenger railway networks, and b) cut-and-cover tunnels with difficulties of recovery in an occurrence of structural damage.

According to the classification rule shown in Table 26, the focused bridge pier was classified to “important structure”.

Table 26 — Classification of importance of bridges (Railway Standard, 1999)

Importance Class	Definitions
Important structures	Structures for the Shin-kansen (high-speed-train) railway network and metropolitan passenger railway networks. Cut-and-cover tunnels with difficulties of recovery in an occurrence of structural damage.
Other structures	Bridges except important structures

5.2.1.2.2 Seismic performance requirements

As shown in Figure 118, the seismic performance of a structure is related to the difficulty of recovery of anticipated damage to it after an earthquake. For a relationship between reference earthquake motion level and expected seismic performance (Table 27), the Seismic Performance I is applied to the Level-1 Earthquake Ground Motion for design. The Seismic Performance II is applied to the Level-2 Earthquake Ground Motion for the important structures, and Seismic Performance III is applied to other structures. (512a, 512b), (512A)

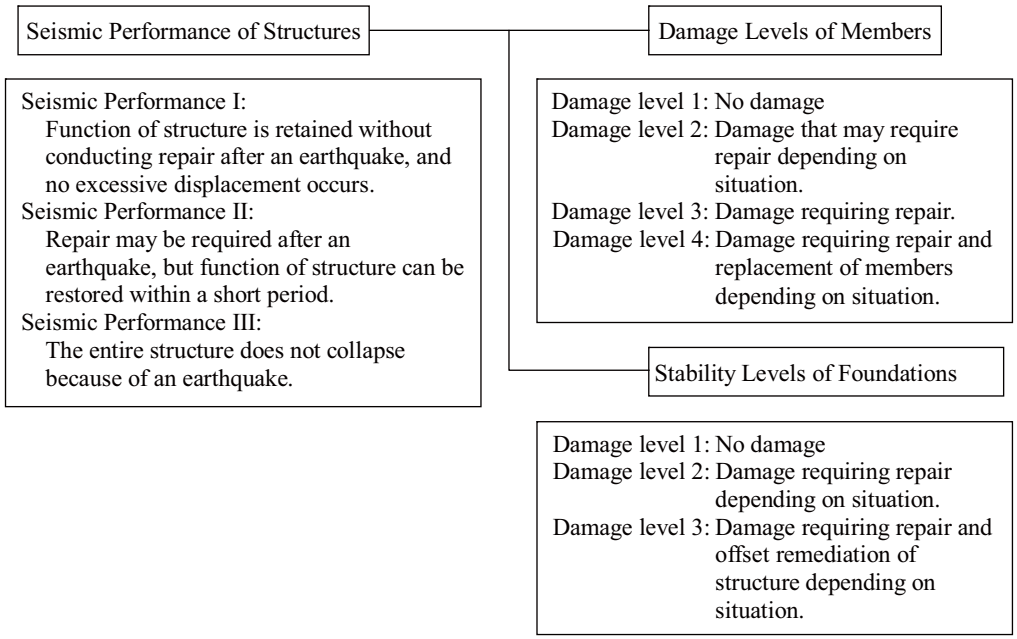

Figure 118 — Seismic performance of railway structures (Railway Standard, RTRI [1])

Table 27 — Performance grades of railway structures (Railway Standard, 1999)

	Design Earthquake Ground Motion	
Importance of structure	Level-1	Level-2
Important structures	Seismic Performance I	Seismic Performance II
Other structures	Seismic Performance I	Seismic Performance III

According to the performance grades specification shown in Table 27, the bridge pier was required to achieve Seismic Performance I for the Level-1 Earthquake Ground Motion and Seismic Performance II for the Level-2 EGM.

5.2.1.2.3 Performance criteria and limit states

The seismic performance of a structure depends on both the degrees of damage to component members of the structure and the degree of stability of its foundation. The damage degree of each member has to be set in consideration of its role during an earthquake. As the stability of a foundation relates to the deformation of a structure, both bearing capacity and displacement are necessary to be taken into account.

The envelope curve of bending moment-curvature relation in a reinforced concrete member is expressed as shown in Figure 119. In Figure 119, the damage level 1 is set within the curvature to make the longitudinal reinforcement steel yield (point B); the damage level 2 is set within the curvature at maximum capacity (point C); the damage level 3 is set within the curvature at which the yield capacity can be sustained (point D); and the damage level 4 is set for the curvature beyond the point D. (514A, 514B, 514C)

For the deformation of bridge is strongly affected by the stability level of foundation, the stability level of foundation should by set based on bearing capacity and displacement. Figure 120 illustrates the relation between the stability level and load-displacement curve of the foundation. The stability levels of foundation are defined in Table 30. (514A, 514B, 514C)

Table 29 summarizes the relations between the seismic performance of bridge pier and the limit values for member damage levels and foundation stability levels.

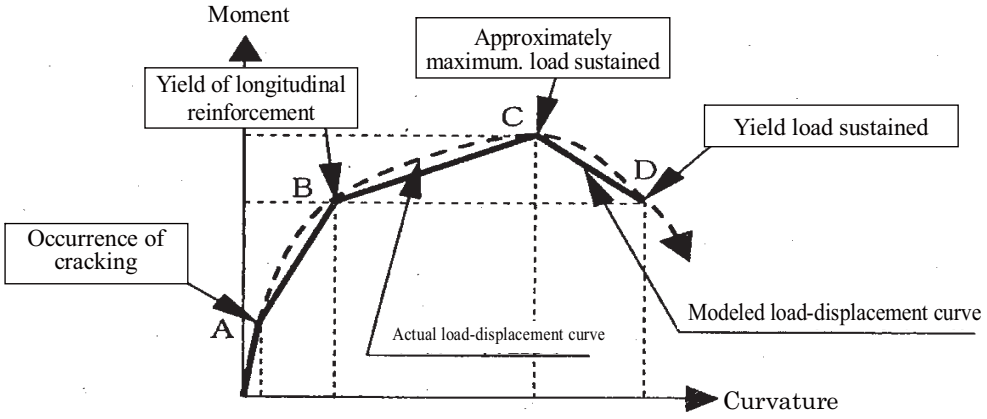

Figure 119 — Envelope curve of moment-curvature relation of reinforced concrete members

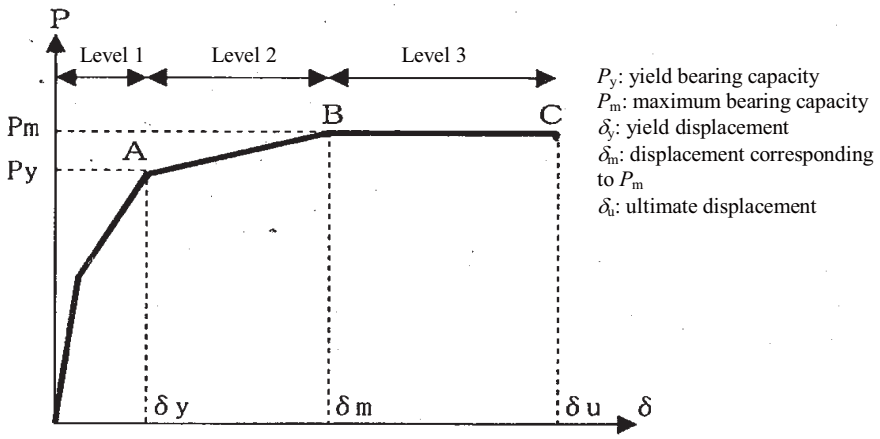

Figure 120 — Load-displacement curve and stability levels of foundation

Table 28 — Stability level of foundation

	Stability Level of Foundation
Stability Level 1	In principle, the load acting on a foundation is smaller than the yielding point of bearing capacity of the foundation, and large displacement does not occur. In addition, the resultant forces in component members of the foundation do not exceed the yielding point of bearing capacity.
Stability Level 2	Underground supporting members may partially or totally yield but maintain a sufficient bearing capacity. In addition, harmful residual displacement potentially reducing the function of structure after an earthquake does not take place.
Stability Level 3	The structure retains the bearing capacity required to prevent its collapse due to failure of the underground supporting members.

Table 29 — Relations among seismic performance of bridges, damage level of members and stability level of foundations (Railway Standard, 1999)

	Seismic Performance I	Seismic Performance II	Seismic Performance III
Damage level of member	1	3	3
Stability level of foundation	1	2	3

*Of the member damage levels, bearing damage level is in accordance with "7.11 Bearings."

5.2.1.3 Reference earthquake ground motions

The Railway Standard prescribes the Level-1 and Level-2 Earthquake Ground Motions as reference earthquake ground motions for design. The Level-1 EGM is set as a reference earthquake motion for serviceability, and the Level-2 EGM is set as that for safety. (513A)

These Level-1 and Level-2 EGMs are provided at a firm ground (so-called engineering base for input motion) and their properties are represented by acceleration response spectra and time histories. The firm ground is generally set to be the upper boundary of a layer whose shear wave velocity is greater than 400 m/sec. (623A)

5.2.1.3.1 Level-1 Earthquake Ground Motion

The intensity of Level-1 EGM is determined as expected value of earthquake ground motion with a return period of 50 years based on an earthquake risk analysis. (621A, 621B)

5.2.1.3.2 Level-2 Earthquake Ground Motions

Earthquakes occurred in and around Japanese archipelago are classified to intra-plate and inter-plate types. The Railway Standard prescribes a principle to take into account both type earthquakes.

The Design Spectrum I is specified in consideration of inter-plate seismic activities involving magnitude 8 class earthquakes. The Design Spectrum II is prescribed with consideration of anticipated intra-plate earthquakes beneath a structure in interest. Figure 121 shows the Design Spectrum I and Spectrum II according to the Railway Standard. These Design Spectra were developed as response spectra with a non-exceedance probability of 90% on the basis of a statistical analysis using a huge dataset of past earthquake ground motions recorded on firm ground. Examples of acceleration time histories for design are demonstrated in Figure 122. These are compatible with the Design Spectrum I and Spectrum II, being synthesized with consideration of the phase characteristics of earthquake ground motion utilizing a statistical model of group delay time based on a concept proposed by Sato *et al*. (2001). (621A, 621C, 622a) Reflecting a current Japanese situation that methods to simulate strong earthquake motions on the basis of theoretical

fault models have become popular in civil engineering field, the design spectrum considering theory of fault mechanism is specified as the Design Spectrum III. The Design Spectrum III may be used instead of the Spectrum II.

A flowchart to determine the Level-2 Earthquake Ground Motion is shown in Figure 123. In this example, it was unknown whether active faults exist near the bridge. The construction site locates in an area with high possibility of existence of active faults but detection of possible faults is not easy because of thick Holocene deposits. The site is, therefore, classified as the area with high uncertainty of faults existence. Following the flowchart shown in Figure 123, the Design Spectrum II was adopted as the Level-2 Earthquake Ground Motion. (622A)

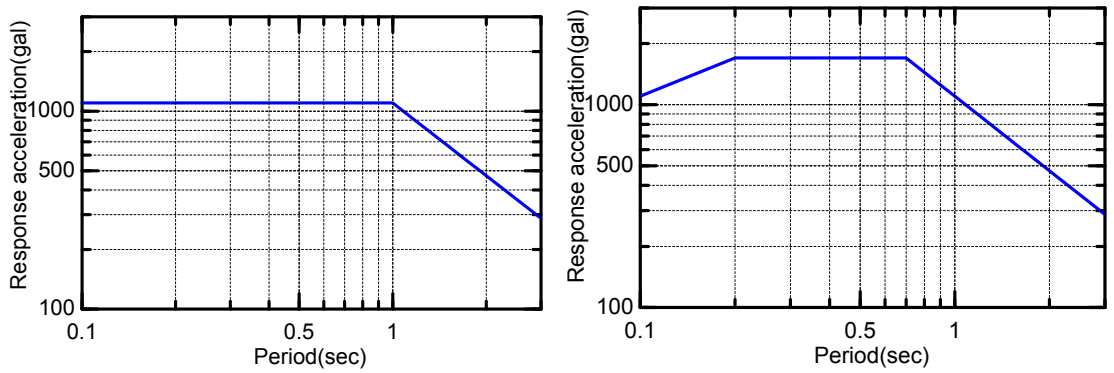

Figure 121 — Acceleration response spectrum of the Design Spectra I and II

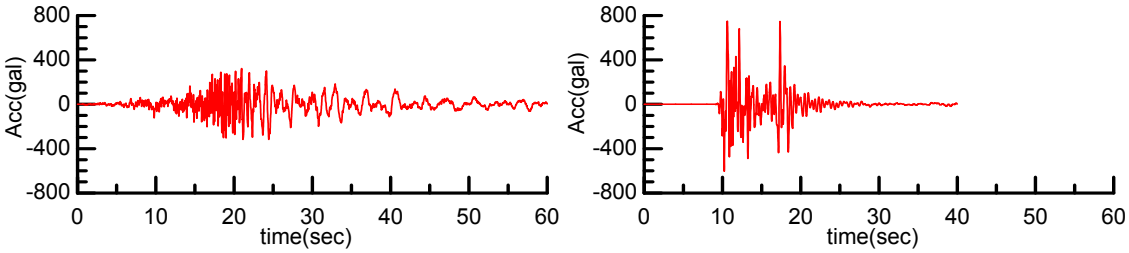

(a) For Design Spectrum I **(b) For Design Spectrum II**

Figure 122 — Acceleration time histories compatible with the Design Spectra I and II

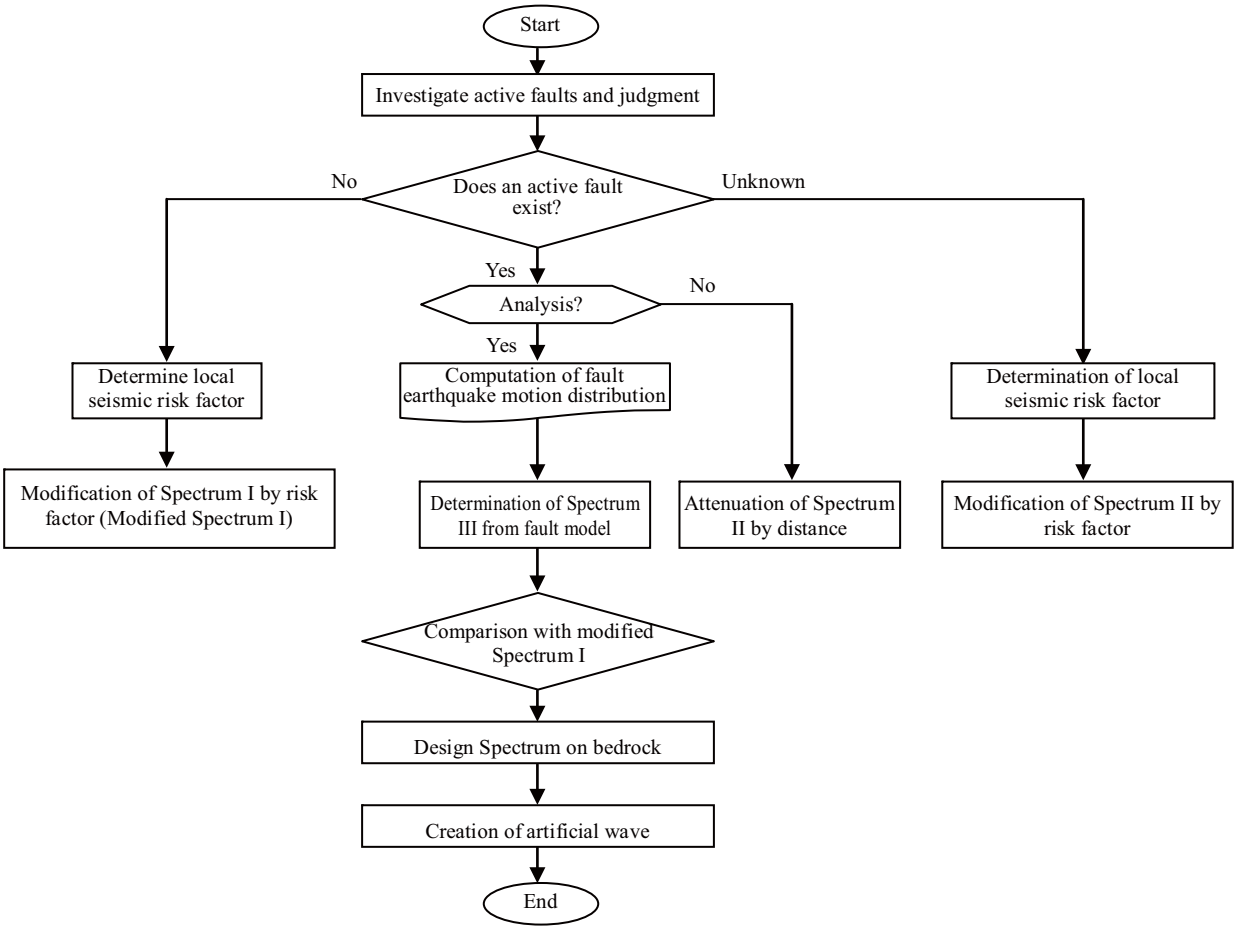

Figure 123 — Flowchart to determine the Level-2 Earthquake Ground Motion (Railway Standard, 1999)

5.2.1.4 Site response analysis and assessment of liquefaction potential

The reference earthquake ground motions at the ground surface and at a reference depth of ground were obtained by a one-dimensional site-specific dynamic response analysis using model properties shown in Table 25. The dynamic analysis is a total stress approach, because the potential of liquefaction in this site is quite low. (631A, 631B, 631C)

The soil column was divided into multiple layers for calculation and was modelled as a column consisting of lumped masses connected with non-linear shear springs. Nonlinear stress-strain properties of soil layers were developed by the general hyperbolic model with S-shape hysteretic model (GHE-S model) (Murono and Nogami, 2006) .

Figure 124 and Figure 125 show the acceleration response spectra and the acceleration time history at the ground surface obtained by the site response analysis, respectively. Figure 126 shows a set of distributions of soil responses along the depth, including (a) maximum response acceleration, (b) maximum soil displacement relative to the firm ground, and (c) maximum shear strain. Relationships of response shear stress and shear strain in two different depths are shown in Figure 127. Non-linear responses remarkably appear at the boundary between the third and the fourth layers, so that soil deformation largely increases at this depth as a result. (623B)

Note Description about the check for the Level-1 Earthquake Ground Motion is omitted here due to page limitation.

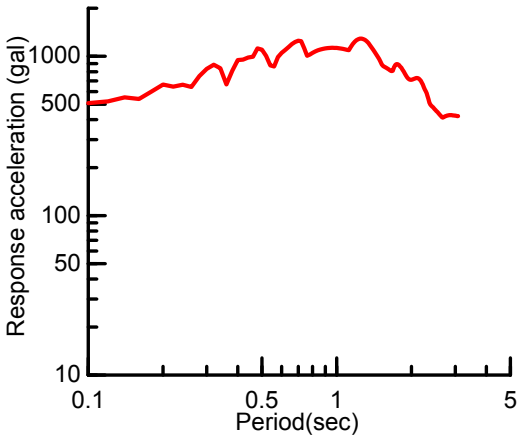

Figure 124 — Acceleration response spectra at ground surface

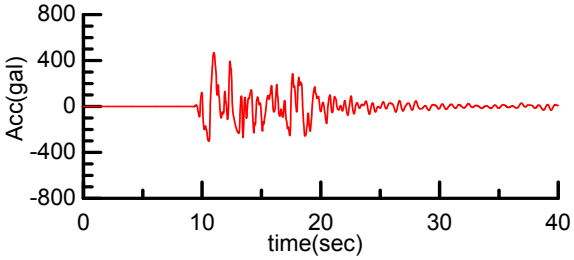

Figure 125 — Acceleration time history at ground surface

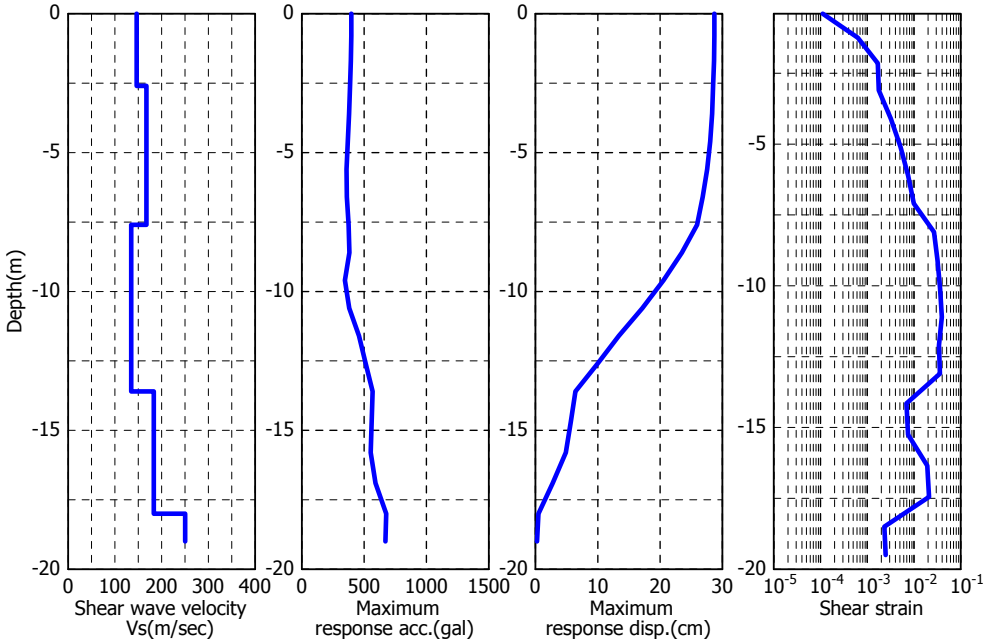

Figure 126 — Distributions of soil responses: maximum response acceleration, maximum soil displacement relative to firm ground, and maximum shear strain along the depth

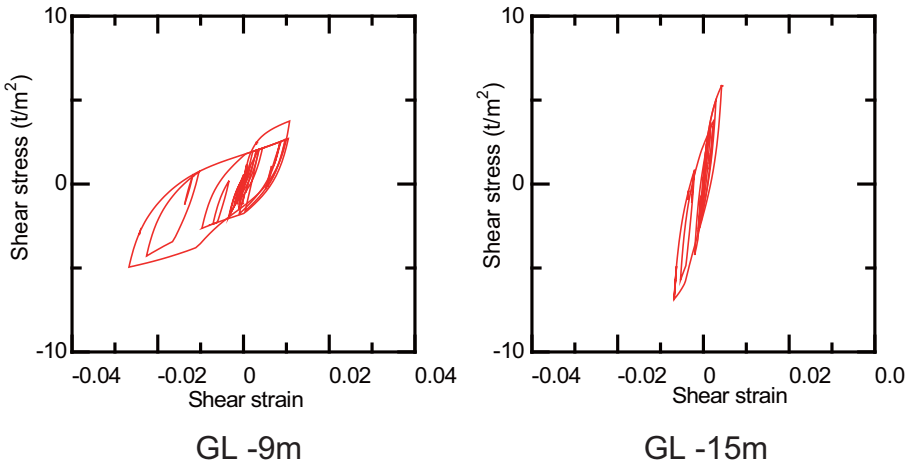

Figure 127 — Relations between response shear stress and shear strain at two different depths

5.2.1.5 Procedure for specifying seismic actions on piles

The seismic response of a pile-foundation embedded in a soft ground is affected by both kinematic and inertial interactions among a superstructure, a foundation and surrounding soils. In order to evaluate resultant forces such as bending moment and shear force in piles, effects of these two types of interactions should be taken into account. Seismic Deformation Method, a simplified equivalent static analysis of applying seismic soil deformations to piles through imaginary interaction springs connecting piles with a soil column, was used in order to evaluate such effects in this example. Figure 128 schematically shows the model of analysis used in the design. (711B, 712A)

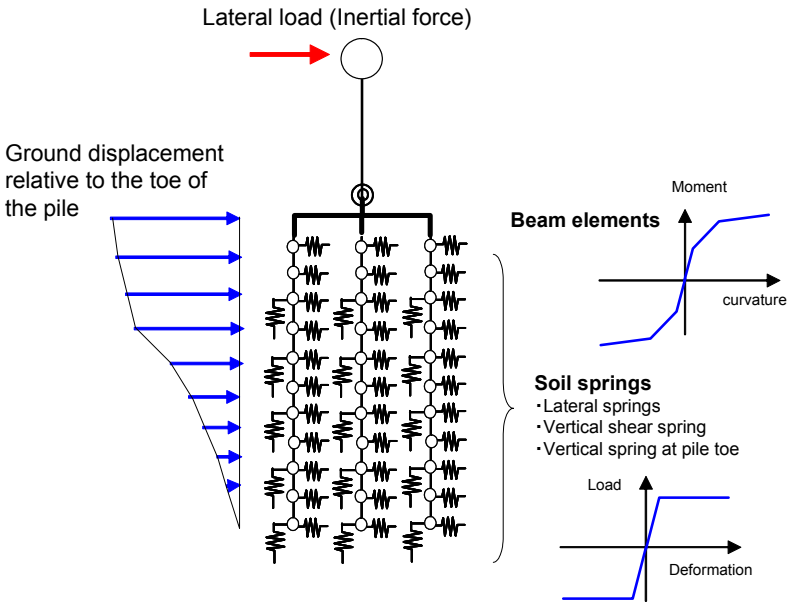

Figure 128 — Calculating model for Seismic Deformation Method

5.2.1.6 Simplified equivalent static analysis - Seismic Deformation Method

5.2.1.6.1 Seismic actions on piles

(1) Equivalent static inertia force

In the Seismic Deformation Method, a seismic action on a foundation induced by the inertial interaction between the superstructure and the foundation-soil system can be modelled as an equivalent static inertia force of the superstructure. This action is specified on the basis of the strength demand spectra provided by Railway Standard, which were developed in a set of nonlinear response spectra. The procedure to compute the equivalent static inertia force of the superstructure using the strength demand spectra is mentioned as follows: (711A, 713A)

a) Calculate a set of strength demand spectra for seismic ground motion at ground surface (see Figure 125) obtained from a site response analysis. Figure 129 shows a set of strength demand spectra.

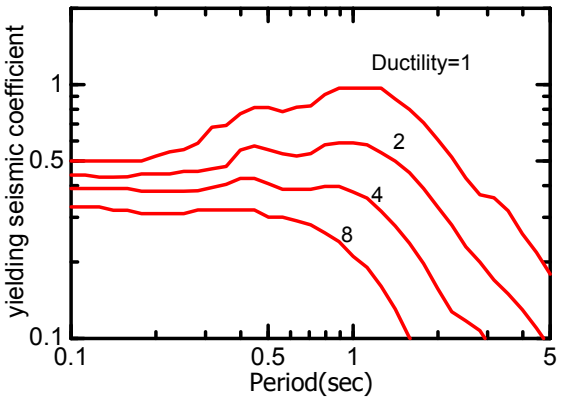

Figure 129 — Strength demand spectra

b) Obtain the value of yielding seismic coefficient K_{hy} using a push over analysis on the superstructure.

c) Obtain the value of equivalent natural period of the superstructure.

d) Obtain the point of intersection of the horizontal line of constant value of yielding seismic coefficient obtained in Step b) and the vertical line of constant value of equivalent natural period obtained in Step c). Then, determine a demand yield seismic coefficient spectrum diagram crossing the obtained intersection by interpolation, and accordingly determine a ductility factor μ at the same time.

e) Calculate a peak response displacement using an equation of μ x δ_y, where δ_y is a yielding displacement.

f) Obtain the seismic coefficient corresponding to the peak response displacement calculated in the previous step in the load-displacement curve previously obtained (see Figure 130). After that, calculate the inertia force by multiplication of the seismic coefficient obtained and the weight of the superstructure. In this example, inertial force is obtained as $0.73 \times W$, where W is the weight of superstructure.

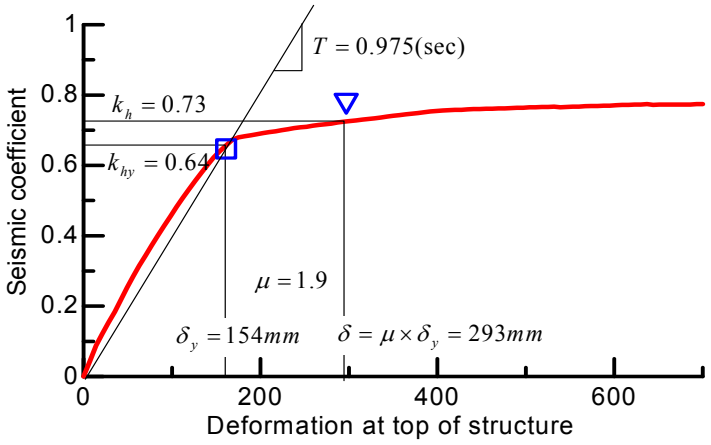

Figure 130 — Lateral load-displacement curve of bridge pier (for transverse direction)

(2) Equivalent static soil deformation

The action on piles induced by a kinematic interaction between piles and soils can be modelled as an equivalent static soil displacement relative to the bottom of the piles. This action can be specified on the basis of a maximum soil displacement distribution obtained as the response of a soil column shown in Figure 126. (711A)

(3) Combination of equivalent inertial force and equivalent static soil displacement

Much attention, however, should be paid to combine the inertial force of superstructure and the soil displacement. It is because that the maximum acceleration response of the superstructure and the maximum displacement response of the soils do not always appear at the same time. (811b)

In general, the characteristics of the soil-pile-structure interaction strongly depend on the relationship between the natural periods of structure T_s and soil deposit T_g. As the result, phase difference between the response of superstructure and the response of free field is generated depending upon to the relationship between their natural periods.

The fundamental characteristics about the phase relation between inertial force and soil displacement can be summarized as follows according to Murono and Nishimura (2000);

a) When $T_g<T_s$, the soil displacement and the inertia force act on the foundation with nearly same phase.

b) When $T_g=T_s$, the actions of inertia force and soil displacement deviate nearly 90 degree with each other.

c) When $T_g>T_s$, the soil displacement and the inertia force act on a foundation with nearly inverse phase.

During an earthquake, a phase relation between the inertial force and the soil displacement may become more complicated. The combination of two kinds of seismic actions due to inertial and kinematic interactions with a phase difference can be expressed in a generalized equation as follows:

$$R_t = \beta \times R_a + \gamma \times R_g \tag{43}$$

,where R_t is the seismic action to be considered in design; R_a is the inertial force based on the maximum response of the superstructure (see Section 6.1(1) and Figure 130) and R_g is the soil displacement based on the maximum displacement distribution of the free field response (see Figure 126), respectively. The coefficients β and γ are the parameters to combine R_a and R_g. The combination of β and γ changes step by step during an earthquake. In the seismic design process, the most critical combination for the resultant forces in piles should be considered as follows;

Combination A: at the instance that the effects of the inertial force are dominant

$$R_t = 1.0 \times R_a + \gamma \times R_g \tag{44}$$

Combination B: at the instance that the effects of the soil deformation are dominant

$$R_t = \beta \times R_a + 1.0 \times R_g \tag{45}$$

The Combination A expresses the situation that the influence of the inertial force becomes largest and the combination B expresses the situation that an influence of the soil deformation becomes largest.

Because the phase difference between the inertial and kinemaic interactions strongly depends on the period ratio $\alpha = T_s / T_g$, as mentioned earlier, the coefficients β and γ also vary with α. When T_s<T_g, the coefficients β and γ are nearly equal to 1.0 because the inertial force and soil deformation act on a foundation in the same phase. The coefficients β and γ decrease for increasing $\alpha = T_s / T_g$, because phase difference increases. Figure 131 shows the one of the example of combination coefficient, which is prescribed in the Seismic Design Standard (1999). Parameters used to specify the seismic actions are summarized in Table 30. (811b)

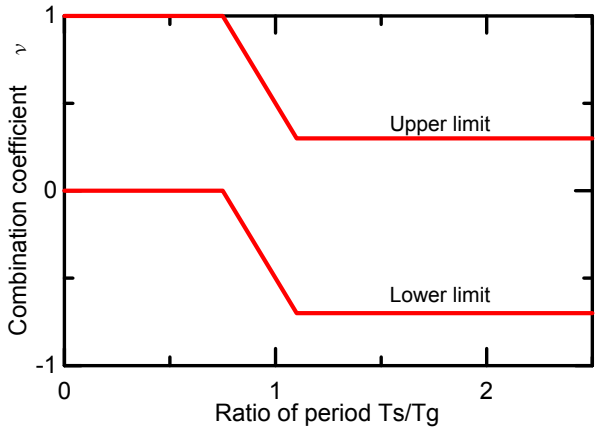

Figure 131 — Combination coefficient (Railway Standard, 1999)

Table 30 — Parameters used to specify the seismic actions

		Longitudinal direction	Transverse direction
Yielding seismic coefficient		0.38	0.64
Response seismic coefficient (Equivalent inertial force)		0.43	0.73
Equivalent Period of structure Ts (sec)		1.063	0.975
Period of soil deposit (sec)		0.47	0.47
Period ratio $\alpha = T_s / T_g$		1.131	1.037
Coefficients $\beta, \gamma = \nu$	Upper*	1.0	1.0
	Lower	-0.7	-0.57

* When load-displacement curve bends obviously, the combination factor ν for upper limit should be 1.0. It has been confirmed that the probability that inertia force and the ground deformation take the maximum value at the same time, when the load-displacement curve of structure bends obviously and the response acceleration of superstructure reaches the ceiling (Murono and Nishimura, 2000).

5.2.1.6.2 Structural modelling and calculating procedure

The pier, the pile and the footing are modelled by beam elements and pile's surrounding soils are modelled by springs, as shown in Figure 128. To express the nonlinearity of reinforced concrete members, a model is required to take account of the influence of cracking in members, yielding of longitudinal reinforcement, spalling of cover concrete, and buckling of longitudinal reinforcement. The tetra-linear model, which can take into consideration the decrease of flexural moment capacity beyond the maximum flexural moment capacity, is used to express the M-ϕ relationship as shown in Figure 119. (811B)

The surrounding soil is modelled into three kinds of springs, such as the lateral springs, vertical shear springs (skin friction), and the vertical spring at pile toe. The shear springs, however, are ignored within the range of $1/\beta$ from the pile head, because the gap between pile and ground would be generated and the friction does not work under an earthquake. The parameter β is defined by Equation (4).

$$\beta = \sqrt[4]{\frac{k_h D}{4EI}} \tag{46}$$

Where, EI is flexural stiffness of a pile, k_h is the coefficient of subgrade reaction and d is the diameter of a pile.

As shown in Figure 132, the soil resistance for each spring is modelled so that the relationship between the subgrade reaction and the displacement is bilinear. The initial values of stiffness, K_V, K_H and K_{SV}, can be determined from the Young's modulus of soil and the pile diameter in accordance with RTRI Design Standard for Foundation (1997). The upper limit for each spring can be determined from the internal friction angle of a soil, the cohesion of a soil, and so on. (812A)

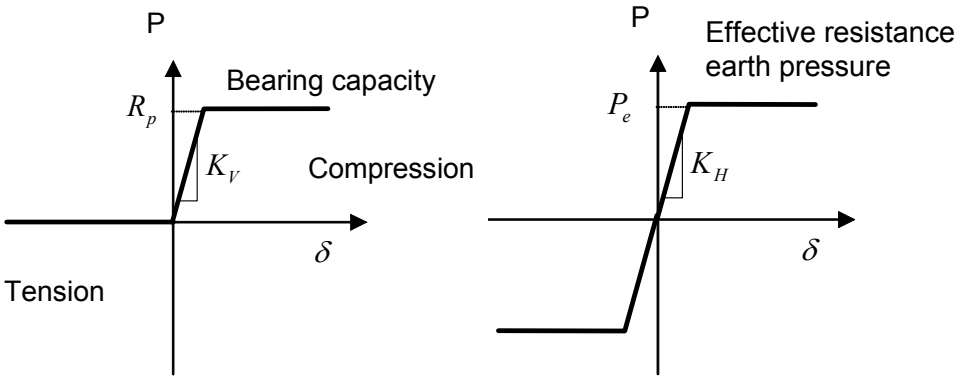

(a) Vertical spring at pile toe **(b) Lateral spring**

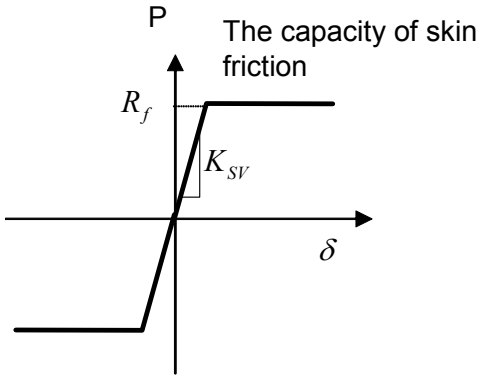

(c) Vertical shear spring (skin friction)

Figure 132 — Models soil springs

5.2.1.6.3 Bending moment and shear force in pile

The distribution of bending moment and shear force as results of calculation are shown in Figure 17. When only the inertial force is considered as the seismic action, the maximum bending moment and the maximum shear force were induced in the top of pile. The magnitudes of the bending moment and the shear forces decrease along the depth. However, when the seismic soil deformation is taken into account, the distributions of resultant forces are quite different from the previous ones. The bending moment and the shear force are largely generated at the depths of 7.5 m and 14 m. It is because the boundaries between soil layers correspond to such depths, and the ground displacement is suddenly magnified here.

It has been confirmed that the design satisfies the required seismic performance.

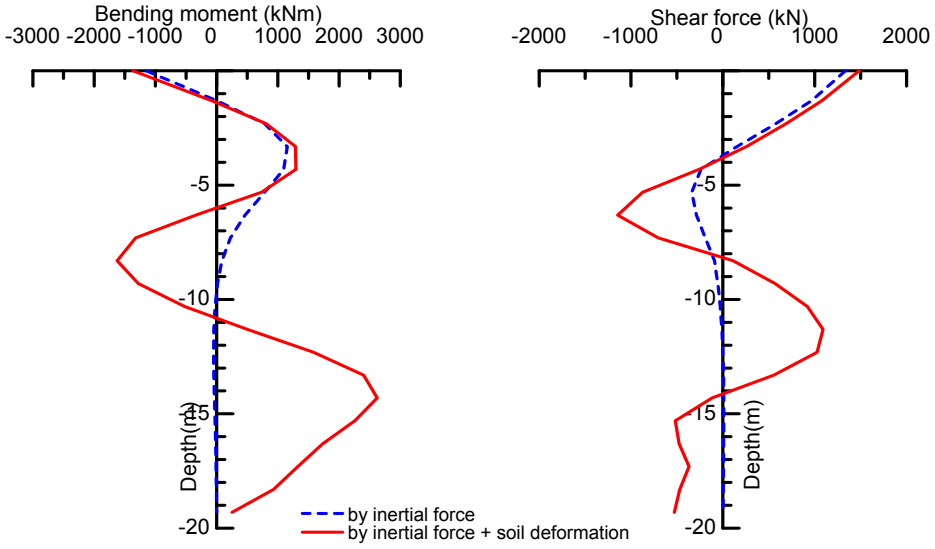

(a) Using combination factor for upper limit

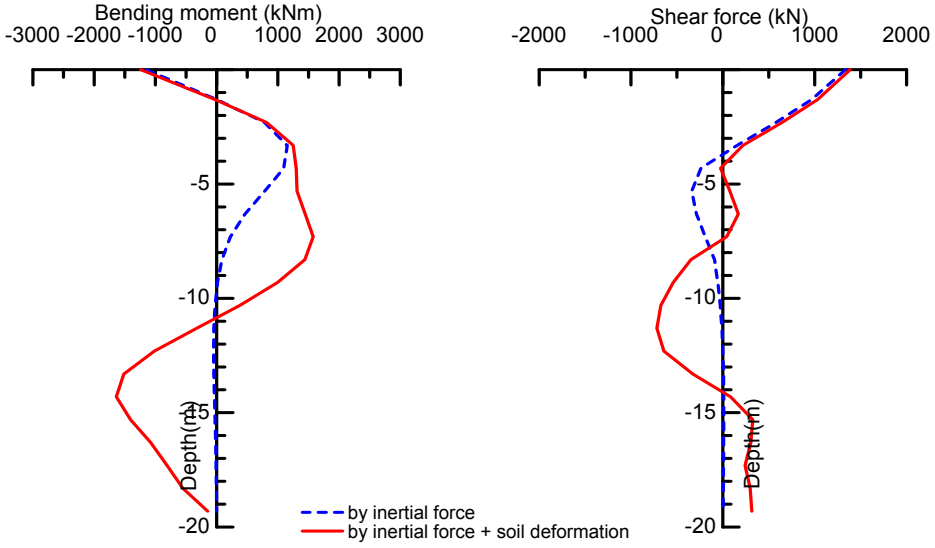

(b) Using combination factor for lower limit

Figure 133 — Distribution of bending moment and shear force induced along pile

5.2.2 Design and actual performance of pile foundation of high R/C smokestack on soft ground

5.2.2.1 General remarks

A high structure with a long fundamental natural period of vibration to be constructed in thick soft soils must be attentively designed for the seismic response of the structure to earthquake ground motions with predominance of components corresponding to the natural period of vibration of the structure. Thus the effect of soil-structure interaction onto the response of the structure and its foundation should be accurately evaluated even when the response of the soil and structure is in a highly nonlinear state, in a region of highly seismic activity.

Considering the importance of a structure during and after an earthquake from a consequence point of view, the design of an important structure should have been performance-based in terms of assuming appropriate performance criteria for action effects evaluated by an attentively-developed model, against proper seismic hazards. After construction, the model is sometime evaluated by various kinds of field tests and monitoring. For its service time, the actual performance of such a soil-structure is often monitored with instruments. Then, the actual behavior of it is sometime recorded during a severe seismic event for it (Kowada et al., 1998). Here is demonstrated with an example of seismic design, tests and monitoring of a high smokestack on soft soils (Mori, 2004, Mori, 2008).

5.2.2.2 Purpose and functions

A 200 m high smokestack for Nanko LNG (liquefied natural gas) thermal power station with a capacity of 1800 MWe by Kansai Electric Power Company had been planned to be newly constructed as a reinforced concrete superstructure, then had been designed two years in 1986 and 1987, checked by a series of vibration tests immediately after skeleton construction in 1989, and was completed in its construction in 1990. Since August of 1990 instrumental monitoring of seismic behavior of soils and smokestack has started. Nanko Power Station initiated commercial operation in November of 1990. A bird's eye view of the smokestack is shown in Figure 134.

The smokestack of the thermal power station, which has been providing huge amount of electricity to Kansai region including Japan's second largest city of Osaka, is essentially categorized to commercial use facility but very important to public, in terms of keeping serviceable functions particularly even during and after an earthquake. Considering the possible consequence of its failure or service disruption, the performance objectives were needed to establish. (511A, 512a)

Figure 134 — Bird's eye view of the smokestack of a thermal power plant

5.2.2.3 Performance objectives for seismic design and reference earthquake motions

According to Building Laws of Japan, the design of a high rise building whose height is equal to or more than 60 m or a high and large structure like this smokestack has been required to be reviewed and approved by one of the two officially designated review organizations in Japan. In this case, the General Building Research Corporation of Japan (GBRC), which is a non-profit foundation established in 1964 in Osaka, was officially assigned as the review organization and it established a Special Review Committee (SRC) consisting of three leading professors in structural, earthquake and geotechnical engineering fields for reviewing the design of this smokestack. Moreover, such a design has been required to follow the document of Recommendations on Earthquake Motions for Dynamic Response Analysis in Design of High-rise Buildings issued by the Committee on Structural Evaluation of High-rise Buildings in the Building Center of Japan (BCJ) in 1986. According to the

BCJ recommendations, the design of such a structure has basically been requested to follow the principle of a kind of performance-based design policy with description of performance objectives. The performance objectives of the smokestack include serviceability for keeping it fully operational during and after an earthquake with a seismic intensity expected 2 to 3 times with a high probability of occurrence in its design working life, 50 years, and safety for minimizing human casualties and damage to structural capacity within limited residual deformation during and after an earthquake generating a seismic intensity of a considerable maximum at an interest site. Eventually, Reference Earthquake Motions (REM) for design are set for two limit states, i.e. serviceability and safety states, as Level 1 Earthquake Ground Motions (Level1 EGM) and Level 2 EGM, respectively as shown in Table 31 (Kida et al., 1992). (512a, 512b, 512A)

Table 31 — Performance objectives for seismic design of smokestack

Reference Earthquake Motions	Annual Return Period (for reference)	Performance objectives
Level 1 Earthquake Ground Motion (Level 1EGM)	200 year	Serviceability: Full serviceability even immediately after an earthquake Safety: Little or no damage to major structural and functional elements and almost elastic behaviors during and after an earthquake
Level 2 Earthquake Ground Motion (Level 2EGM)	more than 1300 year, or maximum considerable earthquake ground motion	Serviceability: Acceptable term loss of serviceability for repair Safety: Severe damage not leading collapse nor harming human lives during and after an earthquake

The reference earthquake motions for designing this smokestack were set as summarized in Table 31 according to the BCJ Recommendation (513A). The earthquake motions for design determined according to these performance objectives will be mentioned later.

Almost four years later this structure was actually attacked by a severe earthquake ground motion equivalent to the Level 1 EGM for designing it during the devastating Kobe earthquake on January 17, 1995. The facilities of the power station were suffered very minor damage but had been keeping fully operational function except a short period necessary for checking. Therefore, it can be understood as an example showing that the performance objective for serviceability of the structure was successfully verified overall (Kowada et al., 1997a).

5.2.2.4 Performance criteria and limit states

The site of Nanko Power Plant is located in a southern part of Osaka Port in Japan as shown in Figure 135 and is characterized as a manmade island newly reclaimed on very soft thick soil deposits overlaying deep Osaka Basin. From a scenery design point of view, the shape and color of the smokestack was requested by the City of Osaka in order to be symbolic for the port as a scenic marine gateway to Osaka. Additionally from a structural design point of view, the structure was required to have a robust long-pile foundation for such a statically determinate, large and heavy structure, with consideration on the consequence of potential damage to it. Thus the foundation of the smokestack was determined to have a rigid footing and long end-bearing pre-cast concrete piles for higher safety level considering the importance of the smokestack. (514C)

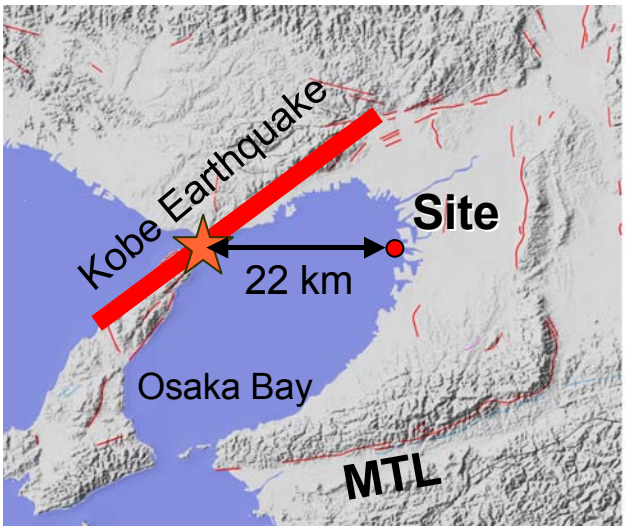

Figure 135 — Location of the site and the epicenter of the 1995 Kobe earthquake

Consequently, the smokestack supported by the long piles was expected to have a long fundamental natural period of vibration, and the ground of the site was anticipated so as well additionally die to a deep basin effect. (622b) As a result, the evaluation of linear and nonlinear soil-structure interaction (SSI) effects was considered to be the most important issue in the design of this smokestack. Because it was worried that some transient resonance between the soils and the structure might take place and nonlinear behavior of soils under severe seismic excitation might advance such resonance. In addition, long piles penetrating an intermediate thin firm layer fairly above their possible bearing base layer may respond to seismic displacements of soils, associating with generation of stress concentration in them. Moreover, the tendency of such stress concentration was anticipated to be accelerated by soil displacement amplified due to nonlinear response to a severe earthquake ground motion. Thus the SSI effects should have been needed to evaluate from viewpoints not only of inertial interaction but also of kinematical interaction for specifying seismic actions on the soils, the smokestack and the foundation in the seismic design of the pile foundation of the smokestack (Kida et al., 1992). (514A, 515A)

For the reason that the smokestack is statically determinate, the foundation of the smokestack ought to have been sufficiently stable even after a considerably intense earthquake ground motion. In other words, the piles of the foundation are essential part of such a statically determinate huge structure. Accordingly, performance objective of the pile foundation is maintaining full operational capacity even in safety limit state. (512a, 512b)

Therefore, the basic policy of seismic design of the smokestack and foundation was determined to be that seismic actions on the smokestack and the foundation would be evaluated by a kind of detailed dynamic analyses with a soil-pile-foundation-smokestack coupled model (a fully coupled model) using reference earthquake ground motions for design specified on the basis of probabilistic and deterministic hazard analyses. (515A) Following above-mentioned policy, performance criteria was specified by ductility factors in terms of maximum curvature for the smokestack, by maximum stresses for the concrete and re-bar of piles, and by maximum stresses and residual displacements for the foundation footing. For structural safety, liquefiable subsurface soils are remedied for no susceptibility to Level 1 EGM (514A, 612B)

As previously described, the importance of the structure and undesirable amplification due to soil-structure interaction require higher safety for this structure. Performance criteria for the structure are determined as shown in Table 32. (514A, 514B, 514C)

Table 32 — Performance criteria for reference earthquake ground motions

Reference Earthquake Ground Motion	Elements	Performance criteria
Level 1 Earthquake Ground Motion (Level 1EGM)	Smokestack	Allowable stress: Factors of safety is greater than 1.5 for re-bar and concrete.
	Smoke pipe	Allowable stress: Factors of safety is greater than 1.5 for FRP.
	Foundation footing	Allowable stress: Factors of safety is greater 1.5 for re-bar and concrete.
	Pre-cast concrete pile	Allowable stress: Factors of safety is greater than 1.5 for re-bar and concrete.
	Subsurface soil	Liquefaction occurrence is not allowed.
Level 2 Earthquake Ground Motion (Level 2EGM)	Smokestack	Allowable flexural deformation: ductility factor is less than 2.0. Allowable shear stress: A factor of safety is greater than 1.2.
	Smoke pipe	Allowable stress: A factor of safety is greater than = 1.05.
	Foundation footing	Allowable stress: A factor of safety is greater than 1.05.
	Pre-cast concrete pile	Allowable stress: N-M combination locates within ultimate limit curve.
	Subsurface soil	Liquefaction is allowed within acceptable influence for upper structure and piles.

5.2.2.5 Policy of determining seismic actions on superstructure and foundation for design

5.2.2.5.1 General

Reference earthquake ground motions were determined through two stages for evaluating serviceability and safety of the smokestack during and after an earthquake. (520A) This site is covered by very thick sediments and no active fault was recognized there and in its vicinity. (650a) Therefore, no consideration of fault displacement was needed in design. (611A)

In principle, the design of this smokestack was requested to follow the BCJ Recommendation that recommends the magnitude of earthquake ground motions be measured by peak ground velocity, the design EGM waves include more than three different kinds of earthquake waves, such as a standard wave, i.e. the El Centro 1940 record, a longer component rich wave, i.e. the Hachinohe 1968 record, and a wave representing site characteristics, i.e. an earthquake ground motion recorded at a site. However, these kinds of earthquake waves recorded at other different sites are not realistic for the construction site. Therefore, an incident wave in an engineering base layer at a recorded site calculated by deconvolution was used in a site response analysis as the incident wave in an engineering base layer at the Nanko site. In such cases, a total motion wave at ground surface obtained from the site response analysis is rightly different from the recorded wave. (Kida et al., 1992) (622A)

For the first stage, earthquake ground motions were evaluated through the following procedures;

— a seismic hazard analysis of peak velocity on seismic bedrock (granite),

— an evaluation of amplification of seismic bedrock motions to ground surface in terms of peak velocity, and

— determination of earthquake motions at the interface between the firm ground and subsurface soils for design.

As the result of a seismic hazard analysis and a 1-D site response analysis, the Level 1 and Level 2 EGMs are specified for the seismic actions necessary for the models of analyses for the smokestack and its foundation with a set of variables including PGV, acceleration time histories, etc. (623A, 623B)

For the second stage, the performance of the smokestack and its foundation was verified through two simplified dynamic analyses and a detailed dynamic analysis using the free field motions at the surface and at the bottom of piles within the subsoil, with consideration of types of analyses, methods of analyses, performance criteria, and geotechnical characterization. (711A, 711B)

5.2.2.5.2 Seismic hazard analysis and site response analysis

A seismic hazard analysis (SHA) was carried out in terms of peak bedrock velocity on the basis of statistical analysis using Kanai's formula in combination with three Japanese historical earthquake datasets, which were covering approximately 1300 years in past. This formula is an attenuation relation that predicts peak velocity of earthquake ground motion on outcropping seismic bedrock, and had been frequently used for SHA in Japan. The uncertainties in parameters applied to this formula were not explicitly considered. (621A, 621B, 621C, 622a, 622c)

The peak bedrock velocity (PBV) with a 200-year annual return period (ARP) is estimated to be 5 cm/s in round-up number for the magnitude of a Level 1 EGM, and the considerably maximum of PBV is evaluated to be 10 cm/s for that of a Level 2 EGM as well. Through this process, scenario earthquakes were specified to be a Nankai subduction zone earthquake as the Level 1 EGM and a close inland intra-plate earthquake as the Level 2 EGM. (611A, 621A, 621B, 621C)

Local site amplification to be considered in design involves both a deep basin effect at the site located in the center of Osaka Basin and a nonlinear amplification effect due to softening of subsurface liquefiable sandy soil layers and soft clayey soil layers. For safer consideration, it was evaluated in two steps.

The first step is to evaluate amplification of PBV by a site response analysis with a 1-D model with linear soil constants for all the sediments overlaying seismic bedrock at a depth of approximately 1,500 m. Considering a deep basin effect, marginal amplification is adopted to be 5.0 based on amplification factors of PBV and peak amplification factors in a lower frequency range of a transfer function. Eventually peak ground velocity (PGV) of Level 1 and Level 2 EGMs were determined as 25 and 50 cm/s, respectively. These values seemed to be proper in comparison with high-rise buildings in Osaka region of which design PGV are 20 and 40 cm/s. (622A, 622b)

The second step to develop the input motions for models of analyses to design smokestack by modification of the design EGM waves through a 1-D nonlinear local site response analyses using a 450 m deep soil model overlaying a firm ground with a shear velocity of 550 m/s. It was necessary to consider enough depth to take account of amplification of 2 to 3 second period of vibration with a limited geologic and geotechnical information of the site. (623A) Through the local site response analyses for the two different levels of earthquake ground motions for design, peak stresses in liquefiable soil layers were calculated for judgment of liquefaction as well as EGMs at the ground surface and within a bearing stratum for input earthquake motions to soil-structure models mentioned later. (612A, 621A, 623A, 623B, 631A)

The nonlinear site response analyses were performed by equivalent linear total stress approach and the assessment of liquefaction was performed using the soil responses of the analyses. (631B, 631C)

Considering the large size of foundation mat, the SRC requested the evaluation of a site-specific spatial variation of earthquake ground motions. Responded to the request, the spatial variation of EGM due to oblique incidental angles of a shear wave and propagation of a Rayleigh wave at the site was considered as an input rotational motion to the base-fixed model of the smokestack. (641A, 641B, 641C) As a result, the increase of the maximum stresses of smokestack and the foundation piles varies from 2 to 3 percent.

Any special detailed analysis was not performed for evaluation of the deep basin effects and the spatial variation of EGM. (644a, 645A, 645B) At the time of the design, the settlement due to consolidation of mid Holocene clay layers at large reclaimed sites in Osaka Bay area was discussed as a serious problem. Thus the un-uniform settlement before the Level 2 EGM was evaluated as an additional P-delta effect on the smokestack and the foundation piles. The evaluation result showed a negligible effect. (650A)

5.2.2.6 Features of smokestack and geotechnical characterization

5.2.2.6.1 Features of smokestack and foundation piles

Figure 136 shows the front and side views of the smokestack together with the arrangement of the accelerometers on the smokestack as well as the ground. The smokestack consists of three internal cylinders made of FRP and an external hexagonal reinforced concrete structure supporting the cylinders. The height of the internal cylinders is 200m and that of the external structure is 194m.

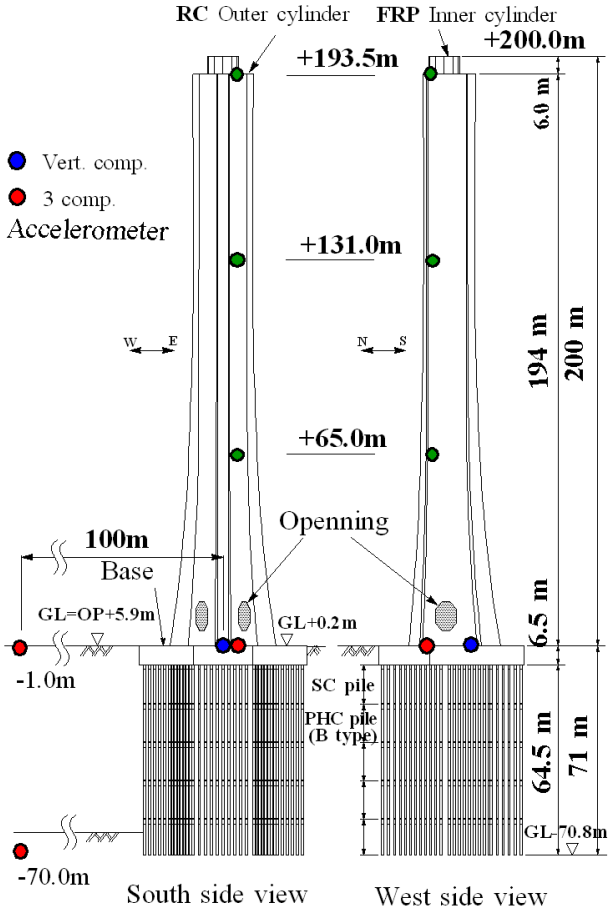

Figure 136 — Front and side views of smokestack and arrangement of accelerometers on it and in ground

The accelerometers, as indicated in Figure 136, consist of two horizontal component accelerometers fixed at 65, 131, and 193.5 m height on the smokestack, and a three component accelerometer on the smokestack base. This arrangement of accelerometers aims at measuring the third vibration mode of the smokestack. Two additional vertical accelerometers on the base aim at extracting two-directional rocking modes of the base. A pair of three component accelerometers was also placed at the depths of 1 m and 70 m below the ground so as to measure the principle behaviour of the ground100m away from the smokestack as the free field.

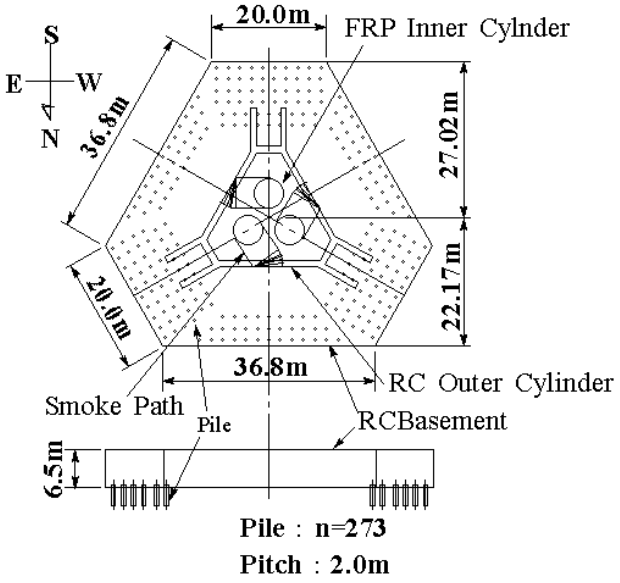

Figure 137 — Plan and side views of basement and arrangement of 273 piles

The plan and elevation of the smokestack base along with the arrangement of 273 piles are shown in Figure 137. The piles were arranged to be near the edges of the basement with at least a 2-meter placing for effectively resisting the rocking of the base. Each pile was made of five pile segments consisting four pre-stressed high strength concrete (PHC) pile segments and one steel reinforced PHC (SC) pile segment on the top of a pile. The external diameter of the pile segments is 80 cm. Each pile has a length of 65 m and reaches a base layer for an end-bearing pile. The bearing base layer is an early Holocene gravelly sand layer appearing at a depth of 72 m. All the piles penetrate soft and hard soil layers down to the bearing layer. Accordingly, seismic ground displacement may induce stress concentrations at boundaries in between. Thus the type of analysis and the model of analysis should be selected in terms of capability of evaluation of such stress concentration. (711A, 711B, 712A, 713A) The base of the smokestack measures 6.5 m deep and 51 m wide having sufficient weight and rigidity against rocking.

5.2.2.6.2 Soil profile and geotechnical characterization

The detailed soil profile at the site is shown in Figure 138 together with the SPT N-value and shear wave velocity profiles. The soil profile consists of different layers, which include 6.5 m thick banked layers, 10.7 m thick filled layer, 25.5 m thick late Holocene clay-silt-sand layer (Ma13), 8 m thick early Holocene gravel layer (Temma Layer), 14.5 m thick clayey layer (Ma12), and 11 m thick second gravely sand layer. The last layer was selected as the bearing layer for end-bearing piles.

Reclamation work for filling and banking had been carried out in 1972 through 1980. The banked layer consists of composite material with soils exploited at mountains and industrial waste from construction sites and the filled layer consists of soils dredged in the vicinity of the front sea. The soil properties of the banked layer were evaluated as a largely uncertain material due to existence of debris. The filled layer has relatively large N-value in the upper portions and relatively small in the lower because of the effect of sand drains in the filled layer and underlying alluvial clay layer. Liquefaction judgment was performed especially to these two

layers for the results of the site response analyses in the first stage. (612A) As a result, liquefaction was judged to be susceptible under the Level 1 and Level 2 EGMs. The policy for measurement of liquefaction was that ground improvement was planned and performed for non-susceptibility of liquefaction under the Level 1 EGM and that the effects of susceptible liquefaction under the Level 2 EGM was considered in a site-specific detailed dynamic analysis for soil-structure. (715B)

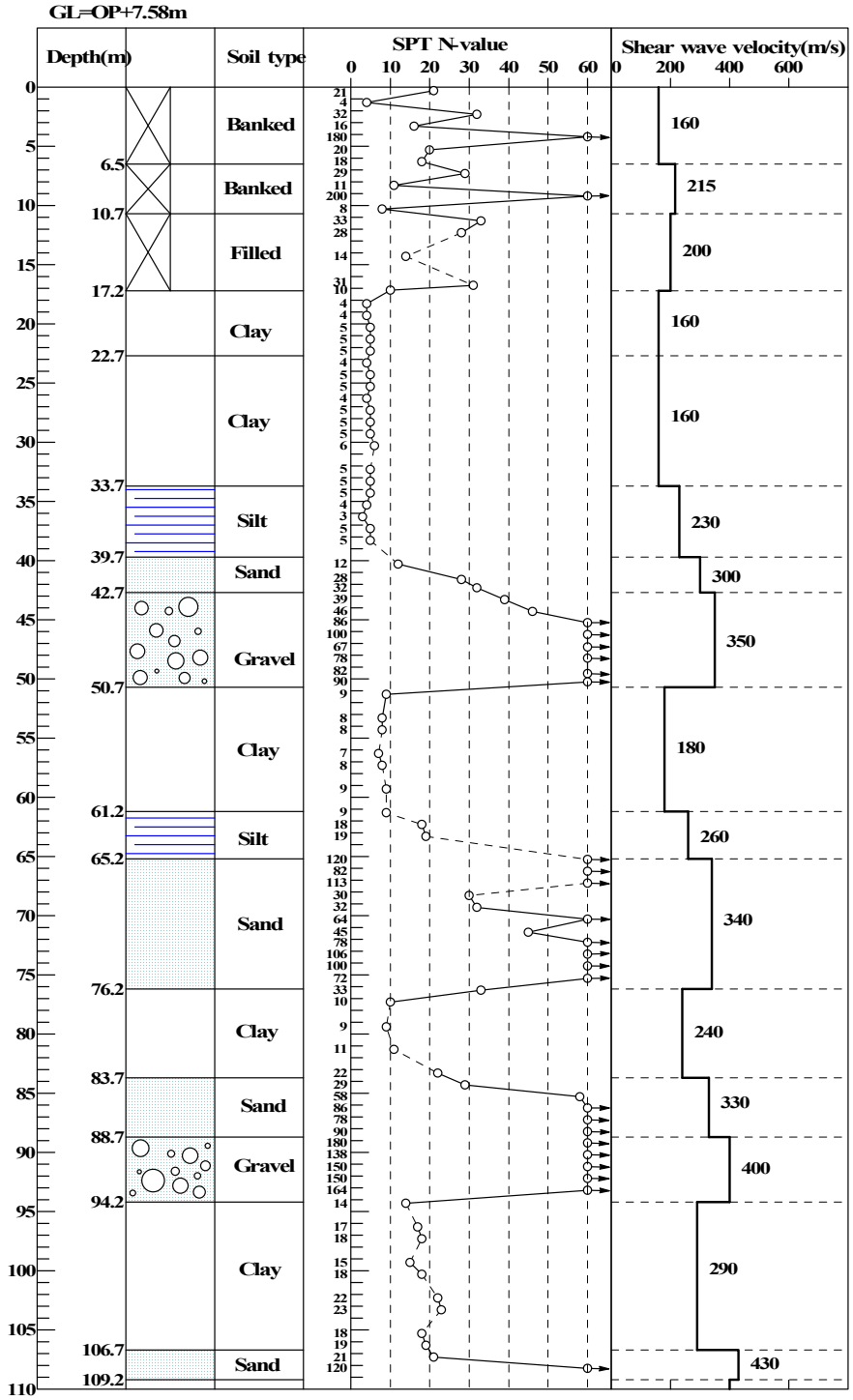

Figure 138 — Soil profile at site including SPT N-value and shear wave velocity profiles

In geotechnical characterization, the ground was assumed to be a horizontally layered system. The data provided for the design included several borehole data and various types of laboratory testing data based on undisturbed and disturbed samples for each layer. The borehole data involved soil profiles, SPT N-values, PS-logging data, lateral loading test in borehole. The laboratory testing data involved physical properties, densities, uniaxial and triaxial compression tests for cohesion and internal friction angle, cyclic triaxial tests for cyclic deformation and resistance characteristics for every layer. Considering such sufficient in-situ and laboratory geotechnical data, site-specific detailed dynamic analyses and detailed equivalent-linear models were adopted in design. (712A, 713A, 715A)

5.2.2.6.3 Linear and nonlinear ground models

Corresponding to three different degree of non-linearity, small intensity EGM, Level-1 and Level 2 EGMs, three different ground models were prepared as shown in Figure 138. The basic model assumed linear elastic properties specified mainly by PS logging data and SPT N-valuese site. This model was planned to be used for verification of model using recorded ground motions with small amplitude in present microtremor data and future earthquake motion records.

The other two models have different values of rigidity and damping ratio under the Level 1 and Level 2 EGMs. The values were determined as an average of three convergent values in the cases of equivalent dynamic analyses with El Centro and Taft as the input motions by using SHAKE program. Each analysis was repeated until the surface velocity response converged to given amplitudes of Level 1 or 2 motions that are 25 or 50 cm/s, respectively. Figure 139 shows the shear wave velocity and damping ratio profiles of these three different models of the ground. The magnitudes of predominant strain in the seismic grounds ranged from 0.03 to 0.2 % for the Level 1 motion and from 0.05 to 5 % for the Level 2 motion. For parameters in the banked and filled layers, the increase of rigidity and resistance due to ground improvement and the reduction of them due to liquefaction were evaluated. (612B, 715A, 715B)

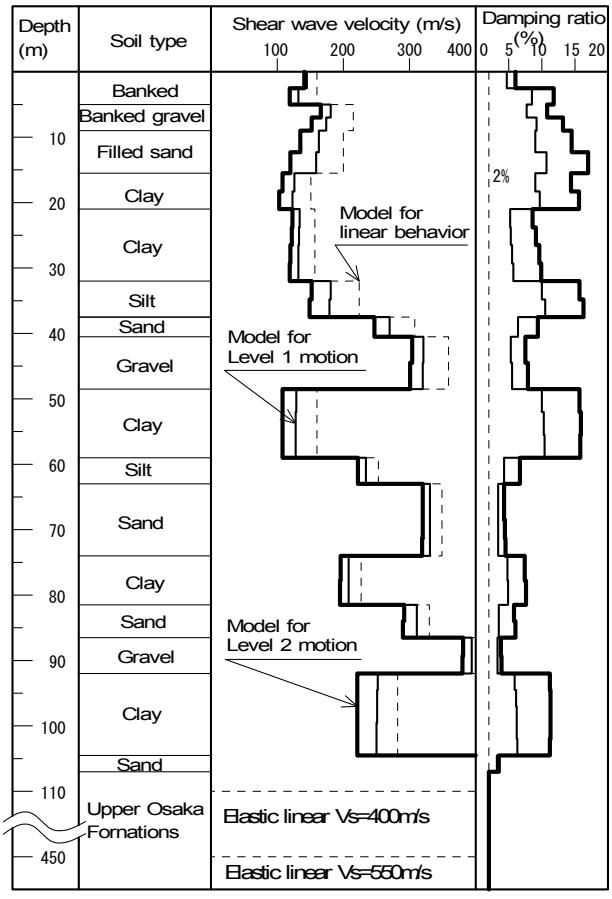

Figure 139 — Three different ground models depending on the degree of non-linearity of soil

5.2.2.7 Models of simplified and detailed dynamic analyses for specifying seismic actions

5.2.2.7.1 Models of simplified and detailed dynamic analyses for seismic design

The second stage for determining seismic actions is specifying seismic actions through simplified and detailed dynamic actions. (520A) In general, a fixed base model had been adopted for seismic design when the effect of soil-structure interaction (SSI) is regarded to be negligible. Even when not negligible, this model was required as a reference model for designers and reviews as a design convention. When the SSI effect is necessary to take into account, a swaying and rocking model had been used for the structures with spread or pile foundations.

It was necessary for the long piles in the soft ground to more carefully take account of the SSI effect on the structure as well as piles with regard to transient resonance due to nonlinear behaviour and stress concentration at boundaries in between soft and hard soil layers due to seismic relative displacement. (913A) Thus soil-pile-structure interaction should be evaluated along the depth of the piles by more appropriate model of analysis. Although a FE model would be powerful in evaluating the SSI effect in linear behaviour, a nonlinear 2-D model had a problem of evaluating 3-D effect of pile behaviour and a 3-D model was difficult in terms of nonlinear behaviour. Eventually, a lumped mass-spring-beam model that is called as a lumped mass SSI model herein was adopted as an appropriate model for taking account of the 3-D SSI effect as well as the material non-linearity in the structure and the ground. The lumped mass SSI model adopted in the design was developed by Mori et al. (1992) and Mori (2000) following the fundamental concept by Penzien et al. (1964). (921A) This lumped mass SSI model was verified by a 2-D FE model in terms of transfer functions at the top of smokestack and at the basement of foundation. (921A, 921B)

In addition to detailed dynamic model of analysis, the fixed base model and the sway-rocking model were also requested by SRC to be adopted for reference models. (911A) Figure 140 shows schematically all the models described previously. Based on the nonlinear properties depending on the intensities of Level 1 and Level 2 EGM, parameters for spring constants in a soil column and springs for interaction in the lumped mass-spring-beam model were determined and parameters for spring constants in the sway-rocking model also determined. (911A, 911C, 912B) Soil-related springs are essentially linear elastic but have reduced rigidity and additional damping ratio as shown in Figure 139. (812A, 911C, 921D) Beam elements representing smokestack was modeled with a fully nonlinear modeling by Takeda Model for a reinforced concrete element. Accordingly, the effect of overstrength in a smokestack was automatically considered. (812A, 911C, 911B) For the Level 2 EGM, the effect of liquefaction was considered as reduction of constants for interaction springs. (922A)

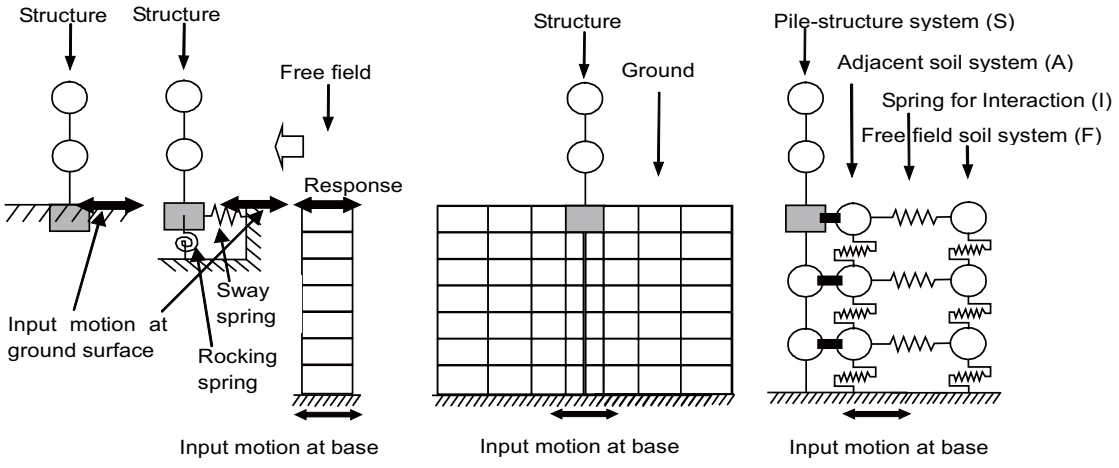

(a) Fixed base model (b) Sway-rocking model (c) 2-D FE model (d) Lumped mass SSI model

Figure 140 — Models of preliminary analyses as candidates for the seismic design

The two different levels of earthquake ground motions for design were obtained by site-specific response analyses at the ground surface and within a bearing stratum for input earthquake motions. The EGMs at the ground surface are input motions for the fixed base and sway-rocking models (912A) and the EGMs at the upper boundaries of the bearing layer. (921B, 921C)

5.2.2.7.2 Verification of adopted model for detailed dynamic analyses by 2-D FE model

In order to verify the appropriateness of the models adopted in design, preliminary analyses were conducted with the ground model for the Level 1 EGM and the results of different models were compared. The actual models employed in the preliminary analyses are shown in Figure 141.

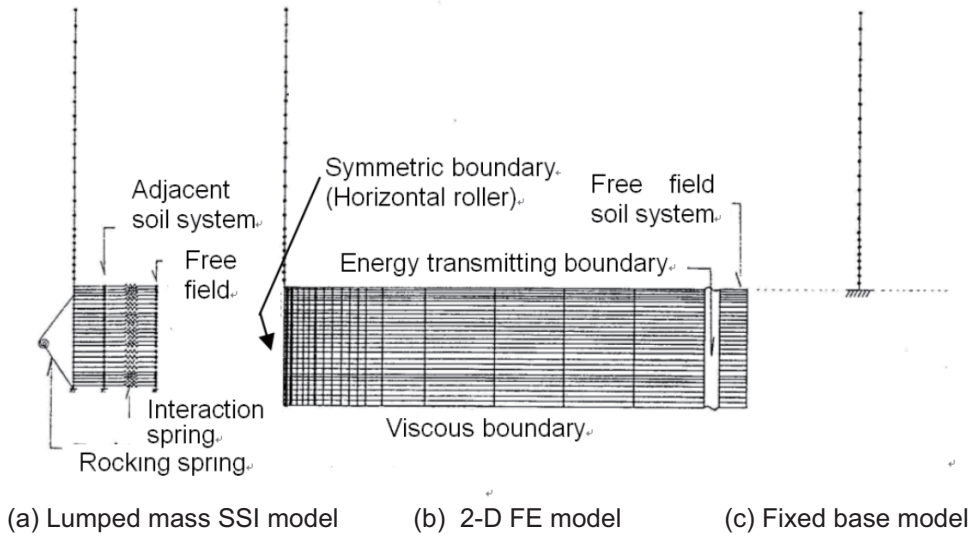

Figure 141 — Three actual models for preliminary analyses

As basic information, the predominant periods of the smokestack obtained from the above-mentioned models are shown in Table 33. In the 2-D FEM model, the predominant periods are specified by its transfer function of the top of smokestack to the base of the ground. In the rest of the models, however they are specified according to the result of eigenvalue analysis.

Table 33 — Predominant periods of smokestack

Mode of smokestack	1st	2nd	3rd		4th	
Mode of foundation			Rocking	Sway	Rocking	Sway
Type of model						
Fixed base model	2.22	0.49	0.2		0.1	
Sway-rocking model	2.33	0.54	0.21	0.25	0.13	
Lumped mass-spring beam model	2.33	0.54	0.21	0.29	0.12	0.11
2D-FEM model	2.38	0.58	0.23		0.12	

Note
1: SSI models are based on the soil properties assumed under Level 2 Earthquake Motions.
2: The detail of the smokestack for preliminary analysis was different from the final structure.

The transfer functions in amplitude, i.e., Fourier spectral ratios, of the top of the smokestack and of its basement to the ground surface of the free field with regard to horizontal movement are compared between the lumped mass SSI model and the 2-D FE model in Figure 142 (a) and (b). As for the top of the smokestack, the predominant periods of these two models match well each other both in the first mode. In spite that the predominant period of the second mode matches each other, the lumped mass model is much greater than the FE model in terms of amplification near this period. The 2-D FEM model may overestimate the dissipation damping of the smokestack and the lumped mass model may overestimate amplification. From an engineering point of view, the proposed model was considered to be more appropriate in the practical seismic design.

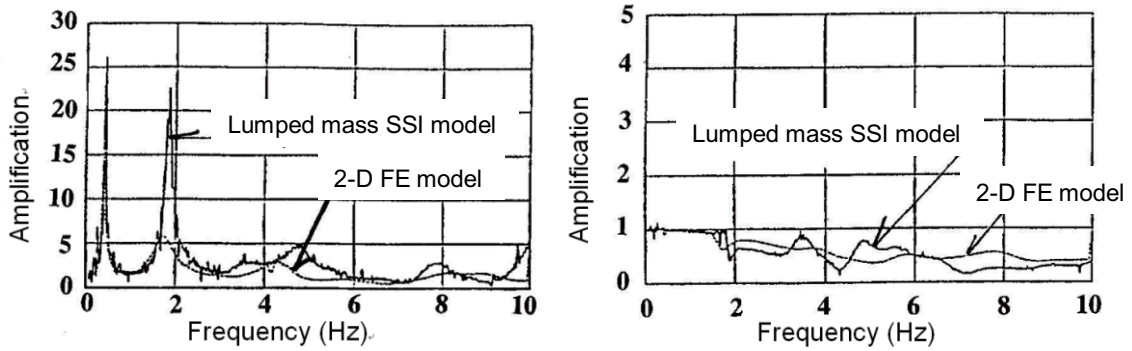

(a) Top of smokestack **(b) Basement**

Figure 142 — Transfer functions in amplitude of the top of the smokestack and of the basement to the ground surface of the free field with regard to horizontal movement

As for the transfer functions of the smokestack base, they imply the input loss effects due to kinematic interaction. These roughly match well each other.

The transfer functions in phase differences are shown in Figure 143. The results from both the models are seen to match well as a whole. As discussed here, the lumped mass SSI model seems overall appropriate in terms of transfer function in amplitude and phase difference. (921A)

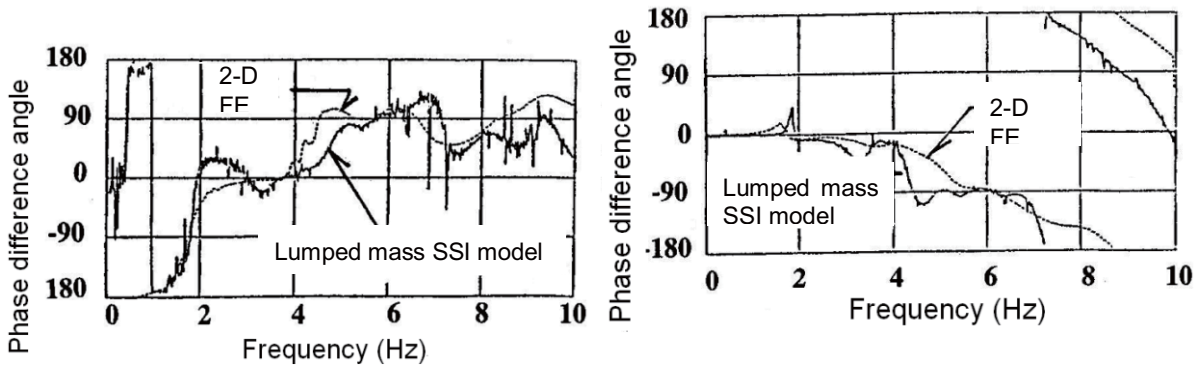

(a) Top of smokestack **(b) Basement**

Figure 143 — Transfer functions in phase difference of the top of the smokestack and of the basement to the ground surface of the free field with regard to horizontal movement

On the other hand, the sway-rocking model for the smokestack was not adopted for the seismic design analysis, because of great discrepancy with the 2-D FE model near and beyond the second predominant frequency in the transfer function both in amplitude and phase difference.

5.2.2.7.3 Appropriateness of adopted model with regard to interaction mode of vibration

In order to understand the natural modes of vibration in the lumped mass SSI model, some lower modes are compared with the fixed base model in Figure 144. As shown in the figure, the modes of sway and rocking of the foundation are clearly recognized and excited modes and amplitudes of the smokestack in the periods of predominant or natural ground vibration can be quantitatively understood (Mori, 2000). (921A)

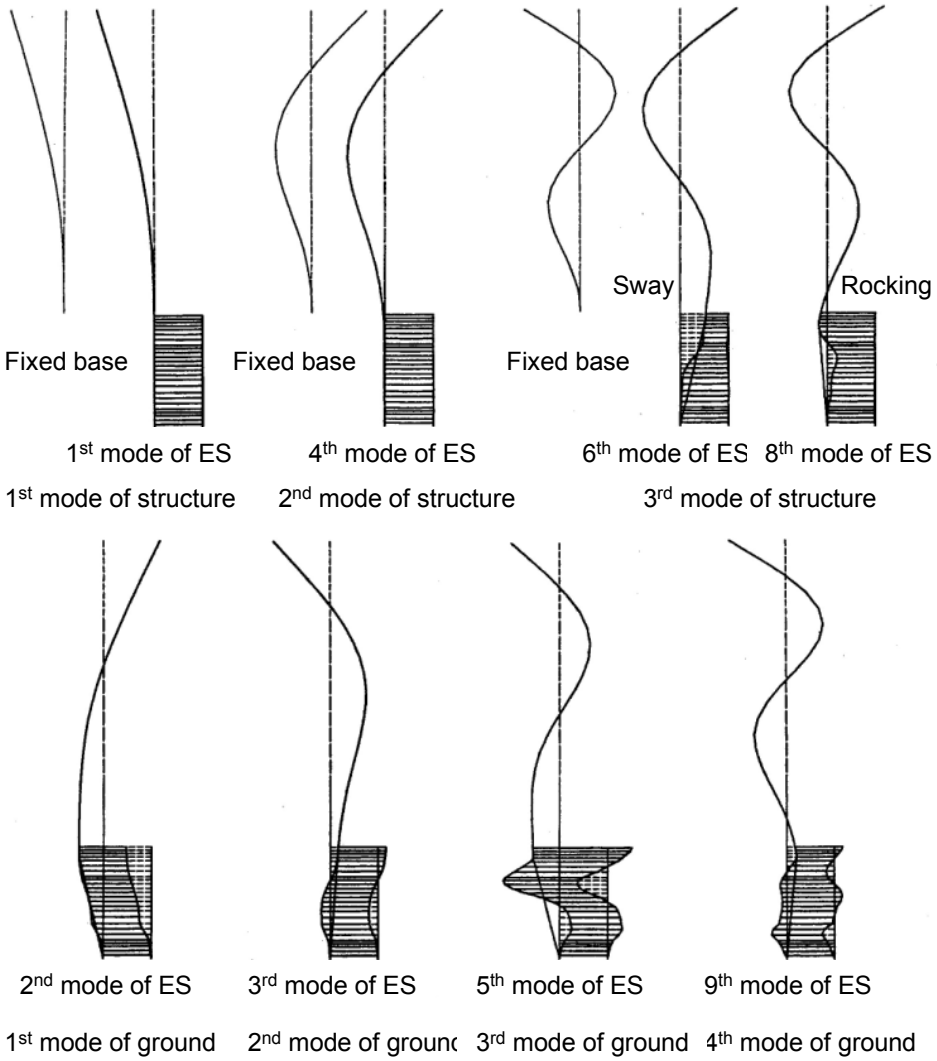

Figure 144 — Lower order modes of vibration in the lumped mass SSI model, which can be identified to the specific modes of the ground, the structure, or the foundation

5.2.2.8 Results of detailed dynamic analyses

The bending moments and shear forces of the piles were obtained directly from the response of beam elements for the pile, and the axial forces of the piles were derived from the response of the reaction of a rotation spring for rocking. The seismic action on each pile can be obtained as a combination of such resultant forces. In the simplified models like the fixed base model and the sway-rocking model, the resultant forces are obtained only at pile heads. On the other hand, the lumped mass SSI model adopted in design provides the resultant forces at any depth along the piles. Therefore, other additional analysis is required for evaluation of piles within the ground in the case of a simplified model. For reference, an equivalent static analysis for

seismic soil displacement was performed for evaluating pile stress within the soil with the results of the simplified models.

According to the results of the detailed dynamic analyses, the maximum bending moment and the maximum shear forces take place at the pile head, but the second maximum of them take place at a depth varying from 40 to 45 m or at a depth varying from 62 to 65 m. These two depths correspond to the upper ends of two different gravelly layers. The combination of the result of the simplified dynamic model and the result of the equivalent linear model for seismic displacement can not simulate such a large magnitude of pile response.

In the design of the pile, performance criteria were met even in such large resultant forces in deep portions of piles.

5.2.2.9 Verification of models based on vibration tests

A series of vibration tests including microtremor measurements and manpower excitation tests were carried out immediately after the completion of the smokestack construction in August 1990 (Kida et al., 1992). The manpower excitation for the first mode of the smokestack was produced by a cyclic movement of individual centers of gravity by 27 persons on the top of smokestack, and for the second mode, produced by applying a simultaneous push the wall at the top by 12 persons.

In order to find a point that could be regarded as the free field for discussing the transfer function of the smokestack-ground system, array observation of microtremor was also carried out. Figure 145 shows the arrangement of the sensors (velocimeters) for the ground and the smokestack during the excitation tests.

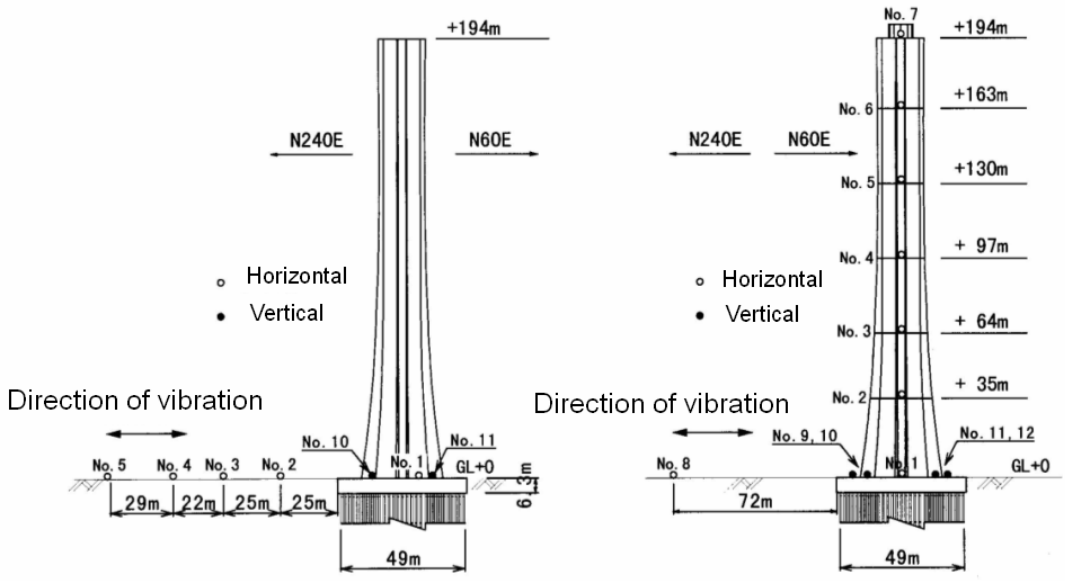

(a) For measurement of the ground **(b) For the measurement of the smokestack**

Figure 145 — Arrangements of sensors for the ground and the smokestack

Figure 146 shows the Fourier spectra of the ground surface and the base of the smokestack, which indicates a gradual decrease of the amplitude of the base in higher frequency compared with the ground surface. Moreover, the spectral ratios of the base to the ground surface obtained from the microtremor measurements as well as the analysis by the lumped mass SSI model are shown in Figure 147(a). This figure clearly shows the input loss effect due to kinematic interaction, which can be successfully simulated by the analysis using the adopted-in-design model. Moreover, the transfer functions with regard to rocking of the smokestack base to the horizontal ground surface motion, as obtained from the measurement and the analysis are compared in Figure147(b). This analytical model may underestimate the amplification of the rocking effect due to SSI, especially around the second predominant period.

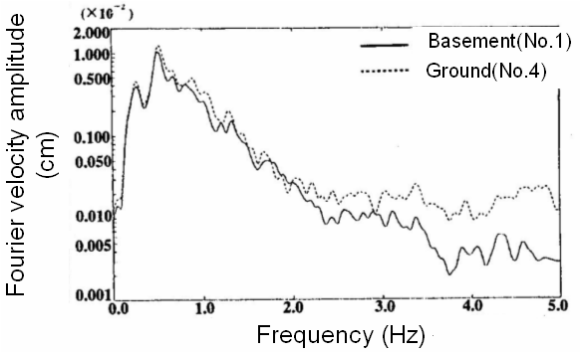

Figure 146 — Fourier spectra of the ground surface and the basement

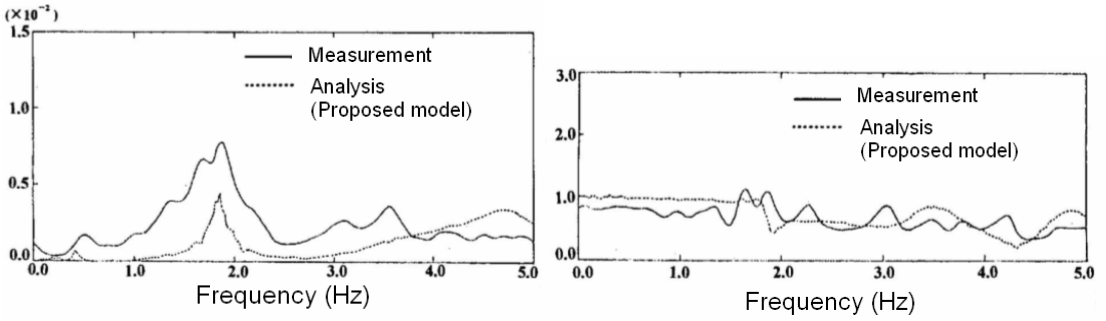

(a) Translation **(b) Rotation**

Figure 147 — Spectral ratios of the basement to the ground surface both by microtremor measurement and the analysis by the lumped mass SSI model adopted in design

Next, the transfer functions of the top of the smokestack to the ground surface of the free field as obtained from the microtremor measurement and the analysis using the adopted model with the soil properties under the Level 2 earthquake motions are compared in Figure 148. Two distinctive features can be seen in this figure. First, the predominant frequencies of the measurement are obviously greater than those of the analysis around the first and the second predominant frequencies, and the ratios of the measured values to the analytical results are almost the same. Second, the shapes of these two transfer functions are almost proportional. These two features are considered to be due to the difference in dynamic properties of the analytical model and the actual structure. The first predominant frequency does not seem to be strongly influenced by the SSI, which means that the difference may be due to the difference of the flexural rigidity of the smokestack.

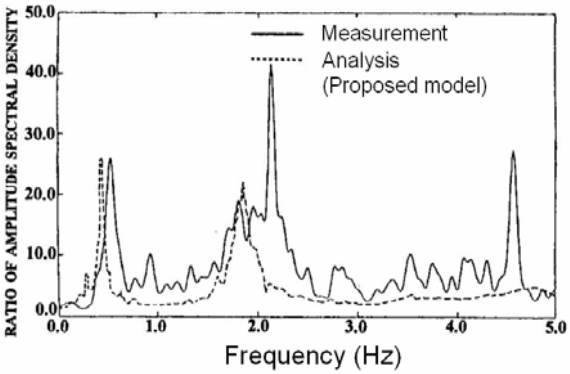

Figure 148 — Transfer functions of the top of the smokestack to the ground surface of the free field by microtremor measurement and analysis with the proposed model

Furthermore, a comparison of the first and second vibration modes of the smokestack as obtained from the measurement and the analysis is made in Figure 149. Both the microtremor measurement and the manpower excitation test have resulted in the same vibration mode.

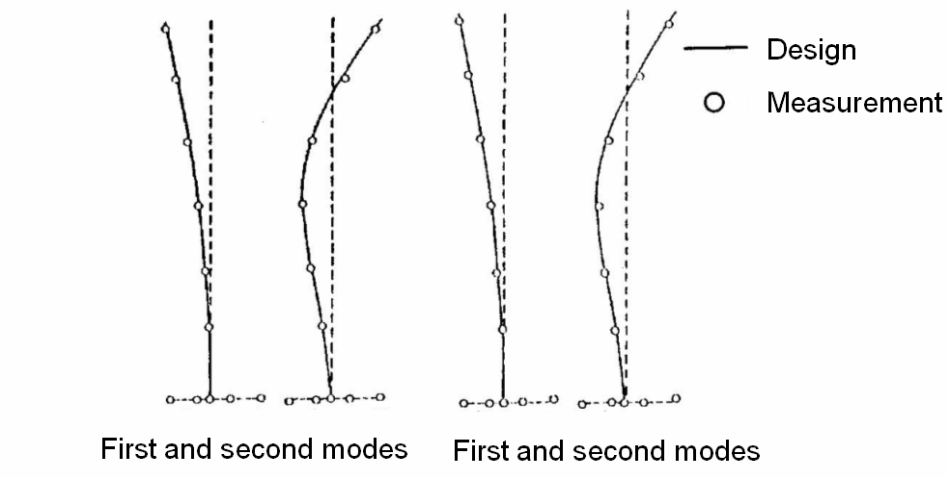

(a) Microtremor measurement **(b) Manpower excitation**

Figure 149 — Comparison of the first and second vibration modes of the smokestack between the measurement and the analysis

Table 34 shows a summary of the predominant periods of the first and second modes as obtained from the analysis and the measurement. There is a big discrepancy of fundamental periods of the smokestack in between. This discrepancy is hereinafter going to be studied from the viewpoint of Young's modulus of concrete. The design value of the Young's modulus of concrete, Ec used for the smokestack was 2.3×10^5 kgf/cm^2, which was estimated by an empirical relationship between Young's modulus and compression strength of concrete, Fc, considered the design strength of concrete, Fc=240 kgf/cm^2.

Table 34 — Summary of predominant periods of the first and second modes by the analysis and the measurement

	Predominant periods for 1st and 2nd modes of smokestack			
	Top/Free field		Top/Basement	
Vibrational mode of smokestack	1st	2nd	1st	2nd
Model and measurement				
Fixed base model	NA	NA	2.22	0.49
Mori's model	2.37	0.54	NA	NA
Microtremor measurement	1.87	0.46	1.89	0.45
Manpower excitation	NA	NA	1.92	0.49

Unit: second

The strengths of the actual concrete used in the smokestack are statistically shown in Figure 150. The average compressive strength of the concrete measured at the construction site was 410 kgf/cm^2, and the average Young's modulus can be estimated to be E=3.3×10^5 kgf/cm^2, which was to be applied in the analysis for vibration experiment. The natural periods according to the adopted model with such modification was almost the same as the measured ones.

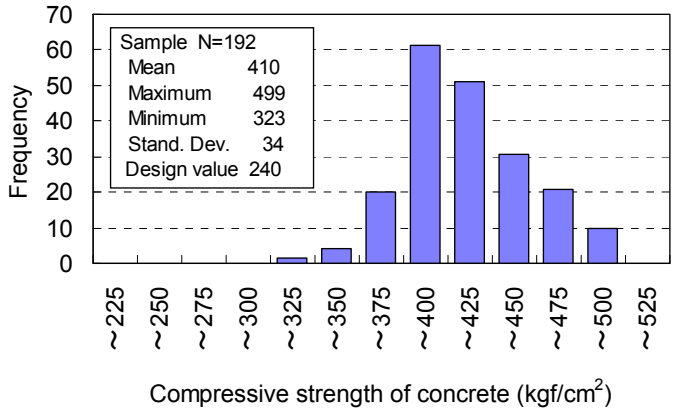

Figure 150 — Histogram of the strength of concrete for the smokestack

The damping ratio was measured based on the free damped vibration after the manpower excitation. Figure 151 shows the time history of displacement at the top during the free damped vibration after the excitation. The damping ratio was measured to be approximately 1.1% at all the heights of sensors from the free vibration. Additionally, the damping ratio estimated by the half power method with the microtremor measurement varied from 1.1 to 1.5%, which is almost the same as the value estimated from the free damped vibration after manpower excitation. The design value of the damping ratio was 2%, which was considered appropriate, taking account of its dependency on the strain of the smokestack.

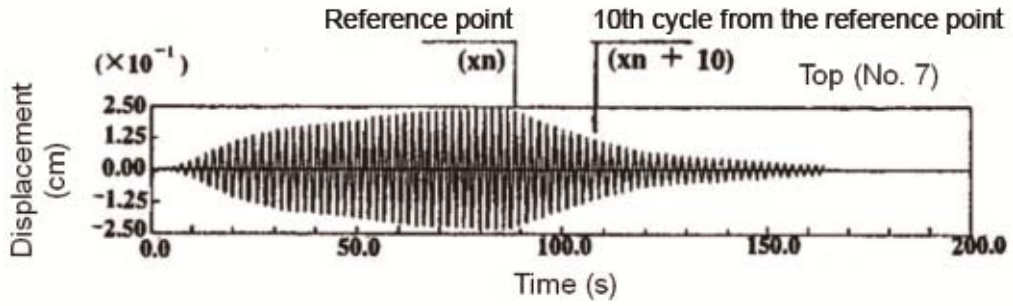

Figure 151 — Time history of displacement at top during free damped vibration

5.2.2.10 Actual seismic behaviour of ground and smokestack

The earthquake observation for the smokestack and the ground was carried out immediately after the completion of construction in March 1990. The arrangement of the seismometers has already been mentioned. Twelve earthquakes had been observed by the end of 1997. The epicenters of those earthquakes are shown in Figure 152 (Kowada et al., 1997a). Ten out of these twelve earthquakes were the main event and the aftershocks of the 1995 Kobe earthquake (see Figure 135).

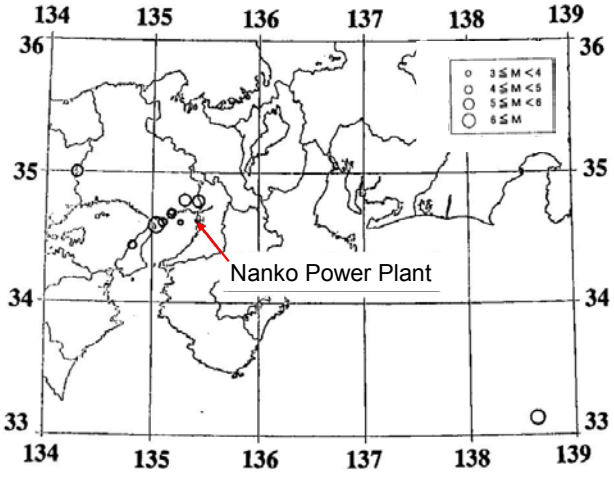

Figure 152 — Location of the epicenters of the earthquakes observed at Nanko site

For grasping the overall amplification or de-amplification through the ground, the foundation, and the smokestack, the relationship of the maximum accelerations among at the base layer, at the ground surface, and on the basement and on the top of smokestack will be discussed on Figure 153. The amplification factor through the subsurface ground is not so great, varying mostly from one to two. From the relationship between the ground surface and the basement of smokestack, de-amplification can be found especially in the range of low amplitude. This de-amplification can be understood as the effect of input loss due to the kinematic interaction between the foundation and the ground, whereas this effect is negligible in the case of the main event of the Kobe earthquake. The amplification through the smokestack varies from two to five times, and the factor seems to be greater when the amplitude of the ground surface acceleration is smaller.

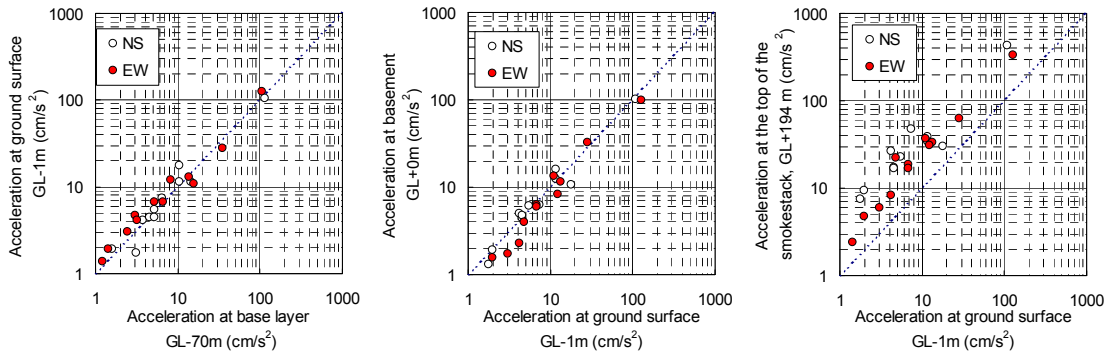

Figure 153 — Relationship of the maximum accelerations among the base layer, the ground surface, and the basement and the top of the smokestack

The predominant frequencies of the ground and the smokestack were determined based on the predominant peaks in the spectral ratios of the ground surface to the base layer and in those of the top to the base of the smokestack, respectively. Figure 154 shows the relationship between the predominant frequencies and the magnitude of the input in the systems of the ground and the smokestack. The dependency of the predominant frequency on the input to the systems, such as the ground and the smokestack, can not be clearly seen.

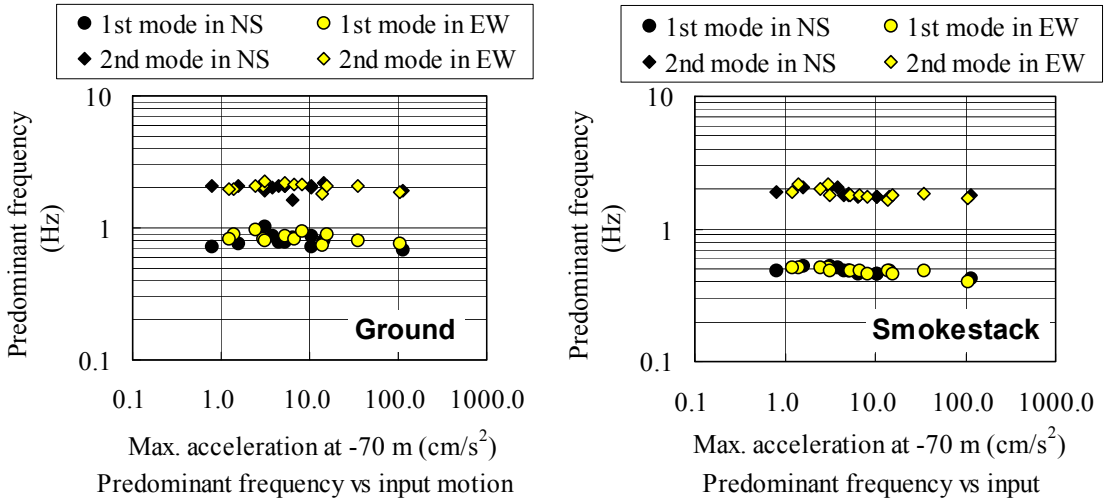

Figure 154 — Relationship between the predominant frequencies and the magnitude of the input in the systems of the ground and the smokestack

In order to study the change of the first and second predominant frequencies along the progress of the time, the change of the predominant periods in the order of the occurrence time of earthquakes is shown in Figure 155.

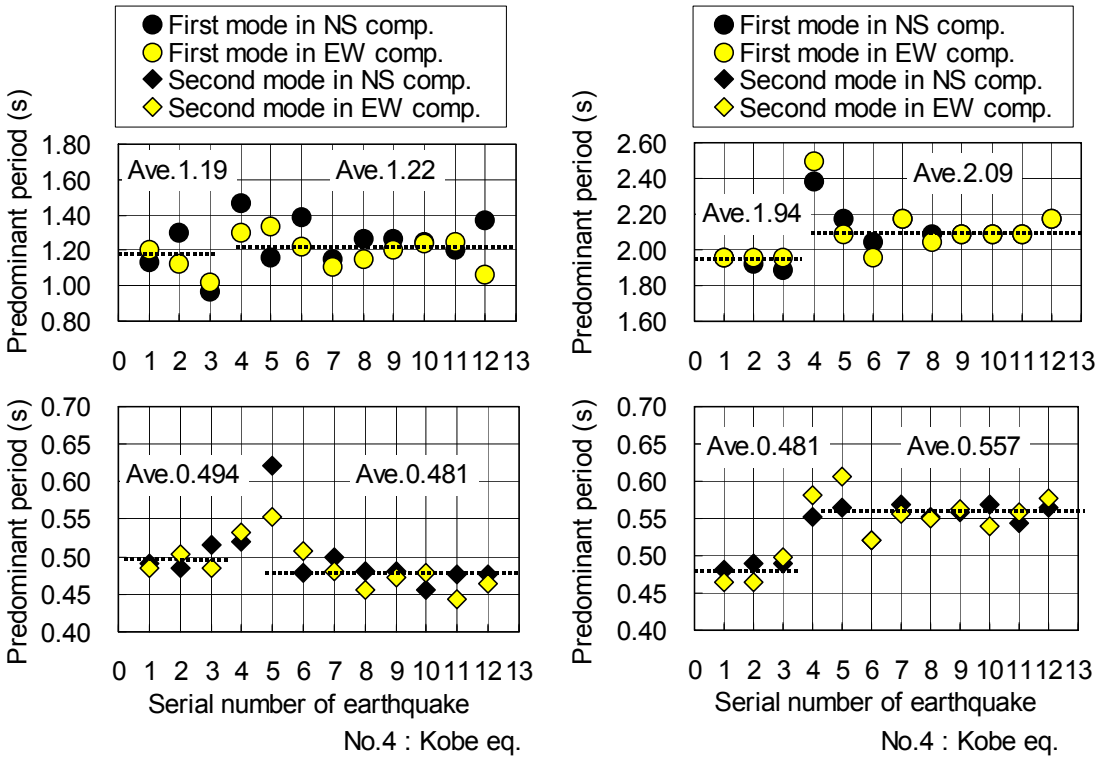

(a) Ground **(b) Smokestack**

Figure 155 — Change of the predominant periods in the order of the time of the earthquakes

As for the predominant periods of the ground, those during the Kobe earthquake are the longest both in the first and second predominant periods, and those after the Kobe are longer than those before in the first predominant period, while the reverse relation can be recognized in the second. The second predominant period can be considered influenced by the soil properties in relatively shallower soils. Accordingly the excitation by the Kobe earthquake might have densificated shallower sandy soil deposits. On the other hand, a slight change of the first predominant period toward the longer side can be supposed to be due to the effect of softening in clayey soil deposits in deeper location. As for the predominant periods of the smokestack, the first one during the main event was significantly long, and those after the Kobe earthquake are longer than those before. The averaged values of the first predominant period before and after the Kobe earthquake are 1.94 and 2.09 seconds, respectively. Moreover, the averaged values of the second predominant period before and after the Kobe are 0.48 and 0.56 seconds, respectively. These irreversible changes of the predominant periods are considered to mean that the stresses in the smokestack had gone far beyond the elastic limit or the cracking limit (Kowada et al., 1998).

5.2.2.11 Verification of models based on strong motion records

5.2.2.11.1 Features of strong motion records obtained during the 1995 Kobe earthquake

The ground motion observed during the Kobe earthquake is approximately equal to the magnitude of the Level 1 EGM for design in terms of PGV. In addition, the behavior of the ground and the smokestack has been clarified to be strongly nonlinear as previously described. Therefore, the numerical simulation by the seismic design models using the record during the Kobe earthquake can be suitable verification of the seismic design of the smokestack.

Figure 156 shows the acceleration time histories of the north-south components on the ground and the smokestack. Figure 157 shows the displacement time histories as well. The principal motions of the ground begin at 16 seconds and end at 28 seconds, which may correspond to the duration time of fault rupture. However, the significant amplitude of vibration, in which a four-second component is highly predominant, takes place in the later time after the principal motion and continues up to 120 seconds in the top of the smokestack. In particular, it is remarkable that the maximum displacement of the top takes place in the later time. This four-second predominant component is also significant in displacement of the ground. This component is considered to be a kind of a surface wave, probably the Love wave due to a deep basin effect.

Some researchers had pointed out that the predominance of components of 3 to 4 seconds had been sometime observed in the central part of Osaka City. From an engineering point of view, the predominance of 3 to 4 period components in Osaka City area was considered in determining reference earthquake ground motions. However, it might be necessary to precisely evaluate the deep basin effect on the smokestack before a Nankai earthquake would attack.

5.2.2.11.2 Verification of models adopted in design

A numerical analysis was conducted by the lumped mass SSI model adopted in the seismic design using the recorded acceleration at the base at a depth of 70 m as the input motion for the model. The analysis by the fixed base model was conducted with the recorded ground surface motion as the input motion. (Kowda et al., 1997, Mori, 2004) Figure 158 shows the acceleration response time histories of the top of the smokestack, the basement of the foundation, and the ground surface together with the measured ones. The response of the top of the smokestack is focused on the time range of the principal motion because this is thought to be dominated by vertically incident shear wave.

In the response of the ground surface, a good agreement is seen in Figure 158. Accordingly, the difference of the ground surface motion between the two models may not be so influential to the response of the smokestack. Comparing the waveform of the basement with that of the ground surface, it is clearly understood that the short period components are obviously reduced. As for the degree of this reduction, the measured one is greater than the analytical one, which means the reduction may not be only due to kinematic interaction along the depth but also due to that in the horizontal plane.

As for the response of the top of the smokestack, both the analytical results roughly match the measured one in terms of amplitude and phase; however, the phase in the response of the fixed base model slightly advances more than the measured one, while that of the proposed model well matches the measured one.

This means that the response of the smokestack from the motion directly transmitted through the pile foundation is presumably dominant in the entire response of the smokestack and the proposed model is able to simulate this mechanism.

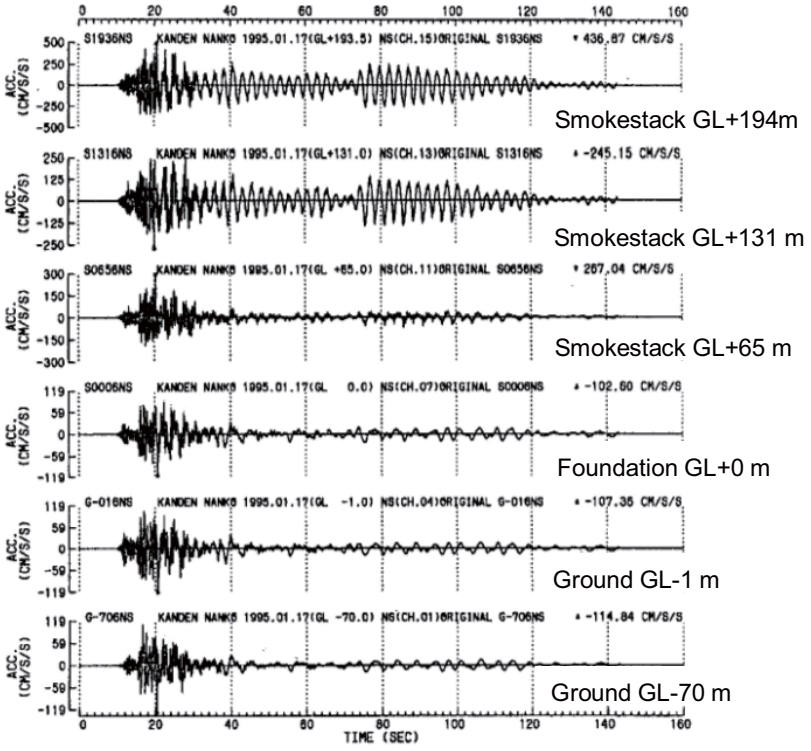

Figure 156 — Acceleration time histories of the north-south components of the ground and smokestack

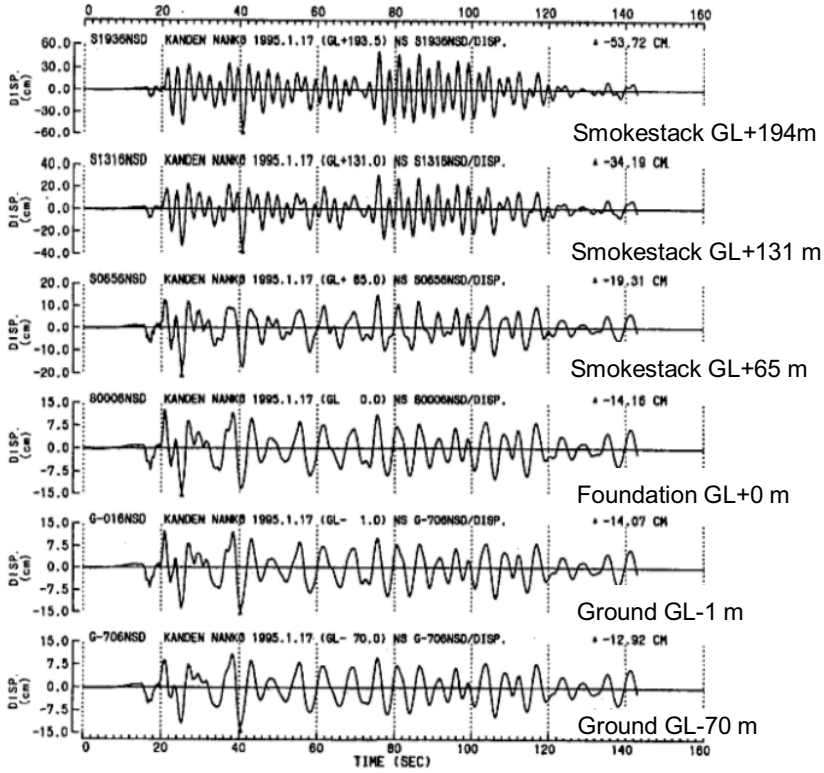

Figure 157 — Displacement time histories of the north-south components of the ground and smokestack

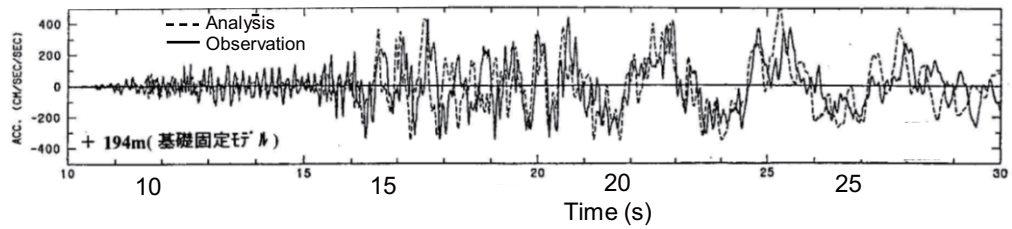

(a) Base fixed model and observation at top of smokestack (GL+194 m)

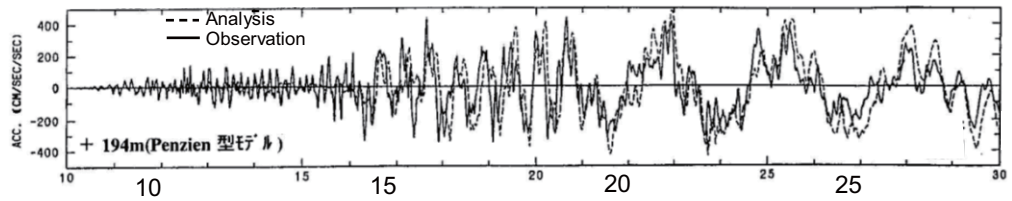

(b) Adopted lumped mass model and observation at top of smokestack (GL+194 m)

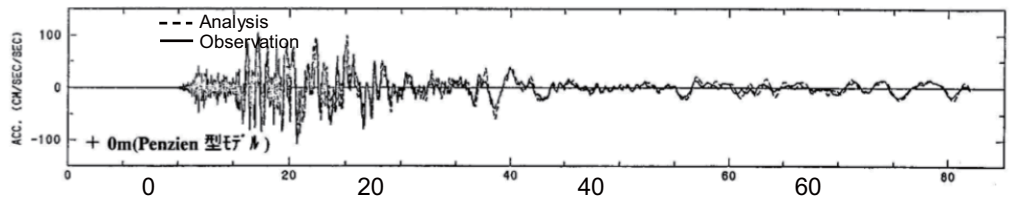

(c) Adopted lumped mass model and observation at basement of smokestack (GL+0 m)

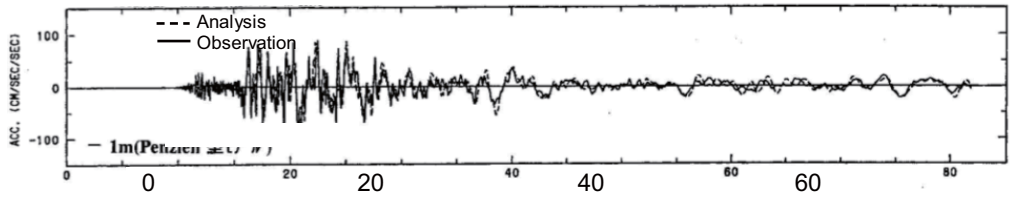

(d) Adopted lumped mass model and observation at ground surface (GL-1 m)

Figure 158 — Acceleration response time histories of the top of the smokestack, the basement of the foundation, and the ground surface together with the measured ones, which is focusing on the time range of the principal motion

Next, the spectral ratios of the top of the smokestack to the ground surface for the north-south component are shown in Figure 159 in order to discuss soil-structure interaction effect from the viewpoint of the transfer function between them. For the first predominant period, the two analysis results match the measurement. For the second predominant period, the result of the proposed model well matches the measured one, but that of the fixed base model is shorter than the measured one. Additionally, a small peak around 1.2 to 1.3 seconds, which may be due to the effect of the first predominant mode of the ground, can be simulated only by the proposed model but not by the fixed base model.

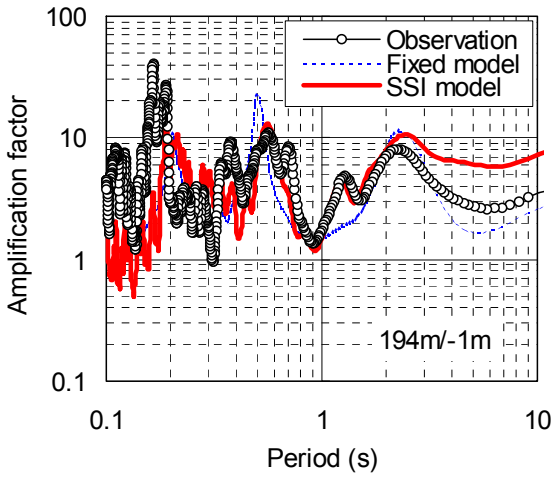

Figure 159 — Spectral ratios of the top of the smokestack to the ground surface and to the base layer for the north-south component

Figure 160 shows various kinds of the spectral ratios of the proposed model and the measurement. That of the top of the smokestack to the base layer, which represents the overall dynamic characteristics of the coupled model, matches the measurement result. That of the ground surface to the base layer, which represents the dynamic characteristics of the ground, also matches the measurement result. As for that of the basement to the ground surface, which represents the effect of input loss in the foundation, both the shapes are roughly the same, whereas the detailed shapes are different.

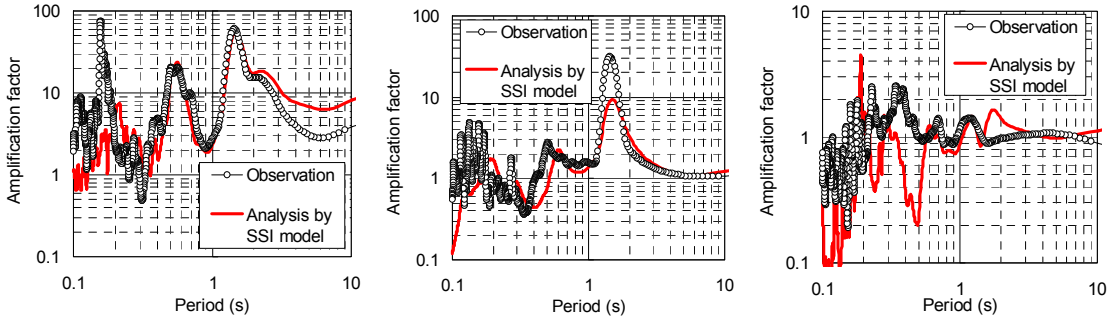

(a) Entire system: Top/GL-70m (b) Ground: GL-1m/GL-70m (c) Basement/GL-1 m

Figure 160 — Spectral ratios of the proposed model and measurement

Figure 161 shows the maximum responses of bending moment and curvature of the smokestack on the skeleton curves with regard to the direction when the north side of the smokestack is in tension and with regard to the east-west direction. In this figure, the two breaking points of each skeleton curve correspond to the cracking and the yielding surfaces. The yielding surface is defined as a situation when the most outer reinforcement bars start to yield. According to the figure, the response of the smokestack went beyond the cracking surface in the range of heights from 20 to 120 m in case of the proposed model, while such situation occurred in a range of heights from 30 to 90 m. The values of residual rigidity of the smokestack estimated from its changed predominant periods, which was mentioned earlier, might correspond to those in case of the proposed model.

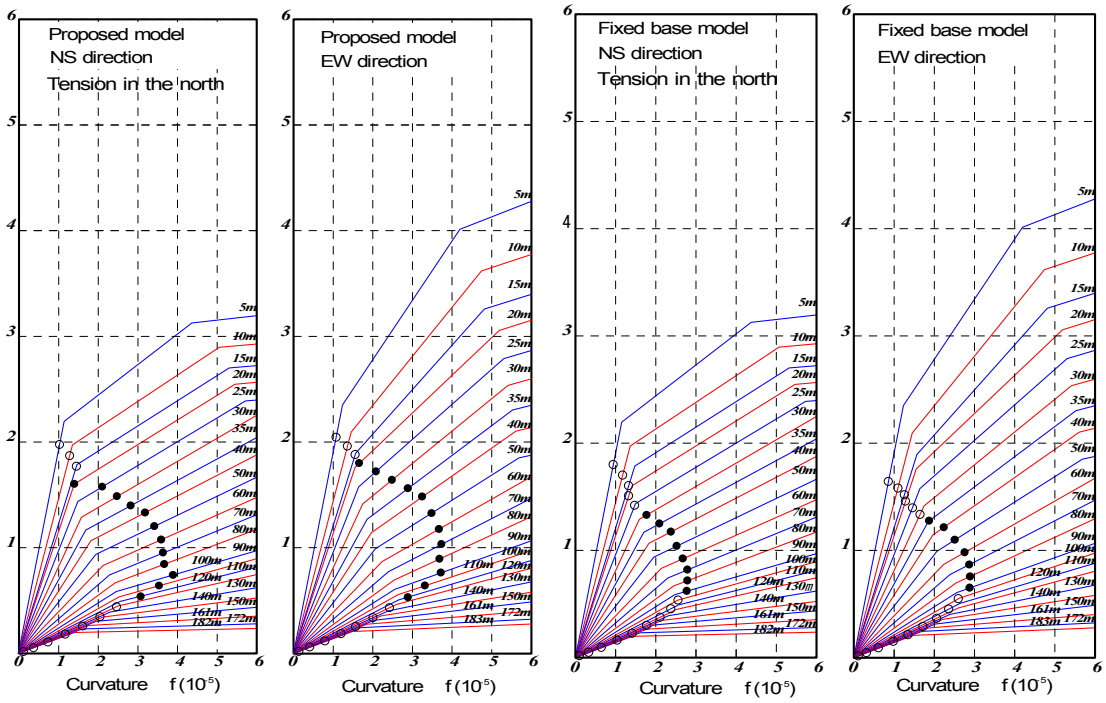

Figure 161 — Maximum responses of bending moment and curvature of the smokestack on the skeleton curves

Based on the comparison of the results of the analyses using the proposed model and the measurement with regard to the time histories of accelerations of the ground and the smokestack, the transfer function of the smokestack, and the relationship between the change of the predominant periods and the nonlinear response of stress-strain of the smokestack, the appropriateness and effectiveness of the proposed model can be verified.

5.2.2.11.3 Confirmation of serviceability and safety of foundation

As previously described, the detailed dynamic model of analysis that is the lumped mass SSI model adopted in design can be verified. Based on the result of the simulation, the response of the piles can be evaluated in terms of integrity. Also in the simulation result, large bending moment take place at pile heads and at boundaries corresponding to the upper ends of the gravel layers. However, the maximum magnitude of the bending moment is smaller than the cracking moment of the piles. Thus the integrity of the pile was successfully confirmed. Actually, no settlement has been observed. In addition, no evidence of liquefaction was observed at the site. This result also harmonized with the result of the simulation analysis. (Mori, 2008)

5.2.3 Shallow immersed rectangular tunnel in soft soils

Underground linear structures refer to a special type of civil construction that having a significant impact on the life quality and economy in densely-populated urban environments. Underground transportation facilities such as metro subways and railway lines, as well as underground road tunnels, , can significantly improve the traffic conditions in large cities. The particular nature of these structures requires a special design approach, under static and especially under earthquake loading in earthquake prone areas. (511A, 512a, 512b)

5.2.3.1 Thessaloniki immersed roadway tunnel

The linear morphology and geographical location of Thessaloniki urban area would require a detour crossing the sea, in order to reduce the traffic and upgrade the life quality in the densely-populated historical centre of the city. The construction of the immersed roadway tunnel that was decided has not begun till recently, since several issues of environmental and operational nature have to be first resolved.

The overall design comprises of a system of cut and cover tunnels (2.9 km length), and underwater immersed tunnel (1.2km) and conjunction ramps to the local road system (1.2 km). A simplified transversal cross section of the RC rectangular tunnel is depicted in Figure 162. The cross-section consists of two separate traffic branches and an escape corridor in the middle. The simplified cross-section geometry used in the present preliminary design initially may be modified in the final design in particular in sections where high stress concentration may demand different plate thickness reinforcement and construction details.

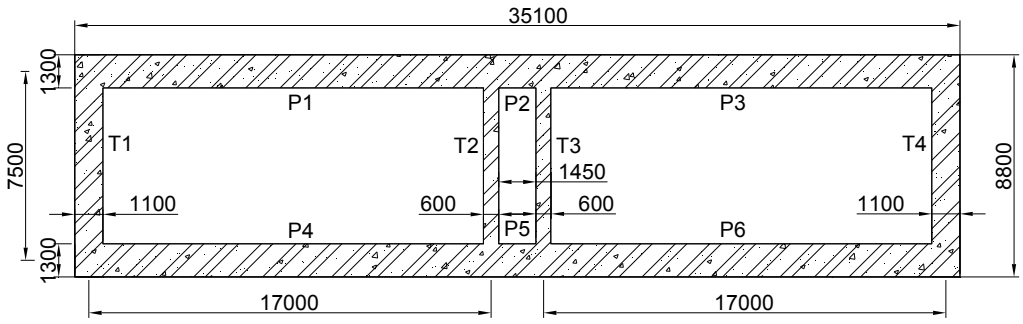

Figure 162 — Simplified tunnel cross-section

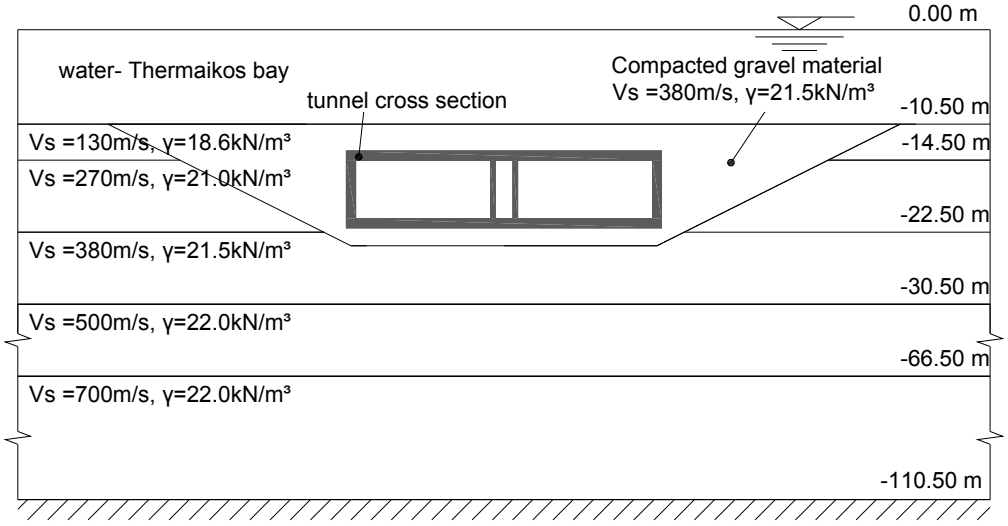

Figure 163 — Simplified tunnel and soil cross-section

A simplified soil profile is depicted along with the tunnel location in Figure 163. Around the tunnel, the initial soft –loose soil (silty clay and loose silty sand),, is replaced with compacted gravel,(slope 1:2), to improve the soil drainage conditions and confinement. A thin (1 m) layer of compacted gravel is also placed below the tunnel to improve the foundation strength and deformability. The average seismic bedrock (Vs>750m/s) is estimated at 110m depth. (715A,715B)

5.2.3.2 Behaviour of longitudinal underground structures under seismic loading

When seismically induced waves propagate across and towards a tunnel, its cross-section is deformed in various modes, both in the longitudinal and transverse direction. For rectangular tunnels, the main transversal seismic load is racking deformation of the rectangular cross-sections (Figure 164). There is a strong time depended interaction effect between the underground structure and the surrounding soil. The soil deformation in the proximity of the structure imposes a displacement constraint on the tunnel's cross-section. Yet, due to the stiffness variation between the two media, the tunnel responds in a different way to the imposed deformation. The overall seismic behaviour of the tunnel depends both on the properties of the surrounding soil and the inertial and material properties of the tunnel's cross-section. Large and thin-plated tunnels tend to

'follow' the deformation of the surrounding soil, whereas more rigid cross-sections are reacting to the imposed soil transient deformation leading to higher strains and stresses. (514A, 514B, 514C)

Taking into consideration the numerous parameters regarding the structural behaviour, the seismic loading and the varying soil properties in the proximity of an underground structure, it is doubtful whether a single, advanced three-dimensional model could accurately reproduce the actual response of the structure. On the other hand, the adoption of a simplified cost-effective two-dimensional approach, employing a parametric investigation of the aforementioned implicated factors, could cover many intrinsic uncertainties of the examined problem. Bearing also in mind that racking deformation, due to vertically propagating seismic waves, is the main seismic input load for rectangular tunnel, it is generally accepted that a well constrained and designed two-dimensional approach can capture the key points of the underground structure's response. (712A, 713A)

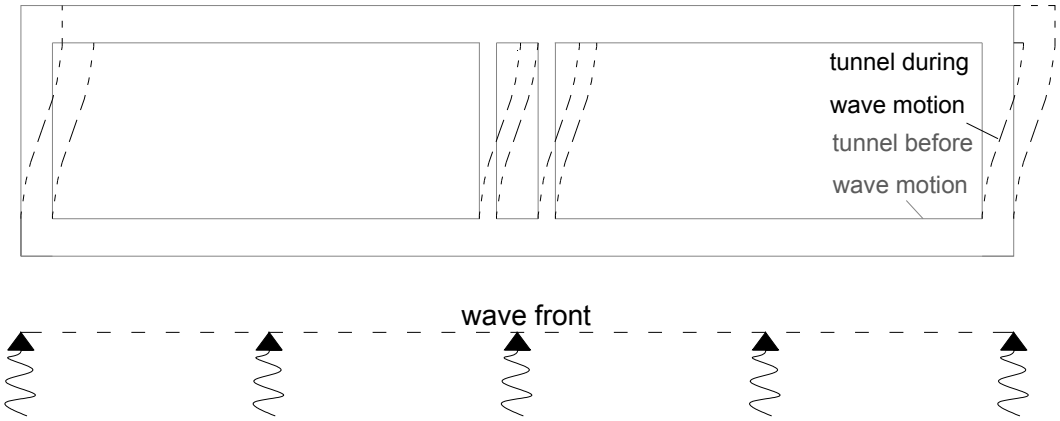

Figure 164 — Racking of rectangular tunnel section

5.2.3.3 Analysis methods

In engineering practice the conventional design method employs equivalent static analysis of the tunnel, applying code regulations (e.g. Greek Seismic Code or EC8). The dynamic earth pressures can be calculated using the Mononobe-Okabe approach, while the inertial forces of the structure are determined after proper estimation of the average acceleration value evaluated along the structure, at depths where it is located. Normally for each site, the code acceleration values are adopted for 500 or 1000y mean return period, disregarding the fact that these values are proposed for the surface ground conditions. Soil-structure interaction is also considered through appropriate spring supports at the tunnel-soil interface. (822A, 822B)

A efficient way to consider the interaction between the tunnel and the surrounding soil, is to model the soil behaviour in the proximity of the structure, employing an adequate numerical code, either by using plane strain elements or by introducing properly calculated impedance functions (springs) at the interface. The "free-field" soil deformations are then imposed at the springs-dashpots, introducing at different depths and locations the seismic loading imposed by the oscillating ground, to the tunnel's cross-section. (821A, 821B, 821C, 821a)

In order to fully capture both the kinematic and the inertial part of the soil-structure interaction effect, a detailed dynamic analysis would be apriori the most appropriate approach. A 2-D discritization of the soil and the structure reproduces efficiently the interaction phenomena, whereas seismic loading is applied on the tunnel through the soil deformation from the propagating upwards seismic SH or SV seismic waves. The input motion is given at the bedrock. Both horizontal and vertical components of the induced input motion may be taken in to account. (921A, 921C, 921D). The present case has been studied using the ADINA code.

5.2.3.4 Determination of input motion

Regardless of the implicated analysis method, an important element in the tunnel's design process is the evaluation of the seismic ground shaking imposed on the structure. Seismic Codes offer some guidelines on the selection of the input motion characteristics, yet those are aimed for above ground structures, and for different return periods and probabilities of exceedance. A complet and site specific seismic hazard analysis is more suitable- if not mandatory- to determine the dynamic loading levels in the case of important underground constructions such as metro lines or underground roadway tunnels, since they specifically address problems related tp local site conditions. In the case of the Thessloniki's immersed tunnel, a full probabilistic seismic hazard analysis has been conducted and the seismic ground motion at outcrop conditions has been properly estimated. Then a typical deconvolution procedure is followed, as schematically described in Figure 165 to estimate the ground motion at the bedrock underlying the tunnels at -110m. The computed ground motion at -110m has been finally used to make a site specific 1D EQL analysis of the ground response, in a typical cross section along the structure, representative of the soil conditions in the area of the immersed tunnels.. (520A,611A,621A,621B,621C,622a,622b,622c,622A,623A,631A)

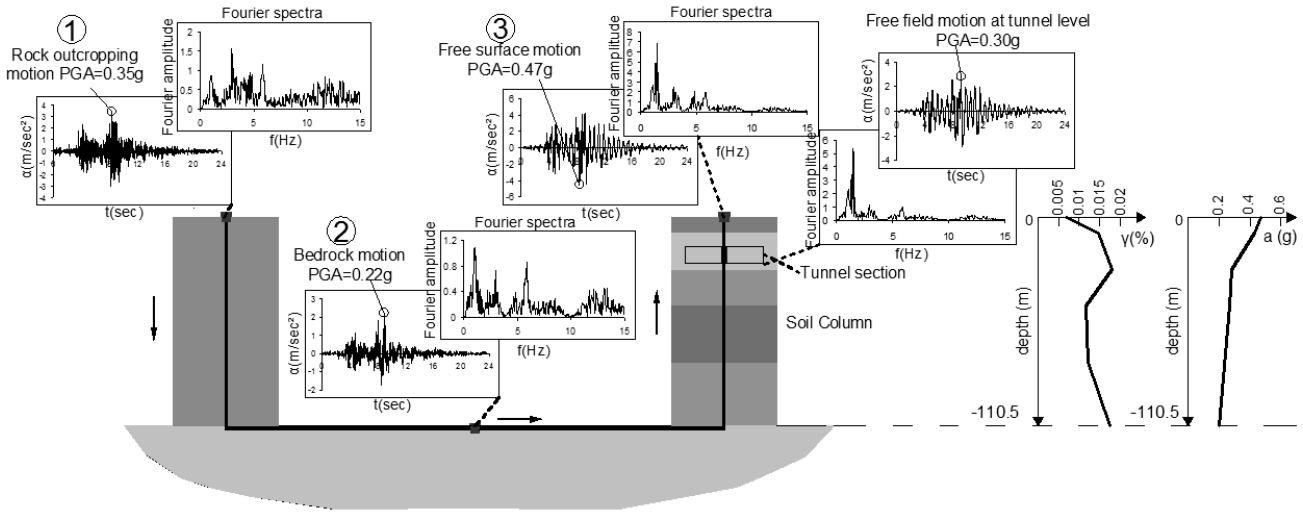

Figure 165 — Deconvolution process (Thessaloniki (1978) seismic scenario): (1) Outcrop target acceleration time history, (2) acceleration time history at the bedrock level, (3) acceleration time history along the soil column

The simplified equivalent static analysis applies "quasi-static" forces upon the structure (slabs and vertical walls). These inertial forces normally correspond to the average acceleration level observed at any depth defined from the 1D free-field ground response analysis. In this case, the simplified equivalent static analysis ignores the kinematic part of soil-tunnel interaction that would normally alter the initial acceleration time-histories at the proximity of the underground structure. If the complete soil profile or the bedrock depth are not available, an acceleration value at the depth of interest could always be estimated (probably conservatively) using the ground acceleration defined by the national seismic code for the investigated site. Along with the deficiencies concerning the kinematic interaction, this simplified approach includes several uncertainties that would only lead to a crude estimation of the actual loading level. (623B)

In the case of detailed equivalent static analysis, the required displacement pattern which will be applied directly upon or in the proximity of the structure, is calculated through a 1D soil-column non-linear or equivalent linear (i.e. SHAKE type) analysis, using as input the bedrock motion that was calculated through the deconvolution process. (623B)

The bedrock motion obtained in the first step of the aforementioned deconvolution procedure can be used for the detailed dynamic analysis, where the soil deposit is simulated using 2-D plane strain elements. The soil-structure system in this case is excited by the upwards propagating seismic waves, from the base of the model towards the surface. (623B)

5.2.3.5 Simplified equivalent static analysis

The approach using static forces to model seismic loading is quite common in several recent seismic codes; it is employed for the study of aboveground structures that meet certain criteria concerning their morphology. It is rather questionable whether a similar method could be used in the case of underground structures, at least in its present form, where the equivalent (to the inertial) static forces obtain a distribution profile that conforms to the dynamic characteristics of an oscillating construction free of lateral supports. Moreover, the determination of the dynamic earth pressures, using methods described in the case of retaining walls, such as the Mononobe-Okabe approach, may be often proved inadequate for underground structures. Nevertheless, several studies utilize an “equivalent static approach” to design tunnels, mainly because the use of static forces is more straightforward and easily controlled by an average engineer using existing commercial software.

The soil-structure model consists of linear frame-type elements for the tunnel’s cross-section and linear springs to simulate the soil support compliancy. A schematic representation of the model concept of the examined case study is depicted in Figure 166. Equivalent static forces on the structure due to seismic loading are determined, based on the average acceleration level calculated at the depth of the tunnel’s cross-section. The base shear force, a term borrowed from the study of aboveground structures, follows a distribution compatible to the first eigen-mode of oscillation of the structure considering the foundation soil compliancy. The calculated static forces are applied at the horizontal diaphragms of the underground structure, in order to correspond to the racking deformation that causes differential displacement between the upper and the lower horizontal diaphragms (slabs) of the tunnel (F_1 and F_2 in Figure 166). Seismic quasi-static forces due to inertial loading are not applied on the side walls, since the mass of the vertical diaphragms is negligible compared to the horizontal diaphragm mass. Considering that this is a single-direction loading approach, and the linear springs used in this analysis work in both directions, the left side wall should not be supported by horizontal springs, as this would relieve the structure from the applied earth pressure. For the same reason, the tunnel should not be supported by horizontal springs in both side walls, when hydrodynamic pressure appied (Figure 167). The roof-slab is free from shear springs it was supposed that the cover thin loose soil layers would move together with the tunnel, rather than provide any shear reaction. (811B, 814a, 815a, 822A, 822B).

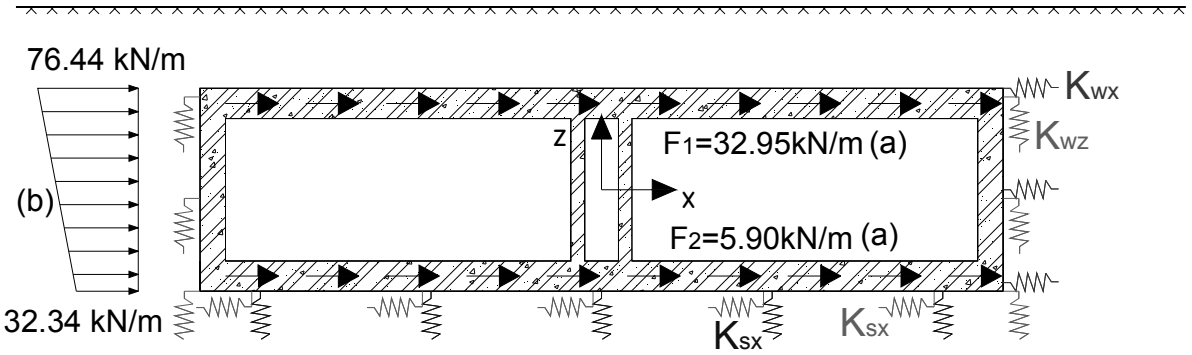

Figure 166 — Equivalent static model: (a: Equivalent static inertial forces, b: Seismic earth pressure)

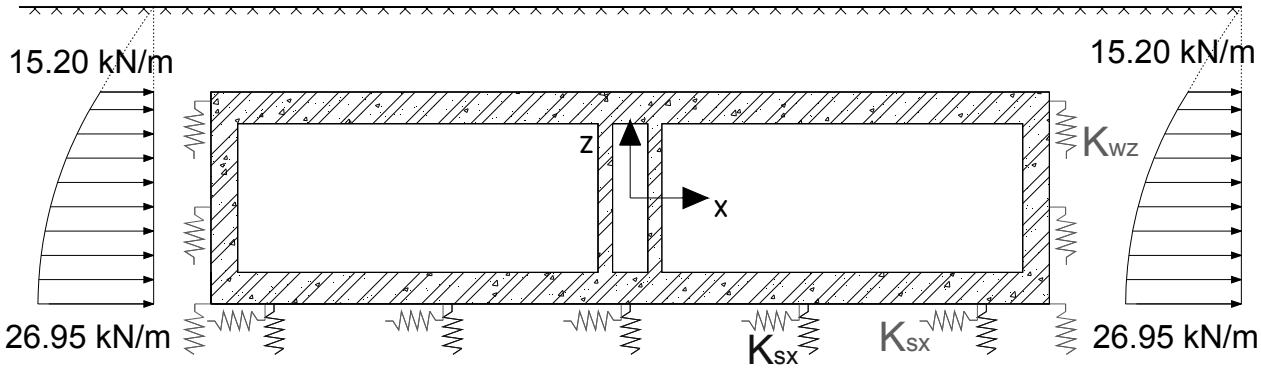

Figure 167 — Equivalent static model for Hydrodynamic pressure

Seismic earth pressures at the tunnel sides are calculated according to the guidelines of the Greek Seismic Code (EAK 2003) for retaining wall, applying two methods; (i) the Mononobe-Okabe approach for walls that can move/tilt sufficiently and (ii) a procedure proposed for rigid non-deformable walls (Figure 168). Finally the procedure for rigid non-deformable walls is adopted, as it gives results closer to those from dynamic analysis. (814a). Hydrodynamic pressures at the tunnel sides are calculated according to the guidelines of the Greek Seismic Code (EAK 2003) for retaining wall. To get the internal forces at the structure, the results from both models (Figures 5 and 6) are companied.

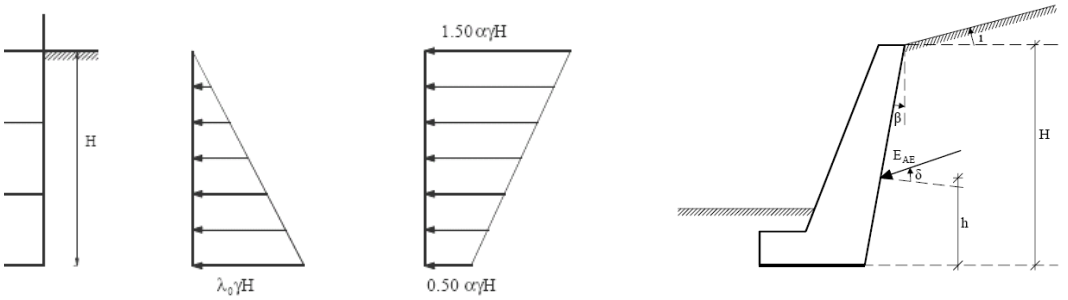

Figure 168 — Geostatic and seismic earth pressures for non-deformable wall (left), and Mononobe-Okabe approach (right).

A rather delicate issue is the determination of the impedance factors for the soil spring-properties and values of the side walls and the slabs of the cross-section. There are several plausible suggestions in the literature for the calculation of horizontal springs on the side walls (K_{wx} in Figure 166 and Figure 167). Almost all are inspired from surface and deep foundations solutions. Yet, in the case of vertical and horizontal soil springs for the cross-section slabs (K_{sz} and K_{sx} in Figure 166 and Figure 167), as well as for the determination of the vertical (shear) soil-springs on the side walls of the tunnel (K_{wz} Figures 166 and Figure 167), few references are roughly compatible to the actual problem configuration and can be applied in this type of structures. A detailed discussion of the impedance factor calculation can be found in [78] and [80].

Several issues, including the concept and distribution of the so called “base shear force” in underground structures, the validity of the seismic earth pressure calculation based on clauses for retaining walls and the estimation of the impedance factors values for static and dynamic loading, discredit the accuracy of this approach. The evaluation of the results in the next few paragraphs confirms the approximate nature and the important uncertainties involved when applying this method.

5.2.3.6 Detailed equivalent static analysis

This type of analysis, although inspired by the previous one, attempts to reproduce more accurately the soil-structure interaction effects during the quasi-static analysis procedure. The calculated “far-field” deformations are now imposed on the soil next to the tunnel’s cross-section, contrary to the previous analytical approach, where a “modified deformation profile” was applied directly on the structure. In this case the final imposed deformations on the tunnel’s side walls, are determined depending on the type of constraint between the structure and the surrounding soil. The soil compliancy is simulated through a finite element code with appropriate constitutive law (i.e. Mohr- Coulomb), either by using 2-D elements for the soil, or via proper springs that correspond to the degree of the support the soil offers to the tunnel’s cross-section. In the example presented herein, the soil surrounding the tunnel is simulated using 2-D plane strain elements to account for the elastic support of the cross-section in the lateral and vertical direction. The deformation profile is imposed at the side FE mesh boundaries of the soil model. (821A, 821B, 821C, 821a)

The determination of the free-field soil deformation profile, which will be imposed on the model, boundaries can be calculated by 1D site response analysis in the same way described in the previous section, supposing free-field conditions. In this case though, it is the complete deformation profile at a specific instance that is required rather than the maximum displacement value at the cross-section’s level. The selected deformation profile corresponds to the time step, where the maximum differential displacement between the base and the top of the cross-section is observed.(811b)

This procedure becomes complicated in case of stratified heterogeneous soil. The presence of the inclined gravel bed for instance, in the examined case study, raises also some modelling questions regarding the geometry of the 1D soil profile that should be used during the calculation of the free-field ground deformations. If the simulated soil area is extended laterally, far away from the gravel bed location, then a single soil column analysis using the in situ soil characteristics is accurate enough to provide the deformation profile for the 2-D analysis (model C in Figure 169 and corresponding simulated area of model C in Figure 170). In the case though, that the modelled soil area is in the edge or inside the gravel bed region, the soil column layering that should be employed in order to obtain a realistic soil deformation profile is not obvious. If, for instance, model A or B of Figure 169 are examined, the soil deposit at this specific location would refer to the initial soil layering. Nevertheless, it is quite obvious that the complex soil geometry of this location after the construction of the gravel bed, will affect the free-field response of the unmodified soil profile, altering the obtained results. Therefore, when the FE model does not extend laterally in the 2-D analysis (Models A, B, D and E of Figure 170), both soil column profiles are employed for the determination of the soil deformations during the 1D analysis, serving as lower and upper bound for the 2-D analysis that will follow. (713A, 715A, 715B)

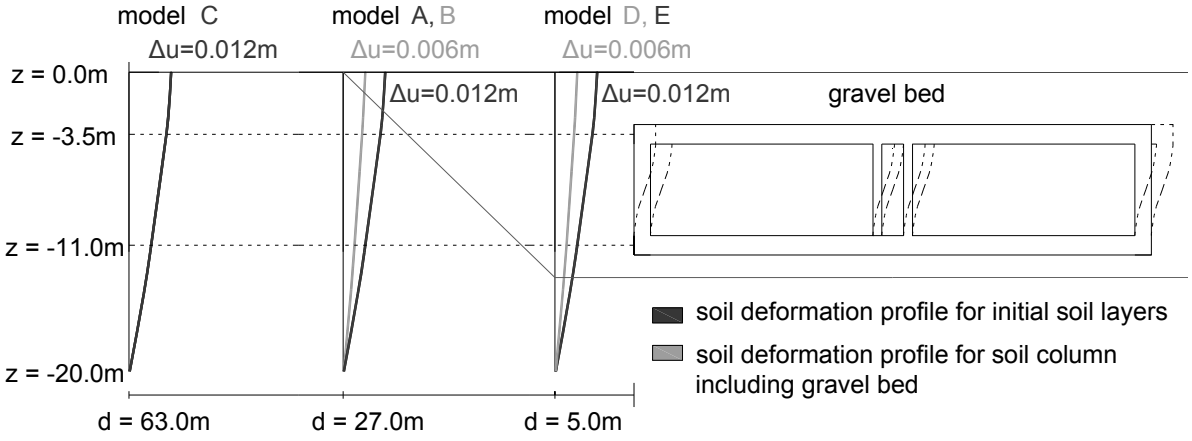

Figure 169 — Soil deformation profile applied in the proximity of the tunnel (at distances d equal to 5m, 27m, 63m).

The 2-D FE models are depicted in Figure 170. The various deformation profiles that were previously calculated are imposed at the side boundaries of the modelled area. Nevertheless, there are no specific guidelines for the distance of the imposed deformations to the tunnel’s cross-section. When the deformation profile is imposed in a long distance from the underground structure, it is possible for the soil elements to

absorb a great amount of induced ground strain, thus “relieving” the structure and altering the analysis results. If, on the other hand, the model is laterally reduced, bringing the side boundaries close to the tunnel, it is doubtful whether the soil-structure interaction mechanisms will deploy to their full extent. (821B, 821a)

Three different models have been proposed, in order to investigate the effect of the side-boundaries distance to the tunnel. Moreover, in each of the reduced size models, two different imposed deformation profiles are utilized, to account for the effect of the surface gravel bed on the free-field response as previously explained. Therefore, in models A and E the imposed seismic equivalent static loading is the seismic displacement profile obtained from the 1D site response analysis of the initial soil profile. In models B and D on the other hand, the imposed ground deformations have been calculated for a soil profile where the surface layer is replaced by compacted gravel material. In the case of model C there is no such dilemma, since the mesh boundaries are far enough to imply any effect of the gravel bed on the ground response. The purpose of this parametric analysis is to form an envelope stress condition for the tunnel, in order to compare the output with the results of the other proposed methods and the detailed full dynamic analysis. (821a)

Being essentially a static analysis, this approach is cost-effective compared to more elaborate full dynamic time-history analysis. However, it is still lacking guidelines concerning several modelling specifics of the soil-structure system.

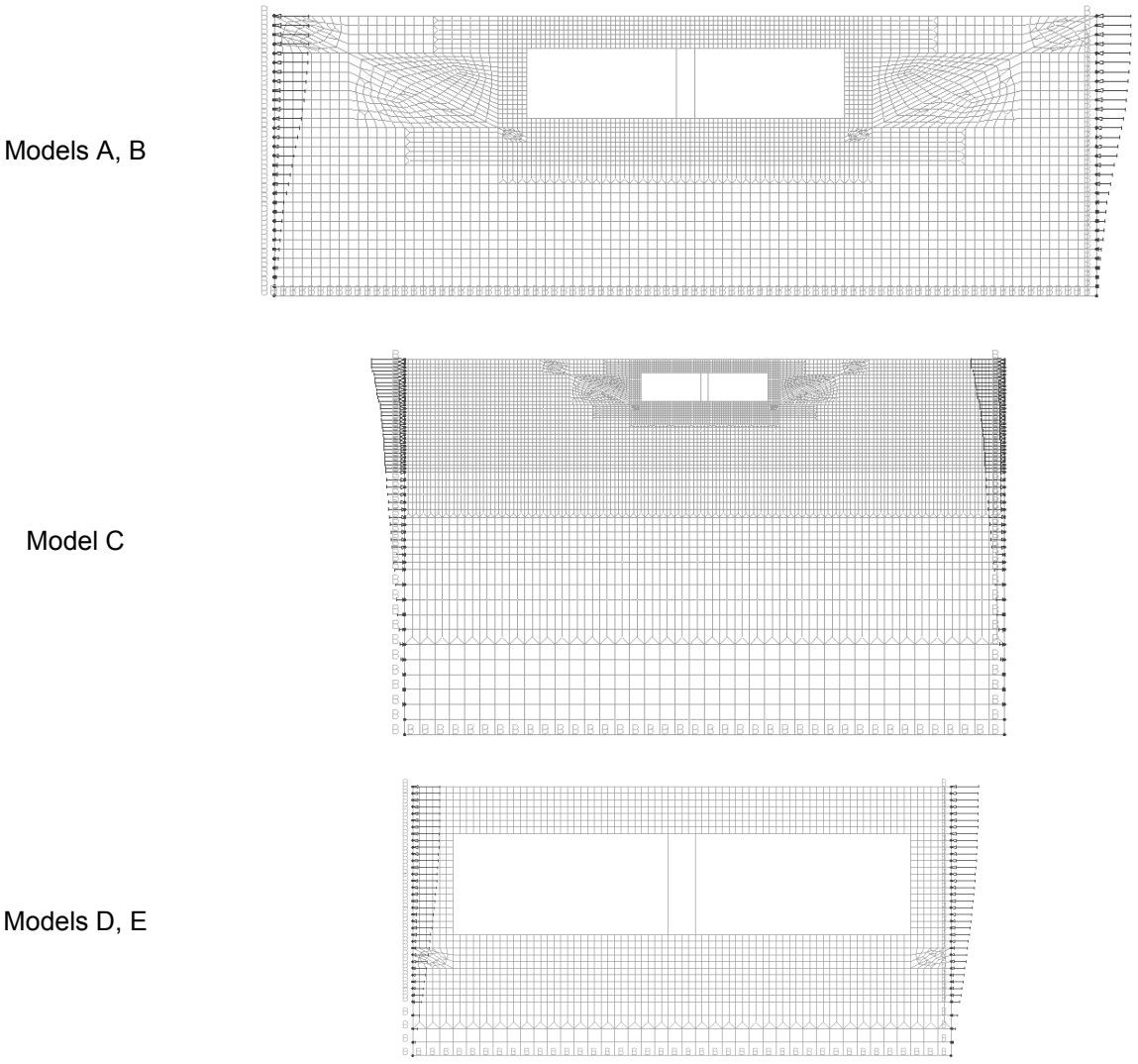

Figure 170 — Application of imposed free-field soil displacement profile for different soil-structure models

5.2.3.7 Detailed full dynamic analysis

The direct consideration of both kinematic and inertial part of the soil-tunnel interaction effects in the time-domain is expected to better consider and highlight various aspects of the underground structure's seismic behaviour that cannot be captured by conventional or improved quasi-static analyses.

Plane strain elements are used to model the soil whereas the tunnel's cross-section is modelled using frame-type elements of proper dimensions. The size of the plane strain elements is carefully selected depending on the soil deposit properties, in order to efficiently reproduce propagation of seismic wave frequencies up to 10~15Hz, an upper frequency bound considered adequate for civil engineering purposes. Detailed dynamic analysis is performed imposing the input motion at the base of the model (i.e. bedrock level at -110m). (921A, 921B, 921C)

Unlike many construction materials, soil exhibits nonlinear behaviour even in small strain levels. An equivalent linear approximation is employed in order to simulate the behaviour of the soil deposit under seismic excitation. The soil shear modulus and damping properties are modified in a multi-step procedure at every analysis cycle, according to the shear deformation level of the soil deposit at each depth. This simple approach is quire efficient for describing the soil inelastic behaviour under seismic loading and is incorporated in many programs specialized in soil seismic response calculations (i.e. code SHAKE). The variation (degradation) of soil shear modulus [G(g)] and material damping increasing [D%(g)] with increasing shear strain (γ), is described by selected G- γ-D curves corresponding to each soil type. (921D)

The material damping of soil materials is normally of hysteretic type and frequency independent. Nevertheless, employing the frequency dependent Rayleigh-type damping facilitates the detailed dynamic analysis. Indeed, since Rayleigh damping is a linear combination of mass and stiffness matrices, it is efficiently incorporated into the analysis procedure. Yet, the selection of the damping parameters and the resulting damping curve should be carefully inspected, in order to achieve constant damping properties at the frequency range of interest.

The final 2-D model for dynamic time-history analysis, incorporating the tunnel's cross-section, is presented in Figure 170. The computed dynamic (seismic) stresses and internal forces are added later to the results of the static loads; the two computations are performed separately as usual.

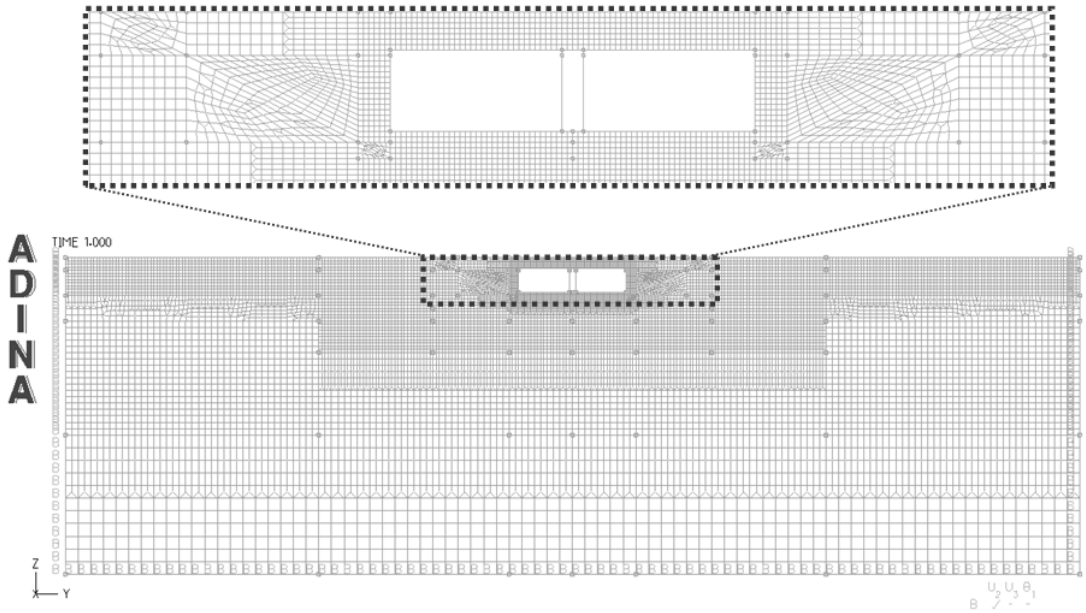

Figure 171 — Numerical FE model

5.2.3.8 Results and discussion

The results of the equivalent static analysis, where quasi-static seismic ground displacements are imposed at the side boundaries of the FE model, are compared with the full dynamic analysis which is considered as apriori being the accurate one. Five different models (A to E) have been used, modifying the lateral boundary sides of the modelled area. Internal forces at the structure are depicted in the diagrams of Figures 172-174 for several locations (see Figure 162), of the tunnel's cross-section. Bending moments in models A and D are almost identical, indicating that a judicious evaluation of the FE mesh dimensions and the seismic ground displacements may be equally acceptable. Indeed, in model A the ground deformations are imposed at a distance of 27m from the cross-section side walls, while the computed peak 1D ground displacements at the surface are equal to 12mm. In model D on the other hand, the computed peak ground displacement are equal to 6mm –due to the existence of the stiff gravel backfill- and they are imposed at a very short distance from the tunnel, On the contrary the with the extended mesh (case C), the computed bending is quite different from the other cases and the full dynamic analysis. It is reminded that the input motion at -110m in all cases is the same. Comparing the results of all models with the results of the full dynamic analysis, it is observed that the better comparison for all internal forces (bending moments, shear and axial forces at several critical sections), is provided when the ground deformation of the unmodified soil (far-field conditions) are applied quite close to the tunnel cross section (model E).

Concerning the simplified equivalent static method, the internal forces on the structure deviate considerably from the results of all other methods, and in particular of the full dynamic analysis. The conventional approach, where seismic earth pressures are simulated by static "inertial" forces, while the tunnel is being supported on the opposite side by linear springs, seems to be rather inaccurate and inconsistent with the reality. The actual dynamic shift between active and passive state of earth pressures cannot be efficiently reproduced in a conventional equivalent static analysis.

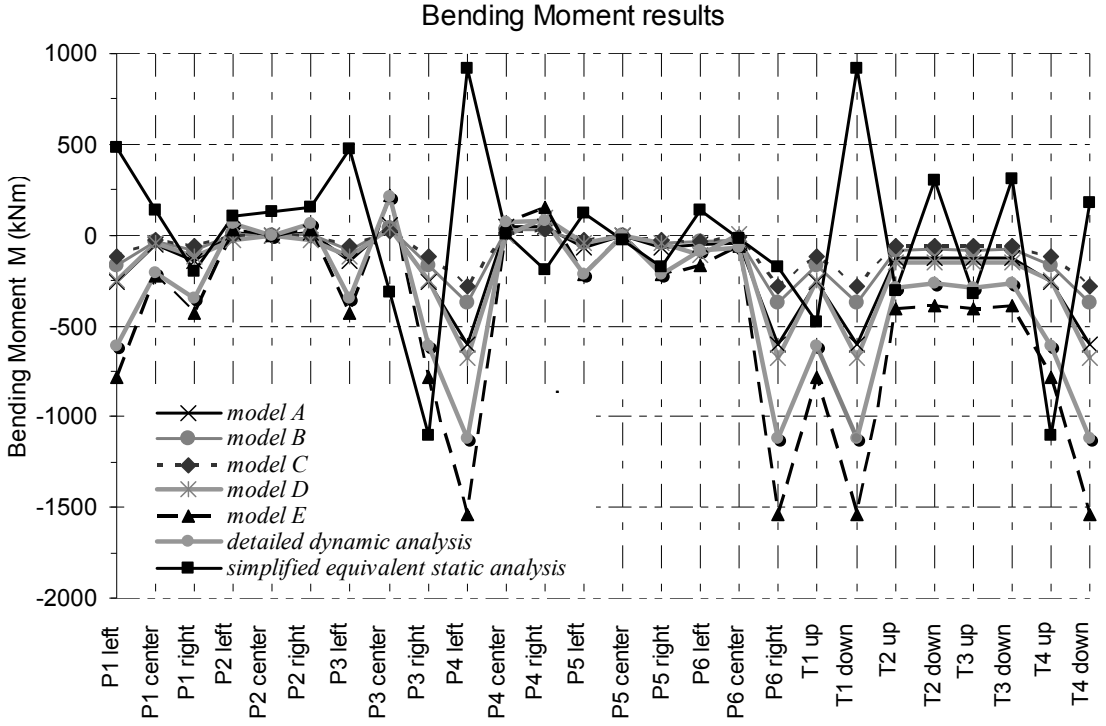

Figure 172 — Bending moments at the cross-section for various analysis cases. Models A to E correspond to equivalent static analysis with imposed quasi static seismic ground deformations displacements at the side boundaries of the FE mesh.

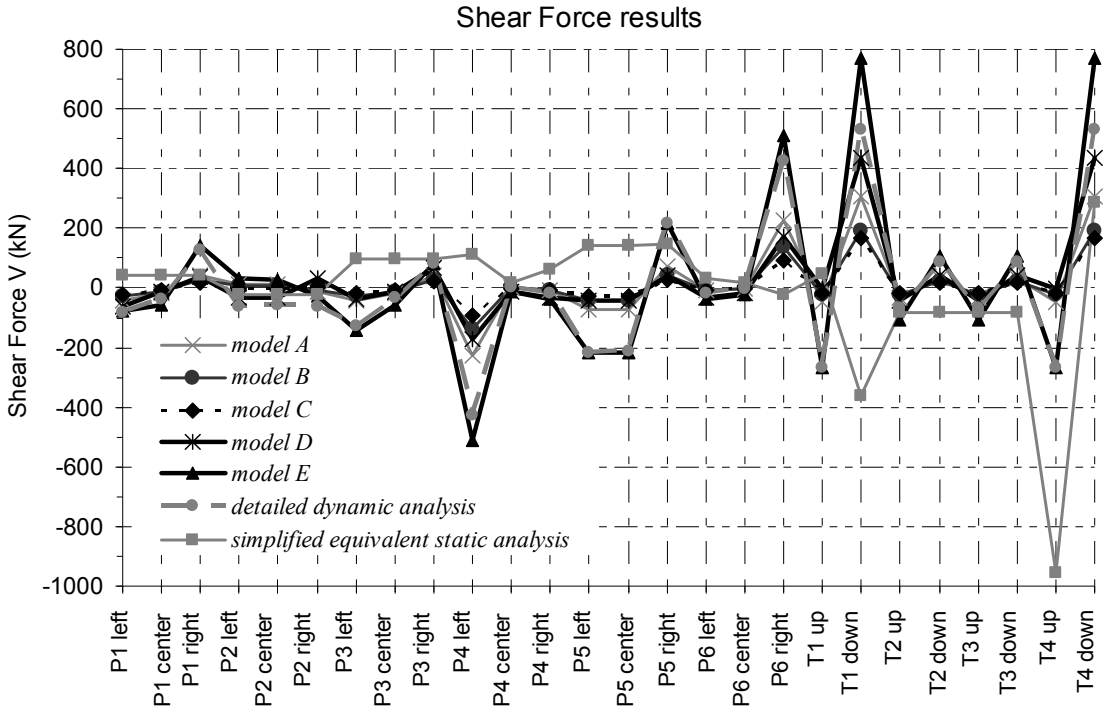

Figure 173 — Shear forces at the cross-section for various analysis cases. Models A to E correspond to equivalent static analysis with imposed quasi static seismic ground deformations displacements at the side boundaries of the FE mesh.

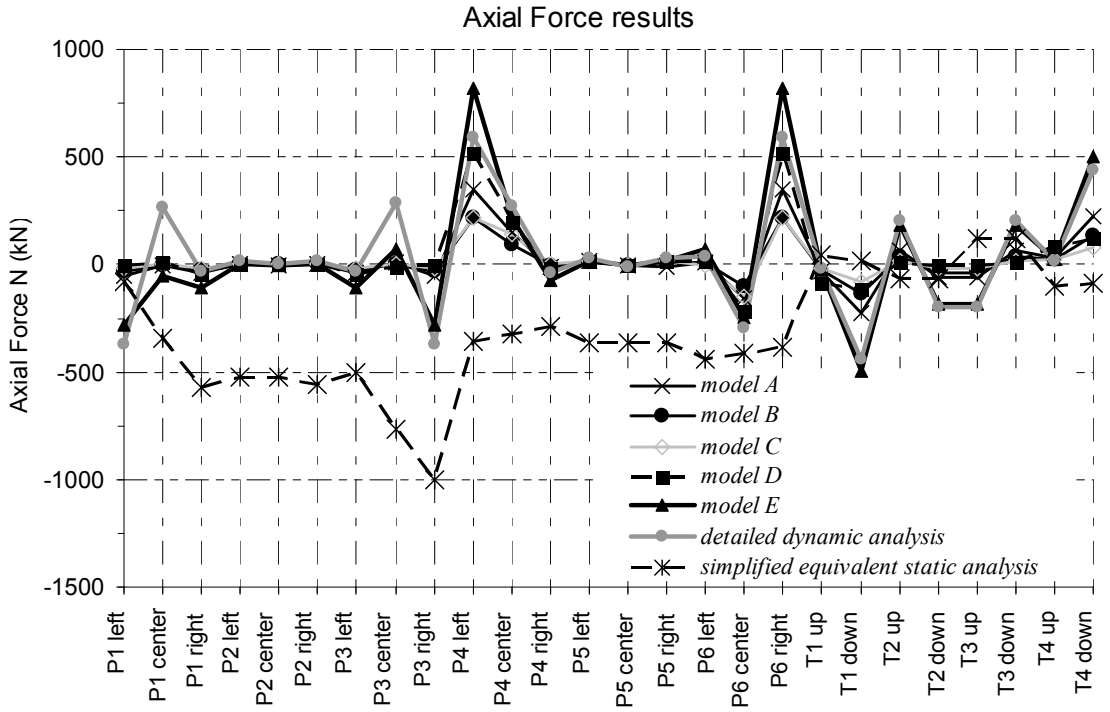

Figure 174 — Axial forces at the cross-section for various analysis options cases. Models A to E correspond to equivalent static analysis with imposed quasi static seismic ground deformations displacements at the side boundaries of the FE mesh.

The main conclusion of this parametric study is that the results of the different approaches and methods may differ significantly under “identical” soil and structure conditions. The detailed full dynamic analysis is considered more accurate. It can describe accurately the tunnel’s geometry, the details of the surrounding soil and the seismic loading conditions. Linear, equivalent linear and non-linear analysis may be used according to the specific features of the problem. Employing a linear elastic analysis scheme, allows for parametric investigation of uncertainties with low computational cost.

The simplified equivalent static analysis, usually applied in engineering practice, has been proved inadequate to model problems of this nature. Moreover, the results, in terms of internal forces, to design the tunnel lining, may not be conservative, leading sometimes to ”unsafe“ structures. The main problems are related to the selection of the appropriate impedance factors and the estimation of the seismic loading conditions (e.g. seismic earth pressures and shear forces round the tunnels cross section).

Given these difficulties, the detailed equivalent static analysis consisting of applying statically an adequate seismic ground displacement pattern in close distance to the structure, and to perform a static numerical analysis in plane strain conditions, may offer an attractive alternative solution.

5.3 Demonstrations evaluating and designing for liquefaction effects

Effects of soil liquefaction on performance of geotechnical works are assessed as per 6.3.1 of ISO 23469. Methods of the assessment may be broadly categorized and selected on the basis of required seismic behaviour specified by performance criteria and quality of geotechnical data of the site. (631B, 631C)

This subclause provides three demonstrations evaluating and designing for the liquefaction effects on pile foundations with importance. All the examples that had already been judged in terms of liquefaction occurrence use site-specific detailed dynamic analyses for incorporating the effects of liquefaction in the 2nd stage as seismic actions or effects on the model of the soil-structure system. (612A, 612B, 712A, 713A, 911A, 911C)

The first example demonstrates three-dimensional (3-D) effects of pile arrangement in the circular plate foundation of a large LNG tank in a liquefiable soil on pile stresses in different locations. It compares a two-dimensional (2-D) model with a 3-D model using the same computer code for effective stress analyses. Consideration of the 3-D effects recognized in this example was reflected into the actual design of the tank. The second example demonstrates 3-D effects of lattice-like rectangular arrangement of piles for the foundation of a huge facility of an electrical power plant in the evaluation of liquefaction effect on pile stresses. It includes comparison similar to the first example and comparison with a unique model using a pile-soil system with periodical boundaries for the 3-D effect of the pile foundation. The 3-D effects can be evaluated by the 2-D model with additional modification, but are evaluated by the unique model with some difficulties. The third example demonstrates pile-volume effects of a foundation supported by a huge amount of piles. It compares four cases of effective stress analyses using the same computer code for effective stress analyses. The four cases involve 2-D and 3-D models wit and without a consideration of pile volume. The result supports the efficiency of an ordinary way modelling a pile to a volume-less beam. (913A, 921A,)

Seismic actions for detailed dynamic analyses are given as input motion time histories at firm ground of the sites. Nonlinear stress-strain behaviour of soils and structures are appropriately modelled for the analyses of the soil-structure systems using appropriate formulations, constitutive models and numerical procedure for evaluating the effects of soil liquefaction. (921B, 921C, 921D, 922A)

5.3.1 Evaluation of 3D SSI effects of pile foundation of LNG tank model by detailed dynamic analyses

5.3.1.1 Problem description

Various detailed analyses have been done by FEM about dynamic analysis of pile foundations. (921A) But most of them were conducted under two-dimensional (2-D) condition, and the detailed analyses for examining the behaviour under three-dimensional (3D) conditions ware few. Especially, it is hard to find the research that treats liquefiable ground. In this sub-sub-clause, behaviours of pile group foundations under two- and 3D condition are discussed using effective stress analysis. (921D)

The ground/foundation/structure system to be analyzed was of a 3D structure composed of piles and walls with varying physical properties and geometric shapes. Three-dimensional models have conventionally been approximated by 2-D models frequently in the case where 3D analysis was difficult. Then, piles were modelled as a sheet pile extending infinitely along the direction of length. Horizontal ground motions have N-S and E-W components and need to be evaluated using multi-directional input ground motions. Two-dimensional models, however, can evaluate only unidirectional component. The results of cyclic element tests (simple shear tests) show that multi-directional shear causes higher dilatancy than unidirectional shear and the resistance to liquefaction is reduced (Ishihara et al 1980[1], Fukutake et al. 1989[3]). The deviation from actual phenomena can be eliminated by 3D analysis. Thus, 2-D analysis has some limitations. Three- dimensional effective stress analysis, however, requires great efforts and is not generally used in design.

A FE code developed for 2-D or 3D effective stress analysis (Fukutake 1997[7]) to assess the dynamic response of structures on liquefiable ground is adopted. (921A) In this method a simplified constitutive model is used to represent the nonlinear behaviour of soil involving liquefaction called “bowl model” (Fukutake, 1989[3] and 1997[7]). Those soil parameters are determined by element tests such as G-γ, h-γ relation obtained by dynamic deformation test, liquefaction strength curves obtained by undrained cyclic test. (913A, 922A) The applicability of the method has been examined by comparing computed results with observed data (Fukutake et al., 1992[4], Ohtsuki et al[9]., 1994, Fukutake, 2008[8]). Behaviors of pile group foundations under two- and 3-D condition are discussed using the effective stress analysis.

In the following section, focuses on the structures supported on pile foundations in soft sandy ground, and presents the forces acting on the cross-section of each pile and the percentage of load carried by each pile, and the behaviour of the ground around the foundation that were obtained from 3-D analysis (Fukutake et al. 1996a[5]). A comparison was also made with the results of 2-D analysis, and the limitations in the application of 2-D analysis are described.

5.3.1.2 Results of analyses and discussion

Figure 175 shows the FE model of the soil-structure system used for the analysis. The model represents a half of the symmetrical system. A cylindrical structure is supported by piles embedded in a Pleistocene sandy layer. The arrangement of the piles is shown in Figure 176. (921A, 921D) Loads were applied only in one direction.

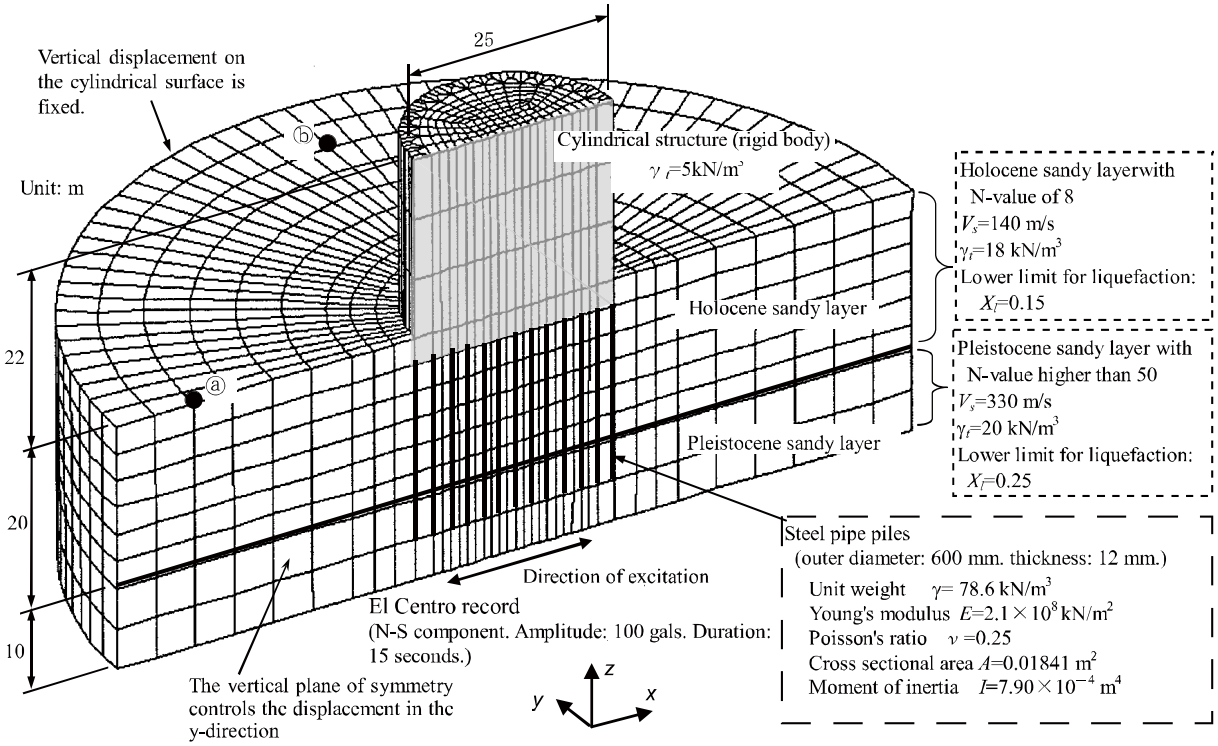

Figure 175 — FEM model of cylindrical structure/ground system supported on a pile foundation (half model)

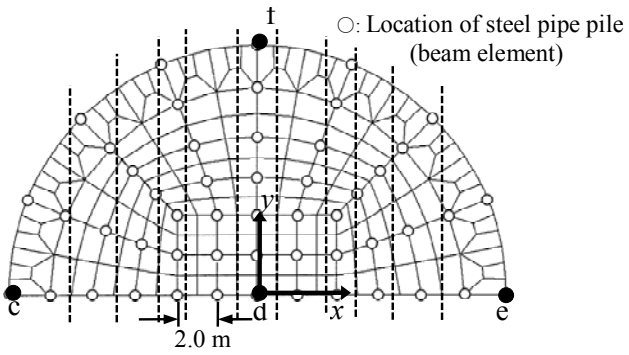

Figure 176 — Finite elements representing the structure and piles

The distribution diagram of the maximum bending moment at pile head is shown in Figure 177. The vertical axis of the diagram indicates the maximum bending moment. Points from “c” to “f” in this figure correspond to the locations of piles shown in Figure 176. The shape of the distribution is like a bowl. The smallest value of maximum bending moment at pile head appears at Point “d” corresponding to the centre of the foundation. The largest appears at Point “f” corresponding to the edge of the foundation that is perpendicularly far from the centre line parallel to excitation direction. If the maximum bending moment is normalized by that of the pile at Point “d”, the normalized values of piles at Points “c” and Point “f” would be 1.22 and 1.53, respectively. Considering simultaneous application of two orthogonal seismic loads during an actual earthquake, seismic forces acting on pile heads along the circle through 3 points corresponding to piles at Points “c”, Point “f” and Point “e” would be almost the same. Thus, piles near the edge of the foundation carry higher percentage of the seismic action on the foundation than those near the centre of the foundation. Figure 178 shows time histories of displacements at Nodes “a” and “b” shown in Figure 175. Both nodes are 40 m distant from the centre of the structure. The displacement at Node “b” was greater than that at Node “a”. The oscillation was greater on the far side than on the near side. Permanent deformation also occurred at Node “b”. Deformation was controlled at a owing to the pile foundation, and the amplitude was also smaller than at Node “b”. Such information on deformation cannot be obtained by 2-D analysis.

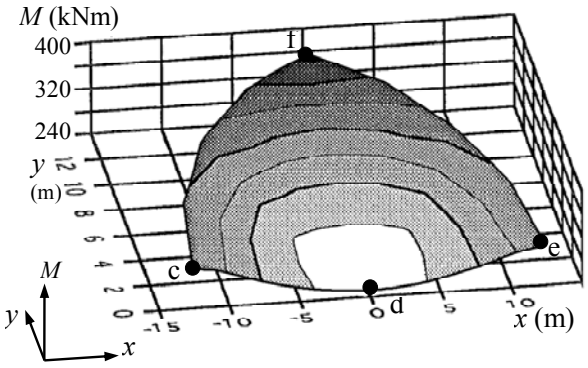

Figure 177 — Isoline map of maximum bending moment at pile head

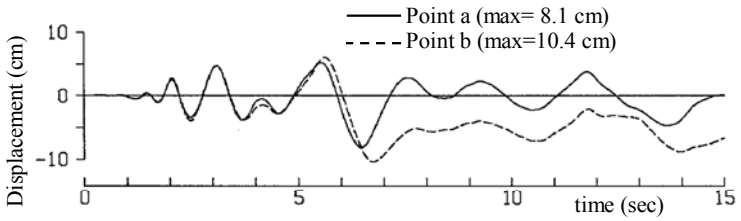

Figure 178 — Displacements of ground surface (x-direction)

In order to identify the applicability of 2-D analysis, the same structure was also analyzed using a 2-D model. The soil-structure system was represented by a 2-D model for a plane strain problem. (i) For representing the cylindrical structure with a diameter of 25 m in 3-D world by a rectangular model for a 2-D analysis, a width of the model was set to be 22.16 m in order that the area of foundation contacting with soil of 2-D model be equal to that of 3-D model. (ii) All the piles of the circular foundation were divided by dotted lines into several groups (Figure 176) and then piles in each group were consolidated into a single model pile equivalent in terms of horizontal and rotational resistance for using a beam element. (iii) The width of ground region was adjusted so as to express the effects of the 3-D analysis as accurately as possible, and the rigidity of soil between piles was adjusted so that the percentages of load carried by the piles might be the same as in the 3-D model.

Figure 179 shows the isolines of the maximum excess pore pressure ratios obtained by the 2-D and 3-D analyses. The both results are nearly the same. The liquefied area extends to soils immediately below the basement and grows thicker in shallow part in the 3-D analysis. In the 3-D analysis, the ground had an oscillation component in the direction of depth (y-direction) although loading was applied in a single direction. On the other hand, no y-direction component existed in the 2-D analysis. As a result, the shear strain of the soil was larger in 3-D analysis. Figure 180 shows the pile stresses in the 2-D and 3-D analyses. There are differences near the head of the pile at Point c, indicating the effect of the 2-D model. The both results agree at the pile of Point “d”. This figure also shows the response of the pile 3-D model at Point “f” with open triangles, which is greater than that of the 2-D model. It is difficult for 2-D analysis to evaluate the response of the pile at Point “f”. The result of the 2-D analysis is on the dangerous side. Figure 180 (b) shows maximum bending moments at pile heads. Those of the 3-D analysis are the response of piles on the centre line of the structure through Point “d” and Point “e”, which coincide with the plane of symmetry. The results of 3-D analysis are higher at the pile end but there is not such a tendency for the results of 2-D analysis. As described before, it is difficult for 2-D analysis to evaluate the response of the pile located far form the centre of a circular plate foundation.

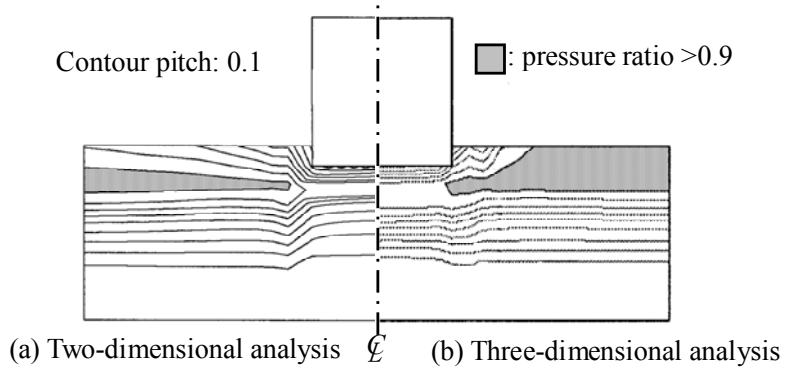

Figure 179 — Isolines of maximum excess pore water pressure ratio

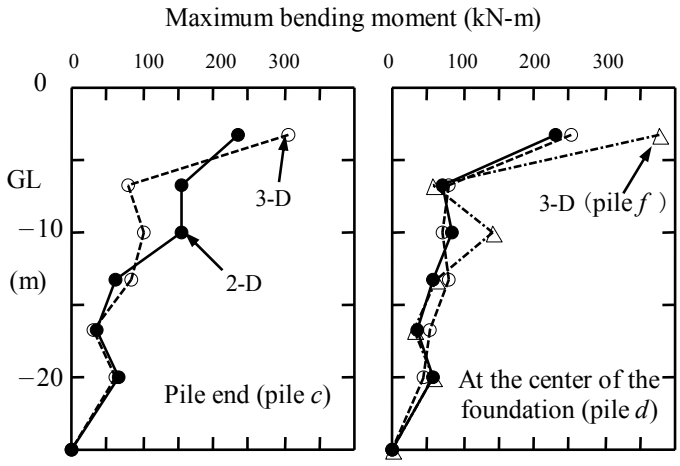

(a) Maximum bending moment of pile at different depths

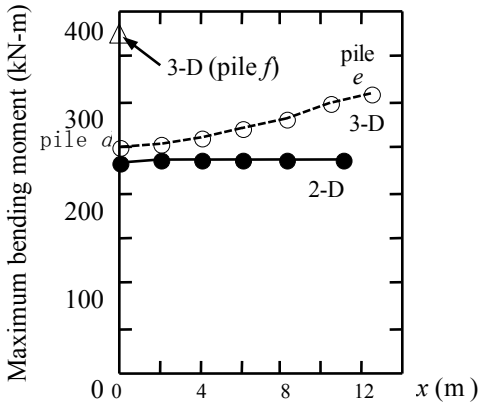

(b) Maximum bending moment at pile head

Figure 180 — Comparison of stresses of piles arranged in circular plate foundations in 2-D and 3-D analyses

5.3.1.3 Consideration of results into design

Behaviours of pile group foundations under 2-D and 3-D conditions are discussed on the basis of effective stress analysis results. In a 3-D model, soils can move relatively freely without constraint due to pile existence. Therefore, larger soil deformation is expected to occur in the 3-D model than in the 2-D model, and liquefaction is as well. As for bending moment of pile at head, the 2-D has relatively uniform distribution and the 3-D has non-uniform one due to 3-D SSI effects. In particular, 3-D analysis can represent non-uniform distribution of load burden ratio of pile in a pile group, which features predominant response at piles located at the outer edge of a circular plate foundation. On the contrary, it is difficult for 2-D analysis to do that.

5.3.2 Evaluation of 3-D effects of lattice-arranged numerous piles by detailed dynamic analyses

5.3.2.1 Objectives

Pile foundations with a large number of piles exhibit complicated behaviour. For example, a load share ratio of pile is influenced by a pile-group effect, a pile spacing, or pile arrangement as a whole. It is ideal to thoroughly examine the behaviour of a pile-group foundation by a 3-D FE analysis with modelling the entire foundation. However, the 3-D FE analysis for a soil-pile-structure system needs very high capability of calculation for a computer. Accordingly, a 2-D model is frequently used for the pile group foundation in general. In the case of a foundation with a huge number of piles, a large-scale model is needed even in 2-D FE analysis. In addition, all piles in-a-row, in 2-D analysis, are forced to be modelled as a wall, which have complete constraint in terms of movement of soil adjacent to piles. Thus a simplified method of modelling a pile-group foundation is demonstrated herein, and its applicability is evaluated. (921D) Constitutive equations and FE computer code used here are the same in the previous sub-sub-clause.

5.3.2.2 Results of analyses and discussion

In order to reduce load of a 3-D analysis for a pile-group foundation, a simple analytical model proposed by Fujikawa et al. (1997) is presented here. The applicability of the simple model is verified by comparing with the results of a 3-D analysis for a model of the entire pile-group foundation. The object for the analysis was a pile-group foundation supporting a gas-insulated switchgear (GIS). Figure 181 shows the 3-D model. In the result of analysis, excess pore pressures were generated but they did not induce liquefaction. The simple model is a model consisting of a beam element for a pile and a solid element for its surrounding soil and it applies MPC (multiple points constraint) condition to each side node for rigidly tying to other nodes in the same level as shown in Figure 184 for realizing an infinitely arranged in horizontal direction. Cases of analysis are shown in Table 35. In the 2-D pile-group model (Case 3), the physical properties of eleven piles along the pile axis were integrated. Eleven times of the values of moment of inertia *I* and cross sectional area *A* for a single pile were assigned to a beam element.

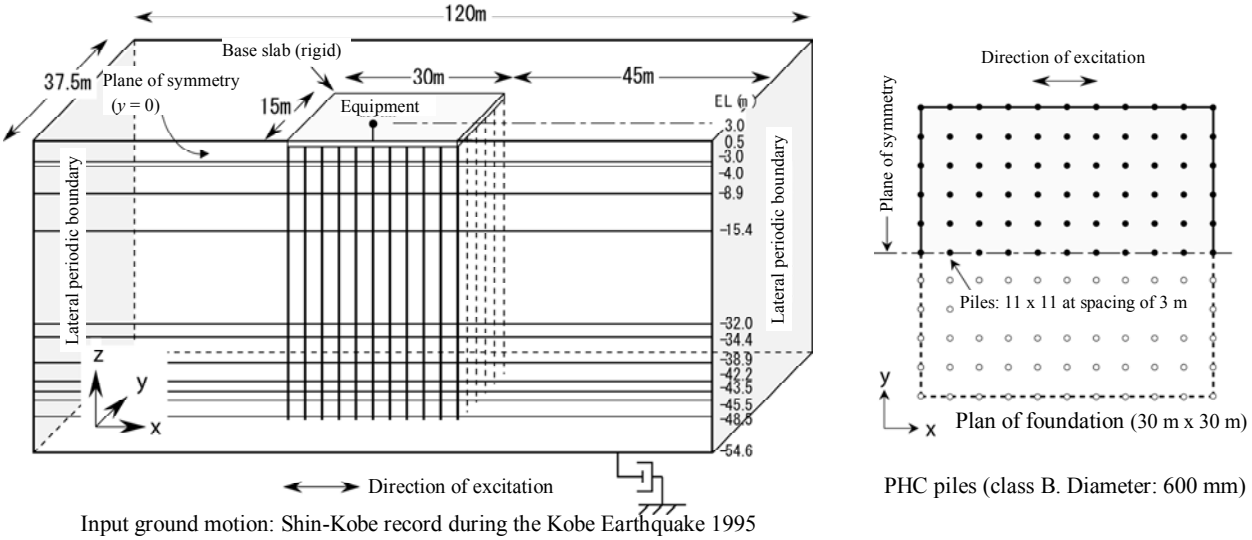

Input ground motion: Shin-Kobe record during the Kobe Earthquake 1995

PHC piles (class B. Diameter: 600 mm)

- Holocene ground: Mainly composed of sandy silt. V_s=130～250 m/s
- Bearing ground: Gravel. V_s=360 m/s

Figure 180 — GIS three-dimensional pile group foundation model (half model)

Table 35 — Analytical cases of pile foundation (4 cases)

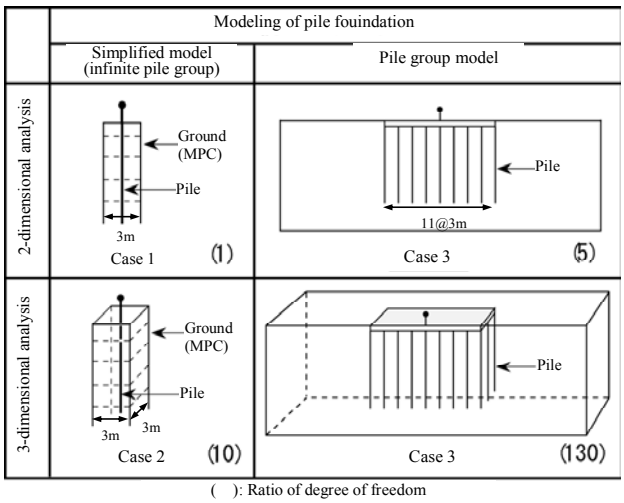

( ): Ratio of degree of freedom

The maximum bending moment, M_{max} in all the piles in two rows are shown in Figure 182. The maximum moment in all the piles take place at the same depth corresponding to a boundary between soil layers. The distribution of M_{max} is higher near both ends than at the centre of the foundation. Comparing the distributions of M_{max} in the 3-D model, the piles locating on the ends shows an approximately 25 % larger value in Row F, whereas almost flat distribution appears in Row A. In the 2-D model, the model for piles arranged in the depth of plane actually behaves like a wall. As a result, a sum of soil reactions on piles is equivalent to the soil reaction on the continuous wall. Such overestimate of soil reaction results in larger response of M_{max}. This figure also shows the estimates by the simple models. Comparing with the full models, these estimates are satisfactory both in 2-D and in 3-D analysis. Thus the effectiveness of the simple model was verified in this case.

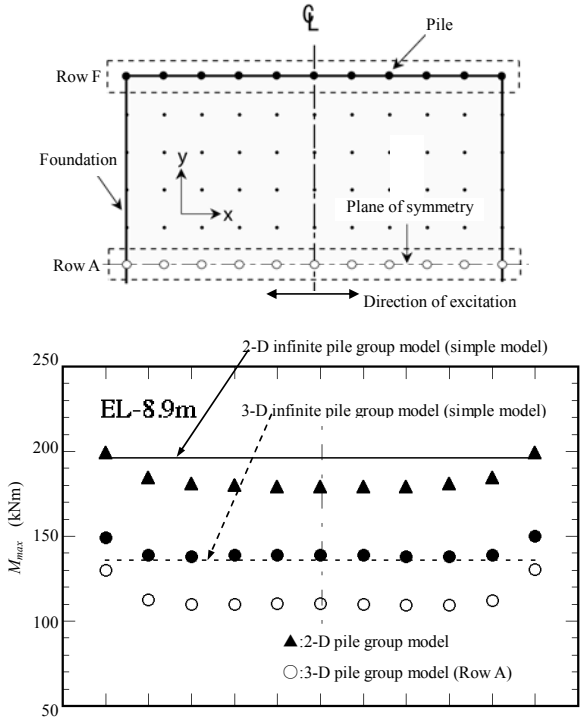

Figure 182 — Maximum bending moment of each pile

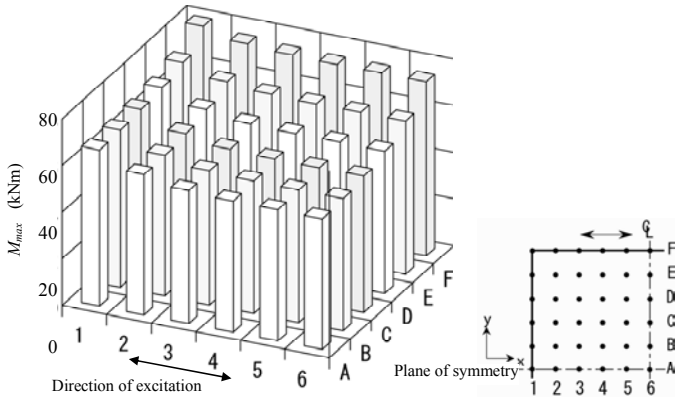

Figure 183 — Maximum bending moment at pile head (three-dimensional model)

Figure 183 shows the distribution-in-plane of M_{max} at the pile head by the 3-D model. The largest value of M_{max} is generated at Pile F1 locating at the corner. This figure can be understood as the in-plane distribution of load share ratio in the pile group.

For applying the simple model to an infinitely continuous pile group, the following points should be kept in mind. In a pile-group foundation, the load share ratio in a pile group depends on the arrangement of piles and on the location of a specific pile. In particular, the outer a pile is located, the higher the stress of the pile becomes. The simple model cannot evaluate such a tendency. The simple model is also unsuitable for the case of a foundation with rocking predominant behaviour. Such limitations for application of the simple model should be considered.

5.3.3 Evaluation of pile-volume effects of a huge number of piles by detailed dynamic analyses

5.3.3.1 Introduction

In general, piles are modelled as beam elements, which are linear and have no volume. If piles are arranged densely, the volumes of the piles are not negligible. (921A, 921D) The example demonstrates here the effect of pile volume according to the results of an effective stress analysis. The constitutive equation and FE analysis program are the same in the previous sub-sub-clause.

5.3.3.2 Results of analyses and discussion

Analysis of a thermal power plant built in the liquefaction-prone soils and supported on a pile group foundation composed of thousands of pilesnote was carried out. A simple analysis model was adopted as shown in Figure 184 (Fukutake et al. 1996b[6]). The piles were installed indefinitely with 2-m spacing in the model. If the number of piles increases and the spacing of piles D is reduced as compared with the pile diameter ϕ, the volumes of piles cannot be ignored. A model was also used for analysis in which the volume of the pile was removed. In the model, space of octagonal cross section circumscribing a 0.6-m diameter 40.6-m deep cylinder was created in a soil mass 2 m long, 2 m wide and 45.6 m deep to represent the volume removed by the pile. The pile was modelled using beam elements, and the node inside the cylinder of octagonal cross section is connected to a node in the beam element at the same depth under the same displacement condition. The analysis cases are shown in Table 36

Table 36 Pile group model composed of an infinite number of piles using a repetitive boundary a single beam element (plan view)

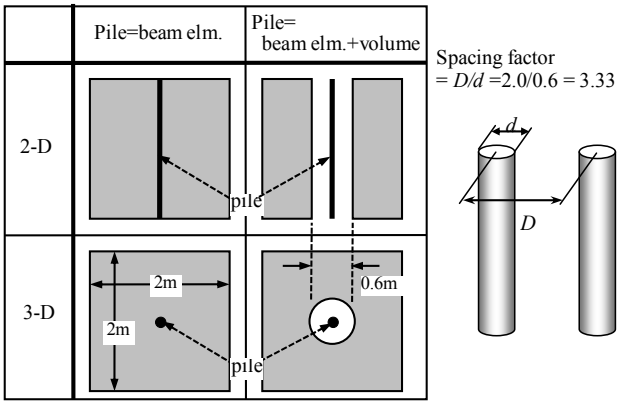

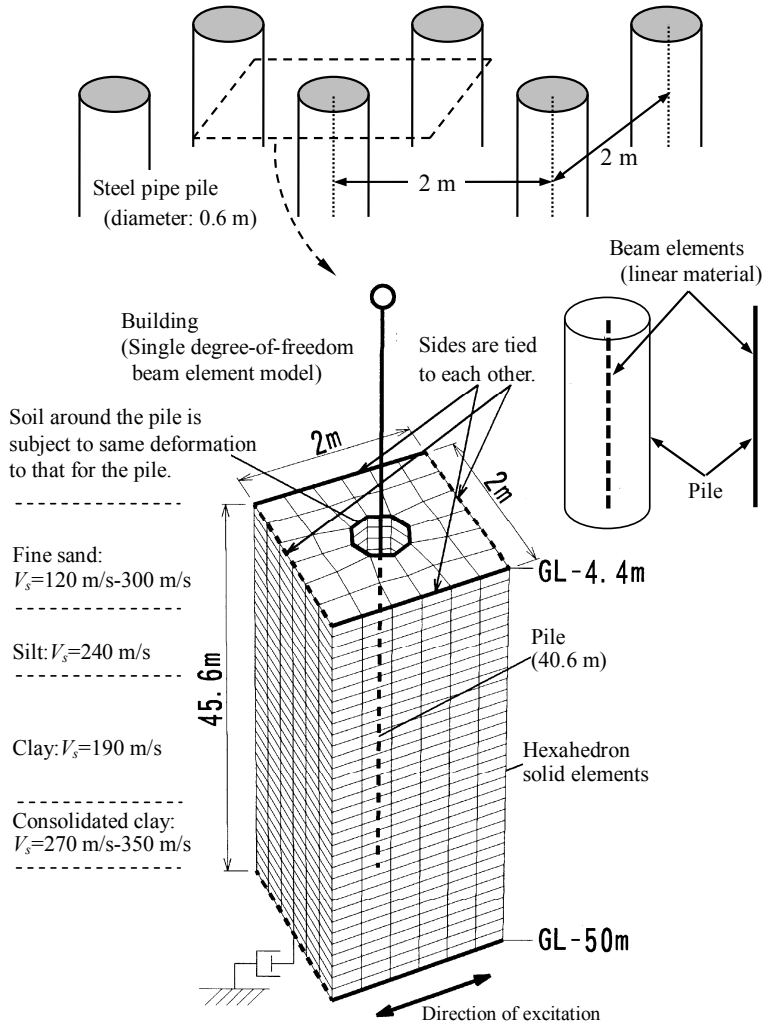

Figure 184 — Consideration of the volume of pile in an infinite pile group model (in the case of three-dimensional analysis)

Figure 185 shows the time histories of excess pore pressures in a fine sand layer (As1 layer) at a depth of 8 m below ground level. The pore pressure increased slightly faster in the case where the volume of the pile was taken into consideration. Little difference was found between two- and 3-D analyses. Few variations were found according to the location at the same depth. (The soil around a pile behaved nearly like the soil between piles.) This is because the soil was deformed like the piles as the piles were installed densely at spacings of 2 m. Figure 186 shows the maximum bending moments at different depths for comparison. The maximum bending moment was highest at the pile head and second highest at a depth of 21 m below ground level in all of the cases. At a depth of 21 m below ground level, there exists a boundary between the As2 (liquefied) layer and Ac1 (non-liquefied) layer. The maximum bending moment near the pile head is slightly higher in the case where the volume of the pile was considered. No significant difference was, however, generally found in all of the four cases. This is true either for two- or 3-D analysis.

5.3.3.3 Consideration of results into design

If focus is placed on the stress of the pile in the pile group model, the volume of the pile has a small effect and a model considering no pile volume is sufficient from an engineering viewpoint. There is little difference in result between two- and 3-D analyses. Two-dimensional analysis is applicable if piles are installed at a small spacing.

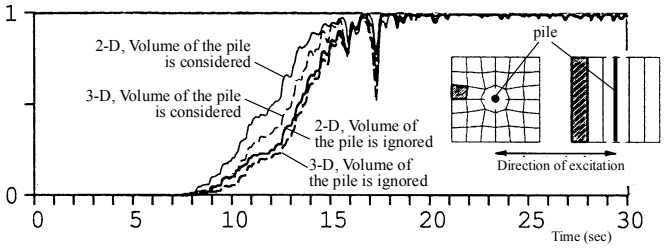

Figure 185 — Time histories of excess pore pressures in fine sand layer (As1 layer) at a depth of 8 m below

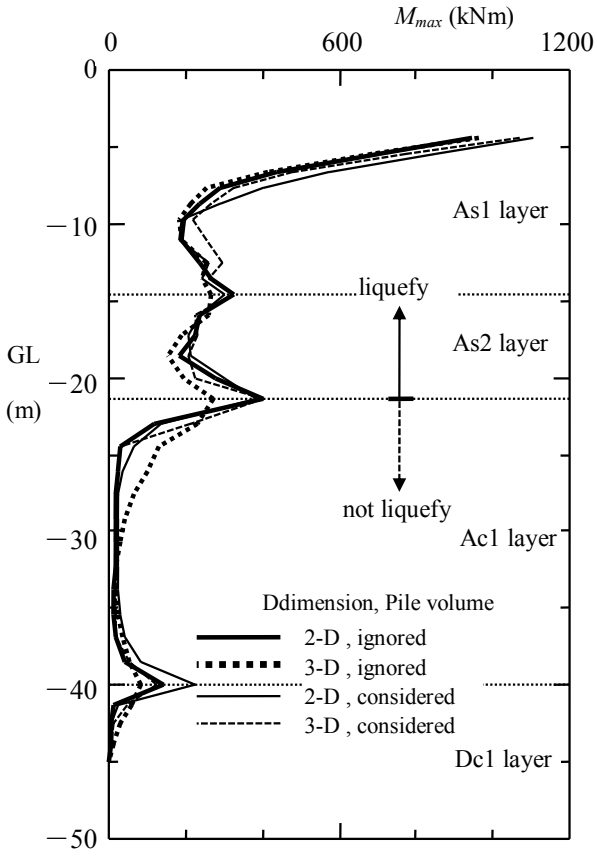

Figure 186 — Maximum bending moment of the pile (infinite pile group model)

5.4 Demonstrations evaluating and designing for fault displacement effects

5.4.1 Seismic design abstract of road embankment taking account of surface fault rupture

5.4.1.1 Purpose and functions

A 30m-high road embankment had been planned as a part of community road and was found to cross over Kaminoyama Fault, which is considered as an active fault. This example is based on “The report on road structure investigation of Kaminoyama-Yamagata Nishi Tendo line (Yamagata New Town District), 2003”. (511A)

5.4.1.2 Performance objectives and ground motions for seismic design

Performance objectives for moderate and large ground motions are shown in Table 37. “Moderate ground motion” is the ground motion that is highly possible to occur in the service period; while “large ground motion” is a very strong one with low probability of occurrence in the service period. (512a, 512b, 513A)

Table 37 — Performance objectives and corresponding levels of ground motion

Level of ground motion	Performance objectives	Remarks
Moderate	Minor or no damage	Based on Japan Road Association (1999)
Large	Restored in 2-3 days	Fault displacement is also taken into account as a seismic action

5.4.1.3 Performance criteria

The performance criteria for the objective “minor or no damage” are the followings.

1) Minimum safety factor for slope stability Fsp>=1.000.

2) Residual settlement S<=Sa, where Sa is the allowable residual settlement and set to be 10cm.

The performance criteria for the objective “Restored in 2-3 days” had not been set in advance. The deformations of the embankment against the seismic actions were analyzed first and then examined if the embankment can be restored in 2-3 days. (514A)

5.4.1.4 Procedure for determining seismic actions

The horizontal seismic coefficient, k_h, for the moderate ground motion was set to be 0.09 from

$$k_h = c_z \cdot k_{h0} = 0.85 \times 0.10 = 0.085 \approx 0.09$$

Where c_z is zone factor and k_{h0} is the standard horizontal seismic coefficient that depends on the ground type.

The NS component of the observed strong motion at the Kobe Marine Observatory, Japan Meteorological Agency during the 1995 Hyogo-ken Nanbu earthquake was used as the large ground motion (Figure 187). (512A, 514A)

According to the results from trench survey, boring survey and absolute age dating, cumulating fault displacement was estimated at 46m in 75,000 years. These values result in the average slip velocity of 0.6m in 1,000 years and the total fault displacement during one event in this area is estimated at 1.8m under the assumption that the recurrence period is 3,000 years. The fault displacement at the target site was set to be 1.5m and the other 0.3m was expected to occur in the other part of this area. Then the horizontal and vertical fault displacements were set to be 1.0m and 0.75m, respectively, considering the fault dip angle and the crossing angle between the fault and the road.

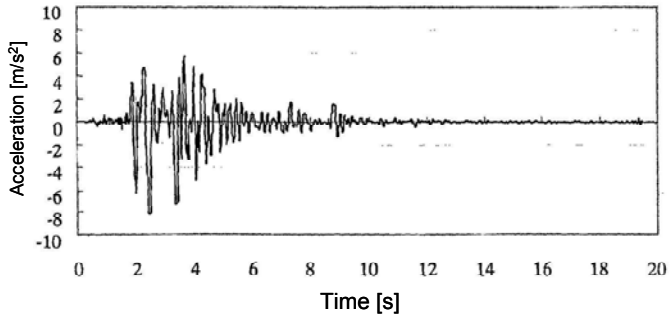

Figure 187 — Large ground motion

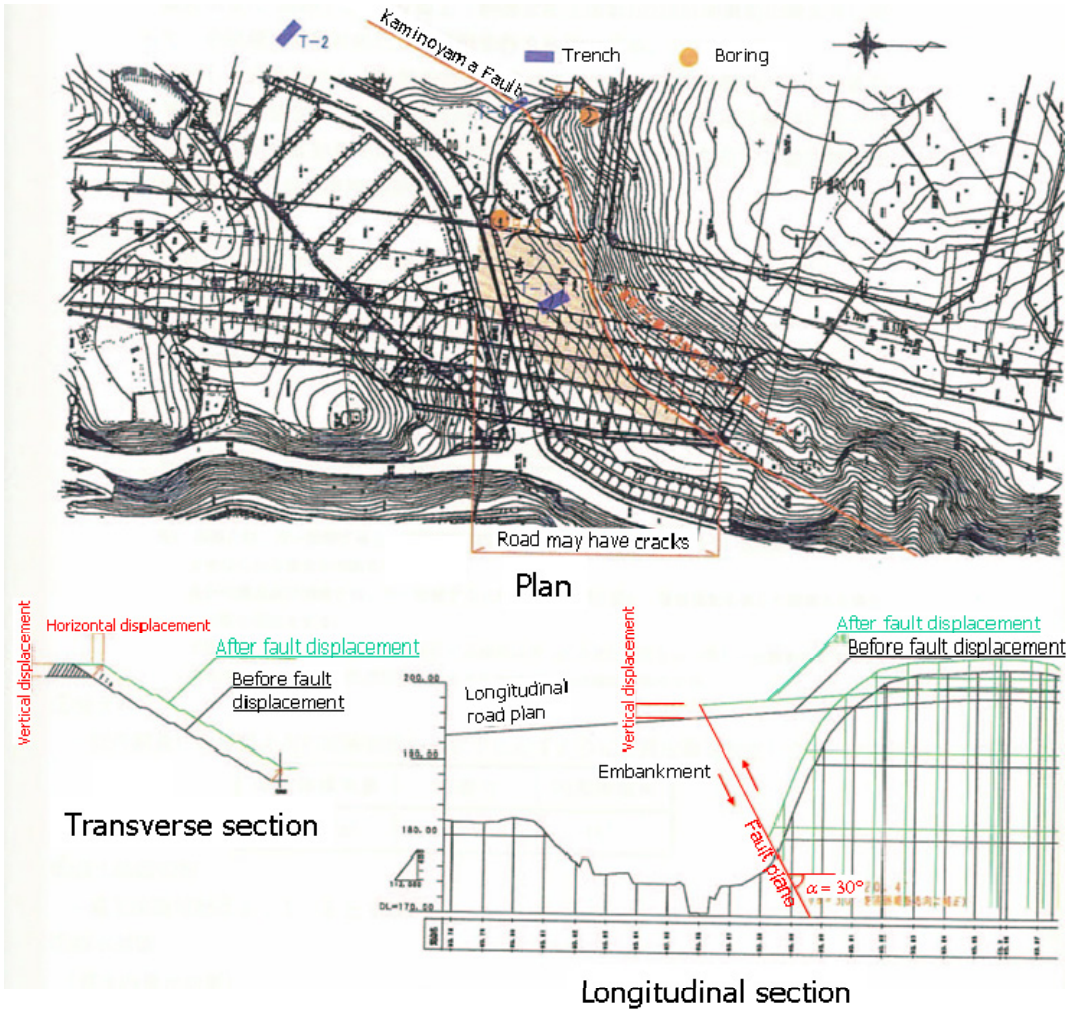

Figure 188 — Plan and sections of the embankment and Kaminoyama Fault

5.4.1.5 Ground failure and other geotechnical hazards

The liquefaction resistant ratio F_L (Japan Road Association, 2002) was used to evaluate the possibility of liquefaction during the moderate ground motion. F_L was estimated at 1.5-3.5, which is greater than the threshold value 1.0, and the possibility of liquefaction was evaluated to be low. (612A)

5.4.1.6 Types of analysis

A simple static and a detailed dynamic analyses were conducted for the moderate and large ground motions, respectively. The circular arch method was employed for the simple static analysis, while the nonlinear FEM was employed for the detailed dynamic analysis. (712A, 713A)

5.4.1.7 Simple static analysis

Figure 189 shows a model with 12 drainage layers and results of the slope stability analyses by the circular arch method. The red curve is the circular arch with the minimum safety factor Fsp=0.863. It was found that nine geotextiles are needed to satisfy the slope stability condition Fsp>=1.000 under the moderate ground motion. One more geotextile, however, was added as safety margin against the surface fault displacement described in Figure 188.

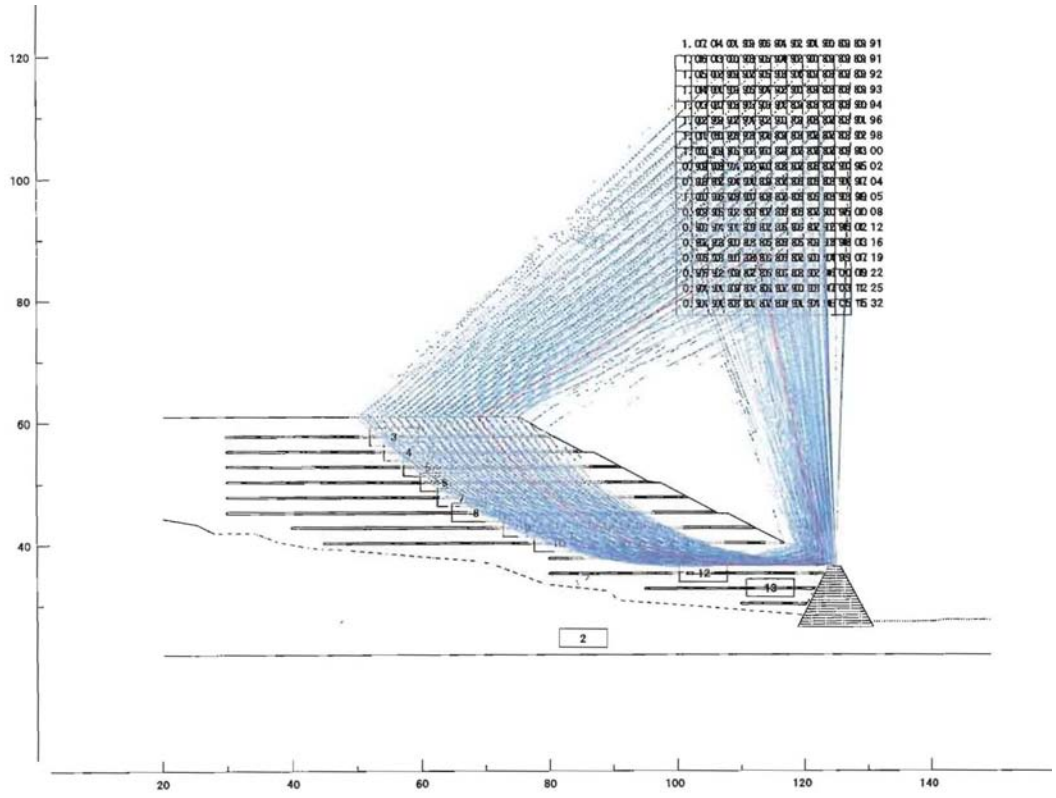

Figure 189 — A model and results of the slope stability analyses by the circular arch method. The blue curve shows the circular arches with the safety factor smaller than 1.0 and the red curve is the circular arch with the minimum safety factor Fsp=0.863.

5.4.1.8 Detailed dynamic analysis

Dynamic elasto-plastic FEM (Wakai and Ugai, 1998) was applied to the detailed dynamic analysis to simulate the response of the embankment subjected to the large ground motion (Figure 187). Figure 190 and191 show the finite element mesh and the layout of the geotextiles and the drainage layers of the model.

Figure 192 shows the residual deformation obtained from the dynamic response analysis. The residual displacement of the road surface was found to be 0.2-0.5m in horizontal and 0.1-0.3m in vertical directions. Relative displacement of the road surface was 0.3-0.4m in horizontal and 0.15m in vertical directions. Residual shear strain of the embankment was less than 5% (2% in average), which is smaller than the product

standard of geotextiles, 10%. The residual displacement and strain were considered to be allowable to achieve the performance objective (restored in 2-3 days) as well as the fault displacement in Figure 188.

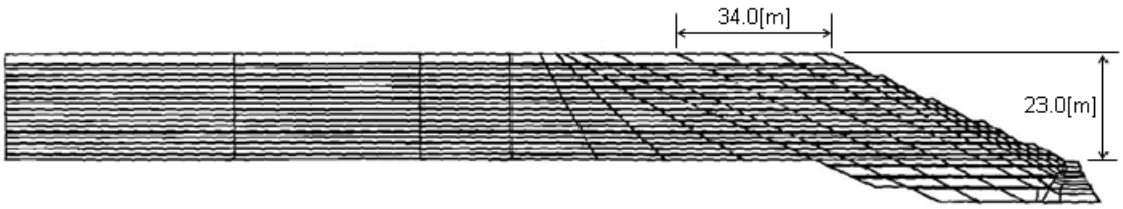

Figure 190 — Finite element mesh of the model.

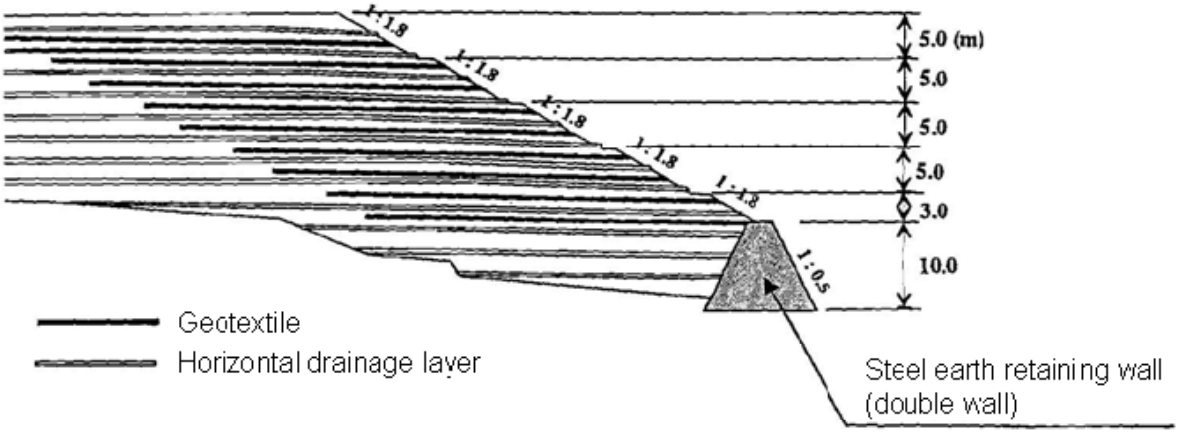

Figure 191 — Layout of the geotextiles and the horizontal drainage layers

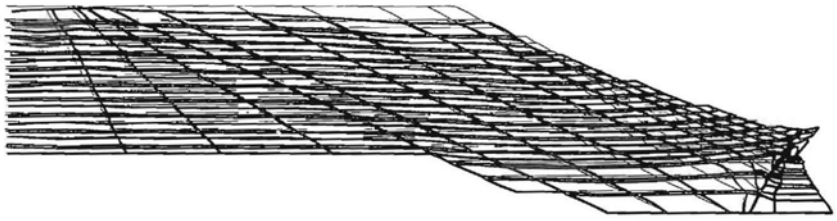

Figure 192 — Residual deformation of the embankment model. Displacement is exaggerated to 10-fold.

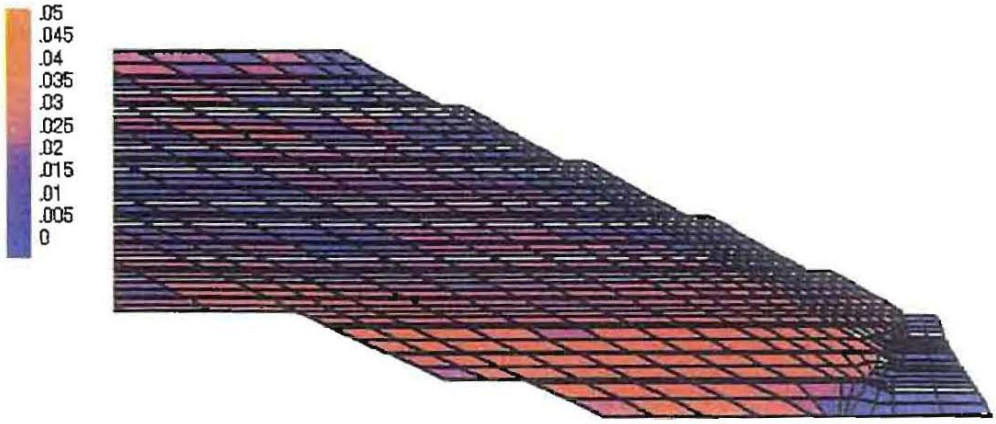

Figure 193 — Residual maximum shear strain.

5.4.2 Shield tunnel subject to fault displacements (Detailed analysis)

5.4.2.1 General remarks

The road tunnel of a project mentioned here is subjected to the risk of influences of fault displacements. Although the construction of a geotechnical structure across an active fault is generally should be avoided if possible, it was very difficult in this project. Therefore, the influences of fault movements to shield tunnel structure such as ground slip, crack, and deformation propagation in sedimentary layer were considered in detail in the design of the tunnel. (520A)(650a)(650A)

The tunnel was planned and constructed by a shield tunnelling method with composite segments. The diameter of the tunnel is 10.6 m.

5.4.2.2 Soil conditions and shield tunnel

The results of investigation on the characteristics of faults are summarized in Figure 194. As a result of a seismic wave reflection survey, four crashed planes were detected in the deposit sediment layer at the construction site. These crashed planes are indicated as I, II, III and IV in Figure 194. In addition, some fault flexure lines on the ground surface were recognized corresponding to the four crashed planes. Therefore, the four crashed planes were recognized as fault planes. The faults are classified to a reverse type, and a detailed investigation revealed that the return period of fault movement was estimated to be approximately 10,000 year. Based on the fault size, the maximum possible magnitude was estimated to be 6.5. (611A, 621A, 650a, 650A)

5.4.2.3 Estimation of fault displacement at base layer

When the magnitude of a fault displacement at a base rock layer is estimated, it is necessary to understand the difference between the fault displacement at the base rock and the slippage (or dislocation) on a fault plane. Therefore the fault dislocation considered in strong motion evaluation cannot be applied to the evaluation of the fault displacement at the base rock. A statistical method based on a relationship between the observed displacements on ground surface and the magnitudes of earthquakes was adopted to estimate the fault displacement at the base rock in this project. (711A)

The observed surface displacements in this statistical relation may involve some effects of subsurface deposit layers, so some consideration may be needed to utilize this statistical relation for estimating the base rock fault displacements. However, such effects were neglected in this project. Because there is an actual previous practice that Freeman et al. (2000) also conducted the safety assessment of a dam against fault displacements under the same assumption. (711A)

The estimation of a fault displacement due to co-seismic fault dislocation produced by an earthquake with the magnitude estimated on the fault at the interested site considered the results in well-known literature, including Matsuda (1975) using the data for intra-plate earthquakes in Japan, Sato et al. (1989) using the data for intra-plate and inter-plate earthquakes in and around Japan, Takemura et al. (1998) using the data for in-crust earthquakes, and Donald et al. (1994) using the data for all the types of earthquakes in the world. Table 38 summarizes the result of the estimation of the base rock fault displacements.

The faults here are classified to an intra-plate earthquake type, and the result by Matsuda's empirical relation seemed to be appropriate. The estimated fault displacement is 80 cm. Considered both that Matsuda's empirical relation gives the mean and that the reduction of displacement may occur through a fault rupture process, an extra displacement of 10 % was additionally considered from an engineering point of view. Eventually, a fault displacement of 90 cm on the base rock was adopted for the design. (621A) (711A)

Among the four crashed planes, the farthest crashed plane from the right end in Figure 194 is due to the latest slip from a geological point of view. However, the thickness of a surface deposit overlaying the bed rock at the zone of this latest crashed plane is the greatest among the four. Considering that the shallower the depth of a soil deposit, the more influential the fault displacement is to a tunnel, the oldest but shallowest crashed plane was taken into account as the fault producing a displacement with the most severe influence to the tunnel for the design. (711A)

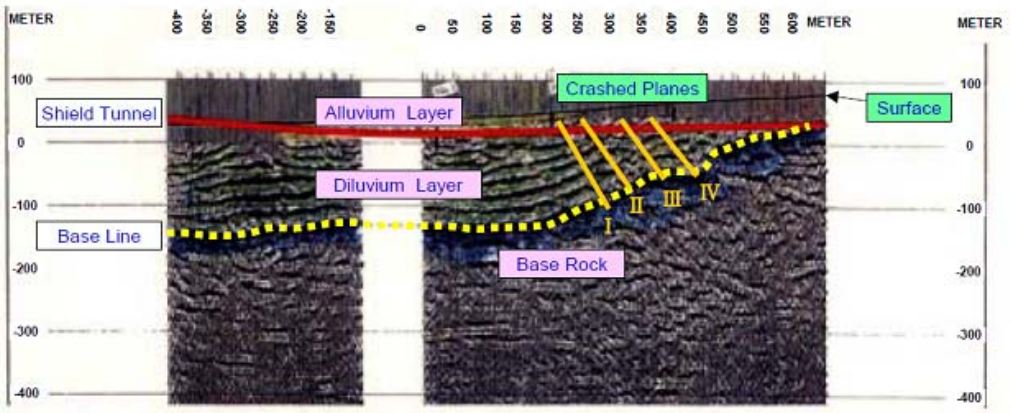

Figure 194 — Ground condition, location of crashed planes, and location of shield tunnel

Table 38 — Estimated ground displacement

Source	Earthquake type	Depth	Displacement (cm)	Remark
Matsuda [*1]	Inland type (Japan)	Surface	79.4	Mean
Satoh et al [*2]	All types (Japan)	Surface	69.2	Mean
Takemura et al [*3]	Inland type (Japan)	NA	56.5	Mean
Donald et al [*4]	All types (World)	Surface	55.4	Maximum
	Reverse fault types (World)	Surface	90.1	Maximum
	All types (World)	Surface	29.9	Mean
	Reverse fault types (World)	Surface	8.4	Mean

*1,*2,*3, and *4 are referred literature numbers.

5.4.2.4 Method of analysis and modelling nonlinear behaviour of soil

To simulate fault rupture propagation through the deposit layers from the base rock, 3-D and 2-D FE analyses were performed. Both linear and nonlinear solid elements were used in the simulation, and joint elements with different properties were also set in each zone adjacent to each crashed plane. (712A) The deposit layers were modelled into three including Holocene layer and two Pleistocene layers (I and II). Figure 195 shows the 3-D FE model. The 2-D FEM model was developed for the section along the tunnel axis were also performed. (713A)

In the 3-D analysis, all the solid elements for the deposit soils are linear. On the other hand, a nonlinear property with a bilinear stress-strain relation with a Mohr-Coulomb type yield condition was modelled in the 2-D analyses. For the soil elements, the basic parameters of elastic media such as density, γ, P-wave velocity, V_p, and S-wave velocity, V_s of modelled a Holocene and two Pleistocene layers were evaluated based on the results of geophysical surveys as shown in Table 39. Then, Poisson's ratio, ν, shear modulus, G, and Young's modulus, E were secondly determined from such basic parameters. (715A)

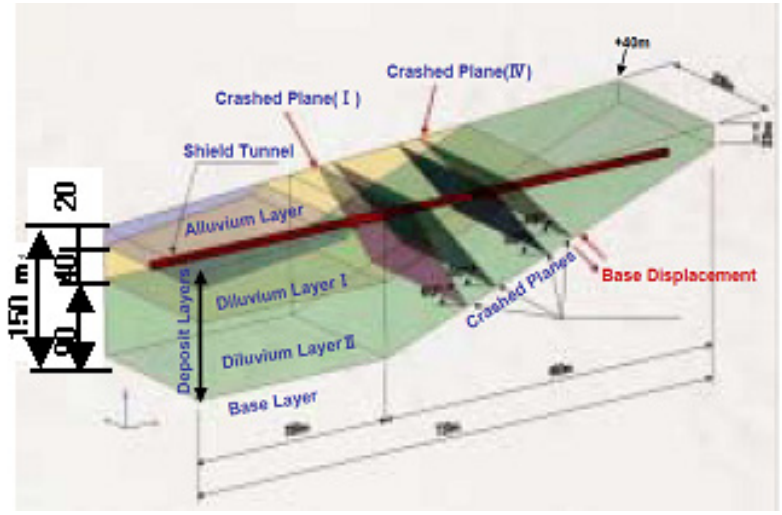

Figure 195 — Model of ground and tunnel for FE analysis

Joint elements to express the slippage and the opening in the deposit soils were set along all the crashed planes. The constitutive model of the joint element is shown with regard to its nonlinearity in Figure 196. Table 40 shows the properties of normal and tangential springs for the joint element such as a normal spring constant, K_n and a sliding or tangential spring constant K_s. Cohesion, c was assumed to be zero (c=0) for a safety side consideration. Internal friction angle ϕ, of sand layers was basically assumed to be 35 degrees, but for joint elements in sand layers it was set to be 20 degrees for resistance against slippage. (715A)

The tunnel is modelled as a set of equivalent beam elements, with effective stiffness as ring joints where necessary. Its physical properties are as shown in Table 41.

The boundaries corresponding to the base rock were set as a fixed boundary in the left-hand side from the focused crashed plane and as a boundary constrained with forced displacements in the right-hand side. The forced displacements along the focused plane with an inclination of 45 degrees were given to the right-hand side boundary both in the 2-D and 3-D models. The magnitude of the displacements is 90 cm as mentioned before.

Table 42 summarizes study cases considering different combinations of model nonlinearity for the design. In all the cases, joint elements were used for all the crashed planes. Case 1 is a 3-D analysis with linear soil elements. Case 2 is a 2-D analysis with linear soil elements. Case 3 is a 2-D analysis with nonlinear soil elements. Case 4 is almost the same with Case 3 except that the internal friction angle for the joint elements is 20 degrees. (821B)

Table 39 — Soil properties of deposit layers

Name of layer	Geological deposit	Unit weight (kN/m^3)	S-Wave velocity (m/s)	P-Wave velocity (m/s)	Poisson's ratio	Shear modulus (kN/m^3)	Young's modulus (kN/m^3)
Alluvium	Holocene	15.7	200	1,600	0.49	63,800	192,000
Diluvium I	Pleistocene I	16.7	400	1,700	0.47	273,000	800,000
Diluvium II	Pleistocene II	18.6	600	1,900	0.44	695,000	1,980,000

Table 40 — Properties of joint elements

	Cohesion, c (kN/m2)	Internal friction angle, ϕ (deg.)	Normal spring constant for unit area, K_n (kN/m^3)	Tangential spring constant for unit area, K_s (kN/m^3)
Model 1	0	35	1000×E	1000×E
Model 2	0	20	1000×E	1000×E

Note: E stands for Young's modulus.

Table 41 — Physical properties of tunnel elements

Unit weight (kN/m^3)	Poisson's ratio	Moment of inertia (m^4)	Young's modulus (kN/m^3)
24.0	0.15	108.9	486,000

Table 42 — Study cases with regard to combinations of model's dimension and nonlinearity

	Model dimension	Nonlinearity of soil model	Modeling of crashed zone	Modeling of tunnel
Case 1	3-D	Linear	Joint model 1	equivalent beams
Case 2	2-D	Linear	Joint model 1	equivalent beams
Case 3	3-D	Nonlinear	Joint model 1	equivalent beams
Case 4	2-D	Nonlinear	Joint model 1	equivalent beams

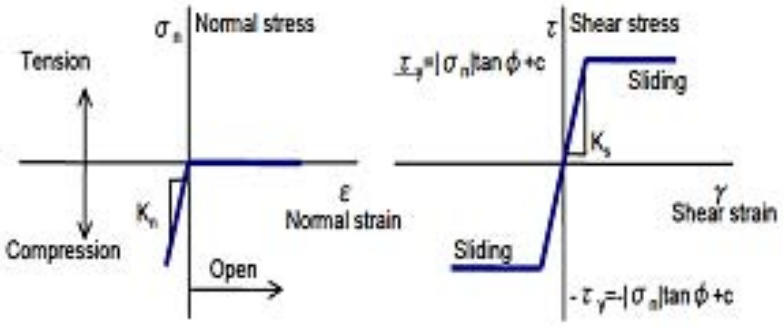

a) Normal direction **b) Sliding direction**

Figure 196 — Model of nonlinearity of joint elements

5.4.2.5 Results of analyses

Figure 197 shows the deformation of the models. In Case1, which is a 3-D analysis, deformation in a plane corresponding to the tunnel axis is shown for easy comparison with other 2-D cases. In each figure, the scale in vertical direction is enlarged by 20 times. No evident gaps are produced along the crashed planes in all the cases. Differences of level at the ground surface are produced at points indicated by arrows in Figure 197. Those are 2.1 cm in Case 1, and Case 2, and 0.0 cm in Case 3 and Case 4, respectively. These values are much smaller than the base offset of 90 cm. Thus it can be concluded that almost all the base offset are absorbed by the compression of the soil deposit in these cases. This result harmonizes the fact that no evident fault line but only flexure lines are observed on the surface at the site. (711A)

According to the previous study (Bray et al. (1992)), fault rupture propagation can reach the ground surface where the base offset is greater than 4 to 5 % of the thickness of a deposit layer overlaying the base. In this case, the offset is only 1% of the deposit layer. Thus the obtained result matches the knowledge of the previous study as well. (711A)

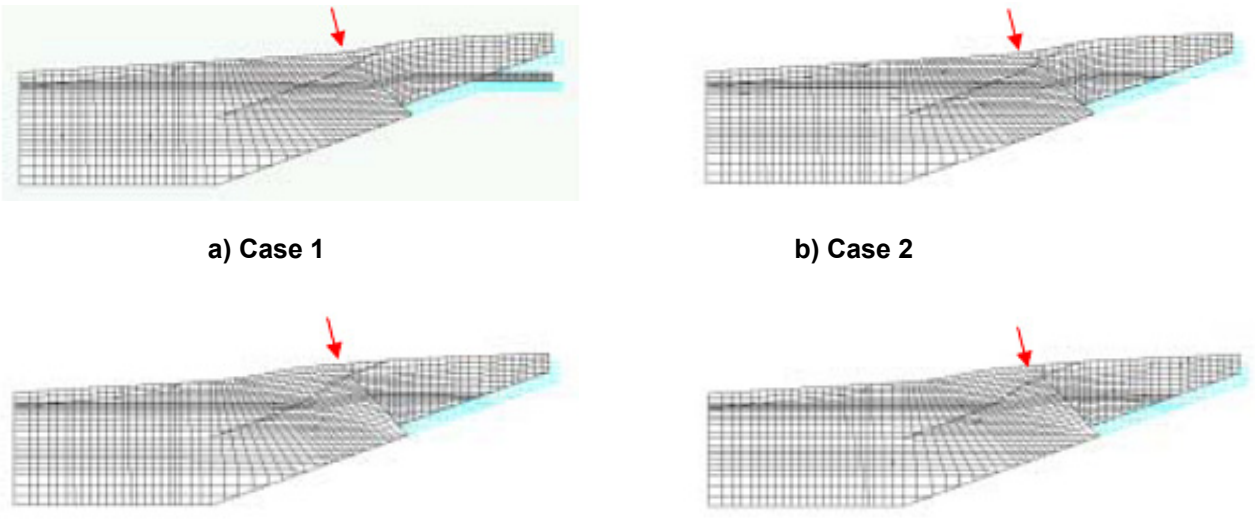

a) Case 1 **b) Case 2**

c) Case 3 **d) Case 4**

Figure 197 — Ground deformation (Arrows indicate the locations of difference of level at ground surface)

As for the deformation mode of the deposit layer, no distinctive difference between the Case 1 (3-D analysis) and Case 2 (2-D analysis) was observed. Therefore, it can be said that there is no 3-D effect in this comparison. In Case 1, there is no clear difference of deformation as a whole in between the plane along the tunnel axis and in the side boundary plane. The reason of that may be said the stiffness of the tunnel is quite small compared with the stiffness of surrounding soil mass.

There are clear differences in the soil deformation modes among Case 2, Case 3 and Case 4. In Case 2, only the right-hand side (hanging wall side) of the deposit is displaced due to the base offset. In Case 3 and Case 4, not only the right-hand side but also the left-hand side of the deposit layer are displaced with deformation of the deposit layer. Accordingly, the difference between with and without consideration of nonlinearity of soil elements must be influential to the difference of deformation mode. Comparison between Case 2 and Case 3 in terms of the horizontal and vertical displacements is made.

Figure 198 shows the contour maps of the horizontal and vertical displacements in the two cases. In Case 2 (linear soil elements), the bottom of the deposit layer does not move vertically but moves horizontally. On the contrary, the area of displacement in Case 3 (nonlinear soil elements) is more broadly developed than that in Case 2. The influence of the fault movement is only limited in the joint elements when the soil elements are linear. On the other hand, it is widely extended to surrounding soil elements when they are nonlinear.

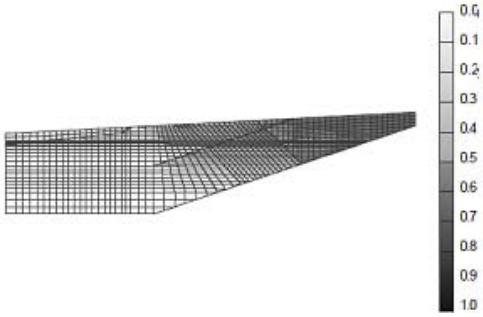

a) Horizontal displacement contour map (Case 2)

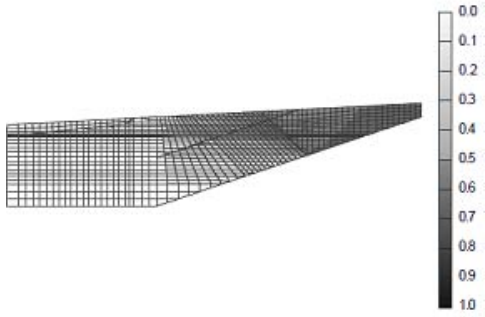

b) Horizontal displacement contour map (Case 3)

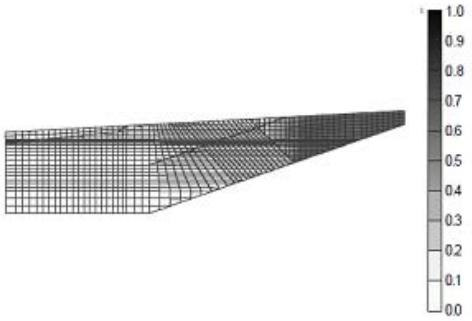

c) Vertical displacement contour map (Case 2)

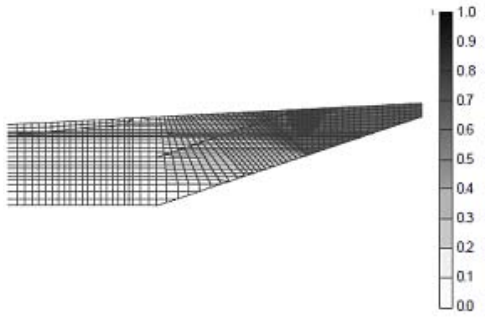

d) Vertical displacement contour map (Case 3)

Figure 198 Horizontal and vertical displacement contour map

Figure 199 shows the deformation situation of the joint elements, such as open, sliding, or close. In Case 2, almost all the joint elements along the crashed plane IV reach sliding situation except elements at the bottom in open situation. Elements along other crashed planes are in close situation, and the displacement occurred only in one crashed plane. Case3 is similar to Case 2 in terms of situation in spite of remarkable deformation in lower region of nonlinear soil elements in Case 3. In Case 4 in which internal friction angle is reduced, the elements along not only the crashed plane subject to the base offset but other crashed planes more or less show sliding situation.

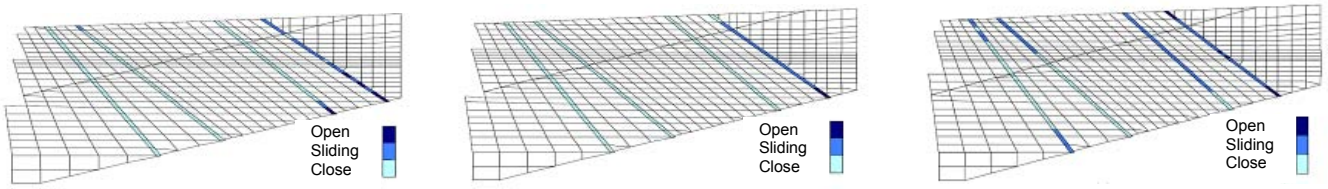

a) Case 2 **b) Case 3** **c) Case 4**

Figure 199 — Situation of joint elements set along four crashed planes

Figure 200 shows the relative displacement in between the right-hand and the left-hand sides in deposit layers along the crashed plane IV. In linear soil element cases, Case 1 and Case 2, the influence of the base rock offset extends approximately 30 m upward. It corresponds to roughly 30 times of the offset. The difference between Case 1 (3-D) and Case 2 (2-D) is slight. In nonlinear soil element cases, Case 3 and Case 4, the influence of the base rock offset recognized in terms of relative displacement suddenly diminishes only within 10 m extension. In these cases, the base offset is absorbed by conversion to deformation of the deposit layer as a whole. (811B)

The results of linear soil element cases such as Case 1 and Case 2 match the finding by Bray et al. (1992) as mentioned before. On the other hand, Case 3 and Case 4 do not match that. The reason is that Bray et al. and the former two cases assumed linear soil, but the latter two cases assumed nonlinear soil model. (711A) (811B)

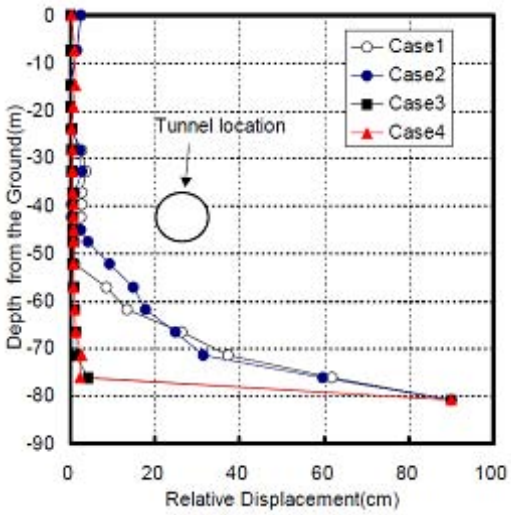

Figure 200 — Relative displacements along the crashed plane where the base offset is applied

Figure 201 shows the vertical displacements of the tunnel in Case 2 and Case 3. The horizontal axis denotes distance from the left end of the model region. In Case 2, the displacement suddenly increases in the immediately right-hand side of the crashed plane IV subject to the base offset and some negative displacement take place in the left-hand side. In contrast with Case 2, the displacement gradually increases in the left-hand side and suddenly increases immediately before the crashed plane IV.

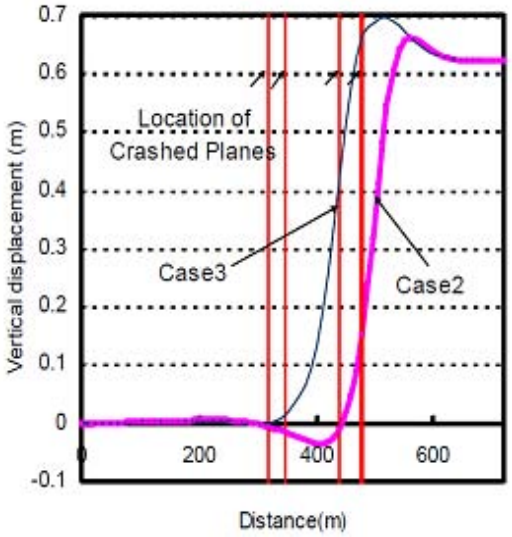

Figure 201 — Vertical displacements of tunnel axis

5.4.2.6 Influence of fault displacement to tunnel

The influence of fault displacement to tunnel can be evaluated based on the result of the FE analyses with regard to stress in beam elements by which tunnel structure is modelled. (713A)(821a) Figure 202 shows the distributions of shear force and bending moment produced in the tunnel as the results in Case 2 and Case 3. The origin of the horizontal axis corresponds to the left end of the model region. As for shear forces, the points of large predominance are observed in the vicinity of the crashed plane IV subject to the base rock offset both in Case 2 and Case 3. However the shear capacity of the segment joints is much greater than the maximum shear force. As for bending moment, the points of large predominance are observed at or near the crashed plane IV. The difference of predominant locations in bending moment distribution is similar to that of displacement. Thus it was clarified that the ultimate resistance against bending moment is greater than the maximum bending moment. Eventually, the safety of the tunnel structure against anticipated fault movements was verified in terms of performance criteria for the design.

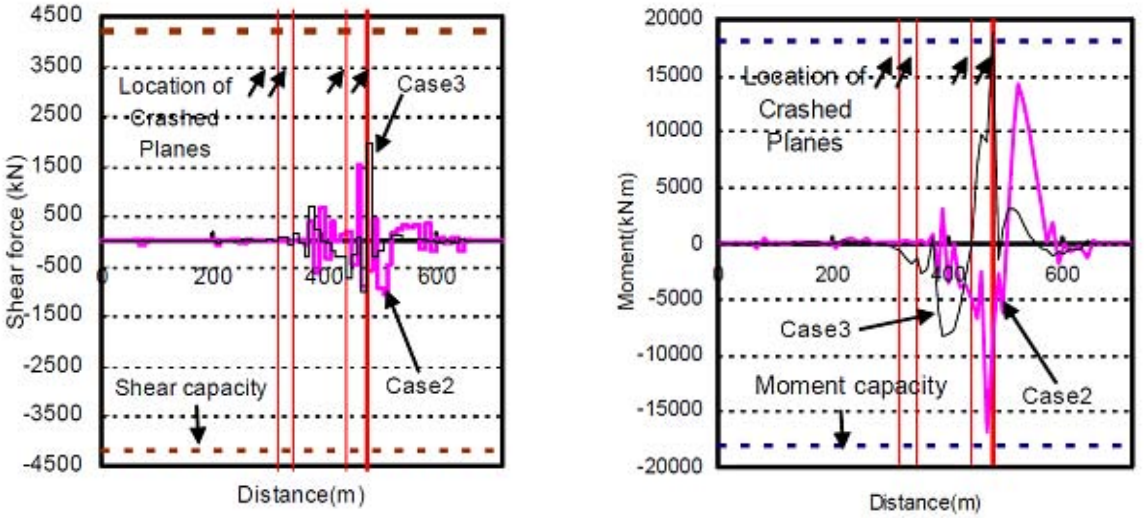

a) Shear force **b) Bending moment**

Figure 202 — Shear force and bending moment produced in the tunnel and capacities for them

5.4.3 Design considerations for a water pipeline access tunnel subject to earthquake hazards

5.4.3.1 Purpose and functions

A water pipeline access tunnel is proposed to replace an existing above-ground water pipe which is part of an aqueduct system to supply water to the City of Los Angeles. The 1971 San Fernando Earthquake and the 1994 Northridge Earthquake caused significant damage to the above-ground water pipe situated on a high steep slope and narrow ridge (Davis and Cole, 1999). Following the Northridge Earthquake, a geological and geotechnical study concluded that future strong ground shaking, amplified by topographic effects, could repeat the damage and cause collateral damage to other nearby aqueducts resulting in significant shut down periods for repairs. In addition, the existing aqueduct pipe and proposed project cross an active fault zone. The proposed project is to construct a new underground pipe in an access tunnel and a shaft to provide critical water supply following shaking or fault displacement from a design seismic event. The design example presented herein is based on an actual project in the Los Angeles area, but parameters and conditions described have been modified to simplify the example and allow it to more easily suit the purposes of this document. (511A, 611A)

5.4.3.2 Project description

Figure 203 shows the proposed water pipeline access tunnel alignment and profile. The main project components include a tunnel portal, tunnel lining system, shaft, water carrier pipe, and an underground vault at the top of hill. The portal will be excavated at the toe of the north-facing slope and a permanent reinforced concrete box structure will be constructed within the portal excavation. Approximately 177 meters (580 feet) of tunnel with an ascending slope of 5.7 percent will be excavated through sedimentary rock between the portal and shaft. The tunnel cross-section will have finished dimensions of 4.1 meters (13.5 feet) wide and 3.6 meters (12 feet) high in a horseshoe-shape. A 2.1 meter (84 inch) inner diameter steel pipe will be supported on reinforced concrete saddles inside the tunnel. The annular space between the pipe and tunnel liner will remain open to allow for future access. The steel pipe will connect to the existing water supply system at the top of the hill through an 88 meter (290 feet) high vertical shaft. The shaft will be excavated through artificial fill and sedimentary rock. The annular space between the pipe and shaft will be backfilled with concrete.

The project is located in one of the most seismically active areas in the Los Angeles area. The tunnel alignment is located near several active (Holocene) or potentially active (late Quaternary) faults that could cause strong ground shaking in the project area. The proposed tunnel will be constructed adjacent to two existing critical aqueduct pipes that must remain in service during the proposed project construction phase.

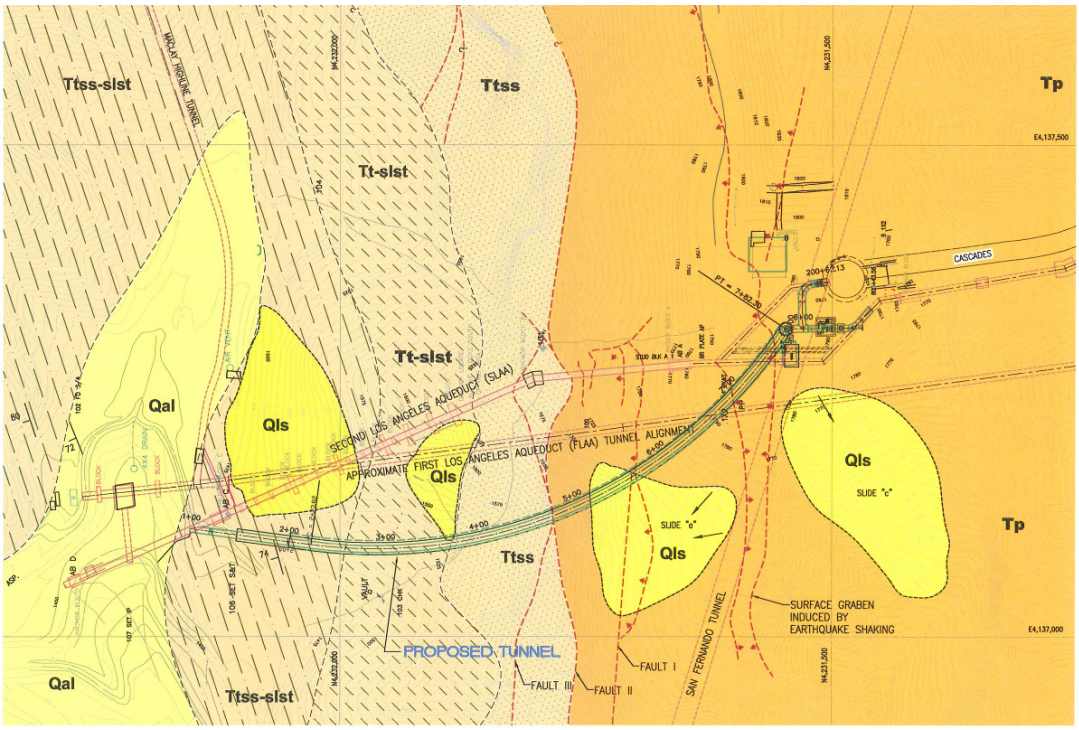

(a) Tunnel alignment

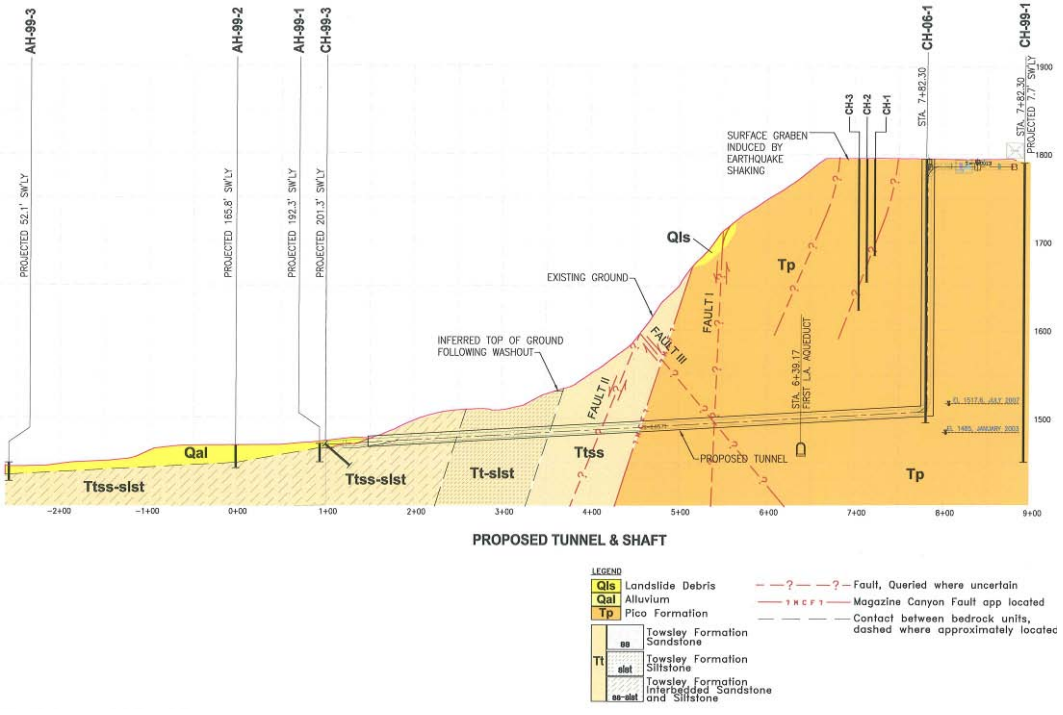

(b) Tunnel profile section

Figure 203 — Proposed water pipeline access tunnel with geological sections (north to the left; 1 station = 100 feet = 30.48 m)

5.4.3.3 Performance objectives and reference earthquake design levels

Performance objectives for the seismic design of the proposed water pipeline access tunnel are determined based on the operational need during and after the earthquake and are related to regional seismicity. Table 42 lists the reference earthquake design level and seismic performance criteria for the water pipeline access tunnel. Four reference earthquake design levels are proposed to construct and operate the water pipeline access tunnel. The design of any temporary structure during the construction phase, such as the tunnel portal and initial support for the tunnel and shaft, must meet the Temporary Design Earthquake (TDE) level having an Annual Return Period (ARP) of 75 years, which corresponds with an annual exceedance of 1% in 1 year. Under the TDE ground motion, it is expected that the structures such as the portal or tunnel initial support will experience acceptable seismic induced structural damage without disruption of construction, protect the safety of crews working in a highly seismically active region, and protect critical operations of nearby pipelines that must remain operable during construction and are supported by the temporary structures. The Operational Design Earthquake (ODE) level has a 475 year ARP, which corresponds with an annual exceedance of 10% in 50 years. The ODE performance criterion stipulates no damage with minor tunnel defections requiring no significant repairs and no operational disruption. (512a, 512b, 512A)

Table 43 — Reference earthquake design level and seismic performance criteria

Reference earthquake design level	Annual return period	Performance criteria
Temporary Design Earthquake (TDE)	75 year	No disruption of construction
Operation Design Earthquake (ODE)	475 year	No significant damage, minor tunnel defections, no operational disruption
Maximum Design Earthquake (MDE)	2,475 year	Serviceable damage, no service disruptions
Severe Design Earthquake (SDE)	20,000 year	Severe damage, limited operational disruption, pipeline repairable with practical design

The Maximum Design Earthquake (MDE) level has a 2,475 year ARP, which corresponds with an annual exceedance of 2% in 50 years. The MDE is consistent with system-wide ground motion design criteria for other critical water system facilities, and the performance criteria is to allow some serviceable damage but the water pipeline will remain in continuous service. The MDE tunnel damage is limited in extent so that operations may continue unimpeded until such a time following the disaster when the aqueduct may be conveniently taken out of service for maintenance type repairs. (621A, 621B, 621C, 622a, 622b, 622c, 622A, 623A, 623B)

The Severe Design Earthquake (SDE) level has a 20,000 year ARP, which corresponds with an approximate annual exceedance of 1% in 200 years. The SDE is only used to evaluate the fault displacement and has an ARP similar to the recurrence intervals of characteristic earthquakes in the region. The SDE level ground motions are too severe for design applications for this type of structure. The SDE performance criteria allows for severe damage to the tunnel lining but the damage will not be devastating to operations or cause total tunnel closure; the interior pipeline will be easily repairable shortly after the design earthquake and will have limited disruptions to operations. The shaft and vault are not subjected to fault displacements.

The project is designed to meet the minimum reference earthquake design levels shown in Table 1 based on the results of a Probabilistic Seismic Hazard Analysis (PSHA). The reference design earthquake levels are used for the following project design aspects: (513A)

- Fault offset;
- Design ground motions;
- Methods of analysis;

- Risk assessment with regards to tunnel operation following a design level seismic event.

The MDE and/or ODE will be used for modelling the response to the seismic ground motions for use in the detailed design. (711A, 711B, 712A, 713A, 715A)

This example does not consider ground improvements (715B)

5.4.3.4 Performance criteria

The design earthquake ground motions will be used to model the effect on the tunnel using the pseudo-static method per Hashash et al., 2001. Numerical modelling of the structure component will be performed to assist the design. For the ODE, the seismic design loading combination depends on the performance requirements of the structural members. Generally speaking, if the members are to experience little to no damage during the lower level event (ODE), the inelastic deformations in the structure members should be kept low. The following loading criteria, based on load factor design, are recommended: (514A, 514B, 514C)

U =1.05D +1.3L +1.3EX +H+EQ

Where U is the required structural strength capacity, D is the dead load effect of structural components, L is the live load effect, EX is the static load effect due to excavation (e.g., O'Rourke, 1984), H is the hydrostatic water pressure effect, and EQ is the seismic ground motion effect.

Given the performance goals for the MDE, the recommended seismic loading combinations using the load factor design method are as follows:

U = D + L + EX +H + EQ

With high ground motions at MDE level, the load factors for the live load and the load due to excavation are reduced to 1.0.

5.4.3.5 Specific issues related to geotechnical works

The seismic design and analysis of the tunnel is based on deformations of the ground and structure. The response of tunnels to seismic ground motions are usually evaluated in terms of three types of deformations (Owen and Scholl, 1981): (515A, 520A)

- Axial
- Curvature
- Ovaling for circular tunnels or racking for rectangular tunnels

Axial and curvature deformations develop in a horizontal or nearly horizontal tunnel when seismic waves propagate either parallel or obliquely to the tunnel. The tunnel lining design considerations for these types of deformations are basically in the longitudinal direction along the tunnel axis. Using the simplified approach, the free-field axial strains and curvature due to shear waves and Rayleigh waves can be expressed as a function of angle of incidence, as shown in Table 43. The most critical angle of incidence and the maximum values of the strains are also included in the table. The peak ground velocity (PGV) and peak ground acceleration (PGA) will be determined through the PSHA. The total free-field axial strains are found by combining the axial and curvature strains assuming the tunnel as an elastic beam.

Table 44 — Free-field axial ground strains and curvature due to shear wave propagation

Wave type		Axial	Curvature
Shear wave	General	$e = \frac{V_S}{C_S} \sin\phi \cos\phi$	$\frac{l}{r} = \frac{A_S}{C_S^2} \cos^3\phi$
	Maximum	$e = \frac{V_S}{2C_S}$ for $\phi = 45$	$\frac{l}{r} = \frac{A_S}{C_S^2}$ for $\phi = 0$

ϕ: Angle of incidence of the wave with respect to tunnel axis

r: Radius of tunnel

V_S: Peak ground velocity for shear wave

C_S: Effective propagation velocity for shear wave

A_S: Peak ground acceleration for shear wave

The ovaling or racking deformations of a tunnel structure may develop when waves propagate in a direction perpendicular or nearly perpendicular to the tunnel axis, resulting in a distortion of the tunnel lining. Usually, it is the vertically propagating shear waves that produce the most critical ovaling distortion of the lining. Design considerations for this type of deformation are in the transverse direction of the tunnel.

For a deep tunnel, as proposed in this project, located in relatively homogeneous soil or rock, the simplified procedure by Newmark (1968) is used to provide a reasonable estimate of the ovaling. The maximum free-field shear strain, γ_{max} , can be expressed as:

$$\gamma_{\max} = \frac{V_S}{C_S}$$

where V_s is the peak particle velocity and C_s is the effective shear wave propagation velocity. This simplified seismic design provides a good estimation for the ground strain for tunnel ovaling effect. The actual liner ovaling depends on the relative stiffness between the ground and lining. It will be better determined by considering the tunnel-ground interaction.

In this design the analysis of liquefaction potential is not necessary. (631B, 631C, 612B, 823A)

5.4.3.6 Evaluation of earthquake ground motions and fault displacements

5.4.3.6.1 Seismic hazard analysis

5.4.3.6.1.1 Peak ground acceleration and spectral acceleration at 1.0-second period

The USGS PSHA model (USGS, 2002) was used to estimate the ground motion parameters for the proposed water pipeline access tunnel. Figures 204 and 205 present the PSHA results in the form of hazard curves expressed for the horizontal PGA and Spectra Acceleration at 1.0-second period (SA1) as a function of annual frequency of exceedance and average return period. Table 44 lists the estimated PGA and SA1 ground motion parameters for the TDE, ODE, and MDE levels, applicable to the design, which were obtained from the USGS website. As previously noted, the SDE level ground motions are considered too severe for use in design of this type of project. The ground motion values in Table 44 are calculated for 'firm rock' sites having an average shear-wave velocity of 760 m/sec in the top 30 m, which corresponds to the National Earthquake Hazards Reduction Program (NEHRP) B or BC category site condition (FEMA, 2003). The TDE SA1 value is shown for completeness, but is not used in this design. The SA1 is used to estimate the PGV, discussed in the next section. (623B)

Table 45 — Strong motion parameters for TDE, ODE, and MDE levels

Reference Earthquake Design Level	ARP	PGA (g)	SA1 (g)
TDE	75 year	0.30	0.25
ODE	475 year	0.93	0.74
MDE	2,475 year	1.52	1.30

Local site subsurface material properties change with depth (e.g., variation in Vs). Based on the shear wave velocity at the site, the tunnel portal area and hill top are categorized as NEHRP site type C, and the tunnel shaft connection is NEHRP site type B. However, the variation in site conditions is not expected to modify the high PGA amplitude at this site due to the nonlinear response in the high frequency range; the NEHRP site correction factor for PGA is determined as 1.0 (FEMA, 2003). The proposed project is located in a steep terrain area. The steep ridge effect may cause the accelerations within the high frequency range to be amplified by factors up to 1.5 to 2 (e.g., Boore 1973; Bouchon, 1973; Yuan and Men, 1992). An exact evaluation of topographic effects is difficult and must account for frequency content and incident angles of seismic waves, and is beyond the scope of this simple evaluation of strong ground motions. An amplification factor of 1.5 due to ground motion ridge effect is selected for the site. Therefore, horizontal PGAs of 0.93 g along the tunnel alignment and 1.4 g at the top of hill are recommended for ODE based on the PSHA results, historical recorded values, and topographic effects. For MDE, the PGA value of 1.52 g is recommended along the tunnel alignment and top of hill. The MDE level PGA accounting for the topographic effects would be 2.28 g; an unreasonably high value not recommended for use in design because the longer return periods capture this range of ground motion. For safety purposes, only the MDE acceleration is used for design of a buried vault structure at the top of the hill. (623A, 641A, 641B, 644A)

In this example the phase velocity, wave length, and direction of propagation need not be evaluated due to the length of tunnel compared to the wavelength. (641C)

This design example does not consider superstructures. (811a, 811b, 821B, 821C)

Detailed dynamic analysis is not used in this example. (645A, 645B, 911A, 911B, 911C, 911a, 912A, 912B, 912a, 913A, 914A, 921B, 921C, 921D, 922A)

This example does not include analysis of non-linear behaviour of the rock. (811B, 812A, 812a, 813A, 814a, 822B)

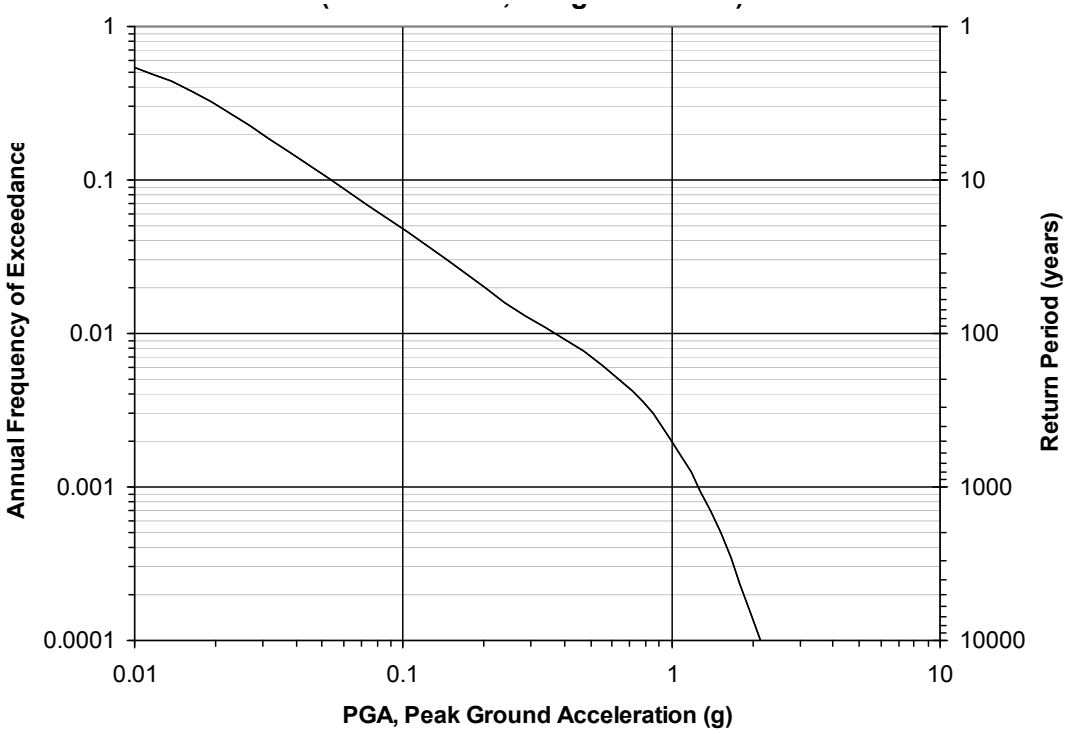

Figure 204 — Peak Ground Acceleration (PGA) probabilistic hazard curve on firm rock site based on USGS 2002 Probabilistic Seismic Hazards Assessment

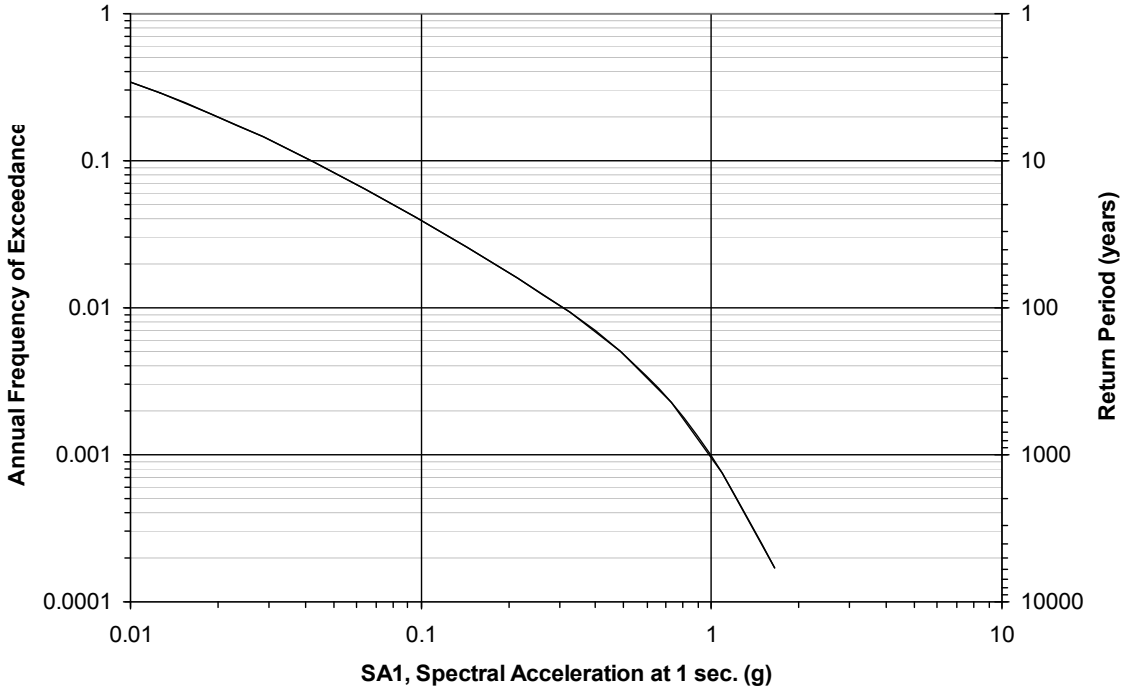

Figure 205 — Spectral acceleration at 1 second period (SA1) probabilistic hazard curve on firm rock site based on USGS 2002 Probabilistic Seismic Hazards Assessment

5.4.3.6.1.2 Peak ground velocity estimation

Few ground motion attenuation relationships are available to estimate the PGV value and they are not included in publicly available PSHA models. The following equation is generally used to estimate the PGV value.

$$PGV = \frac{981.45 \times SA1}{2\pi \times 1.65}$$

PGV is in units of cm/s and SA1 is in units of g. This equation is the relation used by the FEMA HAZUS program to estimate the PGV from the spectra response (FEMA, 1999). The horizontal PGV at the project site is estimated to be 70 cm/s and 123 cm/s for ODE and MDE, respectively, based on this formulation.

However, this relation has a presumably generic amplification factor (1.65), which may not be appropriate for this particular site. For a "site-specific" PGV, the attenuation relationship for PGV provided by Gregor, Silva, and Darragh (2002) was used in the calculation. The computation of PGV through this attenuation relationship requires the value of the distance, magnitude, style of faulting, and site subsurface condition. Furthermore, Gregor, Silva, and Darragh (2002) indicated that in order to obtain the ratio of PGV/SA1 in their work, the spectral acceleration attenuation relationship provided by Abrahamson and Silva (1997) was used to estimate the value of SA1. We assumed that a magnitude (Mw) 7.0 earthquake controlled the shaking at the site, with a thrust style of faulting. In addition, it is assumed that the site is located on the hanging wall side of the fault and is located on a soft rock site condition (NEHRP B or BC). Based on these assumptions, the back-calculated closest distance is 1.3 km, and the resulting PGV value is 76 cm/s and 130 cm/s for ODE and MDE, respectively, which is slightly higher than the value obtained from the FEMA HAZUS formulation.

As discussed in the previous section, this PGV value is calculated for NEHRP B or BC category site conditions. Local site conditions are known to have significant impacts on the PGV amplitudes. Based on the shear wave velocity at the site, the tunnel portal area and hill top are categorized as NEHRP site type C, and the tunnel shaft connection is NEHRP site B. The PGV at these locations need to be corrected for the local site condition. Currently, the most commonly used correction factors are defined in the 2003 NEHRP provision (FEMA, 2003) as listed in Table 45. For NEHRP category C site, the correction factor for SA1 is 1.3. Because of a slight ridge effect expected at the site even in a period range of PGV (1 second), an increase of the design PGV value by 10% is recommended at the hill top. Table 46 provides the recommend PGV for ODE and MDE with correction for site condition and ridge effect at various locations. The recommend PGVs are used in the tunnel lining seismic design. For completeness PGV values are provided at the top of hill in Table 46, but these values are not used in this design example. (631A)

Table 46 — Site condition correction factor for SA1 (FEMA, 2003)

Site Class	SA1≤0.1g	SA1=0.2g	SA1=0.3g	SA1=0.4g	SA1≥0.5g
A	0.8	0.8	0.8	0.8	0.8
B	1	1	1	1	1
C	1.7	1.6	1.5	1.4	1.3
D	2.4	2	1.8	1.6	1.5
E	3.5	3.2	2.8	2.4	2.4
F	---[a]	---[a]	---[a]	---[a]	---[a]

Note: a: Site-specific geotechnical investigation and dynamic site response analyses should be performed.

b: Use straight line interpolation for intermediate values of SA1.

Table 47 — Recommended peak ground velocity (PGV) with site condition and ridge effect corrections

Site	PGV (cm/s)	
	ODE	MDE
Portal	99	169
Tunnel	76	130
Hill top	108	186

5.4.3.6.2 Fault displacements

The proposed water pipeline access tunnel is located within an active fault zone and passes through splay faults branching from the main active fault. As a result, the potential exists for subsidiary displacements on the splay faults in the event of a main fault rupture.

Based on available source and site geology characteristics, a probabilistic fault rupture analysis was completed to estimate subsidiary fault vertical and horizontal displacements. Table 47 presents the fault offset design parameters for the ODE, MDE, and SDE levels. The TDE level is not considered for fault displacement design due to the extremely low probability of the splay faults moving during the construction period. For the ODE level, subsidiary fault displacement parameters of 10 cm (4 inch) vertical and 5 cm (2 inch) horizontal were estimated for the project design; for a normal liner design the tunnel should experience minor effects without service disruptions. Subsidiary fault displacement parameters for the MDE level are 15 cm (6 inch) vertical and 8 cm (3 inch) horizontal, which should be accommodated by a normal liner design with no service outage and the need for minor repairs. The SDE level fault displacements of 1 m (3 feet) vertical and 0.5 meter (1.5 feet) horizontal will severely damage the tunnel, but the design would provide enough space in the tunnel around the pipe to accommodate the 1-meter of vertical off set to reduce the possibility of devastating damage and allow for more rapid repair within a practicable design. (650a, 650A)

Table 48 — Design criteria for fault offset

Reference Earthquake Design Level	Annual Return Period (ARP)	Fault Offset		Performance
		Vertical	Horizontal	
ODE	475 year	10 cm	5 cm	no significant damage, minor tunnel effects
MDE	2,475 year	15 cm	8 cm	serviceable damage, aqueduct remains in service
SDE	20,000 year	1 meter	0.5 meter	Severe damage

5.4.3.7 Simplified equivalent static analysis

5.4.3.7.1 Portal excavation supports

The portal will be excavated in weathered and fresh siltstone (Towsley Formation bedrock). A conceptual layout of the portal configuration is presented in Figure 206. This conceptual portal is approximately 7.2 meters (23.5 feet) wide at the base with sloping side walls on each side. A review of the available geotechnical data indicates that groundwater level should be well below the proposed portal excavation. Therefore, hydrostatic pressures and dewatering were not considered in the portal design. A soil nail wall is proposed as a retaining system to provide the support for the portal excavation. (612C)

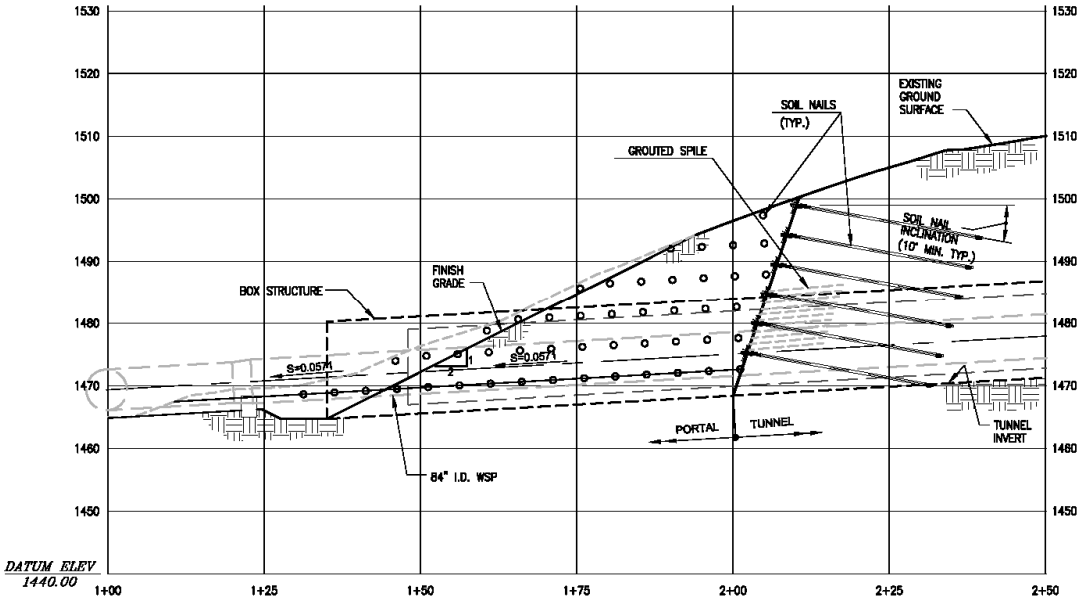

Figure 206 — Tunnel portal cross section with soil nail wall design

The soil nail wall design was based on the design factors recommended by the United States Federal Highway Administration (FHWA) (1998) and listed in Table 48. The static analysis for the soil nails is performed by a computer program SNAIL developed by the California Department of Transportation (Caltrans, 2005). A pseudo-static analysis is used to evaluate the seismic effect on portal design. The non-dimensional pseudo-static seismic coefficient is related to the TDE level site peak ground acceleration. As recommended by FHWA (1998), it is acceptable to select a seismic coefficient between 0.5 and 0.67 of the peak ground acceleration for soil nail wall stability analysis. This range has provided soil nail wall designs that yields tolerable deformations in highway facilities (Kavazanjian et al., 1997). Using the PGA value in Table 44, a seismic coefficient of 0.17 has been determined for the pseudo-static analysis. The plane shear analysis showed the proposed soil nail support system stabilizes the worst possible block with the design factors recommended by FHWA (1998), and the slope stability analysis results satisfied the static and dynamic global Factor Of Safety (FOS) requirements. (822A)

Table 49 — Soil nail design strength factors per FHWA (1998)

Design Strength Factors	Static	Dynamic
Head Punching Shear	0.67	0.89
Tensile Strength	0.55	0.73
Grout Bonding Strength	0.50	0.67
Global FOS	1.35	1.1

5.4.3.7.2 Tunnel lining system

The proposed tunnel will be excavated sequentially in two stages: top heading and lower bench excavation. As shown in Figure 203, approximately 91 meters (300 feet) of new tunnel will be excavated within Towsley Formation bedrock and the last 85 meters (280 feet) will be excavated within Pico Formation bedrock. The Towsley formation is expected to dip at 70° to 80° to the north. Surficial weathering may be present down to the crown of the tunnel over the first 46 meters (150 feet) of the tunnel excavation. The formation is expected

to be weakly cemented and part along bedding planes. The Pico Formation is also dipping steeply to the north. The exploratory drifts excavated as part of the construction of nearby tunnels suggest that the Pico Formation will vary from moderately hard to soft sandstone and conglomerate with high clay content and massive bedding. The tunnel will encounter the fault zone at a distance of approximately 61 meters (200 feet) from the portal. Based on observations logged during construction of a nearby parallel tunnel, it is anticipated that this shear zone will be at least 90 meters (300 feet) wide.

The initial support and final lining design is based on the anticipated ground loads in the shear zone. The static rock load for tunnel support design was estimated using the Modified Terzaghi's Rock Load Classification System by Deere (1970) assuming that the rock can be classified as "completely crushed and above groundwater level". This corresponds to a uniform vertical load equal to a height of rock (H_p) equal to $1.1(B+H_t)/2$, and lateral uniform load (P_h), equal to $0.3\gamma_R(0.5H_t+H_p)$, where B is the tunnel excavation width, Ht is height of tunnel, and γ_R is unit weight of rock. The unit weight of rock, γ_R =21.5 kN/m3 (134 pcf), was estimated by averaging laboratory test values performed on samples taken at 79 meters (260 feet) to 97.5 meters (320 feet) below the top of hill. As a result, the static vertical uniform load, P_v, was estimated as 110 kPa (2.3 ksf) and the static lateral uniform load, P_h, was estimated as 47.88 kPa (1.0 ksf).

5.4.3.7.2.1 Initial support

Steel sets made up of W8x21 curved beams at 0.91 meter (4 feet) spacing with 7.6 cm to 10 cm (3 to 4 inches) of shotcrete lagging is recommended for the initial support. Figure 207 shows typical tunnel sections. The groundwater table was not encountered during the field investigation, therefore external hydrostatic pressures and dewatering were not considered for the design of the tunnel.

The design of the steel sets for initial support was based on the methodology described by Proctor & White (1968). Applying the static vertical rock load, the maximum total stress in the arch portion of the steel set was computed by adding the maximum stress due to thrust and the maximum stress due to bending. The maximum total stress in the arch portion of the steel set was then compared to an allowable stress of 149 MPa (21.6 ksi), or 60% of the yield stress. The stress in the leg portion of the steel sets was computed by adding the compressive stress from the vertical load and the maximum bending stress caused by the lateral rock load. The maximum total stress in the leg portion of the steel set was also compared to an allowable stress of 149 MPa (21.6 ksi).

The steel sets were also checked for a short term seismic loading condition using a pseudo-static analysis with the TDE level peak ground acceleration of 0.3g (horizontal and vertical) applied to the static rock load. The total static and pseudo-static loads were estimated by multiplying the static loads by 1.3. The maximum stress in the steel sets was then compared to an allowable stress for temporary loads equal to 193 MPa (28 ksi) (30% increases in allowable stress). (815a)

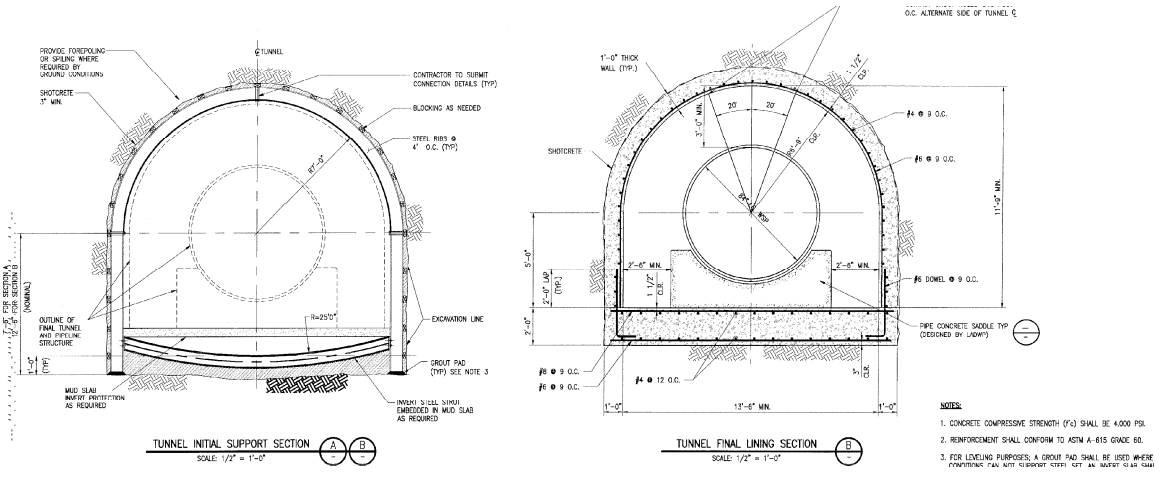

Figure 207 — Typical cross section for tunnel lining system, initial support and final lining

5.4.3.7.2.2 Permanent support lining

For the design of the final lining permanent support, a two-dimensional beam-spring model using the computer program STAAD (STAAD, 2008) was performed to determine the liner thickness and required reinforcement. In the STAAD analysis, the lining is represented by linear beam elements while the ground is represented by equivalent springs. The radial springs attached to the lining are compression-only to simulate the passive support that the ground will provide to the lining. The stiffness of the springs used in the models was calculated based on the modulus of subgrade reaction derived by the following equation:

$$k_r = \frac{E_r}{B \cdot (1 - \nu^2)}$$

where E_r is elastic modulus of rock mass, ν is Poisson's ratio of rock mass, and B is height or width of tunnel. Five load cases were analysed with the STAAD program applying load factor specified in ACI 318-2002 (ACI, 2002) and two scenarios for each load case were investigated assuming the liner is reinforced as necessary to take moment causing tension (negative moments) on the outside face or assuming one layer of reinforcing on the interior lining face such that plastic hinges form at the bottom corner and no negative moment capacity exist in the haunches of the arch. The maximum lining load was then compared to the lining interaction diagrams (Hoek, 1999) for the arch, walls, and invert slab.

For seismic loading, three types of ground deformation were considered: axial compression and extension, curvature (longitudinal bending), and ovaling. The loading conditions for these ground deformation types are described in Section 5 and the ground strains are calculated based on the equations in Table 43 assuming 45 degree angle of wave incidence with respect to tunnel axis. The average shear wave velocity along the tunnel is estimated around 900 m/s (2950 fps) based on down-hole seismic measurement. The total axial strains resulted from the axial and bending deformations were 0.00043 and 0.00074, respectively for ODE and MDE levels, which is less than the 0.003 allowable strain for concrete. (821A, 821a)

For ovaling deformation, the maximum free-field shear strain, over the 12 inch thick concrete tunnel lining was estimated to be 0.00084 and 0.0014, respectively for ODE and MDE levels. Both shear strains were applied to the beam-spring model, and the results were compared to the lining interaction diagrams (Hoek, 1999). Table 49 presents the corresponding thrust force and bending moment due to the shear strain. The maximum thrust was calculated for both full-slip and no-slip conditions. For most tunnels, the interface condition is between full-slip and no-slip with certain degree of separation among the tunnel and the surrounding ground. Full-slip assumptions under simple shear may cause significant underestimation of the maximum thrust, so it has been recommended to investigate both conditions for critical lining forces and deformations (Hashash et al, 2001). The most severe stress conditions, which is caused by the bending moment from full slip and the thrust from no-slip, were determined to be 11.48 MPa (1.665 ksi) and 19.76 MPa (2.866 ksi), respectively for the ODE and MDE levels. With specified concrete strength of 27.58 MPa (4 ksi), stress conditions are satisfied for the ODE and MDE levels.

Table 50 — Tunnel lining loading per unit length due to seismic shear strain

Loading		Design Level	
		ODE	MDE
Thrust kN (kips)	Full-slip	10 (2.26)	17.5 (3.95)
	No-slip	568 (128)	978 (220)
Bending moment m-kN (ft-kips)		25.2 (18.6)	43 (32)
Max. Combined stress MPa(ksi)		11.48 (1.665)	19.76 (2.866)

Using the analysis results, the design requires a minimum 30cm (12 inch) thick concrete lining with #6 bars at 30 cm (12 inch) spacing for the arch and walls, and minimum 45 cm (18 inch) thick concrete lining with #8 bars at 30 cm (12 inch) spacing is recommended for the invert. At the downstream end of the tunnel, a 1.3 cm (1/2-inch) thick bond breaker is recommended for the connection between the tunnel lining and the concrete thrust block to prevent stress concentrations caused by seismic displacement of the shaft lining above the tunnel.

As previously described, the resulting tunnel liner design for seismic ground motions is sufficient to accommodate ODE and MDE level fault displacements shown in Table 46 and meet the performance criteria presented in Table 42. The well reinforced tunnel liner is expected to easily accommodate the small fault displacements specified for the ODE and MDE level designs and do not require a detailed analysis to confirm conformance with the performance criteria.

Figure 207 shows how the tunnel is dimensioned to meet the SDE level fault movements presented in Table 46. An air gap meeting or exceeding the design movements is provided to accommodate the fault displacement without significantly stressing the welded steel carrier pipe. Additionally, the pipe saddle supports are designed to be cast separately from the concrete tunnel invert and to not be firmly anchored to the floor. This will allow the pipe and saddles to flex and bend around the fault displaced tunnel during a SDE level event. The SDE level performance criteria allow for yielding and damage and thus a non-linear analysis of the tunnel liner is not warranted, in fact the tunnel liner is expected to fail in such an event. However, reinforcing is placed in the concrete liner to help prevent large concrete spalling that may impact the steel pipe. Experience in past earthquakes has shown that standard specifications for welded steel pipe used in the Los Angeles area allow for yielding strains (O'Rourke, et al, 1988) over long distances of pipe length with little to no damage to the pressure boundary. As a result, the pipe design within the tunnel is expected to meet the specified performance criteria.

5.4.3.7.3 Shaft excavation supports

The recommended method for shaft construction at the top of the hill is by traditional top-down excavation methods. The shaft will be excavated through three types of ground: soil within the top 1 meter (3 feet), weathered Pico Formation bedrock (sandstones and pebble conglomerate) from 1 meter (3 feet) to 30 meters (90 feet), and fresh Pico Formation bedrock below 30 meters (90 feet). The groundwater table was not encountered in boreholes, therefore hydrostatic pressures and dewatering were not considered in the shaft design. Figure 208 shows the shaft design.

Lateral pressures for designing the excavation support system was calculated by combining the lateral earth pressure and the lateral pressure due to a construction surcharge from a crawler crane and drill rig. The active earth pressure was calculated as based on Coulomb theory for the depth up to 30 meters (90 feet). The lateral pressure due to construction surcharge was estimated following an analytical solution after Das (2004) and simplified as two uniform loads of 28.73 kPa (0.6 ksf) over the depth from 0 meter to 5 meters (0 feet to 15 feet) and 14.36 kPa (0.3 ksf) over the depth from 5 meters to 10 meters (15 feet to 30 feet). Lateral earth pressure below 30 meters (90 feet) was computed from the following equation by Proctor & White (1977):

$Ph=0.4\gamma D$ for depth > 5 times shaft diameter, D, for medium sand

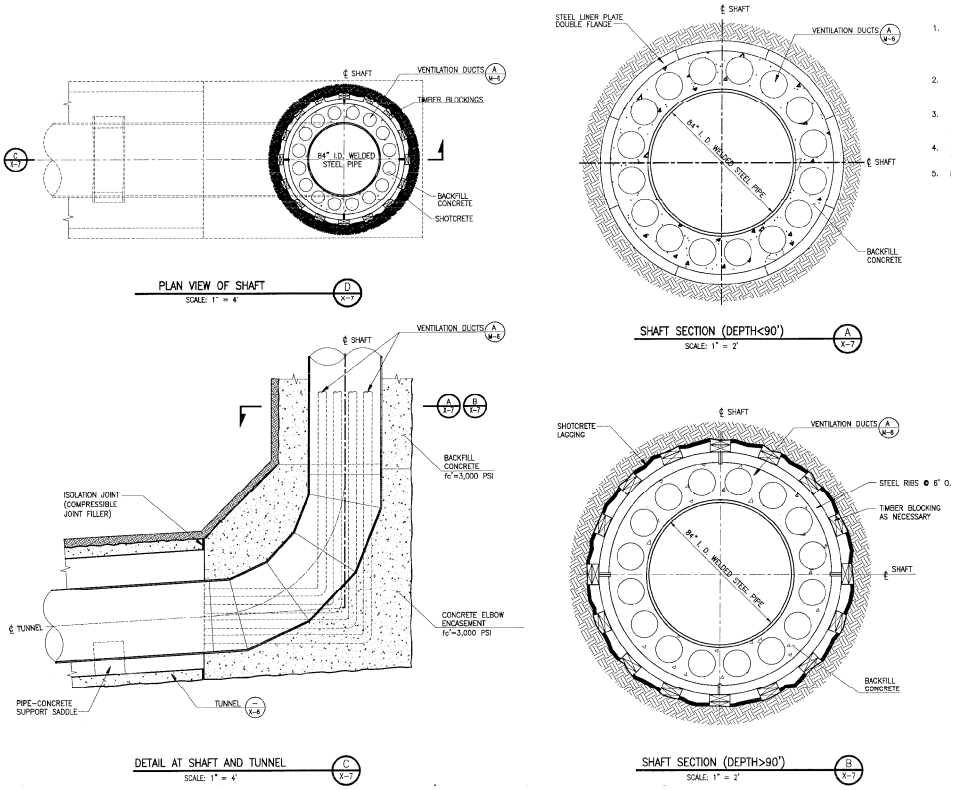

Figure 208 — Shaft section and detail

Although the shaft will be in fresh Pico Formation below a depth of 30 meters (90 feet), the equation for medium sand was taken to be conservative for these depths. Figure 209 shows the lateral pressure diagram along the proposed shaft. Steel liner plate is recommended for initial support for the first 30 meters (90 feet) of shaft excavation and steel ribs and shotcrete are recommended for support below 30 meters (90 feet). Steel ribs and shotcrete can be used in the upper 30 meters (90 feet) if sufficient stand-up time is observed during construction. The analysis of steel liner plates was based on Section 15 Steel Tunnel Liner Plates from AASHTO Standard Specifications for Highway Bridges (AASHTO, 2008). The analysis of steel ribs was based on arch stress calculation described by Proctor & White (1968) following the same total stress calculation with arch steel set design for the tunnel. The steel ribs and steel liner plate were also checked for temporary seismic loading condition using a pseudo-static analysis using the TDE level peak horizontal ground acceleration of 0.3g applied to the lateral pressure load. The total static and pseudo-static loads were estimated as multiplying the static loads by 1.3.

The design for the shaft excavation support consists of 3 mm thick, double flanged steel liner plate for the upper 30 meters (90 feet) and Grade 36 W6x9 ribs spaced every 1.8 meter (6 feet) with shotcrete lagging for the rest of the shaft.

The final constructed shaft liner consists of welded ductile steel carrier pipe encased in thick unreinforced concrete. The shaft is not expected to experience any fault displacements. The final shaft configuration has a section sufficiently strong to resist ODE and MDE level seismic induced pressures and length to provide sufficient flexibility accommodate transient movements.

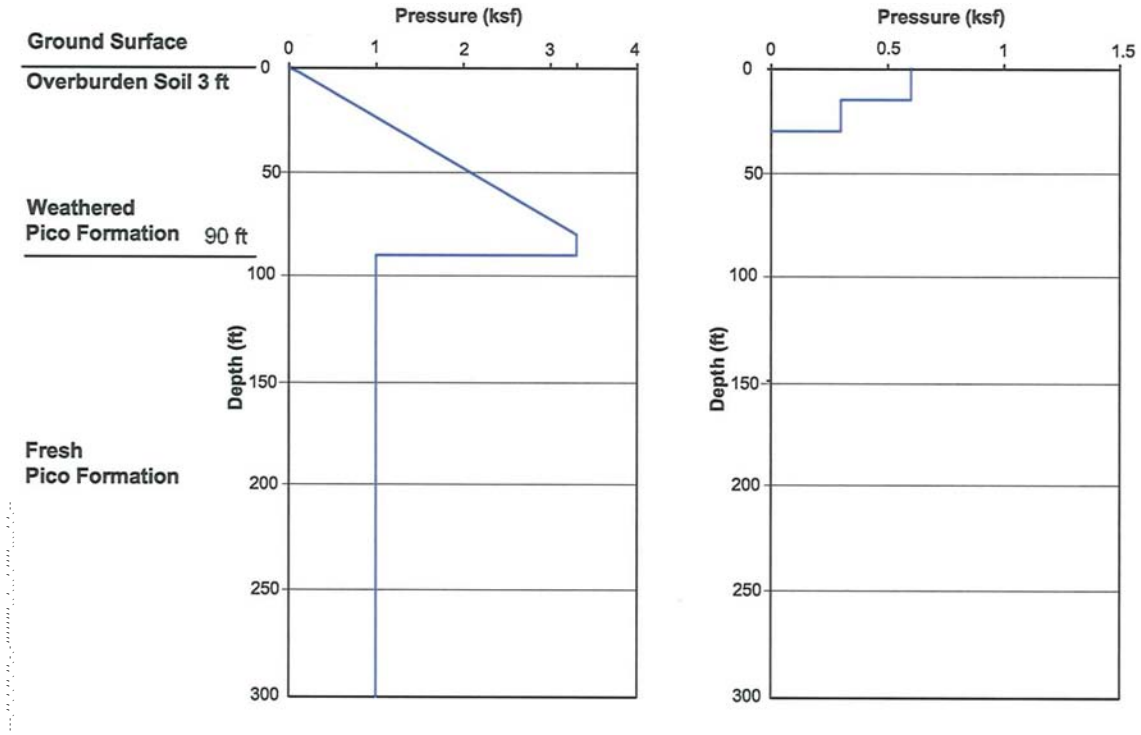

Figure 209 — Minimum lateral pressure and surcharge diagrams for shaft support system

5.4.3.7.4 Lateral seismic wall pressures on vault

A 10 m x 15 m underground vault will be constructed to house the valves, and pipe connections at the top of hill. The vault will not be subjected to fault displacements. The lateral soil pressure sE distribution for seismic loading on the vault was evaluated based on the seismic wave propagation (Davis, 2003). The vault is assumed to be a rigid, non-deflecting structure buried at or below the ground surface as shown in Figure 210. The lateral seismic pressures sE applied to the vault soil retaining walls are determined from the superposition of: (1) lateral stress increases in the free-field soil Dsh that result from densification and dilation of soil particles during shearing (e.g., Youd and Craven, 1975), and (2) transient stresses sx resulting from the passage of seismic waves (e.g., Scott, 1973; Veletsos and Younan, 1994a, 1994b):

$$\sigma_E = \Delta\sigma_h + \sigma_x = K_E \gamma z + k_s (u_f - u_H), \qquad 0 \le z \le H$$

where K_E is lateral earth pressure coefficient resulting from seismic shaking, z is the depth below ground surface, H is the depth to bottom of wall below ground surface, γ is the soil unit weight, u_f is the horizontal soil deformation in the free-field during seismic shaking, u_H is the horizontal soil free-field deformation at depth H, and k_s is a continuous stiffness parameter that relates the free-field horizontal displacement with lateral wall stress.

The free-field displacement u_f is dependent upon the subsurface site conditions and depth of burial. The horizontal acceleration at the ground surface a_h is related to $\overline{u}$ by $a_h = \omega^2 \overline{u}$ and the free-field subsurface displacement profile is evaluated from:

$$u_f = \overline{u} \cos\left(2\pi \frac{z}{\lambda}\right) = \frac{a_h}{\omega^2} \cos\left(2\pi \frac{z}{\lambda}\right)$$

where z is the coordinate depth below ground surface as shown in Figure 210.

Solving the elastic equation of motion, the pressure distribution over the wall height H is determined by:

$$\sigma_E = K_E z\gamma + \frac{a_h}{g}\frac{\gamma\beta\psi_\sigma}{2\pi f}\sqrt{\frac{z}{H}}\left\{\cos\left(\frac{2\pi}{\lambda}z\right) - \cos\left(\frac{2\pi}{\lambda}H\right)\right\} \quad \text{for } 0 \le z \le H$$

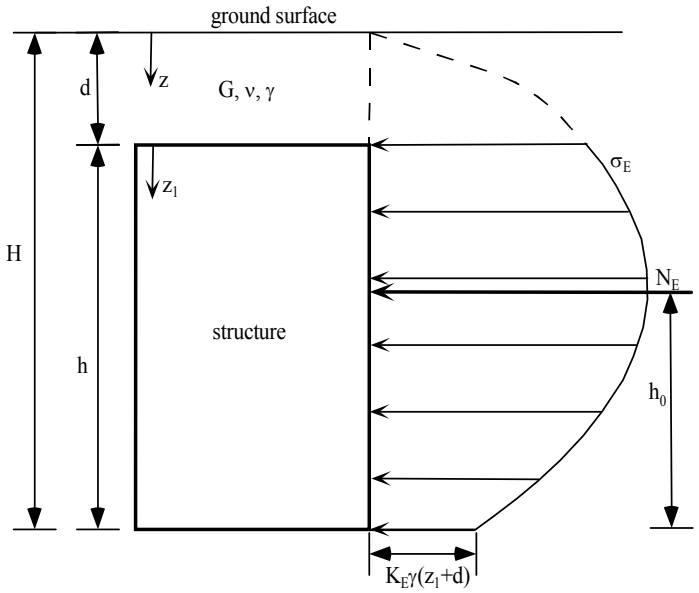

Figure 210 — Lateral stress distribution σ_E, resultant force N_E, and resultant force location h_0 against rigid underground structure

The vault at the top of the hill is proposed with the top of vault at ground surface. The seismic design values at the top of hill were determined using ν = 0.36 and β = 540 m/s (1771 ft/s) obtained from down-hole seismic shear and compression wave measurements. The lateral earth pressure coefficient resulting from seismic shaking as described by Davis (2003), K_E is taken as 0.05 based on results of Youd and Craven (1975) and Sherif et al. (1982). The lateral stress distribution for the MDE level is determined as followings and illustrated in Figure 211:

$$\sigma_E = 6z + 13528\sqrt{\frac{z_1}{H}}\left[\cos(1.356z_1) - \cos(1.356H)\right] \text{ (psf or multiply by 47.88 for N/m}^2\text{)} \quad (2)$$

Based on the performance criterion defined for the project, the vault is only designed for elastic response with the MDE level to ensure safety protection for workers who may need to enter the vault for operational purposes following a design level event to help ensure the water pipeline can flow water. As a result, the vault may perform closer to the ODE criteria under MDE level ground motions.

The resultant seismic force N_E, calculated using the procedure presented in Davis (2003), is determined from the plot in Figure 212a. For the vault with the fixed depth of 6 m (19 feet), the resultant N_E is 163 kN/m (11,003.5 lb/ft), and the resultant N_E is located at a distance h_0 = 0.5H from the base of the wall, determined from Figure 212b. σ_E and N_E only consider seismic shaking and must be added to pre-earthquake and all other appropriate pressure combinations acting on the wall.

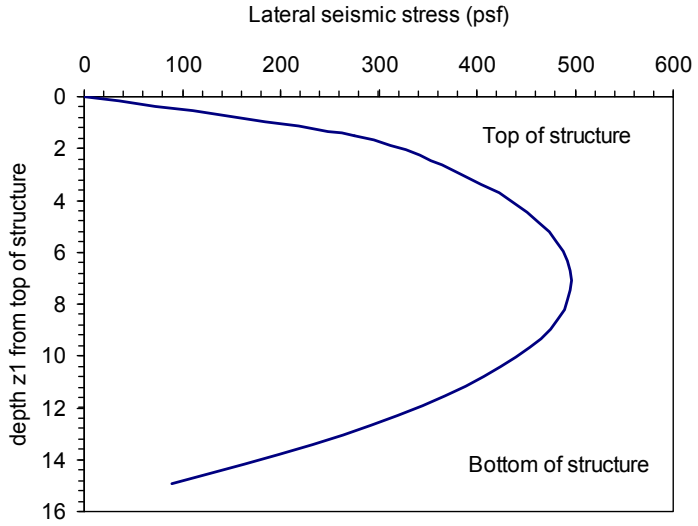

Figure 211 — Lateral wall stresses on vaults at the top of Terminal Hill (vault height=6 m).

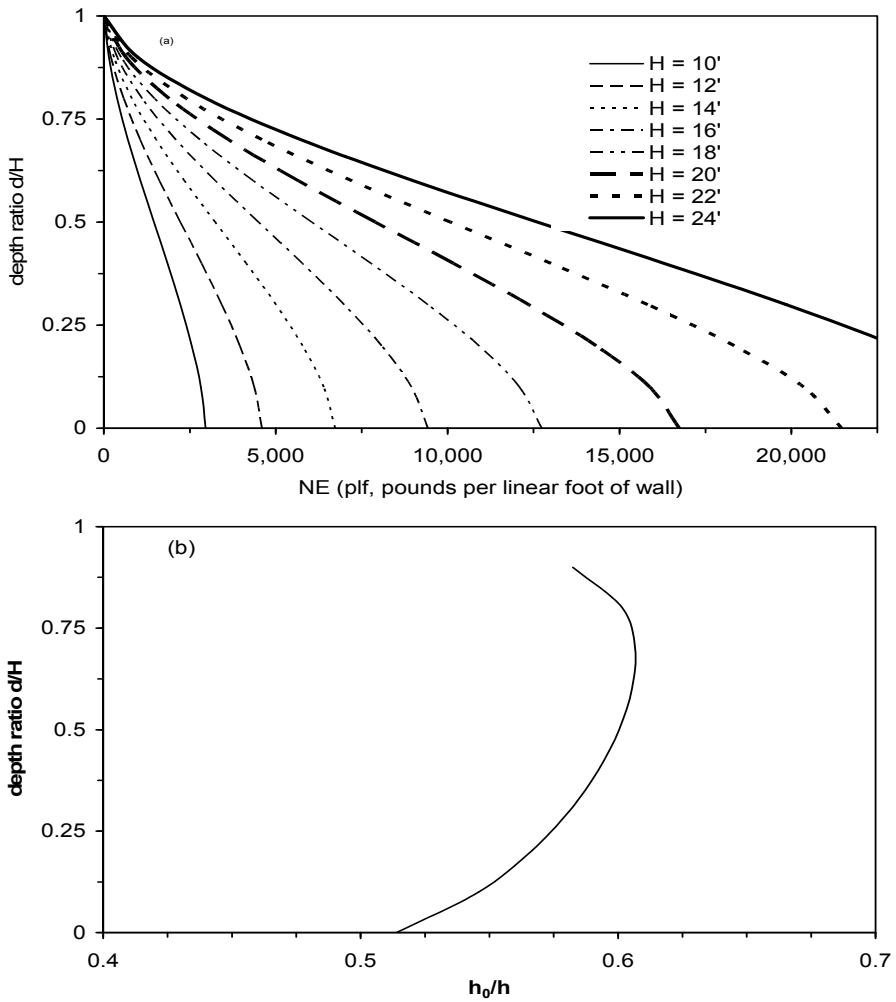

Figure 212 — (a) Resultant lateral seismic force N_E for various H and d/H, and (b) resultant force location variation with depth ratio d/H on vaults at top of the hill

Annex A
(informative)

Conformity with provisional sentences in ISO 23469

A.1 General

In the main text of each sub-sub-clause for a design example, a sentence or a paragraph corresponding to a specific requirement which is provided in a sentence using “shall” in ISO 23469, shall be ended with a corresponding “code” written in parentheses for being checked in terms of conformity with provisional sentences in ISO 23469. A specific recommendation is provided in a sentence using “should” as well. Therefore, this Technical Report adopts a code description in which a code of abbreviation consists of numerals and an alphabet. In the code, consecutive numerals stand for clause, sub-clause, and sub-sub-clause, respectively in principle. An alphabet in capital letter stands for “shall” and that in lower-case letter stands for “should” in appearing order. For examples, the third sentence using “shall” in the sub-sub-clause 6.2.1 in ISO 23469 corresponds to “(621C)” and the first sentence using “should” in sub-sub-clause 8.1.4 corresponds to “(814a).” Exceptionally, zero is placed in the place for sub-clause like “(520A).”

Provisional sentences using “shall” or “should” are extracted from the main body of ISO 23469 with partial reduction if acceptable and shown in appearing order as shown in this A.

Clause and sub-clause	Code	Statement
5 Principles and procedure		
5.1 Principles		
5.1.1 Purposes and functions		
5.1.2 Performance objectives for seismic design	(511A)	In designing geotechnical works, the purposes and functions *shall* be defined in accordance with broad categories of use such as commercial, public and emergency use.
	(512a)	Performance objectives for seismic design of geotechnical works *should* generally be specified on the following basis (serviceability, safety), depending on the expected functions during and after an earthquake.
	(512b)	The performance objectives *should* also reflect the possible consequences of failure.
	(512A)	Seismic actions on geotechnical works *shall* be specified, which are compatible with the performance objectives.
5.1.3 Reference earthquake motions	(513A)	For each performance objective described in 5.1.2, reference earthquake motions *shall* be specified for evaluating seismic performance of geotechnical works as follows (for serviceability, for safety).

5.1.4 Performance criteria and limit states	(514A)	Performance criteria *shall* generally be specified by engineering parameters that characterize the response of geotechnical works to the reference earthquake motions.
	(514B)	These engineering parameters *shall* be specified considering the design working life.
	(514C)	These issues *shall* be taken into account in the formulation of the performance criteria.
5.1.5 Specific issues related to geotechnical works	(515A)	Seismic actions on geotechnical works *shall* be specified taking the following factors (seismic response, mode of failure, performance criteria, soil-structure interaction).
5.2 Procedure for determining seismic actions	(520A)	Seismic actions on geotechnical works *shall* be defined as follows (1st stage [characterize the firm ground motion, the fault displacements, the free field motions, the potential for earthquake-induced phenomena], 2nd stage [Specify the earthquake ground motions, the ground displacement of fault movements, ground failure and other geotechnical hazards]).
6 Principles and procedure		
6.1 General		
6.1.1 Earthquake ground motions and fault displacements	(611A)	For the 1st stage, earthquake ground motions and fault displacements *shall* be evaluated for use as basic variables in subsequent analyses for specifying seismic actions on geotechnical works.
6.1.2 Ground failure and other geotechnical hazards.	(612A)	Liquefaction potential *shall* also be evaluated in the 1st stage.
	(612B)	If liquefaction is judged to occur, the effects of liquefaction *shall* be incorporated in the 2nd stage either as seismic actions or effects on the model of the soil-structure system.
	(612C)	The potential for ground failure in the form of landslides or deformations *shall* be evaluated
6.2 Seismic hazard analysis	(621A)	The earthquake ground motions, liquefaction potential, ground failure, and fault displacement *shall* be determined by either probabilistic or deterministic analyses.
6.2.1 Probabilistic and deterministic analyses	(621B)	The earthquake ground motions for evaluating serviceability *shall* be determined by probabilistic analyses.
	(621C)	The earthquake ground motions for evaluating safety *shall* be determined by either probabilistic or deterministic analyses.
6.2.2 Analysis for evaluation of earthquake Probabilistic and	(622a)	Both probabilistic or deterministic seismic hazards analyses *should* capture the characteristics of the ground motions based on earthquake magnitude, fault type and distance.

deterministic analyses	(622b)	More detailed seismic hazard analysis *should* capture the near source effects and directivity effects and *should* be based on seismic source parameters, attenuation of earthquake motions from the fault, and deep basin effects.
	(622c)	The uncertainties in the model parameters of seismic source parameters, attenuation relations and deep basin effects *should* be considered.
	(622A)	Seismic hazard analysis methods, including empirical, semi-empirical and theoretical methods, *shall* be chosen, (reduced), based on the importance of a structure, and the available information on seismic faults and deep basin structures.
6.2.3 Outputs of seismic hazard analysis.	(623A)	Earthquake ground motions at the interface between firm ground and local soil deposits shall be developed through seismic hazards analysis.
	(623B)	An appropriate set of variables (peak acceleration, peak velocity, peak displacement, Fourier and response spectral values or time histories of acceleration, velocity, displacement) *shall* be evaluated for specifying the seismic actions depending on the models and the methods of analysis.
6.3 Site response analysis and assessment of liquefaction potential	(631A)	The earthquake motions at the ground surface and within the subsoil *shall* be obtained for use in determining seismic actions on geotechnical works.
6.3.1 General	(631B)	The assessment of liquefaction potential *shall* also be performed for evaluating the effects on performance of geotechnical works.
	(631C)	The methods used for site response analysis and assessment of liquefaction potential *shall* be selected on the basis of required seismic behavior specified by performance criteria and quality of geotechnical data from the site.
6.4 Spatial variation	(641A)	The spatial variations of earthquake ground motions *shall* be evaluated for the design of a long or a large structure.
6.4.1 General	(641B)	Appropriate characterisation for lateral variation in these geotechnical conditions （topography, soil properties and stratigraphy） *shall* be performed.
	(641C)	Parameters such as phase velocity, wavelength and direction of propagation *shall* be appropriately defined for evaluating spatial variation.
6.4.4 Site-specific simplified dynamic analysis	(644a)	In site-specific simplified dynamic analysis, the spatial variation such as that due to phase difference at the firm ground *should* be considered.

6.4.5 Site-specific detailed dynamic analysis	(645A)	In site-specific detailed dynamic analysis, earthquake ground motions with the effects of spatial variation *shall* be evaluated based on the effects of lateral geotechnical heterogeneity.
	(645B)	The deep basin effects that depend on the heterogeneity below the local soil deposits *shall* also be considered.
6.5 Fault displacement, ground failure and other geotechnical hazards.	(650a)	Construction of geotechnical works at a site on or in the vicinity of a known active fault *should* be avoided if possible.
	(650A)	Otherwise, the effects of fault displacements, ground failure and other geotechnical hazards *shall* be considered in the design of geotechnical works.
7 Procedure for specifying seismic actions	(711A)	Following assessment of the free field earthquake motions, fault displacements, ground failure and other geotechnical hazards, the seismic actions on the geotechnical works *shall* be appropriately specified
7.1 Types and models of analysis 7.1.1 General procedure	(711B)	The following procedure *shall* be used.(1) select type of analysis → 2) select model and method of analysis → 3) specify performance criteria parameters → 4) perform geotechnical characterization)
7.1.2 Types of analysis	(712A)	The type of analysis to be adopted for evaluating the seismic performance of the geotechnical works *shall* be chosen based on the data, the importance of the structure, the performance criteria parameters and the level of complexity and non-linearity.
7.1.3 Model for analysis	(713A)	The most appropriate model and method of analysis *shall* be used for evaluating the seismic performance of the geotechnical work.
7.1.5 Geotechnical characterisation	(715A)	Geotechnical and material studies *shall* be carried out to determine appropriate input parameters for the selected models and types of analysis.
	(715B)	Effects of response control and ground improvement *shall* also be considered where applicable.
8 Seismic actions for equivalent static analysis	(811A)	The effects of overstrength in a superstructure *shall* be considered when evaluating the seismic actions.
8.1 Seismic actions for simplified equivalent static analysis.	(811B)	Non-linear behavior of foundations and soils *shall* be incorporated in the model of analysis either through linear modeling with reduced stiffness or non-linear modeling.
8.1.1 Seismic actions from a superstructure	(811a)	Further non-linear effects, such as P-delta effects *should* be taken into account where appropriate.
	(811b)	Consideration *should* be given to the possibility that the maximum ground displacements and maximum acceleration of superstructure may not occur at the same time.

8.1.2 Seismic actions without spatial variation	(812A)	Non-linear behavior of foundations and soils *shall* be incorporated in the model of analysis either through linear modeling with reduced stiffness or non-linear modeling.
	(812a)	Further non-linear effects, such as P-delta effects *should* be taken into account where appropriate.
8.1.3 Seismic actions with spatial variation	(813A)	Non-linear behavior of soils *shall* be considered when large relative displacements are expected.
8.1.4 Seismic earth and hydro-dynamic pressures	(814a)	Non-linear behavior of soils *should* be carefully considered as this can lead to amplification or attenuation of the peak acceleration.
8.1.5 Seismic earth on soil and structure masses	(815a)	The inertia force *should* be specified based on the peak acceleration response at the center of gravity of the assumed mass of soil and structure.
8.2 Seismic actions for detailed equivalent static analysis.	(821A)	In the detailed equivalent static analysis, the seismic performance of geotechnical works *shall* be analysed using a global computation model of the soil-structure system.
8.2.1 Detailed equivalent static analysis	(821B)	An appropriate model of the superstructure, if applicable, *shall* also be incorporated in the global model to account for the interaction.
	(821C)	The effects of overstrength in a superstructure *shall* be considered either in the modeling or in evaluating seismic actions from the structure.
	(821a)	Appropriate types of numerical models, such as finite element or lumped mass models, *should* be used for the analysis.
8.2.2 Seismic actions for a seismic coefficient approach	(822A)	In order to take full advantage of a detailed equivalent static analysis, site-specific analysis shall be performed to evaluate the free field acceleration.
	(822B)	Non-linear behavior of soils and structures *shall* be incorporated in the model of analysis either through linear moiling with reduced moduli or non-linear modeling.
8.2.3 Effects of soil liquefaction and induced ground displacement	(823A)	Allowance *shall* be made for differential settlements caused by site heterogeneity, taking into account the characteristics of the structure and simplifications in the analysis.
9 Seismic actions for dynamic analysis	(911A)	In simplified dynamic analysis of a shallow or deep foundation, seismic actions from the superstructure *shall* be specified in terms of the dynamic response of the superstructure.
9.1 Seismic actions for simplified dynamic analysis.	(911B)	The effects of overstrength in a superstructure *shall* be considered either in the modeling or in evaluating seismic actions from the structure.

9.1.1 Seismic actions from a superstructure	(911C)	Non-linear behavior of soils and structures *shall* be incorporated in the model of analysis either through linear moiling with reduced moduli or non-linear modeling.
	(911a)	Further non-linear effects, such as P-delta effects *should* be taken into account where appropriate.
9.1.2 Seismic actions without spatial variation	(912A)	These time histories of ground motion *shall* be based on the free field response to a reference earthquake motion, input at the appropriate level in the free field.
	(912B)	Non-linear behavior of foundations and soils *shall* be incorporated in the analysis either through linear modeling with reduced stiffness or non-linear modeling.
	(912a)	Further non-linear effects, such as P-delta effects *should* be taken into account where appropriate.
9.1.3 Seismic actions with spatial variation	(913A)	Non-linear behavior of soils *shall* be considered when large relative displacements are expected.
9.1.4 Seismic actions on soil and structure masses	(914A)	If the wall or earth structure is relatively large, the spatial variation of the inertia forves arising from the variation of accelerations over the structure *should* be accounted for.
9.2 Seismic actions for detailed dynamic analysis.	(921A)	Appropriate types of computational models, such as finite element or lumped mass models *shall* be used for the analysis.
9.2.1 Seismic actions for a soil-structure system	(921B)	Firm ground motions or motions at the base of the analysis domain *shall* be given as seismic actions for the global computational model.
	(921C)	Input motions for analysis *shall* be determined by a site-specific study.
	(921D)	Non-linear stress-strain behavior of soils and structures, including damping, *shall* be appropriately modelled for the analysis of the soil-structure systems.
9.2.2 Effects of soil liquefaction and induced ground displacement	(922A)	Appropriate formulations, constitutive models and numerical procedure *shall* be used.

Bibliography

[1] Kataoka, S (2008): Empirical method for determining design earthquake motions for civil engineering structures, Technical Reports on Civil Engineering, 50-2, pp. xx-xx. (In Japanese) Drafter Prof. Nakamura has been looking for a related English literature.

[2] AKI, K. (1966): Generation and propagation of G waves from the Niigata earthquake of June 16, 1964. 2. Estimation of earthquake moment, released energy, and stress-strain drop from G wave spectrum, *Bulletin of the Earthquake Research Institute*, Vol.44, pp.23～88.

[3] AKI, K. (1967): Scaling law of seismic spectrum, *J. Geophys. Res.*, Vol.72, pp.1217～1231.

[4] BAZZURRO, P. and CORNELL, C.A. (1999): Disaggregation of seismic hazard, *Bulletin of the Seismological Society of America*, Vol.89, pp.335-341.ISO/IEC Directives, Part 2, *Rules for the structure and drafting of International Standards*, 2001

[5] COHEN, L. (1995): *Time-Frequency analysis*, Prentice-Hall, Englewood Cliffs, New Jersey.

[6] NAGAO, T., YAMADA, M. and NOZU, A. (2005): Probabilistic seismic hazard analysis with focus on Fourier amplitude and group delay time, *Journal of the Japan Society of Civil Engineers*, No.801/I-73, pp.141-158 (in Japanese with English abstract).

[7] SAWADA, S., MORIKAWA, H., TOKI, K. and YOKOYAMA, K. (1998): Identification of path and local site effects on phase spectrum of seismic motion, *Proceedings of the 10th Japan Symposium on Earthquake Engineering*, pp.915-920.

[8] WALD, D.J. and SOMERVILLE, P.G. (1995): Variable-slip rupture model of the great 1923 Kanto, Japan, earthquake: geodetic and body-waveform analysis, *Bulletin of the Seismological Society of America*, Vol.85, pp.159-177.

[9] Committee on Civil Engineering in Energy and Power Industries, Japan Society of Civil Engineers (1999): Guidelines of Performance-Based Structural Evaluation of LNG Underground Tank.

[10] DAN, K., M. WATANABE, T. SATO and T. ISHII (2001), Short-period source spectra inferred from variable-slip rupture models and modeling of earthquake faults for strong ground motion prediction by semi-empirical method, J. Struct. Constr. Eng., AIJ, 545, 51-62. (in Japanese with English abstract)

[11] GRAVES, R. W. (1996), Simulating seismic wave propagation in 3D elastic media using staggered-grid finite differences, Bull. Seism. Soc. Am., 86, 1091-1106.

[12] IRIKURA, K. and H. MIYAKE (2001), Prediction of strong ground motions for scenario earthquakes, J. Geogr., 110, 849-875. (in Japanese with English abstract)

[13] IRIKURA, K., H. MIYAKE, T. IWATA, K. KAMAE, H. KAWABE and L. A. DALGUER (2004), Recipe for predicting strong ground motion from future large earthquake, Proceedings of the 13WCEE, 1371.

[14] KAGAWA, T. (2004), Developing a Stochastic Green's Function Method having more accuracy in long period range to be used in the Hybrid Method, Journal of Japan Association for Earthquake Engineering, 4, 2, 21-32. (in Japanese with English abstract)

[15] KAGAWA, T., H. IEMURA, K. IRIKURA, and K. TOKI (2004), Strong ground motion observation by the Committee of Earthquake Observation and Research in the Kansai Area (CEORKA), Journal of Japan Association for Earthquake Engineering, 4, 3, 128-133.

[16] Kansai Geo-informatics Network (2008), Kansai ground renewed, Osaka plain and Osaka bay.

[17] NAKATA, T., K. SHIMAZAKI, Y. SUZUKI, and E. TSUKUDA (1998), Fault branching and directivity of rupture propagation, J. Geogr., 107, 512-528. (in Japanese with English abstract)

[18] Osaka Prefecture (2007), Study on action for natural disaster prevention in Osaka Prefecture, Earthquake damage anticipation. (in Japanese)

[19] Osaka City (2007), Study on action for natural disaster prevention in Osaka City, Earthquake damage anticipation. (in Japanese)

[20] PITARKA, A. (1999), 3D elastic finite-difference modeling of seismic motion using staggered-grid with non-uniform spacing, Bull. Seism. Soc. Am., 89, 54-68.

[21] SOMERVILLE, P. G., K. IRIKURA, R. GRAVES, S. SAWADA, D. WALD, N. ABRAHAMSON, Y. IWASAKI, T. KAGAWA, N. SMITH and A. KOWADA (1999), Characterizing earthquake slip models for the prediction of strong ground motion, Seism. Res. Lett, 70, 59-80.

[22] OHNISHI, Y. and M. HORIKE (2000), Application of the method for generating 3-componentstrongground motions using the stochastic Green's function to the 1995 Hyogo-ken NANBU earthquake, Journal of Structural Engineering, 46B, 389-398. (in Japanese with English abstract)

[23] AOI, S., OBARA, K., HORI, S., KASAHARA, K. and OKADA, Y. (2000): New strong-motion observation network: KiK-net, *Eos Trans. Am. Geophys. Union*, 81, 329.

[24] BEAUVAL, C., BARD, P-Y, MOCZO, P. and KRISTEK, J. (2003): Quantification of frequency-dependent lengthening of seismic ground-motion duration due to local geology: application to the Volvi Area (Greece). *Bulletin of the Seismological Society of America*, 93, pp.371-385.

[25] BERESNEV, I.A. and WEN, K.L. (1996): Nonlinear soil response: a reality?, *Bulletin of the Seismological Society of America*, 86, pp.1964-1978.

[26] BOORE, D.M. (1983). Stochastic simulation of high-frequency ground motions based on seismological models of the radiated spectra. *Bulletin of the Seismological Society of America*, 73, pp.1865-1894.

[27] BRUNE, J.N. (1970): Tectonic stress and the spectra of seismic shear waves from earthquake, *J. Geophys. Res.*, Vol.75, pp.4997～5009.

[28] BRUNE, J.N. (1971): Correction, *J. Geophys. Res.*, Vol.76, p.5002.

[29] IAI, S., MATSUNAGA, Y. and KAMEOKA, T. (1992): Strain space plasticity model for cyclic mobility, *Soils and Foundations*, Vol.32, pp.1-15.

[30] IWATA, T. and IRIKURA, K. (1986): Separation of source, propagation and site effects from observed S waves, *Zisin 2*, 39, pp.579-593 (in Japanese with English abstract).

[31] KINOSHITA, S. (1998): Kyoshin Net (K-net), *Seim. Res. Lett.*, 69, pp.309-332.

[32] MIYAKE, H., IWATA, T. and IRIKURA, K. (2003): Source characterization for broadband ground-motion simulation: kinematic heterogeneous source model and strong motion generation area, *Bulletin of the Seismological Society of America*, Vol.93, pp.2531-2545.

[33] KOWADA, A., TAI, M., Iwasaki, Y. and Irikura, K. (1998): Evaluation of horizontal and vertical strong ground motions using empirical site-specific amplification and phase characteristics, *J. Struct. Constr. Eng., AIJ*, No.514, pp.97-104 (in Japanese with English abstract).

[34] NOZU, A. and MORIKAWA, H. (2003): An empirical Green's function method considering multiple nonlinear effects, *Zisin 2*, Vol.55, pp.361-374 (in Japanese with English abstract).

[35] NOZU, A. and MORIKAWA, H. (2004): Assessment of soil nonlinearity using empirical Green's function method, *Proceedings of the 13th World Conference on Earthquake Engineering*.

[36] NOZU, A. and T. NAGAO (2005): Site amplification factors for strong-motion sites in Japan based on spectral inversion technique, *Technical Note of the Port and Airport Research Institute*, No.1102 (in Japanese with English abstract).

[37] NOZU, A., NAGAO, T. and YAMADA, M. (2006): Simulation of strong ground motions based on site-specific amplification and phase characteristics, *Third International Symposium on the Effects of Surface Geology on Seismic Motion*, Grenoble, France.

[38] NOZU, A., NAGAO, T. and YAMADA, M. (2008): A strong motion prediction method suitable for areas with less information on subsurface structure – Kowada's method and its application to shallow crustal earthquakes in Japan, *Proceedings of the 14th World Conference on Earthquake Engineering*.

[39] NOZU, A. and SUGANO, T. (2008): Simulation of strong ground motions based on site-specific amplification and phase characteristics – accounting for causality and multiple nonlinear effects -, *Technical Note of the Port and Airport Research Institute*, No.1173 (in Japanese with English abstract).

[40] TSURUGI, M., SAWADA, S., MIYAJIMA, M. and KITAURA, M. (2002): Re-estimation of site amplification effects in Kansai region, *JSCE Journal of Structural Engineering*, Vol.48A, pp.577-586.

[41] YAMADA, M., HIRAI, T., IWASHITA, T., KAMAE, K. and IRIKURA, K. (1999): Simulation of ground motion by the modified fault model of the Hyogo-ken Nanbu earthquake, *Program and Abstracts, The Seismological Society of Japan 1999 Fall Meeting*, A14 (in Japanese).

[42] Iai, S., Matsunaga, Y. and Kameoka, T. (1992): Strain space plasticity model for cyclic mobility, Soils and Foundations, Vol. 32, No. 2, pp. 1-15.

[43] Iai, S., Ichii, K., Liu, H. and Morita, T. (1998): Effective stress analysis of port structures, Soils and Foundations, Special Issue on Geotechnical Aspects of the January 17, 1995 Hyogoken-Nambu Earthquake, No.2, pp.97-114.

[44] Inagaki, H., Iai, S., Sugano, T., Yamazaki, H. and Inatomi, T. (1996): Performance of caisson type quay walls at Kobe Port, Special issue of Soils and Foundations, Japanese Geotechnical Society, pp. 119-136.

[45] Ministry of Transport, Japan (ed) (1999): Design Standard for Port and Harbour Facilities and Commentaries, Japan Port and Harbour Association, 1181p (in Japanese). ; English edition (2001) by the Overseas Coastal Area Development Institute of Japan.

[46] Mononobe, N. (1924): "Considerations on vertical earthquake motion and relevant vibration problems," Journal of Japan Society of Civil Engineers, Vol.10, No.5, pp.1063-1094 (in Japanese)

[47] Okabe, N. (1924): "General theory on earth pressure and seismic stability of retaining wall and dam," Journal of Japan Society of Civil Engineers, Vol.10, No.6, pp.1277-1323.

[48] PHRI (1997): Handbook on Liquefaction Remediation of Reclaimed Land, Port and Harbour Research Institute, A.A. Balkema, Rotterdam, Brookfield.

[49] PIANC (2001): Seismic design guidelines for port structures, International Navigation Association, Balkema, 474p.

[50] Schnabel, P.B., Lysmer, J. and Seed, H.B. (1972): "SHAKE: a Computer Program for Earthquake Response Analysis of Horizontally Layered Sites," Report No. EERC 72-12, Earthquake Engineering Research Center, University of California, Berkeley.

[51] Westergaard, H.M. (1933): "Water pressure on dams during earthquakes," Transactions of ASCE, Vol.98, pp.418-472.

[52] Japan Road Association. *Specifications for Highway Bridges Part V Seismic Design*, 2002.3

[53] Foundation Engineering Research Team Structures Research Group Public Works Research Institute. *Design of Highway Bridge Foundation in Japan*, Technical Memorandum from the Foundation Engineering Research Team, PWRI, No.01-2003, 2003.10

[54] YABE, MASAAKI, SHEC, CHI, YAMASAKI, YASUTUGU. *Assessment of the Seismic Performance of the Sutong Bridge*, Internatinal Conference on Bridge Engineering –Challenges in the 21st Century (CD-ROM), 2006.

[55] YABE, M. AND KAWASHIMA, K. *Nonlinear seismic response of a pile foundation and its push-over analysis*, Journal of Structural Mechanics and Earthquake Engineering, JSCE, No.619, 1999, pp. 91-109. (In Japanese)

[56] MINISTRY OF CONSTRUCTION. *Interim Report on the Damage of Highway Bridges by the Hyogo-ken Nanbu Earthquake*, Committee for Investigation on the Damage of Highway Bridges Caused by the Hyogo-ken Nanbu Earthquake, 1995. (In Japanese)

[57] FOUNDATION ENGINEERING RESEARCH TEAM STRUCTURES RESEARCH GROUP PUBLIC WORKS RESEARCH INSTITUTE. *Design of Highway Bridge Foundations in Japan*, Technical Memorandum from the Foundation Engineering Research Team No.01-2003, Compiled on October 8,2003.

[58] JAPAN ROAD ASSOCIATION: Specifications for Highway Bridges, Part V SEISMIC Design, March 2002.

[59] IAI, S., MATSUNAGA, Y. and KAMEOKA, T. (1992): Strain space plasticity model for cyclic mobility, *Soils and Foundations*, Vol.32, pp.1-15.

[60] ICHII, K., Demonstration of specifying seismic actions in a case of port structures by simplified and detailed analyses, *Proc. of International Workshop on Seismic Design Examples Based on ISO-23469, - Well-chosen Examples of Performance-Based Seismic Design for Geotechnical Works -, Tokyo, Jan. 25, 2010, Japan Association of Earthquake Engineering-Japan Society of Civil Engineers*, CD-ROM, 2010.

[61] Railway Technical Research Institute (1999): The Design Standards for Railway Structures and Commentary (Seismic Design), supervised by Ministry of Land, Infrastructure and Transport, Edited by.

[62] TADANOBU SATO, YOSHITAKA MURONO, HAI-BO WANG and AKIHIKO NISHIMURA (2001) : “Design Spectra and Phase Spectrum Modeling to Simulate Design Earthquake Motions -A Case study through Design Standard of Railway Facilities in Japan”, *Journal of Natural Disaster Science*, Vol.23, pp.89-100, 2001.

[63] YOSHITAKA MURONO and YUTA NOGAMI (2006) : “Shear Stress-Shear Strain Relationship Taking into Account S-Shape Hysteresis Loop”, *Proc. of 12th Japan Earthquake Engineering Symposium* (CD-ROM), pp.494-497

[64] YOSHITAKA MURONO and AKIHIKO NISHIMURA (2000) : “Evaluation of Seismic Forces of Pile Foundation Induced by Inertial and Kinematic Interaction”, *Proc. of 12th World Conference on Earthquake Engineering*, paper No.1496, 2000.

[65] RAILWAY TECHNICAL RESEARCH INSTITUTE (1997): The Design Standards for Railway Structures and Commentary (Foundation structures), supervised by Ministry of Land, Infrastructure and Transport.

[66] THE COMMITTEE ON STRUCTURAL EVALUATION OF HIGH-RISE BUILDINGS IN THE BUILDING CENTER OF JAPAN, Recommendations on Earthquake Motions for Dynamic Response Analysis in Design of High-rise Buildings, *Building Letters*, No.6, pp.49–50, 1986. (in Japanese)

[67] KIDA, T., MORI, S., HARA, E., MASUBUCHI, K., MIKURIYA, K., and YAMANAKA, M., Seismic design of 200 m high R/C smokestack constructed on soft ground and verification of used dynamic analysis model (Part 1) – (Part 6), *Proceedings of the Annual Conference of Architectural Institute of Japan, Vol. Structure-I*, pp. 493-504, 1992.

[68] KOWADA, A., MAEADA, N., MORI, S., IKEDA, T. and GUAN, B., Nonlinear behavior of a towering R/C smokestack on soft ground during the 1995 Hyogoken-Nanbu earthquake, *Journal of Structural and Construction Engineering, Architectural Institute of Japan*, No.512, pp.67-74, 1998. (in Japanese with English abstract)

[69] MORI, S., Proposal of spring-mass model for pile-foundationed structure and its application to really damaged structures, *Journal of Applied Mechanics, Japan Society of Civil Engineers*, Vol.3, pp. 609-620, 2000. (in Japanese with English abstract)

[70] MORI, S., Design and actual performance of a super high R/C smokestack on soft ground, *Proceedings of the 3rd UJNR Workshop on Soil-Structure Interaction, March 29-30, 2004, Vallombrosa Center, Menlo Park, CA, USA*, CD-ROM, 2004.

[71] MORI, S., Design and Its Verification of a High R/C Smokestack Supported by Long Pile Foundation, *Proc. International Conference on Disaster and Development, Kathmandhu, November 23-24, 2008*, pp. 240-257, 2008.

[72] MORI, S., IKEDA, T., TAKIMOTO, Y., MUTO, M. AND TOHAYA, T., Influence of soil liquefaction on dynamic response of structure on pile foundation, *Proceedings of the 10th World Conference of Earthquake Engineering, Madrid, Spain*, Vol.3, pp.1777-1780, 1992.

[73] PENZIEN, J., SCHEFFEY, C. F. and PARMELEE, R. A., Seismic Analysis of Bridges on Long Piles, *Proceedings of ASCE*, Vol. 90, EM3, pp. 223-254, 1964.

[74] Y.A. HASHASH, J. HOOK, B. SCHMIDT, YAO, J. I-CHIANG , *Seismic design and analysis of underground structures*, Tunelling and Underground Space Technology, 16(4), 2001, pp.247-293.

[75] J.-N. WANG, Seismic Design of Tunnels-A simple state-of-the-art design approach, William Barclay Parsons Fellowship Parsons Brinckerhoff, Monograph 7, 1993.

[76] AFPS/AFTES, Guidelines on earthquake design and protection of underground structures. Washington D.C. , 2001.

[77] C.M. ST. JOHN, T.F. ZAHRAH, *Aseismic design of underground structures*, Tunnelling Underground Space Technology, **2(**2), 1987, pp.165-197

[78] K. PITILAKIS, A. CHALATIS, G. TSINIDIS, E. KIRTAS, *Numerical analysis and seismic design of shallow tunnels in soft alluvial deposits*, Proceedings in COMPDYN 2009, Rhodes, Greece, 2009.

[79] G. TSINIDIS, A. CHALATIS, *Seismic design of immersed tunnels – Application at the Thessaloniki immersed roadway tunnel*. MSc thesis (in Greek with extended English abstract), Civil Engineering Dept., Aristotle University of Thessaloniki, Greece, 2008.

[80] K. PITILAKIS AND ASSOCIATES, Design principles of underground metro stations under earthquake loading according to the equivalent static force method. Technical Report no. 2 (in Greek with English summary), Thessaloniki, 2007.

[81] MINISTRY OF PUBLIC WORKS, Greek Seismic Code EAK2000. Athens (in Greek), 2000.

[82] Ishihara, K. and Yamazaki., F. (1980): Cyclic simple shear tests on saturated sand in multi-directional loading, Soils and Foundations, Vol. 20, No. 1, pp. 45-59.

[83] Fujikawa, S., Ueda, M., et al.. (1997): A study on simplified method for pile group modelling in nonlinear dynamic analysis, JSCE Journal of Earthquake Engineering, Vol. 24, pp. 629-632.

[84] Fukutake, K. and Matsuoka, H. (1989): A unified law for dilatancy under multi-directional simple shearing, Proceedings of Japan Society of Civil Engineers, 412/III, pp. 143-151

[85] Fukutake, K., Ohtsuki, A. and Fujikawa. S. (1992): Three-dimensional liquefaction analysis for simulating response of ground due to Superstition Hills earthquake 1987, Proc. Annual convention of JSSMFE, PP. 1103-1106

[86] Fukutake, K., Ohtsuki, A. and Yoshimi, Y. (1996a): Analytical evaluation of reducing stress in piles with soil cement improvement, 11th World Conference on Earthquake Engineering, Acapulco

[87] Fukutake, K., Ohta, Y., et al. (1996b): A Study on Modelling of Structure- Pile- Ground System for Effective-Stress-Analysis Part 5, comparison between 3D and 2D analysis, and effect of pile volume, Annual Meeting Architectural Institute of Japan, Structures II, pp. 465-466.

[88] Fukutake, K. (1997): Studies on three-dimensional liquefaction analyses of soil-structure system considering multi-directional shearing of soil, doctoral thesis of Nagoya Institute of Technology.

[89] Fukutake, K., Sato, M., Tabata, K. and Taji, Y. (2008): E-Defence shaking table tests on soil-pile-foundation interaction in liquefiable deposit Part 3:Prediction analyses using R-O model & Bowl model, Annual Meeting Architectural Institute of Japan, Structures I, pp. 709-710.

[90] Ohtsuki, A., Fukutake, K., Fujikawa, S. and Sato, M. (1994): Three dimensional effective analysis for evaluating response of group pile foundation under liquefaction, Proceedings of Japan Society of Civil Engineers, 495/I, pp. 101-110.

[91] Committee on road structure investigation of Kaminoyama-Yamagata Nishi Tendo line (Yamagata New Town District)(2003): “Report on road structure investigation of Kaminoyama-Yamagata Nishi Tendo line (Yamagata New Town District)”.

[92] Japan Road Association (1999): “Highway earthwork series – Manual for slope plotection”.

[93] Japan Road Association (2002): “Specifications for highway bridges Part V: Seismic design”.

[94] Committee on road structure investigation of Kaminoyama-Yamagata Nishi Tendo line (Yamagata New Town District)(2003): “Report on road structure investigation of Kaminoyama-Yamagata Nishi Tendo line (Yamagata New Town District)”.

[95] ADACHI Y., YOSHIMURA S., and NAKATA T. , Influence to underground structure by ground displacement, Proc. of 12th Japan earthquake engineering symposium, JEES, 2003 (In Japanese)

[96] Azuma H. and KIYOMIYA O., Reliability evaluation of sea bed pipeline suffered from base offset caused by fault, Proc. of 2nd improvement of seismic disaster prevention symposium by failure process analysis, JSCE, 2001. (In Japanese)

[97] BRAY J.D., SEED R.B. and SEED H.B., Analysis of earthquake fault rupture propagation through cohesive soil, Journal of geotechnical engineering, ASCE, 120, 3, pp. 562-580, 1994.

[98] Cole, D. A., Jr. and Lade, P. V., Influence zones in alluvium over dip-slip faults, Journal of Geotechnical Engineering, ASCE, Proc. Paper 18788, Vol. 110, No. GT5, pp. 599-615, 1984.

[99] DONALD L., et al.(1994) “New empirical relationships among magnitude, rupture length, rupture width, rupture area, and surface displacement”, Bulletin of the seismological society of America, Vol.84, No.4, pp974-1002

[100] Freeman T., GILLON M., BERRYMAN K., MORIWAKI Y., SOMERVILLE P. and MEJIA L. (2000) “MATAHINA dam-fault surface displacement design criteria”, CD-ROM of the twelfth world conference on earthquake engineering, Auckland NZ

[101] IRIKURA K. and MIYAKE H. (2001) “Prediction of strong motion based on scenario earthquake”, Earthquake, Vol. 110, No. 6, pp. 849-875, SSJ (In Japanese)

[102] KENNEDY, R.P., Chow, A.W. and WILLIAM, R.A. (1977) “Fault movement effects on buried oil pipeline”, Transportation Engineering J., ASCE, Vol. 103, No.TES, pp. 617-633

[103] KONAGAI K. and JOHANSON J. (2001) “Lagrangian particles for modeling large soil deformations”, Proc. of a workshop on seismic fault-induced failures, pp. 99-106

[104] MATSUDA T. (1975) “Magnitude and return period of the earthquakes caused by active faults, Earthquake, Vol.2 No.28, pp. 269-283, SSJ (In Japansese)

[105] NEWMARK N. W. and HALL W. J. (1975) “Pipeline design to resist large fault displacement”, Proceedings of the U.S. National Conference on Earthquake Engineering-1975, EERI, pp. 416-425

[106] ONIZUKA N., HAKUNO N., IWASHITA K., and SUZUKI T. (1999) “Stress and strain propagation due to base displacement caused by reverse fault activities”, Journal of Applied Science, JSCE, 2, pp. 533-542 (In Japanese)

[107] RAMANCHARLA P. K. and MEGRO K. (2001) “Non-linear numerical modeling of dip-slip faults for studying ground surface deformation”, Proc. of 2nd improvement of seismic disaster prevention symposium by failure process analysis, JSCE

[108] RAMANCHARLA P. K. and MEGRO K. (2001) “Applied simulation of non-linear behavior of dip-slip faults for studying ground surface deformation”, Proc. of a workshop on seismic fault-induced failures, JSPS, pp. 109-114

[109] SATO Y., ABE K., OKADA Y., SIMAZAKI K., and SUZUKI Y. (1989) “Relation between [7] earthquake magnitude and fault parameters”, Fault parameters handbook of Japan, Vol.2 2nd chapter, pp. 82-92,

[110] KAJIMA books TAKADA S., NEMAT H., and FUKUDA K. (2001) “Propose of simplified design method for buried pipes crossing earthquake fault”, Journal of structural engineering, JSCE, No.668, □-54, pp. 187-194 (In Japanese)

[111] TAKEMURA M. (1998) “Scaling rule of crust type earthquake in Japan”, Zisin, Vol.2 No.51, pp. 221-228, Seismological Society of Japan (In Japanese)

[112] TANI K. and UEDA K. (1991) “Location and shape of discontinuous plane in sandy layer by base fault displacement”, Proc. of 26th geotechnical engineers meeting, pp. 1185-1188 JSCE (In Japanese)

[113] TANIYAMA T. and WATANABE H. (1998) “Deformation propagation in sandy surface layer caused by reverse fault activities, Journal of Geotechnical Engineering, JSCE, 591/ III-43, pp. 313-325 (In Japanese)

[114] Y.A. HASHASH, J. HOOK, B. SCHMIDT, YAO, J. I-CHIANG , *Seismic design and analysis of underground structures*, Tunelling and Underground Space Technology, 16(4), 2001, pp.247-293.

[115] AASHTO, 2008, “Standard Specifications for Highway Bridges,” American Association of State Highway and Transportation Officials, Washington D.C.

[116] AMERICAN CONCRETE INSTITUTE (ACI), 2002, “Building Code Requirements for Reinforced Concrete (ACI 318-2002),” American Concrete Institute, Detroit, Michigan.

[117] BOORE, D., 1973, “The Effect of Simple Topography on Seismic Waves: Implications for Accelerations Recorded at Pacoima Dam, San Fernando Valley, California,” Bull. of the Seism. Soc. of Am., Vol. 63, No. 5, Oct., pp. 1603-1609.

[118] BOORE ET AL., 1997, “Equations for Estimating Horizontal Response Spectra and Peak Acceleration from Western North American Earthquakes: A Summary of Recent Work,” Seismological Research Letters, Volume 68, Number 1, January/February, pp. 128-153.

[119] BOUCHON, M., 1973, "Effect of Topography on Surface Motion," Bull. of the Seism. Soc. of Am., Vol. 63, No. 3, April, pp. 615-632.

[120] CALIFORNIA DEPARTMENT OF TRANSPORTATION (CALTRANS), 2005, "SNAILZ – Soil Reinforcement Program", Office of Roadway Geotechnical Engineering, Caltrans, Sacramento, CA

[121] DAVIS, C. A., 2003, "Lateral Seismic Pressures for Design of Rigid Underground Structures," Proc. 6th U.S. Conf. on Lifeline Earthquake Engineering, Monograph 25, ASCE, Long Beach, Aug., 10-13, pp. 1001-1010.

[122] DAVIS, C. A. AND S. R. COLE, 1999, "Seismic Performance of the Second Los Angeles Aqueduct at Terminal Hill," Proc. 5th U.S. Conf. on Lifeline Earthquake Engineering, ASCE, Seattle, Aug., pp. 452-461.

[123] DEERE, D.U., PECK, R.B., PARKER, H., MONSEES, J.E., AND SCHMIDT, B., "Design of Tunnel Support System," Highway Research Record, No. 339 (1970)

[124] FEDERAL EMERGENCY MANAGEMENT AGENCY (FEMA), 2003, "FEMA-450: NEHRP Recommended Provisions for Seismic Regulations for New Buildings and Other Structures," 2003 Edition, Washington, D. C., Developed by the Building Seismic Safety Council (BSSC) for FEMA.

[125] FEDERAL EMERGENCY MANAGEMENT AGENCY (FEMA), 1999, "HAZUS - FEMA's Software Program for Estimating Potential Losses from Disasters", Washington, D. C.

[126] FEDERAL HIGHWAY ADMINISTRATION (FHWA), 1998, "Manual for Design and Construction Monitoring for Soil Nail Walls," FHWA Publication No. SA-96-069R, October 1998

[127] GREGOR, N., W. SILVA, W., AND B. DARRAGH, 2002, "Development of Attenuation Relations for Peak Particle Velocity and Displacement," A PEARL Report to PG&E/CEC/Caltrans, Prepared by Pacific Engineering and Analysis, June 12, 2002.

[128] HASHASH, Y.M.A., HOOK, J.J., SCHMIDT, B., AND YAO, J.I.C., 2001, "Seismic Design and Analysis of Underground Structures," Tunneling and Underground Space Technology 16

[129] HOEK, E., 1999, "SUPPORT FOR VERY WEAK ROCK ASSOCIATED WITH FAULTS AND SHEAR ZONES." Proc. International Symposium on Rock Support and Reinforcement Practice in Mining, Kalgoorlie, Australia, 14-19 March, 1999.

[130] KAVAZANJIAN, E. JR., MATASOVIĆ, N., HADJ-HAMOU, T., AND SABATINI, P.J., 1997, "Design Guidance: Geotechnical Earthquake Engineering for Highways, Volume I, Design Principles," Geotechnical Engineering Circular No. 3, Report FHWA-SA-97-076, Federal Highway Administration, Washington, D.C.

[131] NEWARK, N. M., 1968, "Problems in Wave Propagation in Soil and Rock," International Symposium on Wave Propagation and Dynamic Properties of Earth Materials.

[132] O'ROURKE, M. J., HMADI, K.E., 1988, "Analysis of continuous buried pipelines for seismic wave effects." Earthquake Engrg. and Struct. Dyn., 16, 917-929.

[133] O'ROURKE, T. D., "Guidelines for Tunnel Lining Design," ASCE Technical Committee on Tunnel Lining Design of the Underground Technology Research Council, 1984.

[134] OWEN, G. N., AND SCHOLL, R. E., 1981, "Earthquake Engineering of Large Underground Structures," prepared for the Federal Highway Administration, FHWA/RD-80/195.

[135] PROCTOR, ROBERT V. & WHITE, THOMAS L., 1977, "Earth Tunneling with Steel Supports," Commercial Shearing and Stamping Company.

[136] PROCTOR, ROBERT V. & WHITE, THOMAS L., “Rock Tunneling with Steel Supports,” Commercial Shearing and Stamping Company (1968).

[137] SCOTT, R. F., 1973, “Earthquake-Induced Pressures on Retaining Walls,” Proc., 5th World Conf. On Earthquake Engr., Int. Assn. of Earthquake Engr., Tokyo, 2, 1611-1620.

[138] SHERIF, M. A., I. ISHIBASHI, AND C. D. LEE, 1982, “Earth Pressures Against Rigid Retaining Walls,” Journal of the Geotechnical Engineering Division, ASCE, Vol. 108, No. GT5, pp. 679-695.

[139] STAAD, 2008, “STructural Analysis And Design software,” Bentley System, Exton, PA USA, www.bentley.com.

[140] UNITED STATES OF GEOLOGICAL SURVEY (USGS), 2002, “Documentation for the 2002 Update of the National Seismic Hazard Maps”, Open-File Report 02-460, U.S. Geological Survey, Washington D.C..

[141] VELETSOS, A. S., AND A. H. YOUNAN, 1994a, “Dynamic Soil Pressures on Rigid Vertical Walls,” Earthquake Engineering and Structural Dynamics, Vol. 23, pp. 275-301.

[142] VELETSOS, A. S., AND A. H. YOUNAN, 1994b, “Dynamic Modeling and Response of Soil-Wall Systems,” J. of Geo. Eng., ASCE, Vol. 120, No. 12, pp. 2155-2179.

[143] YOUD, T. L., AND T. N. CRAVEN, 1975, “Lateral Stress in Sands During Cyclic Loading,” J. Geo. Eng. Div., ASCE, Vol. 101, No. GT2, pp. 217-221.

[144] YUAN, X. AND FU-LU MEN, 1992, “Scattering of Plane SH Waves by a Semi-Cylindrical Hill,” Earthquake Engineering and Structural Dynamics, Vol. 21, pp. 1091-1098.

ICS 91.080.01; 93.020

Price based on 215 pages